MINNESOTA DEPARTMENT OF TRANSPORTATION

RESEARCH

2007-05

Resilient Modulus and Strength of Base Course with Recycled Bituminous Material

LRRB
LOCAL
ROAD RESEARCH
BOARD

Take the steps... Research...Knowledge...Innovative Solutions!

Transportation Research

Technical Report Documentation Page

1. Report No.	2.	3. Recipients Accession No.
MN/RC-2007-05		

4. Title and Subtitle	5. Report Date
Resilient Modulus And Strength Of Base Course With Recycled Bituminous Material	January 2007
	6.
7. Author(s) Woosung Kim and Joseph F. Labuz	8. Performing Organization Report No.
9. Performing Organization Name and Address Dept. of Civil Engineering University of Minnesota 500 Pillsbury Drive SE Minneapolis, MN 55455	10. Project/Task/Work Unit No. 11. Contract (C) or Grant (G) No. (c) 81655 (wo) 132
12. Sponsoring Organization Name and Address Minnesota Department of Transportation 395 John Ireland Boulevard Mail Stop 330 St. Paul, Minnesota 55155	13. Type of Report and Period Covered Final Report 14. Sponsoring Agency Code

15. Supplementary Notes
http://www.lrrb.org/PDF/200705.pdf

16. Abstract (Limit: 200 words)

The objective of the research was to determine the strength and deformation characteristics of base material produced from recycled asphalt pavement (RAP) and aggregate. Various samples with different ratios of RAP and aggregate base were mixed (% RAP/aggregate): 0/100, 25/75, 50/50, 75/25. Laboratory compaction testing and field monitoring indicated that gyratory compacted specimens were closer to the densities measured in the field. Resilient modulus (MR) tests were generally conducted following the National Cooperative Highway Research Program 1-28A test protocol. MR increased with increase of confining pressure, but MR showed little change with deviator stress. The specimens with 65% optimum moisture contents were stiffer than the specimens with 100% optimum moisture contents at all confining pressures. Cyclic triaxial tests were conducted at two deviator stresses, 35% and 50% of the estimated peak stress, to evaluate recoverable and permanent deformation behavior from initial loading to 5000 cycles. The specimens with RAP exhibited at least two times greater permanent deformation than the 100% aggregate material. As %RAP increased, more permanent deformation occurred. In summary, the base material produced with various %RAP content performed at a similar level to 100% aggregate in terms of MR and strength when properly compacted.

17. Document Analysis/Descriptors	18. Availability Statement
Recycled asphalt pavement, Resilient modulus, Aggregate base	No restrictions. Document available from: National Technical Information Services, Springfield, Virginia 22161

19. Security Class (this report)	20. Security Class (this page)	21. No. of Pages	22. Price
Unclassified	Unclassified	270	

Resilient Modulus and Strength of Base Course with Recycled Bituminous Material

Final Report

Prepared by:

Woosung Kim and Joseph F. Labuz
Department of Civil Engineering
University of Minnesota

January 2007

Prepared for:

Minnesota Department of Transportation
Office of Materials and Road Research
1400 Gervais Avenue
Maplewood, MN 55109

Published by:

Minnesota Department of Transportation
Research Services Section
395 John Ireland Boulevard, MS 330
St. Paul, Minnesota 55155-1899

Acknowledgements

Partial support was provided by the Local Road Research Board and the Minnesota Department of Transportation (Mn/DOT). Special thanks are extended to (a) Mn/DOT Office of Materials, especially Shongtao Dai, Marc Loken, Tim Anderson, Jerry Geib, Bruce Chadbourn, and John Siekmeier; and (b) Wright County Engineers Wayne Fingalson and Virgil Hawkins.

Table of Contents

List of Figures

List of Tables

Executive Summary

Full-depth reclamation is a recycling technique in which the existing asphalt pavement section and all or a predetermined portion of the underlying aggregate are uniformly reclaimed and blended to produce a base course. Full-depth reclamation has been proposed as a viable alternative in road rehabilitation, where asphalt and aggregate resources are conserved, and material and transportation costs are reduced. The objective of the research was to determine the strength and deformation characteristics of base material produced from recycled asphalt pavement (RAP) and aggregate.

Various samples with different ratios of RAP and aggregate base were mixed (% RAP/aggregate): 0/100, 25/75, 50/50, 75/25. Sieve analyses were performed, and it was found that as % RAP increased the material became coarser. Laboratory compaction testing and field monitoring indicated that gyratory compacted specimens were closer to the densities measured in the field. Resilient modulus (M_R) tests were generally conducted following the National Cooperative Highway Research Program 1-28A test protocol. M_R increased with increase of confining pressure, but M_R showed little change with deviator stress. The specimens with 65% optimum moisture contents were stiffer than the specimens with 100% optimum moisture contents at all confining pressures, with the effect increasing at higher confining pressures.

Cyclic triaxial tests were conducted at two deviator stresses, 35% and 50% of the estimated peak stress, to evaluate recoverable and permanent deformation behavior from initial loading to 5000 cycles. The specimens with RAP exhibited at least two times greater permanent deformation than the 100% aggregate material, and a steady state condition was reached after approximately 1000 cycles. As %RAP increased, more permanent deformation occurred. The secant Young's modulus (E_{secant}) increased as the number of cycles increased. Initially, E_{secant} was larger for the 100% aggregate specimens, but after approximately 100 cycles the 25% aggregate – 75% RAP specimens had the highest E_{secant}. The cyclic tests at the 50% peak stress ratio exhibited greater permanent deformation by a factor of 2-3 compared to the 35% peak stress ratio tests, and E_{secant} was about 15% greater at the higher deviator stress. In summary, the base material produced with various %RAP content performed at a similar level to 100% aggregate in terms of M_R and strength when properly compacted.

Chapter 1
Introduction

Full-depth reclamation is a recycling technique in which all of the existing pavement section and all or a predetermined portion of the underlying aggregate are uniformly blended to produce a base course [1, 2]. Full-depth reclamation has been proposed as a viable alternative in road construction, where asphalt and aggregate resources are conserved, and material and transportation costs are reduced because recycling eliminates the need for hauling new materials and disposing of old materials [3, 4]. The mixture of recycled asphalt pavement (RAP) and aggregate produced from full-depth reclamation (Fig. 1.1) has the potential to have engineering properties that exceed those of a 100% aggregate base material, although little data are available to substantiate the claim [5].

Figure 1.1: Full Depth Reclamation and Recycled Asphalt Pavement (RAP).

Pavements are located on material layers called the base and sub-grade. It has been proven that the mechanical properties of the base layer greatly affect the pavement performance. Therefore, it is important to determine stiffness, strength, and permanent deformation characteristics of the base. By conducting cyclic triaxial testing that simulates traffic load, the recoverable and permanent axial strain can be measured and used to estimate the performance of the pavement structure (Fig. 1.2).

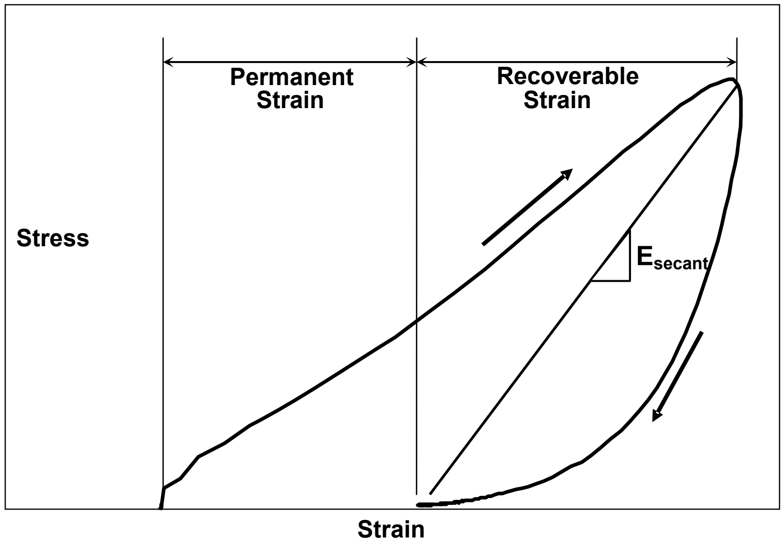

Figure 1.2: Element Response during Cyclic Triaxial Testing.

In this research, resilient modulus (M_R) tests were conducted to measure recoverable (resilient) behavior of base materials with various mixtures of RAP and aggregate. In addition, shear strength tests were performed to measure strength of the different mixtures. Cyclic triaxial tests were also designed and conducted to measure permanent deformation (axial strain) of the mixtures.

1.1 Background

Although there are potential benefits in cost and improvements in engineering properties of RAP as a base material, laboratory and field data are not extensive. Highter et al. [6] conducted M_R tests with different ratios of RAP and aggregate (crushed stone and gravel) mixtures. Standard Proctor tests provided compaction characteristics, and the dry density of the mixtures decreased as the percentage of RAP increased. No trend for moisture content was observed. The M_R test results showed an increase of M_R with the addition of RAP to the aggregate mixtures.

Papp et al. [7] compared engineering properties of RAP and dense-graded aggregate base course. Various ratios of RAP and aggregate mixtures were prepared. From the grain size distribution, aggregate contained more fines than RAP mixtures. From the standard Proctor tests, it was noticed that the maximum dry density and optimum moisture content decreased as the percentage of RAP increased. By using a vibratory hammer, specimens were compacted to 154.2 mm diameter and 304.8 mm height, and M_R and permanent deformation were measured. The RAP blended mixtures obtained higher M_R than the pure aggregate. However, the RAP blended mixtures had higher permanent deformation from cyclic triaxial tests of 100,000 loading cycles at 103 kPa confining pressure and 310 kPa deviator stress. It was explained that higher RAP content specimens had higher permanent deformation from the conditioning and first 95 cycles from each sequences, and stiffened enough before M_R values were measured from the last five cycles, which are used to calculate M_R. From the shear strength tests, aggregate had higher friction angle and cohesion compared to the RAP mixtures.

1.2 Objectives

This report presents M_R, shear strength and cyclic triaxial test results on specimens with various blends of RAP and base aggregate. The effects of %RAP and moisture content on M_R, strength, and permanent deformation are discussed. The results will be useful in helping Minnesota Department of Transportation (Mn/DOT) develop specifications for the use of RAP materials as a base course.

The resilient modulus (M_R) tests were conducted on specimens with various mixtures of RAP and aggregate. M_R is similar to (a secant) Young's modulus based on the recoverable axial strain due to cyclic axial stress:

$$M_R = \frac{\Delta\sigma_a}{\Delta\varepsilon_a^{\ r}} \tag{1.1}$$

where $\Delta\sigma_a$ = cyclic axial (deviator) stress and $\Delta\varepsilon_a^{\ r}$ = recoverable axial strain. The M_R tests were conducted in the laboratory generally following the National Cooperative Highway Research Program (NCHRP) 1-28A test protocol [8]. Cyclic axial stress (Fig. 1.3), which simulates traffic loading, was applied to a cylindrical specimen at a given confining pressure within a conventional triaxial cell, and the recoverable axial strain was measured (Fig. 1.2).

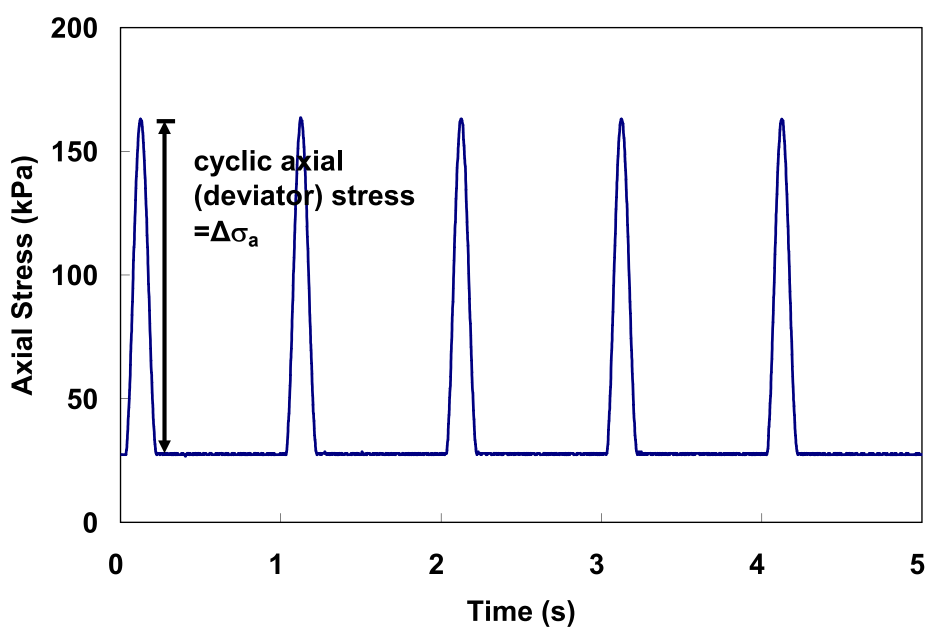

Figure 1.3: Example Cyclic Axial Stress.

Shear strength tests were also conducted on the same specimens after M_R tests. For each mixture, the maximum axial stresses at two different confining pressures were measured (Fig. 1.4). From the principal stress data, friction angle (ϕ) and cohesion (c) were calculated, and the orientation of the failure plane (θ) was noted.

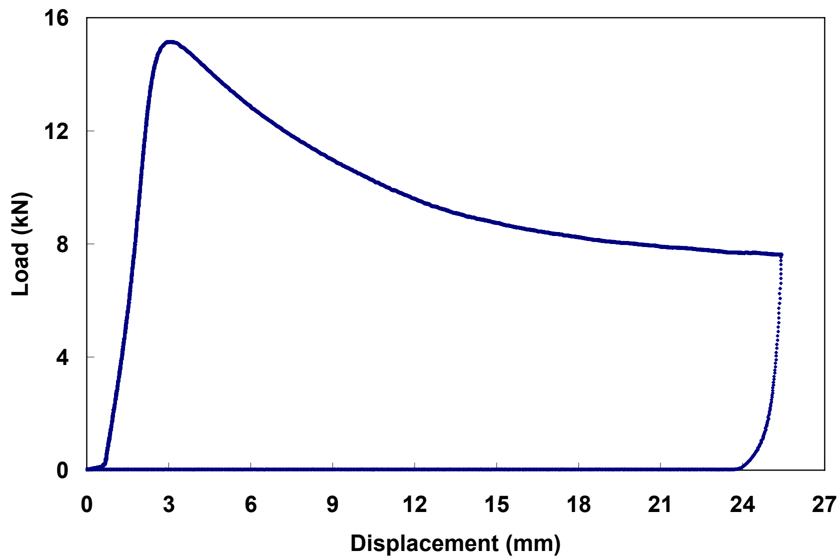

Figure 1.4: Mechanical Response from a Strength Test.

Although permanent deformation of pavement base is critical for pavement performance, it has not received much attention by the researchers compared to the recoverable deformation [9]. From previous research, the cyclic triaxial test has been tried and proved as an acceptable test method in analyzing not only recoverable deformation but also permanent deformation [10, 11]. However, there is no standard protocol of the cyclic triaxial test to measure the mechanical response of base materials [12]. Cyclic triaxial tests were designed and performed on specimens from different mixtures at two different deviator stresses, and the deformation behavior (permanent and recoverable deformation) of each mixture at two different deviator stresses was measured.

1.3 Organization

Chapter 2 contains descriptions of the sample preparation procedure including gradation tests, Proctor and gyratory compaction tests, and the mechanical testing procedures. Chapter 3 describes quality control / quality assurance criteria for the tests, including angle of rotation and signal-to-noise ratio. Chapter 4 contains the test results of M_R, shear strength and cyclic triaxial tests, and data interpretation. Chapter 5 summarizes and concludes the findings of the research.

Chapter 2
Experimental Procedures

2.1 Sample Preparation

Reclaimed materials were obtained from County Road (CR) 3 in Wright County, Minnesota (Fig. 2.1). An in-situ blend (the mixture of RAP and aggregate) was taken during full-depth reclamation.

Figure 2.1: RAP, Aggregate, and In-situ Blend Produced from County Road (CR) 3.

In addition, pure RAP and pure aggregate materials from CR 3 were sampled separately, and various blended mixtures with different ratios of RAP and aggregate base were produced (% RAP/aggregate): 0/100, 25/75, 50/50, 75/25. RAP and aggregate materials were poured into a splitter provided by the Minnesota Department of Transportation (MnDOT) Office of Materials Laboratory (Fig. 2.2) according to the specified ratio by mass, and mixed several (4-6) times until the materials were visually well-mixed. Finally, the five different blended mixtures from CR 3, one in-situ and four laboratory samples, were prepared for testing.

Figure 2.2: Soil Splitter.

In-situ blends (the mixture of RAP and aggregate) were also sampled from Trunk Highway (TH) 23 (Wikipedia, MN), TH 200 (Ada, MN) and TH 5 (St. Paul, MN) during full-depth reclamation. The sample from TH 5 was provided to compare densities in the field with those measured by standard Proctor and gyratory compaction (Tables 2.1 and 2.2).

2.1.1 Gradation Test Procedure

Sieve tests for each material were conducted according to the procedure from the American Society for Testing and Materials (ASTM) Standards C136-01, "Standard Test Method for Sieve Analysis of Fine and Coarse Aggregate [13]." About 5 kg of representative material of each sample were collected. Then, the representative material of each sample was put into the coarse grained soil sieve shaker (Fig. 2.3), and masses on each pan were measured after 10 minute shaking.

Figure 2.3: Sieves for Coarse Grained Soil (Left) and Fine Grained Soil (Right).

Among the material that passed all the sieves and was collected by the bottom pan, about 600 g of representative material was selected and dried at 140ºF for about 2 hr, and then sent to the fine grained soil sieve shaker (Fig. 2.3). The soil retained on each sieve was measured after shaking. Based on the mass ratio, a gradation curve was plotted and compared with the MnDOT specification bands [14].

2.1.2 Gradation Test Result

Gradation curves from the sieve analysis are shown in Figs. 2.4 and 2.5 (detail gradation results are contained in Appendix A.1). For CR 3 material, "Blend" represents in-situ blend material, and "number A – number R" represents percentage of aggregate and RAP. For example, 75% aggregate and 25% RAP sample is expressed as 75A – 25R. Samples from TH 23, TH 200 and TH 5 were all in-situ blend material.

From Fig. 2.4, it is noticed that samples with more RAP are more granular and have less fines content, and the gradation curve for the Blend sample is close to that of 50A – 50R sample. From Fig. 2.5, it is noticed that in-situ blend materials from three Trunk Highways have very similar gradation curves.

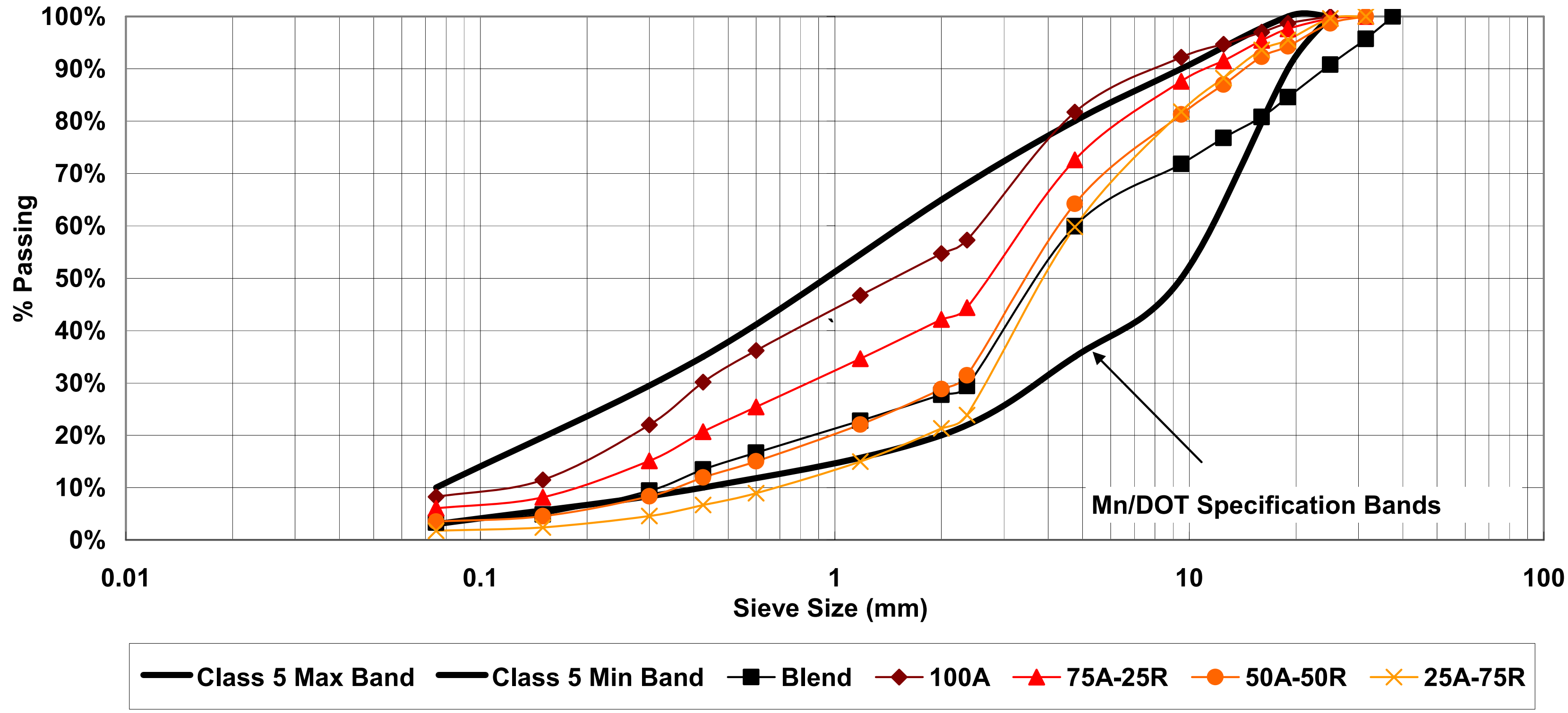

Figure 2.4: Gradation Curves for CR 3 Materials.

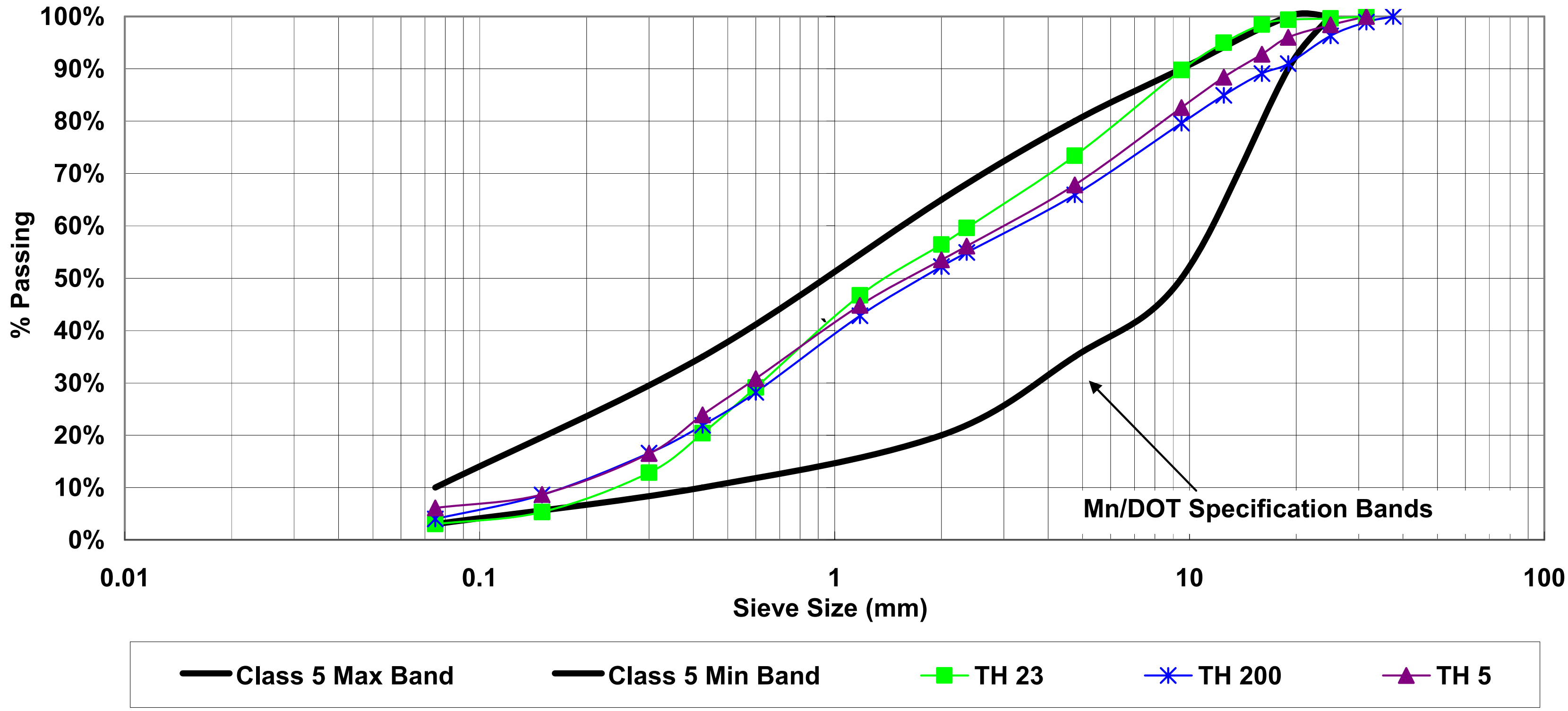

Figure 2.5: Gradation Curves for TH 23, TH 200 and TH 5 Materials.

2.2 Compaction Tests

The Proctor compaction test is typically performed for soils. However, compaction by the drop of a mass has been questioned as the appropriate procedure for simulating field compaction of granular materials, with an additional problem that excess moisture can escape from a Proctor mold. For these reasons, gyratory compaction was investigated for determining the maximum dry density and optimum moisture content. Both standard Proctor and gyratory compaction tests were performed for the eight mixtures and the results were compared (Table 2.1).

2.2.1 Standard Proctor Compaction Test

Standard Proctor compaction tests were performed following the procedure from the American Association of State Highway and Transportation Officials (AASHTO) T99, “The Moisture-Density Relations of Soils Using a 2.5 kg (5.5 lb) Rammer and a 305 mm (12 in) Drop [15].” Also, ASTM Standard D698-00ae1, “Standard Test Method for Laboratory Compaction Characteristics Using Standard Effort” was referenced [16]. Method C was chosen from the AASHTO T99, which specifies a 101 mm mold size, materials smaller than 19 mm, and 3 layers of 25 blows each (Fig. 2.6).

Figure 2.6: Proctor Compaction Test Hammer and Mold.

Although there were some materials larger than 19 mm, AASHTO allows the following:

“If it is necessary to maintain same percentage of coarse material (-50 mm., +4.75 mm) in a sample as in the original field sample, +19 mm material can be replaced as follows: mass of -50 mm, +19 mm material determined and replaced with equal mass of -19 mm,

+4.75 mm material. Replacement material should be taken from the remaining portion of the sample."
Therefore, 5.4 kg of the representative samples were prepared for each sample and those materials larger than 19 mm were replaced by equal mass of -19 mm, +4.75 mm materials. From the Proctor compaction tests, density at different moisture contents were measured, and the maximum dry density and optimum moisture content for each different mixture were estimated. Moisture content was determined by obtaining about 500 g of material from the center of the mold and drying in an oven at 40^{o}C for 48 hours.

2.2.2 Gyratory Compaction Tests

Gyratory compaction tests were performed with a 152 mm diameter specimen mold, and the base rotated at a constant 30 revolutions per minute during compaction with the mold positioned at a compaction angle of 1.25 degrees [17, 18]. A compaction pressure of 600 kPa with 50 gyrations was selected [19]. By comparing field density and moisture content (Table 2.2), and comparing the M_R of specimens compacted by 50 and 75 gyrations, 50 gyrations was recommended for the specimen compaction [19]. Therefore, 5.4 kg of the representative samples (+12.5 mm material were replaced with -12.5 mm , +4.75 mm material for material homogeneity) with different moisture contents were compacted by 50 gyrations, and the maximum dry density and optimum moisture content for each different mixture were calculated (detailed testing procedure is contained in Appendix A.5). Moisture content was determined by obtaining about 200 g of material from the center of the mold and drying in an oven at 40^{o}C for 6 days [19]. Figure 2.7 shows the gyratory compactor and Fig. 2.8 shows a specimen after gyratory compaction.

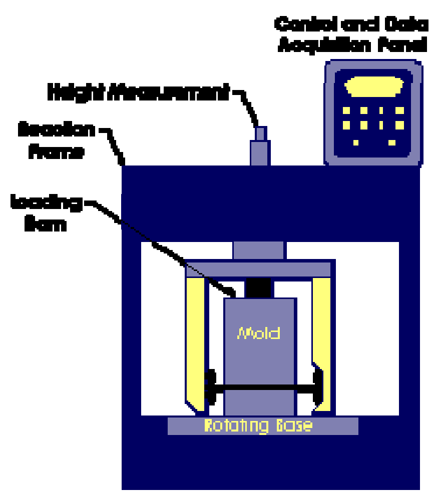

Figure 2.7: Gyratory Compactor and Diagram.

Figure 2.8: Gyratory Compacted Specimen.

2.2.3 Results and Selection of Compaction Method

Eight different mixtures, including their identification letters, descriptions, maximum dry densities and optimum moisture contents from two different compaction methods (Proctor and gyratory), are summarized in Table 2.1. Detailed test results including Proctor and gyratory compaction curves for the mixtures are in Appendix A, and examples of Proctor and gyratory compaction curves for CR 3 50% Aggregate – 50% RAP sample are shown in Fig. 2.9. For some samples (CR 3 Blend, CR 3 100% Aggregate and CR 3 50% Aggregate – 50% RAP), duplicate tests were conducted for Proctor to check on repeatability.

Table 2.1: Proctor and Gyratory Compaction Test Results.

Soil Identification Letter	Description	Proctor		Gyratory	
		Maximum Dry Density (kg/m^3)	Optimum Moisture Content (%)	Maximum Dry Density (kg/m^3)	Optimum Moisture Content (%)
S	In-situ Blend, CR 3	1984	9	2032	7.8
T	100% Aggregate, CR 3	2000	10	2032	8.8
U	75% Aggregate - 25% RAP, CR 3	2000	10	2032	8.7
V	50% Aggregate - 50% RAP, CR 3	1952	9.5	2032	8.0
W	25% Aggregate - 75% RAP, CR 3	1920	8.5	2032	7.2
X	In-situ Blend, TH 23	2000	7	2080	5.4
Y	In-situ Blend, TH 200	2096	6.5	2144	5.7
Z	In-situ Blend, TH 5	1984	8.5	2112	6.6

Table 2.2: TH5 Sand Cone Test Values.

Sand Cone	Dry Density (kg/m^3)	Moisture Content (%)
4 in.	2165	4.2
	2200	3.6
	2196	3.6
	2300	4.5
	2124	3.1
6 in.	2169	3.7
	2266	3.8
	2175	3.2

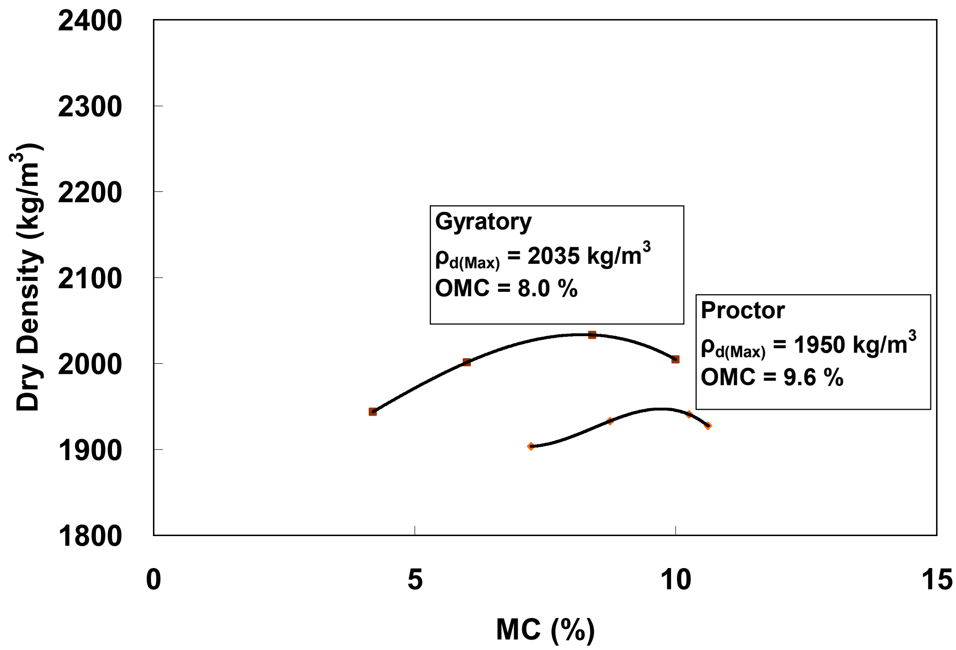

Fig 2.9: Compaction Method Comparison CR 3 50% Aggregate – 50% RAP.

Results from the gyratory compaction tests, as compared to the Proctor tests, showed increased maximum dry densities (32 – 128 kg/m^3) and reduced optimum moisture contents (0.8 – 1.9%). The optimum moisture contents for the CR 3 materials decreased by 0% – 1% as 25% of RAP material increased from the two compaction test. However, the maximum dry density for the CR 3 materials decreased by 0 – 38 kg/m^3 as 25% of RAP material increased from the Proctor, and remained more or less constant regardless of the RAP content for the Gyratory compaction.

Compaction by a vibratory hammer following the maximum dry density from the standard Proctor test is suggested by the M_R testing protocols. However, as mentioned previously, compaction by the drop of a mass has been questioned as the appropriate procedure for simulating field compaction of granular materials. As shown in Tables 2.1 and 2.2, both standard Proctor and gyratory compaction tests were performed for the TH 5 in-situ blend material, and the results were compared with the field sand cone (4 in. and 6 in.) test values. From Fig. 2.10, the maximum dry density and optimum moisture content obtained from a gyratory compaction test were closer to the field compaction values compared to the values from a standard Proctor test. Thus, gyratory compaction seemed to better simulate field conditions.

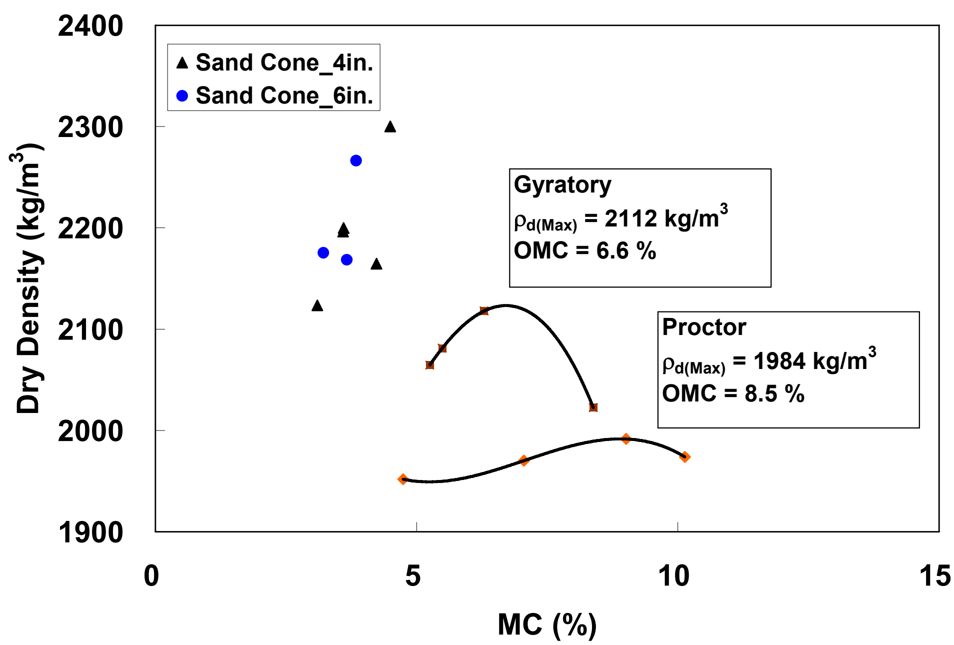

Figure 2.10: Compaction Method Comparison: TH 5 Blend.

To compare the effect of the different laboratory compaction methods on M_R, two M_R tests were conducted on specimens from TH 5 in-situ blend material compacted by different compaction methods (vibratory hammer and gyratory compaction). The results showed that the specimen compacted by the vibratory hammer using the maximum dry density from a standard Proctor test did not provide sufficient density; the specimen was stiffening (an increase of M_R) with increasing deviator stress and significant permanent deformation was recorded (Figs. 2.11 - 2.14). It appeared that compaction was not complete. With gyratory compaction, the specimen response was typical of well-compacted granular soil. Note that the nonlinear and relatively soft response due to incomplete compaction was changed to a stiffer response with the gyratory compactor. As shown in Fig. 2.15, 100% gyratory density specimen is stiffer than 100% Proctor density specimen. Therefore, it was decided to use a gyratory compactor for specimen compaction.

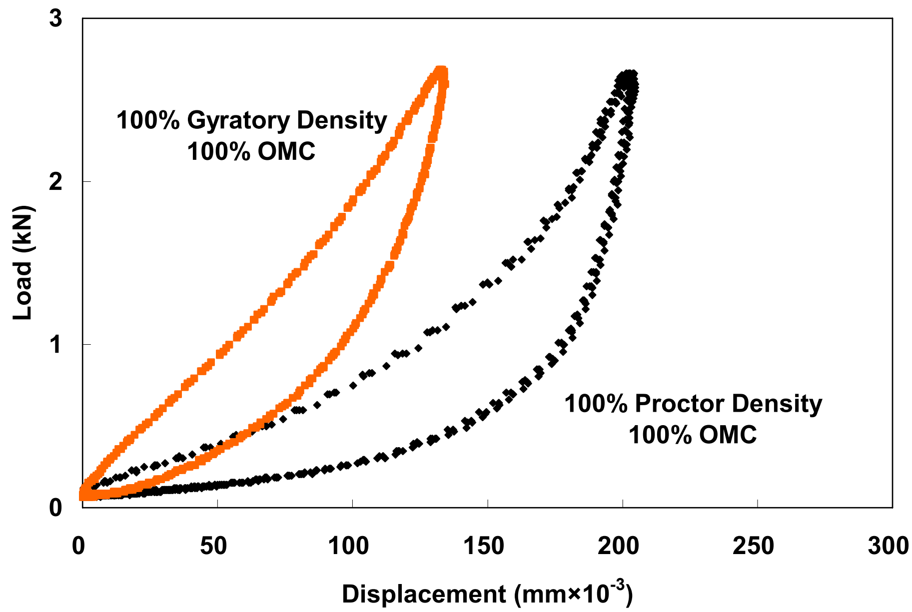

Figure 2.11: Last Five Cycles: Sequence 26: TH 5 Blend.

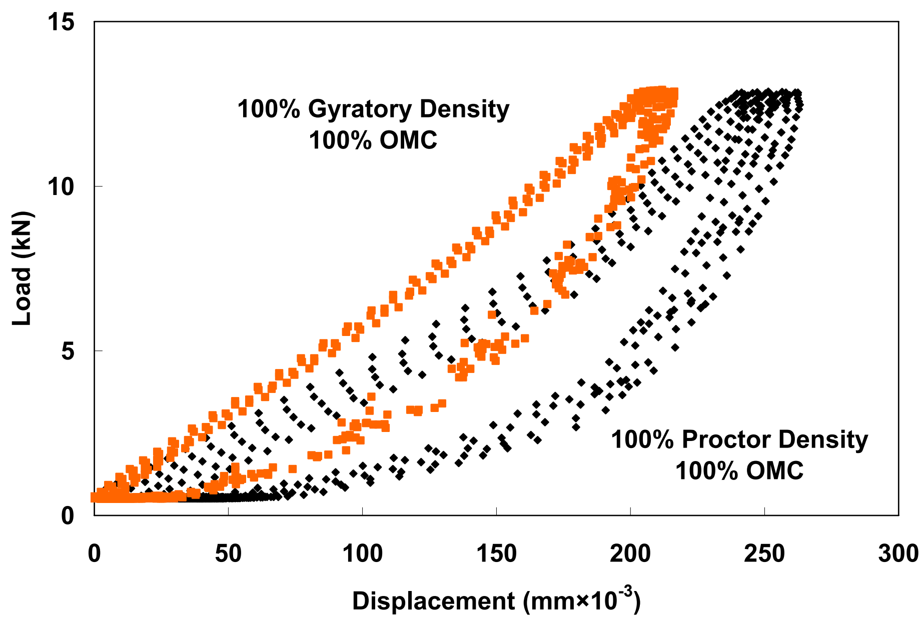

Figure 2.12: Last Five Cycles: Sequence 25: TH 5 Blend.

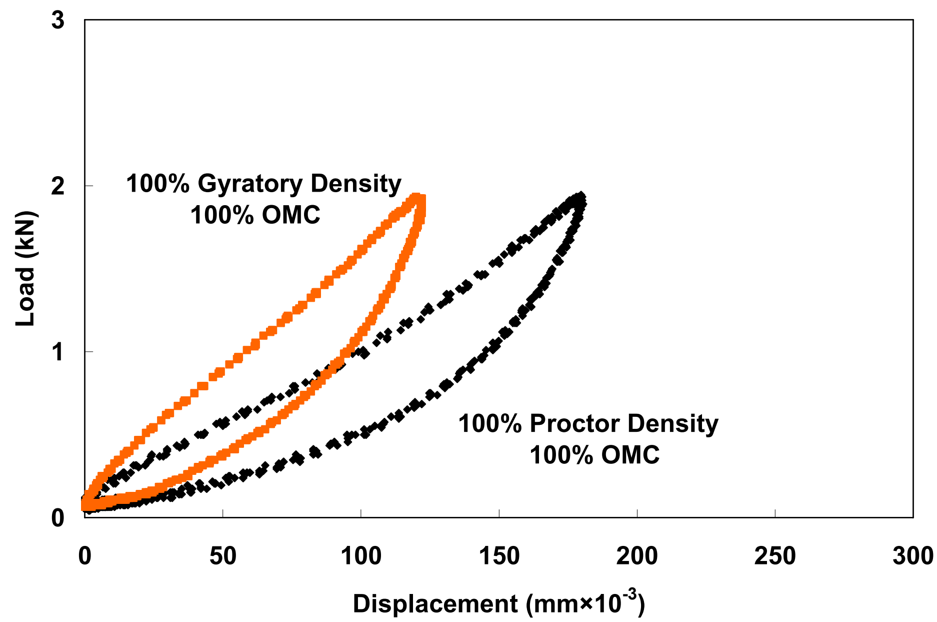

Fig 2.13: Last Five Cycles: Sequence 20: CR 3 100% Aggregate.

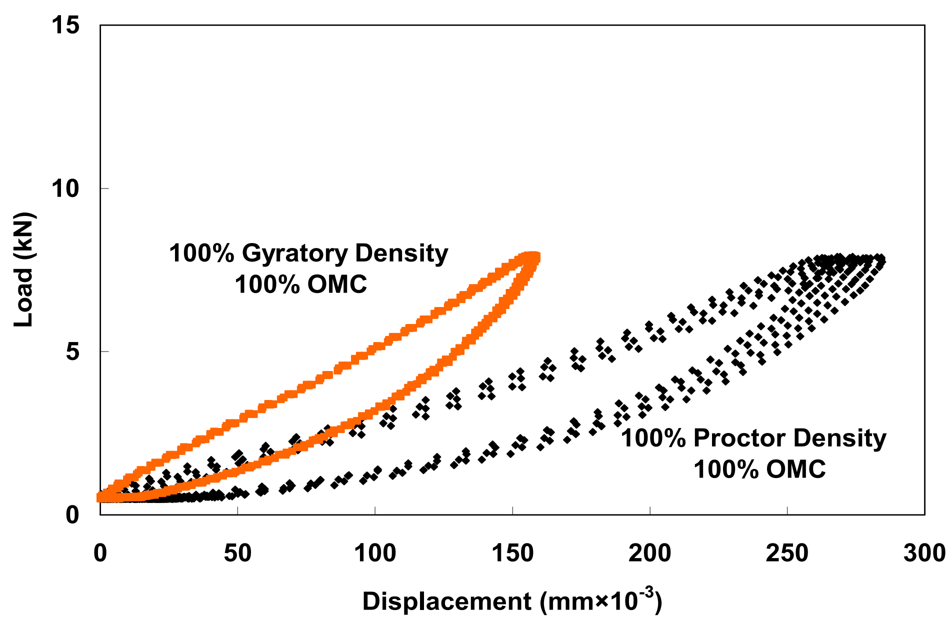

Fig 2.14: Last Five Cycles: Sequence 21: CR 3 100% Aggregate.

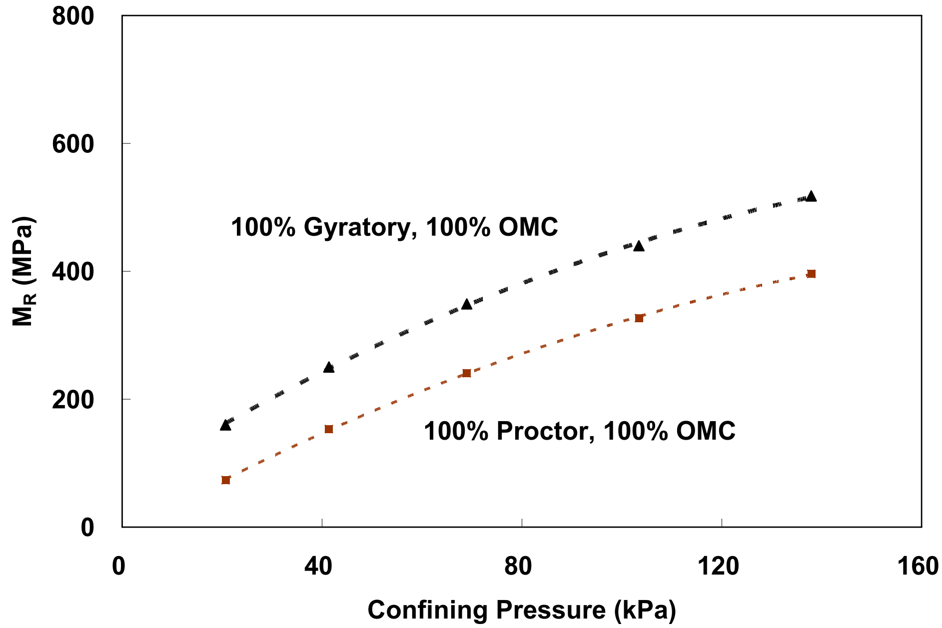

Figure 2.15: Comparison of Resilient Modulus (M_R): TH 5 Blend.

2.3 Test Equipment

The resilient modulus (M_R) test system consists of all appropriate sensors and data acquisition necessary for conducting the test, generally following the NCHRP 1-28A protocol [20]. Figure 2.16 shows the triaxial cell used for the M_R tests. The specimen is located inside the chamber, which acts as a pressure vessel [21]. The interior of the cell is 495 mm in height, 241 mm in diameter, and is surrounded by a plexiglass chamber 13 mm in thickness, which is large enough to contain a 152 mm diameter and 305 mm high specimen. The base contains a port for the air supply for confinement, and it also contains seven electrical feed throughs for LVDTs and internal load cell [20].

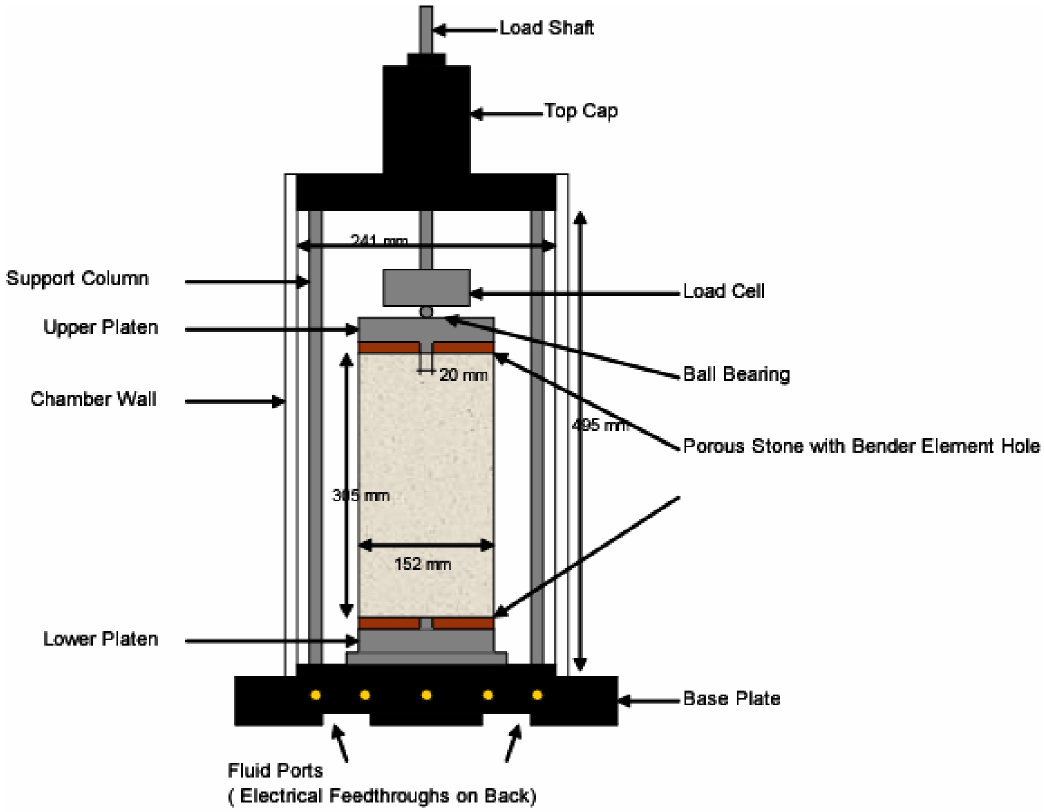

Figure 2.16: Triaxial Cell Diagram [20].

Axial load is applied by a servo-hydraulic load frame (MTS Systems, Eden Prairie, MN), which has a 22.2 kN capacity and 102 mm stroke. The MTS system is operated by a controlling program named TestStar (Fig. 2.17). The load cell has a 22.2 kN capacity (Fig. 2.17). The calibration chart for the load cell is included in Appendix B.1. Load and displacement data are collected by a LabView program named "M_R Data Acquisition." Comparison between the data acquired from the LabView program and the data from the MTS computer is contained in Appendix B.2.

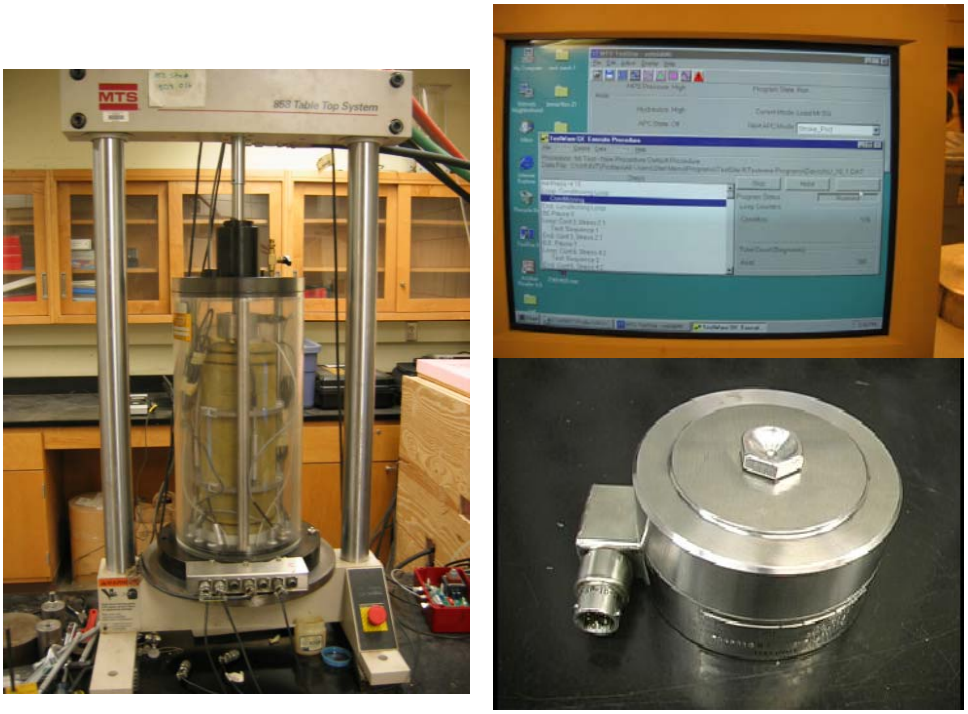

Figure 2.17: Load Frame, TestStar Program and Load Cell.

Since the M_R is calculated from recoverable axial strain, and the recoverable axial strain is determined from recoverable axial displacement, it is important to measure accurately the axial displacement. In this research, three interior Linear Variable Differential Transformers (LVDTs) were used (Fig. 2.18).

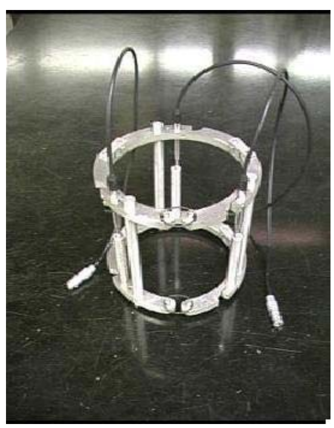

Figure 2.18: LVDT Collars with Spacers [20].

Three LVDTs are positioned at equi-angular positions around two parallel aluminum collars, which are attached to the specimen. On the lower collar, columns are mounted below the LVDTs as contacts for the spring-loaded tips of the LVDTs. This arrangement allows the two collars to move independently of each other. Spacers maintain a parallel distance between the collars while the apparatus is placed on the specimen [20]. This LVDT system has a 152 mm gage length, and the three LVDTs have a ±2.5 mm stroke range. The transducers were calibrated by measuring voltage change per unit displacement and the results are presented in Appendix B.3.

2.4 Resilient Modulus Test Protocol

For M_R testing, two protocols are commonly used: (a) Long Term Pavement Program (LTTP) P46 by the Strategic Highway Research Program (SHRP) [22], and (b) National Cooperative Highway Research Program (NCHRP) 1–28A [8]. In both protocols, repeated cycles of axial stress (Fig. 1.3) are applied to a cylindrical specimen (152 mm diameter and 305 mm height for base material) at a given confining pressure within a conventional triaxial cell. Each cycle is 1 s in duration, consisting of a 0.1 or 0.2 s haversine pulse followed by a 0.9 or 0.8 s rest period for coarse- and fine-grained soils respectively.

From NCHRP 1–28A, which was chosen as the test protocol for the load sequences, each test specimen experience, at 103.5 kPa confining pressure, 1000 cycles of 207 kPa deviator stress to condition the specimen before M_R data collection. The cycles are then repeated 100 times for 30 loading sequences with different combinations of confining pressures and deviator stresses. The M_R is calculated from recoverable axial strain (Fig. 1.2) and cyclic axial stress values from the last five cycles of each sequence. The loading sequences for base materials are shown in Table 2.3.

Table 2.3: Testing Sequences for Base/Sub-base Materials (NCHRP 1–28A) [8].

Sequence	Confining Pressure (kPa)	Contact Stress (kPa)	Cyclic Stress (kPa)	Maximum Stress (kPa)	N_{rep}
Conditioning	103.5	20.7	207.0	227.7	1000
1	20.7	4.1	10.4	14.5	100
2	41.4	8.3	20.7	29.0	100
3	69.0	13.8	34.5	48.3	100
4	103.5	20.7	51.8	72.5	100
5	138.0	27.6	69.0	96.6	100
6	20.7	4.1	20.7	24.8	100
7	41.4	8.3	41.4	49.7	100
8	69.0	13.8	69.0	82.8	100
9	103.5	20.7	103.5	124.2	100
10	138.0	27.6	138.0	165.6	100
11	20.7	4.1	41.4	45.5	100
12	41.4	8.3	82.8	91.1	100
13	69.0	13.8	138.0	151.8	100
14	103.5	20.7	207.0	227.7	100
15	138.0	27.6	276.0	303.6	100
16	20.7	4.1	62.1	66.2	100
17	41.4	8.3	124.2	132.5	100
18	69.0	13.8	207.0	220.8	100
19	103.5	20.7	310.5	331.2	100
20	138.0	27.6	414.0	441.6	100
21	20.7	4.1	103.5	107.6	100
22	41.4	8.3	207.0	215.3	100
23	69.0	13.8	345.0	358.8	100
24	103.5	20.7	517.5	538.2	100
25	138.0	27.6	690.0	717.6	100
26	20.7	4.1	144.9	149.0	100
27	41.4	8.3	289.8	298.1	100
28	69.0	13.8	483.0	496.8	100
29	103.5	20.7	724.5	745.2	100
30	138.0	27.6	966.0	993.6	100

In Table 2.3, contact stress is axial stress applied to a specimen to maintain a positive contact between the specimen cap and specimen. Contact stress is set to maintain a constant confining stress-ratio: (contact stress + confining pressure)/confining pressure = 1.2. Cyclic stress is a repeated haversine axial stress applied to a test specimen. Maximum stress is the sum of contact stress and cyclic stress.

The NCHRP 1-28A protocol was released in 2002 as an improvement of the LTTP P46 protocol, released in 1996. For base course material, the primary differences of the NCHRP 1-28 A protocol from the LTTP P46 protocol are a larger number of loading sequences (30 for NCHRP 1-28 A and 15 for LTTP P46), and larger (confining and deviator) stress ranges [20].

It is common in triaxial testing to remove all aggregate larger than 10% of the specimen diameter (152 mm) for specimen homogeneity [20]. Therefore, all the aggregates larger than 12.5 mm were removed before the specimen compaction (Fig. 2.19). Detail test procedure, following the procedure and requirements for NCHRP 1-28 A protocol is listed in Appendix C.

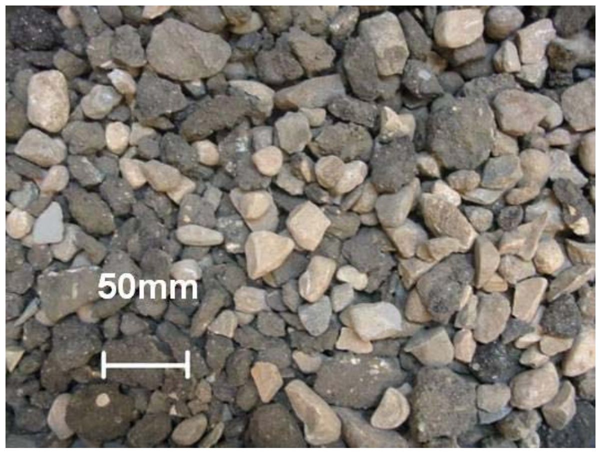

Figure 2.19: Removed Aggregates.

A total of 28 M_R and shear strength tests were conducted: seven different blend types at one density, two moisture contents and one set of replicates. Each specimen was labeled "letter_number1_number2," where the letter represents the sample identification, number1 shows the moisture content, and number2 shows whether it is the first or second test. Dry densities from gyratory compaction were chosen as the target densities (100% maximum), and the target moisture contents were 100% and 65% of optimum (Table 2.4). After completion of M_R tests, shear strength tests were performed at 34.5 kPa and 69 kPa confining pressures, 0.03mm/s loading rate, and the maximum deviator stresses at two confining pressures were measured for two replicate test specimens.

Table 2.4: Test Matrix.

Specimen ID	Description	Target MC (%)	Target Dry Density (kg/m^3)
S_5.1_1	CR 3_Blend_65%OMC_1	5.1	2032
S_5.1_2	CR 3_Blend_65%OMC_2	5.1	2032
S_7.8_1	CR 3_Blend_100%OMC_1	7.8	2032
S_7.8_2	CR 3_Blend_100%OMC_2	7.8	2032
T_5.7_1	CR 3_100%A_65%OMC_1	5.7	2032
T_5.7_2	CR 3_100%A_65%OMC_2	5.7	2032
T_8.8_1	CR 3_100%A_100%OMC_1	8.8	2032
T_8.8_2	CR 3_100%A_100%OMC_2	8.8	2032
U_5.7_1	CR 3_75%A-25%R_65%OMC_1	5.7	2032
U_5.7_2	CR 3_75%A-25%R_65%OMC_2	5.7	2032
U_8.7_1	CR 3_75%A-25%R_100%OMC_1	8.7	2032
U_8.7_2	CR 3_75%A-25%R_100%OMC_2	8.7	2032
V_5.2_1	CR 3_50%A-50%R_65%OMC_1	5.2	2032
V_5.2_2	CR 3_50%A-50%R_65%OMC_2	5.2	2032
V_8_1	CR 3_50%A-50%R_100%OMC_1	8	2032
V_8_2	CR 3_50%A-50%R_100%OMC_2	8	2032
W_4.7_1	CR 3_25%A-75%R_65%OMC_1	4.7	2032
W_4.7_2	CR 3_25%A-75%R_65%OMC_2	4.7	2032
W_7.2_1	CR 3_25%A-75%R_100%OMC_1	7.2	2032
W_7.2_2	CR 3_25%A-75%R_100%OMC_2	7.2	2032
X_3.5_1	TH 23_Blend_65%OMC_1	3.5	2080
X_3.5_2	TH 23_Blend_65%OMC_2	3.5	2080
X_5.4_1	TH 23_Blend_100%OMC_1	5.4	2080
X_5.4_2	TH 23_Blend_100%OMC_2	5.4	2080
Y_3.7_1	TH 200_Blend_65%OMC_1	3.7	2144
Y_3.7_2	TH 200_Blend_65%OMC_2	3.7	2144
Y_5.7_1	TH 200_Blend_100%OMC_1	5.7	2144
Y_5.7_2	TH 200_Blend_100%OMC_2	5.7	2144

2.4.1 Moisture Content

NCHRP 1-28A protocol specifies that the moisture content of the specimens should be within ±0.5% from the target moisture content. As seen from Table 2.5, all 28 specimens had moisture contents within ±0.5% from the target. Moisture contents were also measured after testing, and did not show much difference with the moisture contents before testing. Details of the moisture content control procedures are contained in Appendix C.

Table 2.5: Moisture Content Control.

Specimen ID	Description	Target MC (%)	MC Before (%)	MC After (%)	ΔMC (%)
S_5.1_1	CR 3_Blend_65%OMC_1	5.1	5.1		0.0
S_5.1_2	CR 3_Blend_65%OMC_2	5.1	4.9	4.6	-0.2
S_7.8_1	CR 3_Blend_100%OMC_1	7.8	7.4		-0.4
S_7.8_2	CR 3_Blend_100%OMC_2	7.8	7.7	7.1	-0.1
T_5.7_1	CR 3_100%A_65%OMC_1	5.7	6.0		0.3
T_5.7_2	CR 3_100%A_65%OMC_2	5.7	6.2	5.8	0.5
T_8.8_1	CR 3_100%A_100%OMC_1	8.8	9.1		0.3
T_8.8_2	CR 3_100%A_100%OMC_2	8.8	9.1	8.3	0.3
U_5.7_1	CR 3_75%A-25%R_65%OMC_1	5.7	6.1		0.4
U_5.7_2	CR 3_75%A-25%R_65%OMC_2	5.7	6.0		0.3
U_8.7_1	CR 3_75%A-25%R_100%OMC_1	8.7	8.3		-0.4
U_8.7_2	CR 3_75%A-25%R_100%OMC_2	8.7	8.8		0.1
V_5.2_1	CR 3_50%A-50%R_65%OMC_1	5.2	5.1	4.9	-0.1
V_5.2_2	CR 3_50%A-50%R_65%OMC_2	5.2	5.7	5.2	0.5
V_8_1	CR 3_50%A-50%R_100%OMC_1	8	8.4	7.5	0.4
V_8_2	CR 3_50%A-50%R_100%OMC_2	8	8.0	7.8	0.0
W_4.7_1	CR 3_25%A-75%R_65%OMC_1	4.7	4.5	4.3	-0.2
W_4.7_2	CR 3_25%A-75%R_65%OMC_2	4.7	4.3	3.9	-0.4
W_7.2_1	CR 3_25%A-75%R_100%OMC_1	7.2	7.3	6.8	0.1
W_7.2_2	CR 3_25%A-75%R_100%OMC_2	7.2	7.7	6.3	0.5
X_3.5_1	TH 23_Blend_65%OMC_1	3.5	3.6	3.3	0.1
X_3.5_2	TH 23_Blend_65%OMC_2	3.5	3.6	3.6	0.1
X_5.4_1	TH 23_Blend_100%OMC_1	5.4	5.4	5.4	0.0
X_5.4_2	TH 23_Blend_100%OMC_2	5.4	5.6	5.3	0.2
Y_3.7_1	TH 200_Blend_65%OMC_1	3.7	4.0	3.7	0.3
Y_3.7_2	TH 200_Blend_65%OMC_2	3.7	3.9	4.0	0.2
Y_5.7_1	TH 200_Blend_100%OMC_1	5.7	5.6	5.4	-0.1
Y_5.7_2	TH 200_Blend_100%OMC_2	5.7	5.9	5.2	0.2

2.4.2 Specimen Compaction

The compaction pressure ranged from 500 – 700 kPa, and up to 150 gyrations (for the dry of optimum specimen) were used to produce the target dry densities (Table 2.6). Two specimens around 140 mm in height were compacted separately and then placed one on top of the other; the surfaces in contact between the two specimens were scratched, and the joined specimens were compacted again by a vibratory hammer to achieve a specimen height of 280 mm. The interface between the two 140 mm specimens was not pronounced, and no separation was noticed during any of the tests (Fig. 2.20). Although a 305 mm height is required by the NCHRP 1-28A protocol to achieve a 2:1

(length:diameter) ratio, the gage length of 152 mm (as specified by the protocol) was used to measure axial deformation so that it is anticipated that the slightly (< 10%) short specimen had no effect on the M_R.   The compaction procedure is listed in Appendix C.

Figure 2.20: Specimen Compacted by Gyratory Compactor After Strength Testing.

Table 2.6: Specimen Compaction Control.

Specimen ID	Description	Gyration1 (kPa-#)	Gyration2 (kPa-#)	Height (mm)	Actual / Target (%)
S_5.1_1	CR 3_Blend_65%OMC_1	700-150	700-150	292	96.8
S_5.1_2	CR 3_Blend_65%OMC_2	700-150	700-150	291	98.2
S_7.8_1	CR 3_Blend_100%OMC_1	600-150	600-150	282	100.0
S_7.8_2	CR 3_Blend_100%OMC_2	500-150	500-120	282	100.6
T_5.7_1	CR 3_100%A_65%OMC_1	700-150	700-150	290	96.6
T_5.7_2	CR 3_100%A_65%OMC_2	700-150	700-150	290	96.5
T_8.8_1	CR 3_100%A_100%OMC_1	500-90	500-90	281	100.5
T_8.8_2	CR 3_100%A_100%OMC_2	500-140	500-150	282	100.2
U_5.7_1	CR 3_75%A-25%R_65%OMC_1	700-150	700-150	287	98.5
U_5.7_2	CR 3_75%A-25%R_65%OMC_2	700-150	700-150	283	96.4
U_8.7_1	CR 3_75%A-25%R_100%OMC_1	600-83	600-90	287	100.9
U_8.7_2	CR 3_75%A-25%R_100%OMC_2	600-67	600-75	281	100.9
V_5.2_1	CR 3_50%A-50%R_65%OMC_1	700-150	700-150	285	98.3
V_5.2_2	CR 3_50%A-50%R_65%OMC_2	700-150	700-150	288	96.7
V_8_1	CR 3_50%A-50%R_100%OMC_1	500-97	500-92	282	100.8
V_8_2	CR 3_50%A-50%R_100%OMC_2	500-110	500-115	283	100.9
W_4.7_1	CR 3_25%A-75%R_65%OMC_1	700-150	700-150	284	98.4
W_4.7_2	CR 3_25%A-75%R_65%OMC_2	700-150	700-150	286	97.8
W_7.2_1	CR 3_25%A-75%R_100%OMC_1	500-80	500-95	279	101.0
W_7.2_2	CR 3_25%A-75%R_100%OMC_2	500-150	600-75	281	100.0
X_3.5_1	TH 23_Blend_65%OMC_1	500-125	500-118	275	100.8
X_3.5_2	TH 23_Blend_65%OMC_2	500-200	500-122	276	100.7
X_5.4_1	TH 23_Blend_100%OMC_1	500-77	500-100	280	101.0
X_5.4_2	TH 23_Blend_100%OMC_2	500-68	500-60	280	100.5
Y_3.7_1	TH 200_Blend_65%OMC_1	500-73	500-66	278	99.9
Y_3.7_2	TH 200_Blend_65%OMC_2	500-88	500-80	277	100.1
Y_5.7_1	TH 200_Blend_100%OMC_1	500-57	500-56	277	100.8
Y_5.7_2	TH 200_Blend_100%OMC_2	500-64	500-54	277	100.4

For the lower moisture content specimens, more compaction energy was required (Table 2.6). However, for CR 3 materials, with the highest compaction pressure (700 kPa) and number of gyrations (150), it was still difficult to produce a 100% (gyratory) dry density specimen at the lower moisture content. Therefore, for the lower moisture content specimens from CR 3, around 98% of the target dry density was achieved instead of 100% (Table 2.6). The lower moisture content specimens from CR 3 could not satisfy the NCHRP 1-28A protocol for the variation (±1%) in dry density.

2.4.3 LVDT Displacement Range

Although the NCHRP 1-28A protocol specified the LVDT minimum stroke range requirement as ±6.3 mm, a ±2.5 mm range was used for the tests for more accurate data with less noise effects. LVDT ranges were always checked before the tests to make sure that all three LVDTs were within range (Fig. 2.21). When the LVDTs were about to reach their limit during the M_R tests, the loading was stopped and the LVDTs were re-zeroed. For the last sequence (sequence 30), the displacement was so large that the LVDTs sometimes reached the range limit (even though the LVDTs were re-zeroed before the sequence).

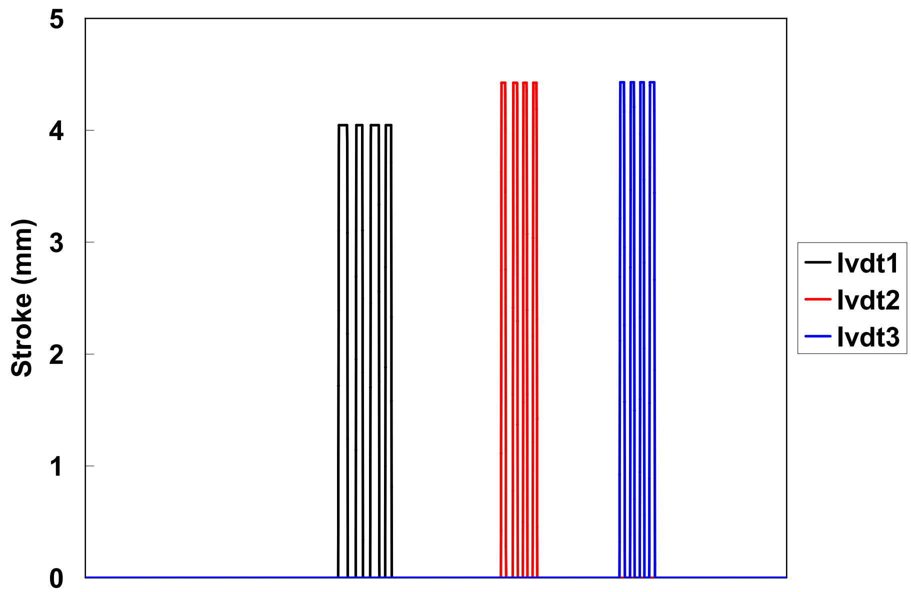

Figure 2.21: Example of the LVDT Range Check.

2.4.4 Permanent Strain

The NCHRP 1-28A protocol requires stopping the M_R test when 5% axial permanent strain is reached [8]. Specimen heights were compared before and after the M_R tests, and the permanent strain was calculated (Table 2.7). None of the specimen reached 5% permanent strain. From Table 2.7, it is noticed that the lower moisture content specimens usually had smaller permanent strain.

Table 2.7: Permanent Strain.

Specimen ID	Description	Permanent Strain (%)
S_5.1_1	CR 3_Blend_65%OMC_1	0.7
S_5.1_2	CR 3_Blend_65%OMC_2	0.7
S_7.8_1	CR 3_Blend_100%OMC_1	1.4
S_7.8_2	CR 3_Blend_100%OMC_2	2.5
T_5.7_1	CR 3_100%A_65%OMC_1	0.3
T_5.7_2	CR 3_100%A_65%OMC_2	0.7
T_8.8_1	CR 3_100%A_100%OMC_1	3.9
T_8.8_2	CR 3_100%A_100%OMC_2	2.5
U_5.7_1	CR 3_75%A-25%R_65%OMC_1	0.3
U_5.7_2	CR 3_75%A-25%R_65%OMC_2	0.4
U_8.7_1	CR 3_75%A-25%R_100%OMC_1	1.0
U_8.7_2	CR 3_75%A-25%R_100%OMC_2	2.5
V_5.2_1	CR 3_50%A-50%R_65%OMC_1	0.4
V_5.2_2	CR 3_50%A-50%R_65%OMC_2	2.1
V_8_1	CR 3_50%A-50%R_100%OMC_1	1.8
V_8_2	CR 3_50%A-50%R_100%OMC_2	3.9
W_4.7_1	CR 3_25%A-75%R_65%OMC_1	0.7
W_4.7_2	CR 3_25%A-75%R_65%OMC_2	0.7
W_7.2_1	CR 3_25%A-75%R_100%OMC_1	3.2
W_7.2_2	CR 3_25%A-75%R_100%OMC_2	2.1
X_3.5_1	TH 23_Blend_65%OMC_1	2.5
X_3.5_2	TH 23_Blend_65%OMC_2	2.9
X_5.4_1	TH 23_Blend_100%OMC_1	2.1
X_5.4_2	TH 23_Blend_100%OMC_2	3.2
Y_3.7_1	TH 200_Blend_65%OMC_1	1.4
Y_3.7_2	TH 200_Blend_65%OMC_2	2.5
Y_5.7_1	TH 200_Blend_100%OMC_1	2.5
Y_5.7_2	TH 200_Blend_100%OMC_2	3.2

2.5 Cyclic Triaxial Test Procedure

The cyclic triaxial tests were conducted with 21 kPa confining pressure, 4 kPa contact stress and 193 kPa and 286 kPa cyclic axial (deviator) stresses; 5,000 repeated cycles of axial stress was applied to a soil specimen. Each cycle was 1 s in duration, consisting of a 0.1 s haversine pulse followed by a 0.9 s rest period, following the M_R protocol for base materials [8]. Specimens had the same dimensions (152 mm diameter and 280 mm height) as the specimens for the M_R tests. Detail test design procedure is in Appendix C. From the tests, displacement behavior (permanent and recoverable deformation) of each mixture was measured.

A total of 14 cyclic triaxial tests were conducted: seven different mixtures of RAP and aggregate at one density and moisture content at two different deviator stresses. Each specimen was labeled "letter_number," where the letter represents the sample identification and number shows the peak stress ratio; the peak stress ratio of 35% is for a 193 kPa deviator stress and 50% is for a 286 kPa deviator stress. The target dry densities and moisture contents were from gyratory compaction tests (100% maximum dry densities and 100% optimum moisture contents, Table 2.8). Detailed testing procedures are contained in Appendix C.

Table 2.8: Test Matrix.

Specimen ID	Description	Target MC (%)	Target Dry Density (kg/m^3)
S_50	CR 3_Blend_50% Peak Stress Ratio	7.8	2032
S_35	CR 3_Blend_35% Peak Stress Ratio	7.8	2032
T_50	CR 3_100%A_50% Peak Stress Ratio	8.8	2032
T_35	CR 3_100%A_35% Peak Stress Ratio	8.8	2032
U_50	CR 3_75%A-25%R_50% Peak Stress Ratio	8.7	2032
U_35	CR 3_75%A-25%R_35% Peak Stress Ratio	8.7	2032
V_50	CR 3_50%A-50%R_50% Peak Stress Ratio	8.0	2032
V_35	CR 3_50%A-50%R_35% Peak Stress Ratio	8.0	2032
W_50	CR 3_25%A-75%R_50% Peak Stress Ratio	7.2	2032
W_35	CR 3_25%A-75%R_35% Peak Stress Ratio	7.2	2032
X_50	TH 23_Blend_50% Peak Stress Ratio	5.4	2080
X_35	TH 23_Blend_35% Peak Stress Ratio	5.4	2080
Y_50	TH 200_Blend_50% Peak Stress Ratio	5.7	2144
Y_35	TH 200_Blend_35% Peak Stress Ratio	5.7	2144

All 14 specimens had the moisture contents within ±0.5% from the target (Table 2.9). Moisture contents were also measured after testing, and did not show much difference with the moisture contents before testing. Specimens were compacted and prepared same way as the specimens for the M_R tests. The compaction pressure ranged from 400 – 500 kPa, and up to 200 gyrations were used to produce the desired dry density (Table 2.9). All 14 specimens had the dry densities within ±1% from the target (Table 2.10).

Table 2.9: Moisture Content Control.

Specimen ID	Description	Target MC (%)	Actual MC_1 (%)	Actual MC_2 (%)	ΔMC_1 (%)	ΔMC_2 (%)	MC After_1 (%)	MC After_2 (%)
S_50	CR 3_Blend_50% Peak Stress	7.8	8.0	7.8	0.2	0.0	7.9	8.2
S_35	CR 3_Blend_35% Peak Stress	7.8	8.0	7.8	0.2	0.0	7.9	8.2
T_50	CR 3_100%A_50% Peak Stress	8.8	9.0	8.6	0.2	-0.2	9.0	8.5
T_35	CR 3_100%A_35% Peak Stress	8.8	9.0	8.5	0.2	-0.3	8.5	8.9
U_50	CR 3_75%A-25%R_50% Peak Stress	8.7	8.9	8.6	0.2	-0.1	8.5	8.7
U_35	CR 3_75%A-25%R_35% Peak Stress	8.7	8.9	9.0	0.2	0.3	8.6	8.7
V_50	CR 3_50%A-50%R_50% Peak Stress	8.0	8.1	8.5	0.1	0.5	8.0	7.9
V_35	CR 3_50%A-50%R_35% Peak Stress	8.0	8.1	8.5	0.1	0.5	8.0	7.9
W_50	CR 3_25%A-75%R_50% Peak Stress	7.2	7.0	7.2	-0.2	0.0	6.8	6.9
W_35	CR 3_25%A-75%R_35% Peak Stress	7.2	6.9	6.7	-0.3	-0.5	6.6	6.7
X_50	TH 23_Blend_50% Peak Stress	5.4	5.3	5.8	-0.1	0.4	5.4	5.4
X_35	TH 23_Blend_35% Peak Stress	5.4	5.3	5.8	-0.1	0.4	5.4	5.4
Y_50	TH 200_Blend_50% Peak Stress	5.7	5.9	6.2	0.2	0.5	5.3	5.2
Y_35	TH 200_Blend_35% Peak Stress	5.7	5.9	6.2	0.2	0.5	5.3	5.2

Table 2.10: Specimen Compaction Control.

Specimen ID	Gyration1 (kPa-#)	Gyration2 (kPa-#)	Height (mm)	Target Dry Density (kg/m3)	Actual Dry Density (kg/m3)	Actual / Target (%)
S_50	500-152	500-124	288	2032	2036	100.2
S_35	500-131	500-151	288	2032	2033	100.1
T_50	400-100	400-89	285	2032	2030	99.9
T_35	400-95	400-96	284	2032	2038	100.3
U_50	400-99	400-88	285	2032	2041	100.5
U_35	400-82	400-70	285	2032	2036	100.2
V_50	500-77	500-93	287	2032	2038	100.3
V_35	500-119	500-132	286	2032	2040	100.4
W_50	500-89	500-78	290	2032	2041	100.5
W_35	400-200	400-182	291	2032	2038	100.3
X_50	400-95	400-79	287	2080	2094	100.7
X_35	400-102	400-115	287	2080	2089	100.5
Y_50	400-93	400-93	284	2144	2144	100.0
Y_35	400-95	400-88	283	2144	2147	100.1

Chapter 3
Quality Control / Quality Assurance

M_R data from a test should represent element response at a given density and moisture. However, due to imperfections of the specimen and test equipment, some error occurs. Therefore, it is important to control the quality of the data through various criteria. M_R data were checked for angle of rotation, signal-to-noise ratio (SNR) and coefficient of variation (COV). M_R tests for a synthetic specimen were conducted to evaluate the testing measurement system.

3.1 Rotation

An element test assumes that the material deforms in a uniform manner. A specimen that is originally cylindrical in shape remains a cylinder during testing. Ideally, the kinematic boundary condition imposed by a rigid platen means that the loading platen should not rotate but remain normal to the longitudinal axis of the specimen. However, some rotation is typically allowed and when multiple displacement measurements are compared, non-uniformity between readings is inevitable. In this chapter, the degree of non-uniformity due to rotation is quantified, and the relation between the degree of non-uniformity and the specimen deformation is discussed to evaluate the influence of rotation on the measured displacements (Fig. 3.1).

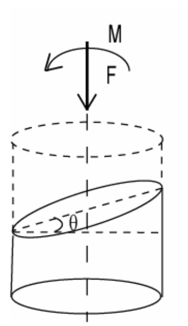

Figure 3.1: Axial Force and Bending Moment Imposed by Rigid Platens That Rotate.

3.1.1 Non-uniformity of Displacement

M_R test data typically display non-uniform displacement histories between three LVDT readings during the loading sequences (Fig. 3.2). Because the M_R value is calculated from the axial displacement of a specimen during cyclic loading, it is critical to have reliable displacement values from at least three LVDTs (two LVDTs are not sufficient to evaluate the non-uniformity).

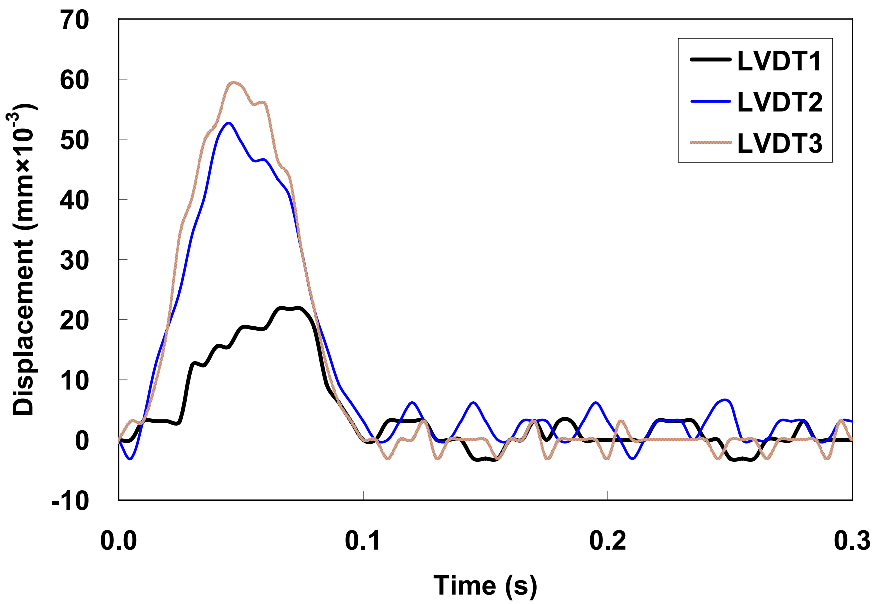

Figure 3.2: Example Three LVDT Displacement Time Histories.

Consider the boundary condition imposed by a rigid platen that can rotate (Fig. 3.1). The distribution of normal stress varies and the resultant is composed of an axial force and a bending moment. Thus, the total displacement can be decomposed into

$$\delta_{(i)} = \delta_{(i)F} + \delta_{(i)M} \tag{3.1}$$

where

$\delta_{(i)}$ = total displacement of LVDT 'i'
$\delta_{(i)F}$ = displacement of LVDT 'i'due to the axial force
$\delta_{(i)M}$ = displacement of LVDT 'i'due to the bending moment

Displacement due to the axial force (δ_F) will be the same for the three LVDTs. However, displacement due to the bending moment (δ_M) will depend on the angle of rotation of the platen (θ) and the position of the LVDT relative to the axis of rotation (Fig. 3.3). To describe the rotated plane, consider three LVDTs positioned at equi-angular positions, 120° apart. Because the axis of rotation is assumed to go through the center of the specimen, displacement of each LVDT due to the bending moment will be decided by the position of the LVDT in relation to the axis of rotation. If an LVDT is on the axis of rotation, displacement due to bending moment is zero, and total displacement will be the same as axial displacement. If an LVDT is located on a line perpendicular to the axis of rotation, displacement due to the bending moment will be either maximum δ_{max} or minimum δ_{min} (Fig. 3.3).

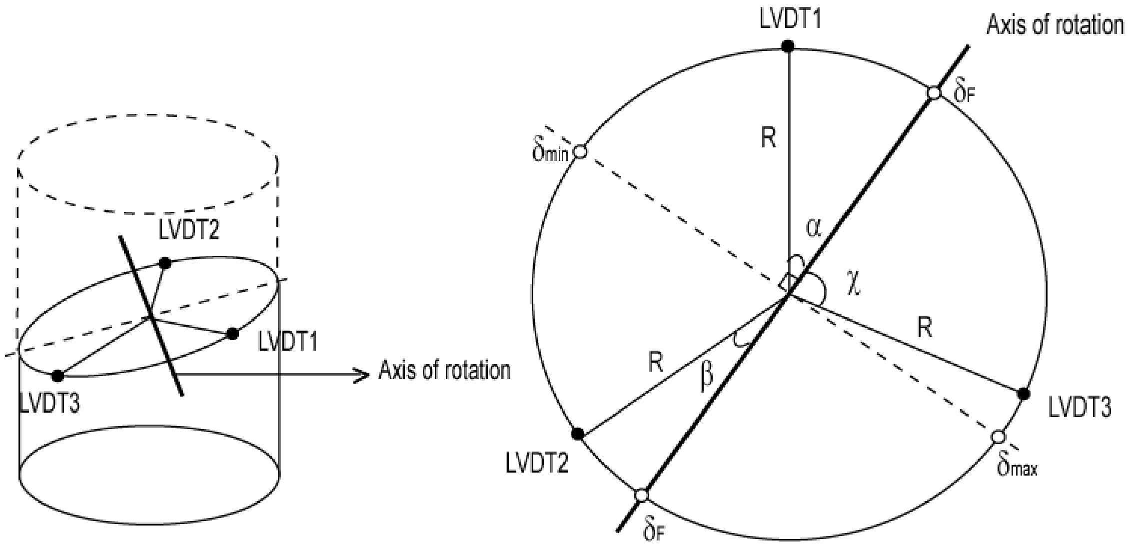

Figure 3.3: Geometry of Specimen and LVDTs with Respect to the Axis of Rotation.

For a cylindrical specimen of radius R, define angles α, β, and χ as the angles between a line from the center of the specimen to each LVDT and the axis of rotation such that the location of δ_{min} is between LVDT1 and LVDT2. Therefore, the displacements of the three LVDTs are

$$\begin{aligned} \delta_1 &= \delta_F - R\, sin(\alpha)\, sin(\theta) \\ \delta_2 &= \delta_F - R\, sin(\beta)\, sin(\theta) \\ \delta_3 &= \delta_F + R\, sin(\chi)\, sin(\theta) \end{aligned} \tag{3.2}$$

and the sum is

$$\delta_1 + \delta_2 + \delta_3 = 3\delta_F - R\, sin(\theta)\, (sin(\alpha)+sin(\beta)-sin(\chi)) \tag{3.3}$$

For equi-angular placement of the three LVDTs, the last term in equation (3.3) becomes

$$sin(\alpha) + sin(\beta) - sin(\chi) = sin(\alpha) + sin(60°-\alpha) - sin(120°-\alpha) = 0 \tag{3.4}$$

From equations (3.3) and (3.4),

$$\delta_F = (\delta_1 + \delta_2 + \delta_3)/3 = \delta_{average} \tag{3.5}$$

Consequently, the displacement due to axial force, even if rotation occurs, is simply the mean of the displacement values from the three LVDTs. This means that the angle of rotation does not affect the value of the axial displacement for stiffness calculations. This does not mean that the angle of rotation should not be limited, as the assumption of uniform deformation may be violated as rotation increases. In addition, the angle of rotation can be used a s a quality assurance parameter.

3.1.2 Angle of Rotation

To estimate the angle of rotation, note that θ is the angle between the normal vectors of the plane before loading (the horizontal plane) and the rotated plane, defined by the (minimum) three LVDT displacement values. Recalling that a plane is described by

$$Ax + By + Cz + D = 0 \tag{3.6}$$

the angle between the normals of the two planes is [23]

$$\cos\theta = \frac{A_1A_2 + B_1B_2 + C_1C_2}{\sqrt{A_1^2 + B_1^2 + C_1^2}\sqrt{A_2^2 + B_2^2 + C_2^2}} \tag{3.7}$$

In addition, a plane passing through three points $\mathbf{P}_i\,(x_i, y_i, z_i)$, $\mathbf{P}_j\,(x_j, y_j, z_j)$, $\mathbf{P}_k\,(x_k, y_k, z_k)$ is determined by

$$\begin{vmatrix} y_i & z_i & 1 \\ y_j & z_j & 1 \\ y_k & z_k & 1 \end{vmatrix} x + \begin{vmatrix} z_i & x_i & 1 \\ z_j & x_j & 1 \\ z_k & x_k & 1 \end{vmatrix} y + \begin{vmatrix} x_i & y_i & 1 \\ x_j & y_j & 1 \\ x_k & y_k & 1 \end{vmatrix} z = \begin{vmatrix} x_i & y_i & z_i \\ x_j & y_j & z_j \\ x_k & y_k & z_k \end{vmatrix} \tag{3.8}$$

The plane before loading is the horizontal plane:

$$z = 0 \tag{3.9}$$

The plane at a particular load is defined by the three LVDT readings:

$$LVDT_1 = (R, 0, \delta_1) \tag{3.10}$$

$$LVDT_2 = \left(-\frac{R}{2}, \frac{R\sqrt{3}}{2}, \delta_2\right) \tag{3.11}$$

$$LVDT_3 = \left(-\frac{R}{2}, -\frac{R\sqrt{3}}{2}, \delta_3\right) \tag{3.12}$$

Thus, the equation of the rotated plane at a particular load is

$$\sqrt{3}R\left(\frac{\delta_2}{2}+\frac{\delta_3}{2}-\delta_1\right)x+\frac{3}{2}R(\delta_3-\delta_2)y+\frac{3\sqrt{3}}{2}R^2z-\frac{\sqrt{3}}{2}R^2(\delta_1+\delta_2+\delta_3)=0 \quad (3.13)$$

Substituting equations (3.9) and (3.13) into equation (3.7), the angle of rotation θ is

$$\cos\theta=\frac{\frac{3}{2}R}{\sqrt{\delta_1^2+\delta_2^2+\delta_3^2-\delta_1\delta_2-\delta_1\delta_3-\delta_2\delta_3+\frac{9}{4}R^2}} \quad (3.14)$$

The axis of rotation is the line of intersection of the rotated plane with the horizontal plane, with

$$z=\frac{\delta_1+\delta_2+\delta_3}{3} \quad (3.15)$$

The equation for the intersection of two planes in the *xy* plane is [23]

$$\begin{vmatrix} C_1 & C_2 \\ A_1 & A_2 \end{vmatrix}x+\begin{vmatrix} C_1 & C_2 \\ B_1 & B_2 \end{vmatrix}y+\begin{vmatrix} C_1 & C_2 \\ D_1 & D_2 \end{vmatrix}=0 \quad (3.16)$$

Substituting equations (3.13) and (3.15) into equation (3.16) results in the equation for the axis of rotation:

$$\sqrt{3}R\left(\frac{\delta_2}{2}+\frac{\delta_3}{2}-\delta_1\right)x+\frac{3}{2}R(\delta_3-\delta_2)y=0 \quad (3.17)$$

In summary, from three sensors placed equi-angular to measure axial displacement, the angle of rotation and the position of the axis of rotation can be calculated.

3.1.3 Uniformity Ratio

In NCHRP 1-28A, the uniformity ratio, γ, is given as

$$\gamma=\frac{\delta'_{\max}}{\delta'_{\min}} \quad (3.18)$$

where $\delta_{max,\ min}$ are the maximum and minimum displacements *measured* by two LVDTs; $\gamma \leq 1.1$ defines an acceptable test [8]. However, when rotation occurs during the load application, γ values will vary depending on where the LVDTs are located with reference to the axis of rotation. Even if rotation is substantial, $\gamma = 1$ can be obtained if two LVDTs are located on the axis of rotation. Thus, γ does not provide an objective measure of uniformity.

The maximum uniformity ratio γ_{max} can be introduced based on the maximum and minimum displacements *calculated* from three LVDTS:

$$\gamma_{\max} = \frac{\delta_{\max}}{\delta_{\min}} = \frac{\delta_{avg} + R\sin\theta}{\delta_{avg} - R\sin\theta} \tag{3.19}$$

This provides some improvement, as a test result may show that γ is within some acceptable limit, but the same test result may not satisfy the condition if γ_{max} is estimated. What is still needed, however, is an evaluation of the strain state at various values of γ_{max} to establish a limit for γ_{max} where displacement measurements can still provide a reasonable estimate of material response.

Obviously, γ_{max} depends on both the uniform and non-uniform components of displacement, and for a constant value of rotation, γ_{max} will vary with the amount of uniform deformation, as measured by the average displacement or the recoverable axial strain $\Delta\varepsilon_a$. As shown in Fig. 5, the same value of rotation could result in different values of γ_{max} depending on the stiffness of the specimen and the applied stress, both of which influence $\Delta\varepsilon_a$. In evaluating test results, it is recognized that some minimal amount of rotation cannot be eliminated, so it may be more reasonable to set a limit on θ together with γ_{max}. For example, given a gage length = 100 mm and rotation = 0.04°, $\gamma_{max} = 1.36$ when $\Delta\varepsilon_a = 0.2\%$ and $\gamma_{max} = 1.17$ when $\Delta\varepsilon_a = 0.4\%$. To produce $\gamma_{max} = 1.17$ when $\Delta\varepsilon_a = 0.2\%$, the rotation would need to be reduced to 0.02°. This improved performance of the testing system may not result in a change in measured response, although further research is needed to evaluate an acceptable level of γ_{max}.

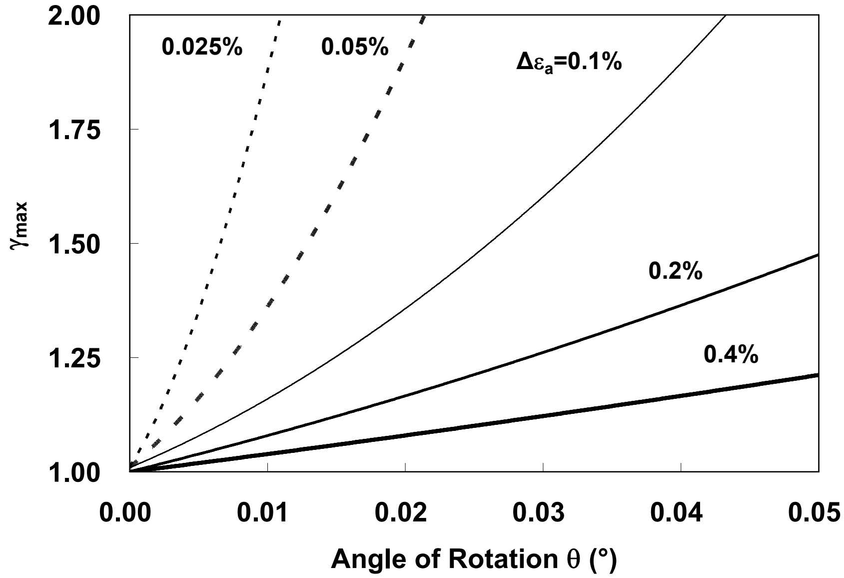

Figure 3.4: Influence of Rotation on the Uniformity Ratio γ_{max} at Various Levels of Axial Strain $\Delta\varepsilon_a$ (Gage Length = 100 mm).

Angle of rotation , which is defined in equation (3.14), of the last five cycles of the 30 sequences of all specimens were analyzed, and those cycles that failed to pass the maximum limit of 0.04°, set by the Minnesota Department of Transportation were withdrawn.

3.2 Signal to Noise Ratio (SNR)

Because specimen stiffness and applied deviator stress may require the LVDTs to measure very small amount of displacement, noise acting during a M_R test can seriously affect the results. Therefore, a coefficient called the signal-to-noise ratio (SNR), which compares the peak displacement to the standard deviation (SDev) of the noise, was introduced [24]:

$$SNR = \frac{Peak}{3 \times SDev(Baseline)} \tag{3.20}$$

SNR value of 3 was chosen for the minimum limit for each three LVDTs at each cycle by the Minnesota Department of Transportation (Figs. 3.5-3.6). Also, SNR value of 10 was used for each loading cycle. All cycles that failed to pass the limits were withdrawn.

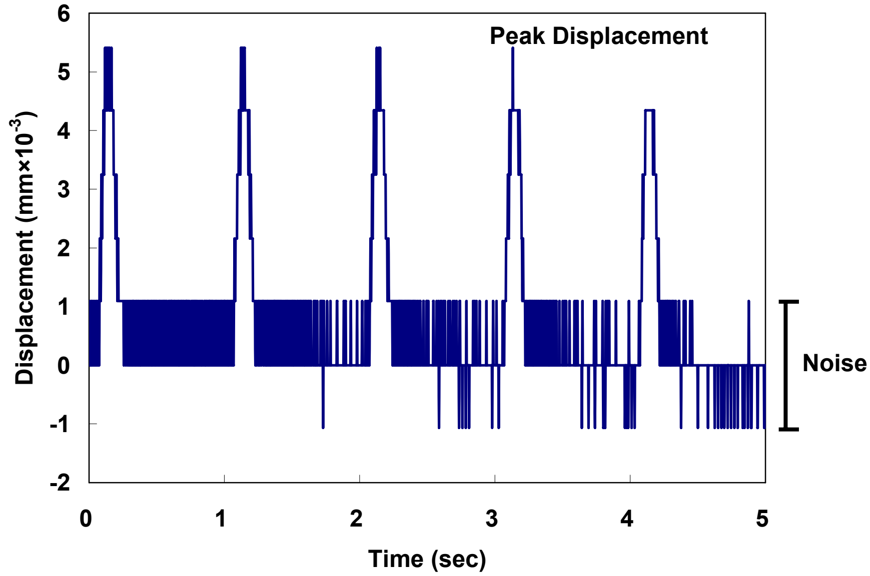

Figure 3.5: Example Displacement History: SNR=3.

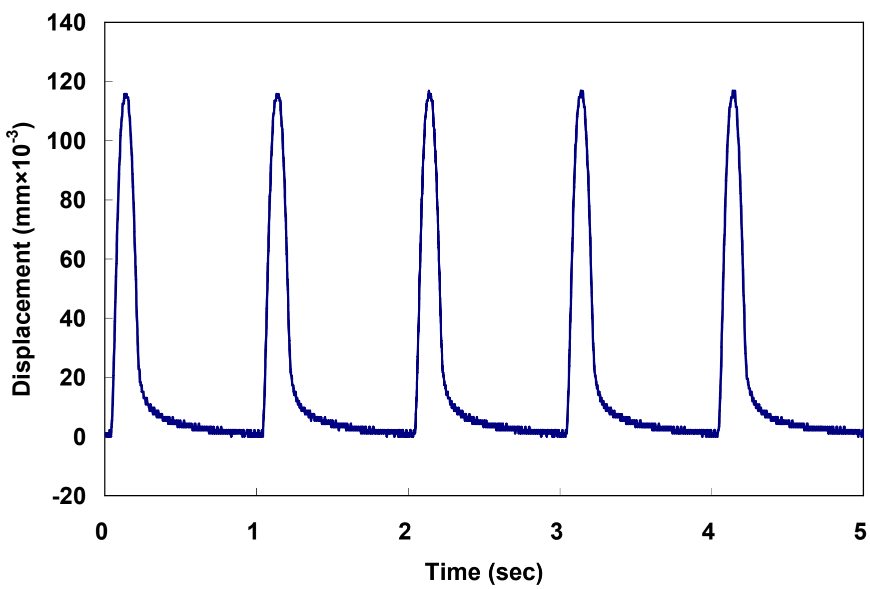

Figure 3.6: Example Displacement History: SNR=30.

Standard deviation is defined as

$$SDev = \sqrt{\frac{\sum_{0}^{N} (Y(n) - \mu)^2}{N - 1}} \tag{3.21}$$

where μ = mean of the baseline, Y(n) = value at point n, and N = total data points.

Root mean square (RMS) is defined as

$$RMS = \sqrt{\frac{\int_0^N Y^2(n)dn}{N}} \tag{3.22}$$

When N is very large, root mean square will be close to

$$RMS = \sqrt{\frac{\sum_0^N Y^2(n)}{N}} \tag{3.23}$$

Therefore, root mean square can be used for SNR instead of standard deviation only when N is very large and $\mu = 0$.

3.3 Coefficient of Variation (COV)

For a specimen at a given sequence, M_R values for the last five cycles should be similar. However, there will be some variation in M_R between the cycles and it is important to control the maximum amount for each sequence. Therefore, the coefficient of variation (COV), defined as

$$COV(\%) = \frac{SDev}{Average} \tag{3.24}$$

must be less than 10%. The M_R values from last five cycles were analyzed by this criterion. Those sequences that failed to pass the maximum COV limit (10%) were withdrawn.

3.4 LVDT Range

As mentioned previously, LVDT ranges were checked before the tests to make sure that all three LVDTs were within the stroke range. Also, when the LVDTs were about to reach their limit during a test, the loading was stopped and the LVDTs were re-zeroed. However, for some sequences (usually sequence 30), the displacement was so large that the LVDTs sometimes reached the limit even though it was re-zeroed and checked before the sequence. If at least one of the LVDTs reached its range limit, those cycles were withdrawn.

3.5 Synthetic Specimen Testing

Resilient modulus testing was conducted with a neoprene spring rubber specimen, 102 mm diameter × 152 mm height. The loading surfaces of the specimen were machined perpendicular to the longitudinal axis within ±0.01°. The displacements were measured with three LVDTs with 102 mm gage lengths (Fig. 3.7). A total of six tests were performed, with four of the tests conducted at MnDOT Office of Materials Laboratory. Among the two tests from the UM, one was performed with the specimen ends lubricated by using two teflon sheets. The NCHRP 1-28A testing protocol was used. In addition, one bender element test was performed on the specimen. The results are shown in Fig. 3.8.

The Young's modulus of the synthetic specimen, determined from wave speeds obtained through bender element testing, was 94 MPa (Table 3.1), and this value is associated with very small strain. In addition, with lubricated ends (two teflon sheets), the value of Young's modulus was 1-10% higher than the value without lubricated ends. The results from MnDOT and UM compared very well.

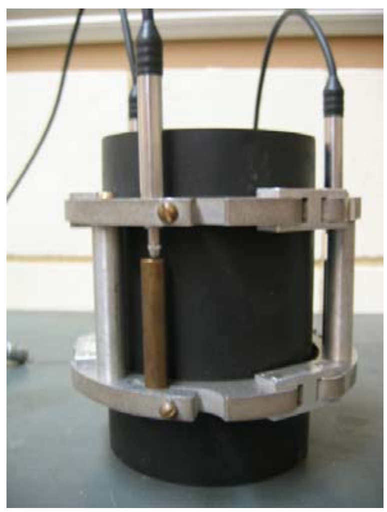

Figure 3.7: Synthetic Specimen

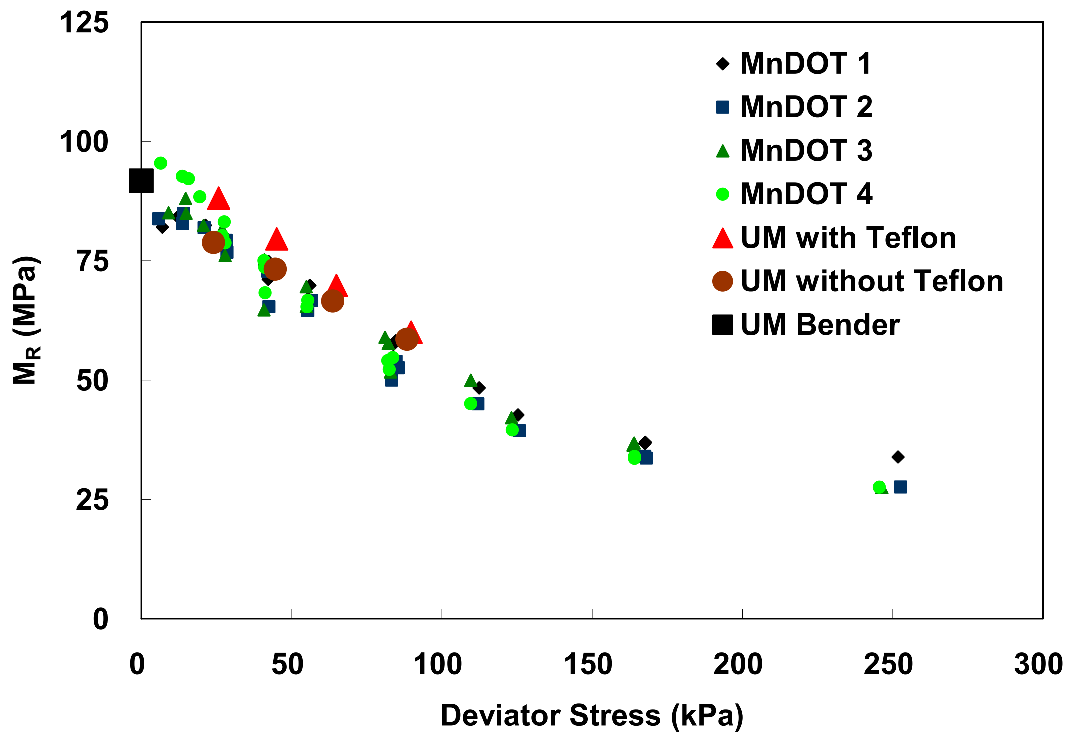

Figure 3.8: Modulus Data of Synthetic Specimen.

Table 3.1: Bender Element Test Result for Synthetic Specimen.

c_P	p-wave speed	250	m/s
c_S	s-wave speed	39	m/s
v	Poisson's ratio	0.49	
G	Shear Modulus	32	MPa
E	Young's Modulus	94	MPa

For the same deviator stress, E_{secant} difference due to confining pressure change was small (within 2%). However, for the same confining pressure, E_{secant} decreased significantly as deviator stress increased (Fig. 3.8). Fig. 3.9 shows the stress-strain response of the rubber specimen (with teflon sheets) at one confining pressure and four deviator stresses. As the deviator stress increased, the synthetic specimen showed a decrease in secant modulus.

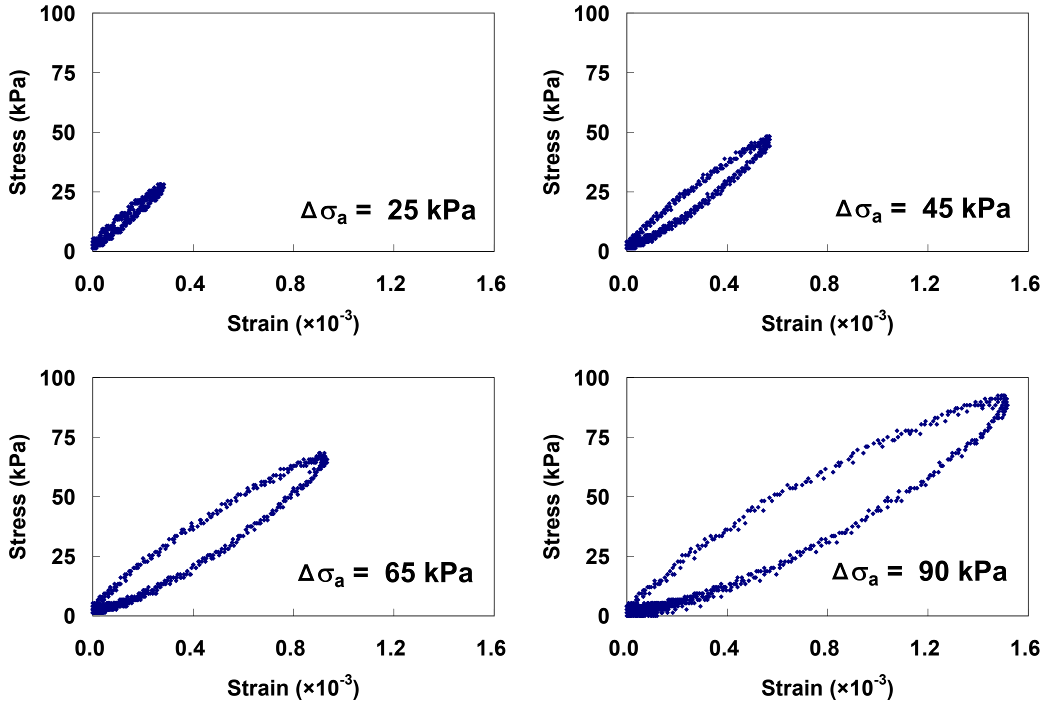

Figure 3.9: Stress-Strain Behavior of Synthetic Specimen: σ_3 = 13.8 kPa.

Chapter 4
Discussion of Results

4.1 Resilient Modulus (M_R) Data

The load and displacement data recorded by M_R data collection were stored in 30 separate files. Each of these data files consisted of the load, stroke, and three LVDT displacement values recorded during the test. A spreadsheet was used to convert these data files into resilient modulus values. The algorithm searched for local maxima in the load and three displacement data sets; these peak values correspond to the peak load and displacement pulses observed during the haversine load pulse. The baseline load and displacement values during the material recovery periods of each cycle were calculated by averaging the data over the final 0.75 seconds of each one second cycle.

M_R tests were conducted on seven different blend types at one density, two moisture contents and one set of replicates. As seen from Table 4.1, replicate tests usually showed very similar M_R values (within 20% difference) for each sequence. Therefore, M_R values for each sequence from replicate tests were averaged for the discussion of the result. Tables of M_R values for each sequence from all 28 specimens are contained in Appendix D.1.

Figures 4.1 – 4.2 show M_R versus deviator stress at different confining pressures for CR 3 materials. M_R versus deviator stress from all 28 soil specimens are contained in Appendix D.2. Generally, as deviator stress increased, M_R decreased. However, for higher moisture content specimens at lower confining pressures (21 and 41 kPa), M_R values increasing as deviator stress increased were also noticed (Fig. 4.2). Because the deviator stress effect on M_R change was less pronounced compared to the confining pressure effect, relations between M_R with confining pressure are plotted without considering deviator stress in Figs. 4.3 – 4.12. Examples that show the combined influence of confining pressure and deviator stress are shown in Figs. 4.13 and 4.14.

Table 4.1: Resilient Modulus of CR 3 100% Aggregate
(T_5.7, 98% Gyratory = 1981 kg/m^3, 65% OMC = 5.7%).

Sq	Confining kPa	Deviator kPa	M_R MPa	Sq	Confining kPa	Deviator kPa	M_R MPa
1	21	10.2	242	1	21	10.2	230
2	41	19.7	292	2	41	19.6	292
3	69	32.5	347	3	69	33.7	348
4	103	51.1	418	4	103	50.6	421
5	138	68.2	501	5	138	67.5	507
6	21	20.5	236	6	21	19.8	215
7	41	40.7	278	7	41	40.1	255
8	69	67.9	329	8	69	67.4	311
9	103	101.9	396	9	103	101.5	386
10	138	136.3	468	10	138	135.5	468
11	21	40.6	214	11	21	40.6	195
12	41	81.7	256	12	41	81.2	237
13	69	136.3	314	13	69	135.7	302
14	103	204.9	394	14	103	203.5	386
15	138	272.8	457	15	138	270.3	453
16	21	61.4	203	16	21	60.9	181
17	41	122.9	251	17	41	121.8	231
18	69	204.8	317	18	69	200.8	306
19	103	306.9	388	19	103	303.2	384
20	138	409.1	442	20	138	405.2	440
21	21	99.4	196	21	21	99.6	175
22	41	203.7	249	22	41	202.6	236
23	69	342.3	322	23	69	339.6	317
24	103	511.9	386	24	103	507.6	378
25	138	679.1	444	25	138	676.6	433
26	21	143.4	190	26	21	141.9	172
27	41	287.0	246	27	41	284.8	233
28	69	477.0	325	28	69	473.1	316
29	103	711.2	395	29	103	707.4	389
30	138	946.1	435	30	138	940.5	434

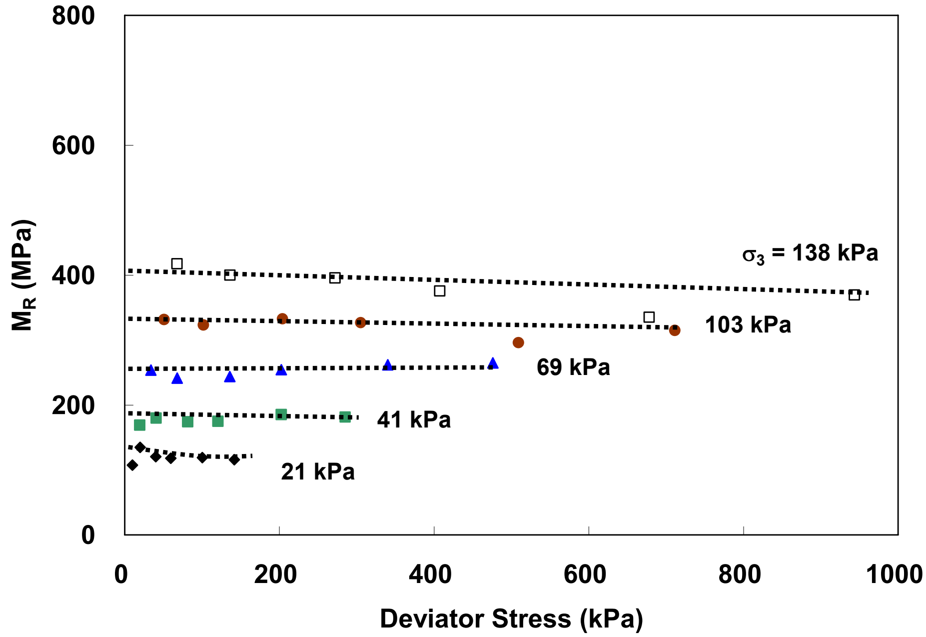

Figure 4.1: Resilient Modulus of CR 3 100% Aggregate
(100% Gyratory = 2032 kg/m^3, 100% OMC = 8.8%).

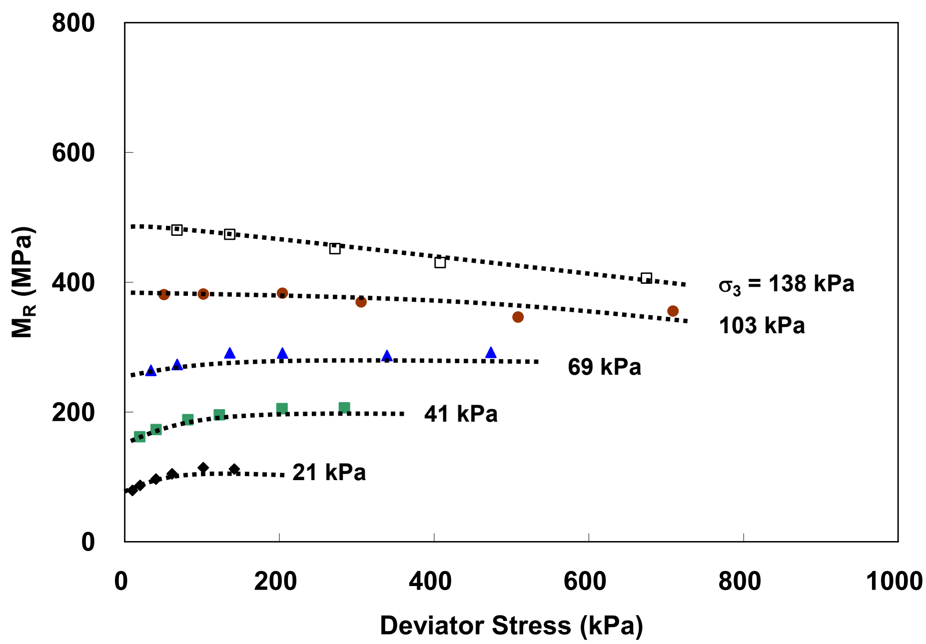

Figure 4.2: Resilient Modulus of CR 3 50% Aggregate – 50% RAP
(100% Gyratory = 2032 kg/m^3, 100% OMC = 8%).

M_R versus confining pressure plots for the seven different mixtures at two different moisture contents are shown in Figs 4.3 – 4.9. The spread in the data at a constant confining pressure represents the M_R at various deviator stresses. The curve fit is based on a square-root dependence on confinement. Typical of granular materials, the M_R increased with increase of confining pressure consistently. The specimens with 65% optimum moisture contents (OMC) were 10% – 116% stiffer than the specimens with 100% optimum moisture contents at all confining pressures. It is noticeable that the M_R values were larger for the dry of optimum specimens even though the lower moisture content specimens could not reach 100% gyratory dry density (approximately 98% gyratory dry density).

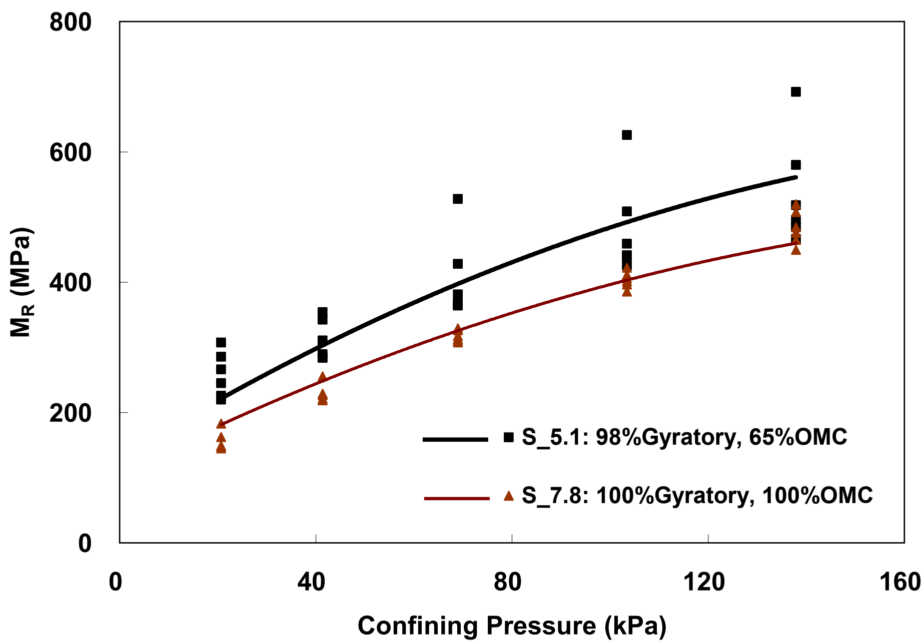

Figure 4.3: Resilient Modulus of CR 3 Blend
(100% Gyratory = 2032 kg/m^3, 100% OMC = 7.8%, 65% OMC = 5.1%).

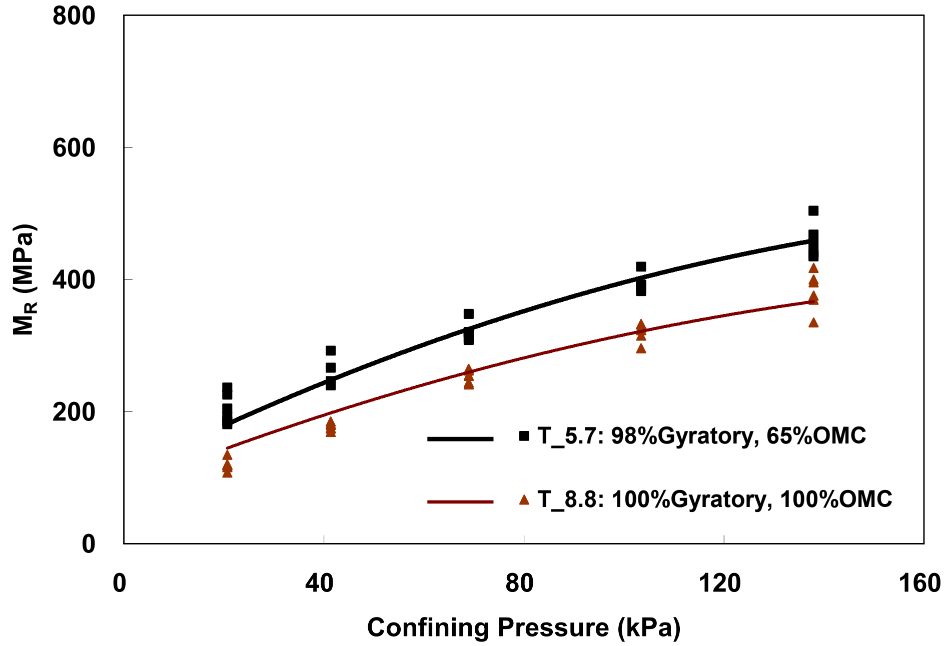

Figure 4.4: Resilient Modulus of CR 3 100% Aggregate
(100% Gyratory = 2032 kg/m^3, 100% OMC = 8.8%, 65% OMC = 5.7%).

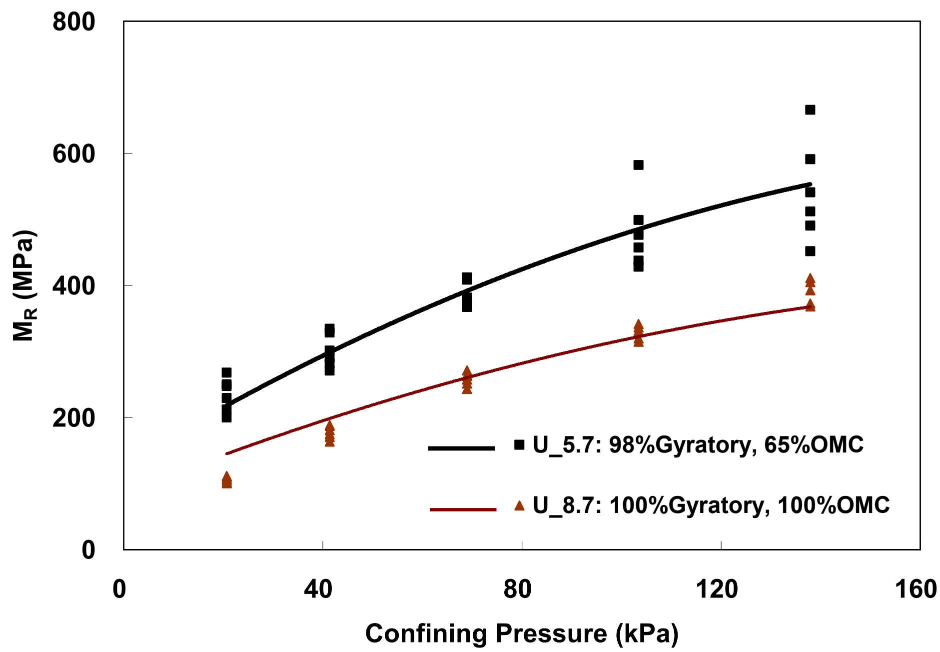

Figure 4.5: Resilient Modulus of CR 3 75% Aggregate – 25% RAP
(100% Gyratory = 2032 kg/m^3, 100% OMC = 8.7%, 65% OMC = 5.7%).

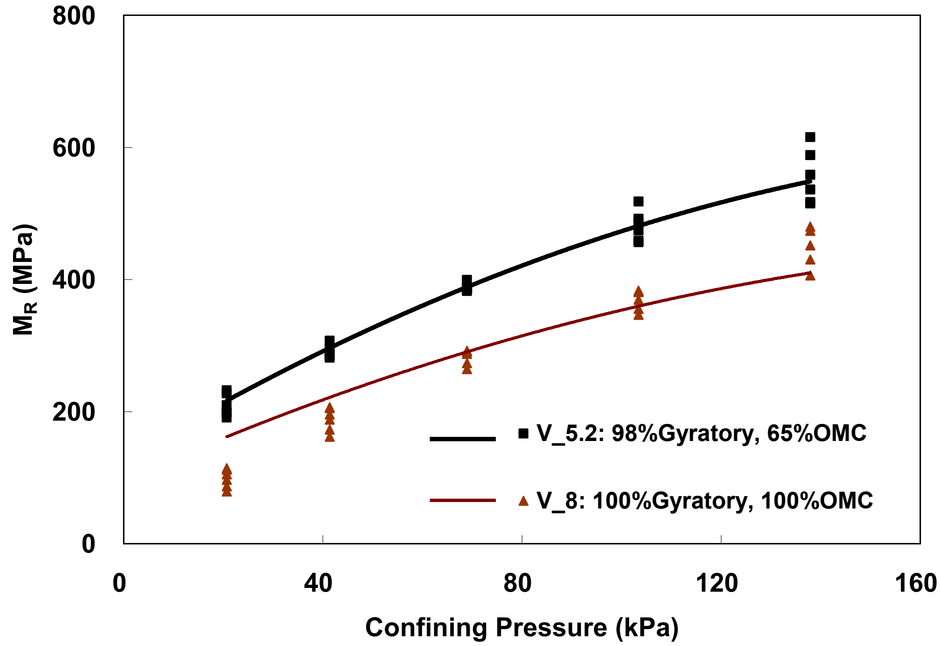

Figure 4.6: Resilient Modulus of CR 3 50% Aggregate – 50% RAP
(100% Gyratory = 2032 kg/m^3, 100% OMC = 8%, 65% OMC = 5.2%).

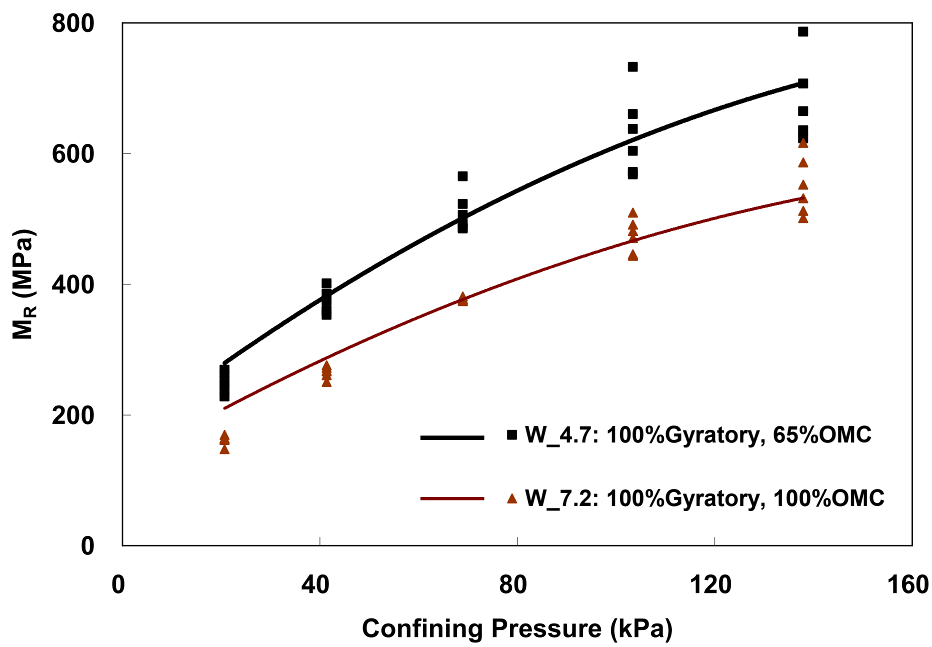

Figure 4.7: Resilient Modulus of CR 3 25% Aggregate – 75% RAP
(100% Gyratory = 2032 kg/m^3, 100% OMC = 7.2%, 65% OMC = 4.7%).

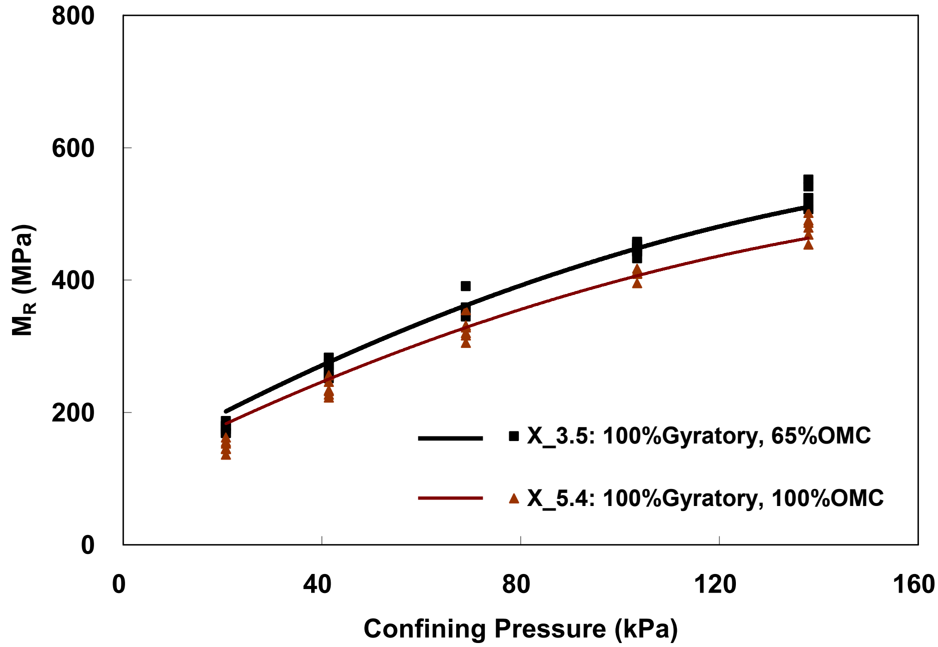

Figure 4.8: Resilient Modulus of TH 23 Blend
(100% Gyratory = 2080 kg/m^3, 100% OMC = 5.4%, 65% OMC = 3.5%).

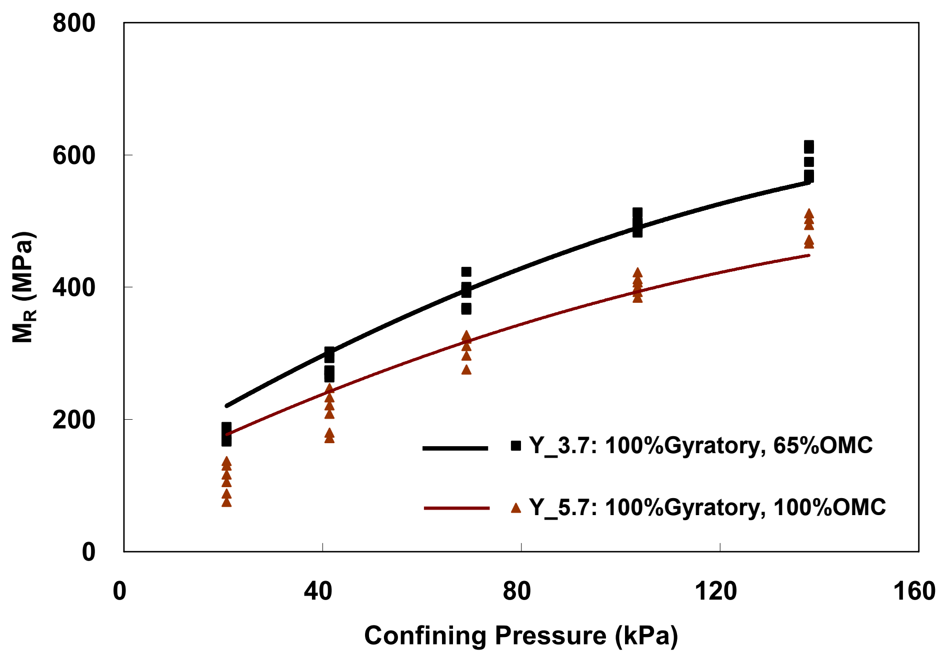

Figure 4.9: Resilient Modulus of TH 200 Blend
(100% Gyratory = 2144 kg/m^3, 100% OMC = 5.7%, 65% OMC = 3.7%).

A summary of the M_R results is presented in Figs 4.10 – 4.11, for CR 3 samples at 65% OMC and 100% OMC, respectively. The 25% aggregate – 75% RAP specimens exhibited the highest M_R, and the 100% aggregate specimens exhibited the lowest M_R. In addition, the blend produced from the reclaimer during full-depth reclamation behaved similar to the 50% aggregate – 50% RAP specimens. Plots of Figs 4.10 – 4.11 at different confining pressure and deviator stresses are contained in Appendix D.3.

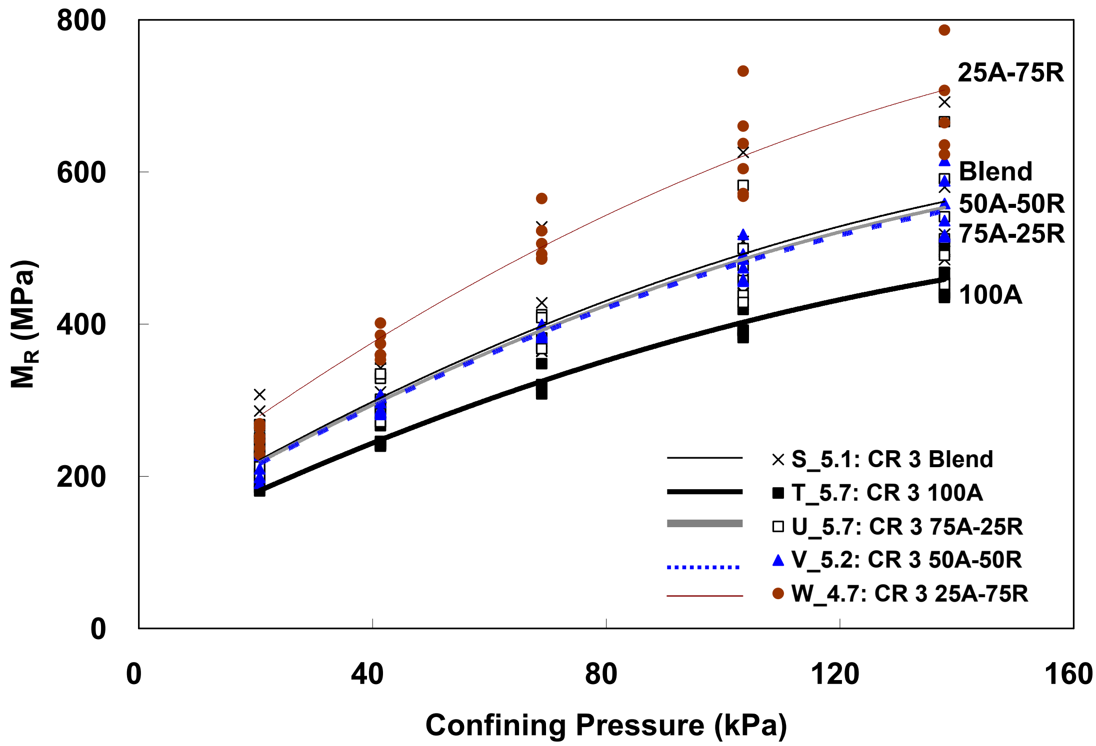

Figure 4.10: Resilient Modulus of CR 3 Materials at 98% Gyratory and 65% OMC.

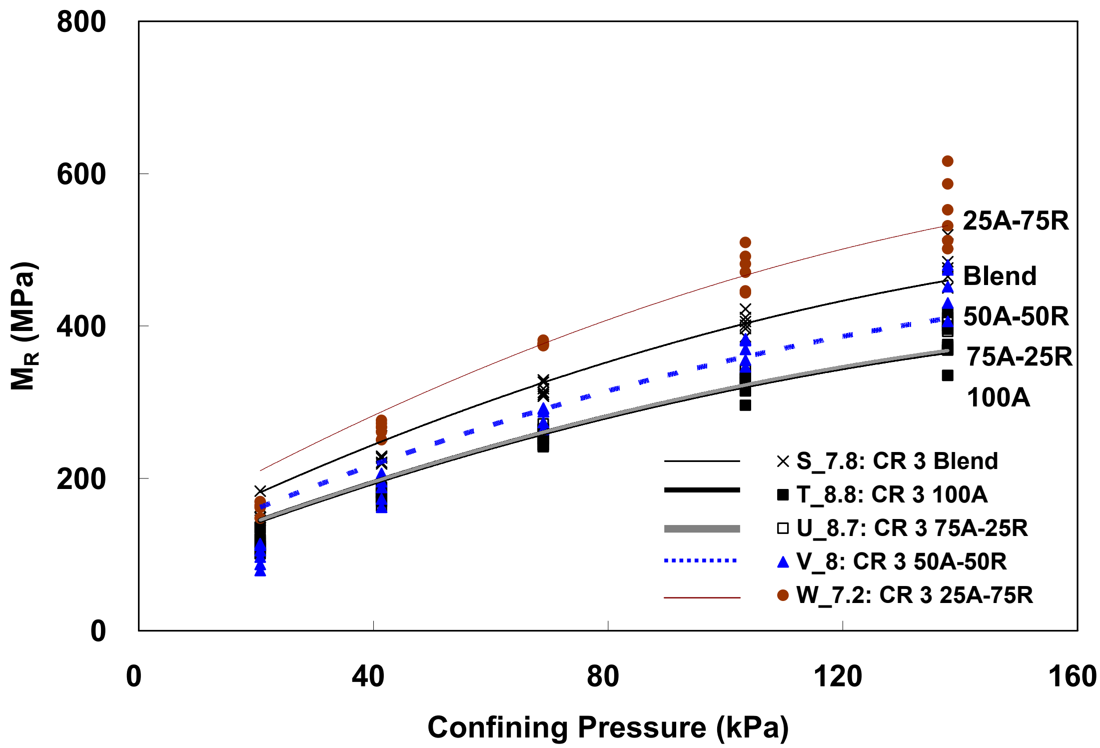

Figure 4.11: Resilient Modulus of CR 3 Materials at 100% Gyratory and 100% OMC.

4.1.1 Resilient Modulus (M_R) Data Interpretation

The M_R of granular material depends on the state of stress during loading. Therefore, several models have been proposed to describe the stress dependency of M_R [25]. Some researchers [26-27] have noted that the M_R increases with an increase in confining pressure:

$$M_R = k_1 \cdot \left(\frac{\sigma_3}{P_a}\right)^{k_2} \tag{4.1}$$

where k_1, k_2 = regression coefficients
P_a = atmospheric pressure (0.101 MPa)
σ_3 = confining pressure

Others [28-29] have suggested that M_R should be given as a function of bulk stress:

$$M_R = k_1 \cdot \left(\frac{\theta}{P_a}\right)^{k_2} \tag{4.2}$$

where k_1, k_2 = regression coefficients
P_a = atmospheric pressure (0.101 MPa)
θ = bulk stress = $\sigma_1 + \sigma_2 + \sigma_3 = \sigma_1 + 2\sigma_3$

Including deviator stress into equation (4.2) was suggested by [30]:

$$M_R = k_1 \cdot \left(\frac{\theta}{P_a}\right)^{k_2} \cdot \left(\frac{\tau_{oct}}{P_a} + 1\right)^{k_3} \tag{4.3}$$

where k_1, k_2, k_3 = regression coefficients
P_a = atmospheric pressure (0.101 MPa)
θ = bulk stress = $\sigma_1 + \sigma_2 + \sigma_3 = \sigma_1 + 2\sigma_3$
τ_{oct} = octahedral shear stress = $(2^{0.5}/3)$×deviator stress

Figures 4.12 – 4.14 show the curve fit plots by equations (4.1) – (4.3) for the same material. As seen from Fig 4.13, the data did not fit well with equation (4.2). Although test data fit well with equation (4.3), both bulk and octahedral shear stresses contain deviator stress, which has less of an effect on M_R compared to the confining pressure (Fig 4.14). However, as seen from Fig 4.12, test data fit well with equation (4.1) assuming $k_2 = 0.50$, and M_R could be expressed as a function of confinement only.

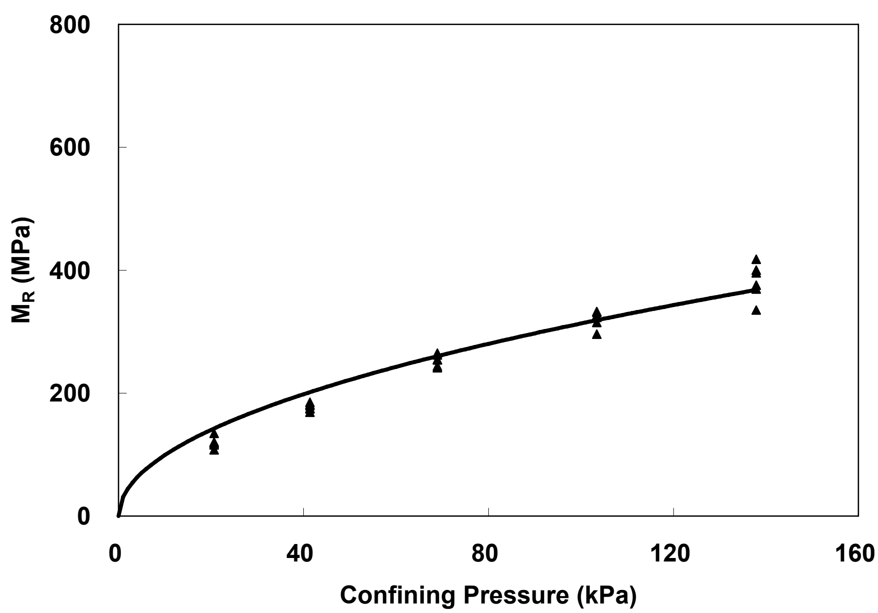

Figure 4.12: Example Curve Fit of CR 3 100% Aggregate by (4.1) (R^2 = 0.97) (T_8.8, 100% Gyratory = 2032 kg/m^3, 100% OMC = 8.8%).

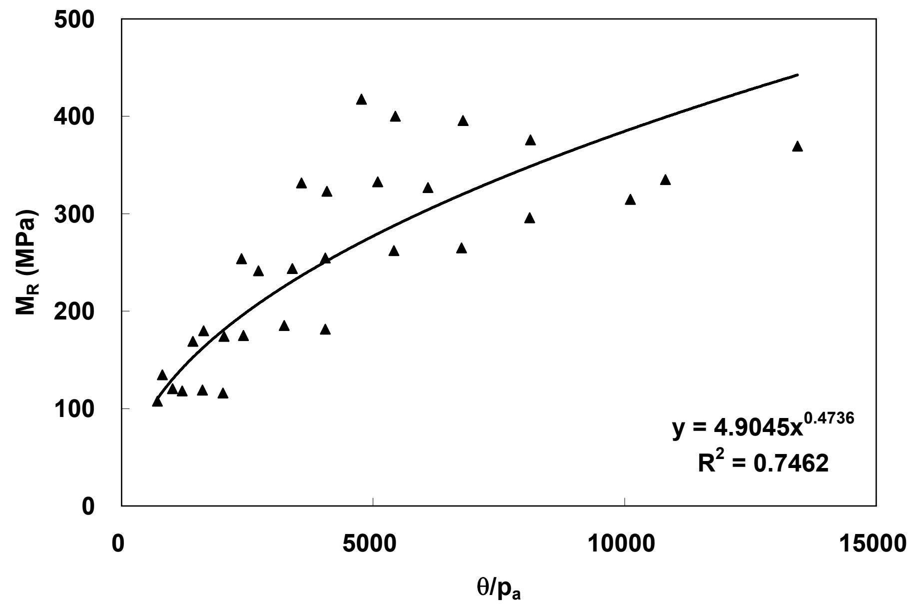

Figure 4.13: Example Curve Fit of CR 3 100% Aggregate by (4.2) (R^2 = 0.75) (T_8.8, 100% Gyratory = 2032 kg/m^3, 100% OMC = 8.8%).

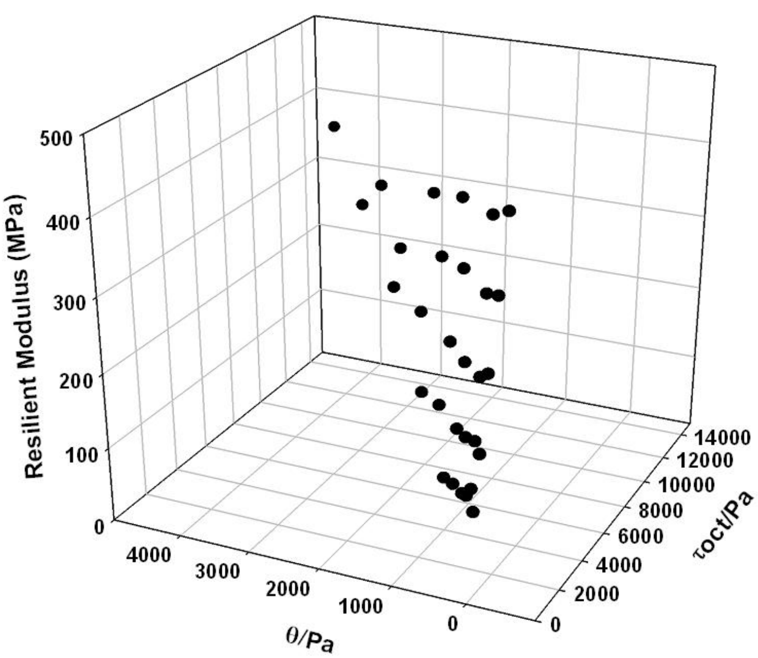

Figure 4.14: Example Curve Fit of CR 3 100% Aggregate by (4.3) (R^2 = 0.95) (T_8.8, 100% Gyratory = 2032 kg/m^3, 100% OMC = 8.8%).

As seen from Figs 4.3 – 4.11, M_R increased as confining pressure increased. For simplicity, a square-root dependency between confining pressure (mean stress before application of the deviator stress) and M_R was assumed:

$$\frac{M_R}{P_a} = k \cdot \left(\frac{\sigma_{mean}}{P_a}\right)^{0.5} \tag{4.4}$$

where $\sigma_{mean} = (\sigma_1 + \sigma_2 + \sigma_3)/3$ = confining pressure
P_a = atmospheric pressure (0.101 MPa)
k = regression coefficient

From the Herzian contact theory of spheres subjected to normal load, it can be shown that the tangent modulus depends on the cube root of stress [31]. However, a square-root dependence fits the data better (Fig. 4.15).

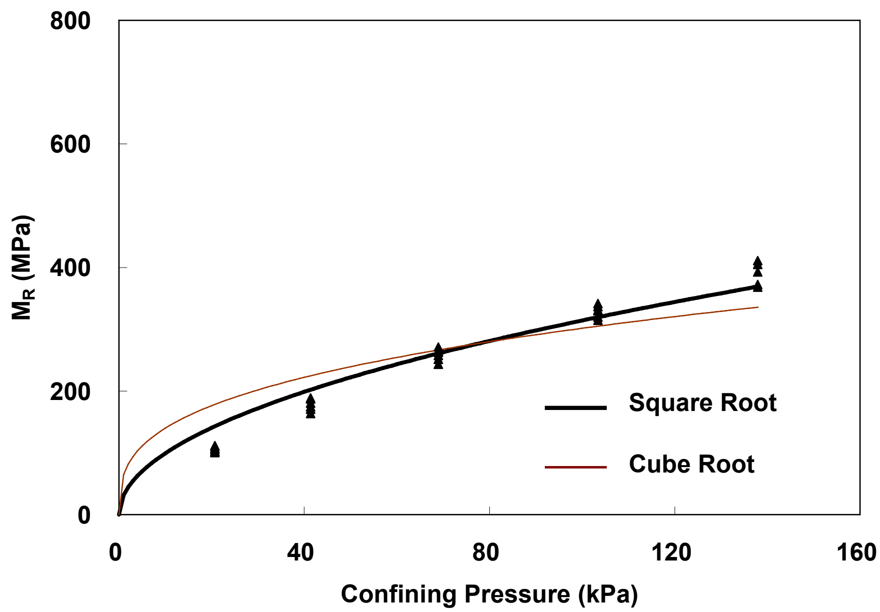

Figure 4.15: Example Curve Fit Comparison of CR 3, 75% Aggregate – 25% RAP (U_8.7, 100% Gyratory = 2032 kg/m^3, 100% OMC = 8.7%).

Coefficient k and R^2 values from equation (4.4), or equation (4.1) with $k_2 = 0.50$, for the seven different mixtures at two different moisture contents are shown in Table 4.2. The M_R test results strongly correlate with the model (R^2 values > 0.9). Lower moisture content specimens have 10 – 50% higher k_1 values for the seven different mixtures, indicating more confining pressure dependency. For CR 3 samples, as % RAP increased, the value of k_1 increased indicating more confining pressure dependency. The k_1, k_2, k_3 model represented by equation (4.3) was also used to fit the data (Table 4.2).

Table 4.2: Coefficients *k* and R^2.

Spec ID	Description	Equation (4.1)			Equation (4.3)			
		k_1	k_2	R^2	k_1	k_2	k_3	R^2
S_5.1	CR 3_Blend_65	4764	0.50	0.97	269	0.74	-0.91	0.84
S_7.8	CR 3_Blend_100	3903	0.50	0.97	153	0.94	-0.83	0.94
T_5.7	CR 3_100%A_65	3895	0.50	0.98	199	0.69	-0.64	0.87
T_8.8	CR 3_100%A_100	3112	0.50	0.97	117	0.98	-0.87	0.96
U_5.7	CR 3_75%A-25%R_65	4697	0.50	0.99	239	0.80	-0.90	0.91
U_8.7	CR 3_75%A-25%R_100	3122	0.50	0.95	113	1.02	-0.89	0.98
V_5.2	CR 3_50%A-50%R_65	4657	0.50	1.00	211	0.83	-0.79	0.94
V_8	CR 3_50%A-50%R_100	3481	0.50	0.91	110	1.16	-1.03	0.99
W_4.7	CR 3_25%A-75%R_65	6009	0.50	0.99	268	0.92	-0.97	0.95
W_7.2	CR 3_25%A-75%R_100	4515	0.50	0.97	172	1.00	-0.93	0.98
X_3.5	TH 23_Blend_65	4334	0.50	0.99	180	0.86	-0.75	0.97
X_5.4	TH 23_Blend_100	3934	0.50	0.98	153	0.91	-0.76	0.97
Y_3.7	TH 200_Blend_65	4739	0.50	0.97	177	0.95	-0.79	0.98
Y_5.7	TH 200_Blend_100	3804	0.50	0.92	121	1.12	-0.94	0.99

4.1.2 Quality Control / Quality Assurance

The M_R data were analyzed by LVDT range, angle of rotation, signal-to-noise ratio (SNR) and coefficient of variation (COV), and those that failed to pass the limit were withdrawn. The % passing rate of each specimens for each criterion of all 28 specimens are in Table 4.3, and summary of % passing rate for each criterion and total % passing rate are in Table 4.4. A total of 95.2% of the test data passed all the criteria. Those sequences that failed to pass the LVDT range and rotation limits were usually higher loading sequences (sequences 29 and 30), and those sequences that failed to pass the SNR limit were usually lower loading sequences (sequences 1 and 2). Appendix D.9 contains the detailed QC / QA evaluation of the particular M_R sequences that did not pass the criteria; all sequences of all tests passed the SNR for load.

Table 4.3: Quality Control / Quality Assurance of Resilient Modulus (M_R) Data.

Specimen ID	Description	% Passing				
		LVDT range	Rotation <0.04°	SNR >3	SNR F >10	COV <10%
S_5.1_1	CR 3_Blend_65%OMC_1	100	97	97	100	100
S_5.1_2	CR 3_Blend_65%OMC_2	100	100	93	100	100
S_7.8_1	CR 3_Blend_100%OMC_1	90	100	100	100	100
S_7.8_2	CR 3_Blend_100%OMC_2	100	97	98	100	100
T_5.7_1	CR 3_100%A_65%OMC_1	100	100	97	100	100
T_5.7_2	CR 3_100%A_65%OMC_2	100	100	98	100	100
T_8.8_1	CR 3_100%A_100%OMC_1	97	100	100	100	100
T_8.8_2	CR 3_100%A_100%OMC_2	100	93	93	100	100
U_5.7_1	CR 3_75%A-25%R_65%OMC_1	100	100	98	100	100
U_5.7_2	CR 3_75%A-25%R_65%OMC_2	100	93	87	100	100
U_8.7_1	CR 3_75%A-25%R_100%OMC_1	97	100	100	100	100
U_8.7_2	CR 3_75%A-25%R_100%OMC_2	97	100	100	100	100
V_5.2_1	CR 3_50%A-50%R_65%OMC_1	100	100	100	100	100
V_5.2_2	CR 3_50%A-50%R_65%OMC_2	100	100	100	100	100
V_8_1	CR 3_50%A-50%R_100%OMC_1	97	100	100	100	100
V_8_2	CR 3_50%A-50%R_100%OMC_2	97	97	100	100	100
W_4.7_1	CR 3_25%A-75%R_65%OMC_1	100	100	97	100	100
W_4.7_2	CR 3_25%A-75%R_65%OMC_2	100	100	100	100	100
W_7.2_1	CR 3_25%A-75%R_100%OMC_1	100	100	100	100	100
W_7.2_2	CR 3_25%A-75%R_100%OMC_2	100	100	93	100	100
X_3.5_1	TH 23_Blend_65%OMC_1	93	100	97	100	100
X_3.5_2	TH 23_Blend_65%OMC_2	97	100	100	100	100
X_5.4_1	TH 23_Blend_100%OMC_1	100	100	100	100	100
X_5.4_2	TH 23_Blend_100%OMC_2	100	93	99	100	100
Y_3.7_1	TH 200_Blend_65%OMC_1	97	100	100	100	100
Y_3.7_2	TH 200_Blend_65%OMC_2	100	95	100	100	100
Y_5.7_1	TH 200_Blend_100%OMC_1	97	100	100	100	100
Y_5.7_2	TH 200_Blend_100%OMC_2	97	100	100	100	100

Table 4.4: Quality Control / Quality Assurance of Resilient Modulus (M_R) Data: Total

% Passing					
LVDT Range	Rotation <0.04°	SNR >3	SNR F >10	COV <10%	Total
98.3	98.7	98.1	100	100	95.2

4.2 Shear Strength Test Result

After completion of M_R tests, shear strength tests were performed at 34.5 kPa and 69 kPa confining pressures at 0.03mm/s loading rate. The maximum deviator stresses at two confining pressures were measured for two test specimens. From the principal stress data, friction angle (ϕ) and cohesion (c) can be calculated:

$$\sigma_{1f} = 2c\sqrt{K_p} + K_p\sigma_3 \tag{4.5}$$

$$K_p = \frac{1+\sin\phi}{1-\sin\phi} \tag{4.6}$$

where σ_3 = confining pressure
σ_{1f} = confining pressure + deviator stress

Also, the relation between the orientation of the failure plane (θ) and friction angle (ϕ) can be used to estimate ϕ:

$$\theta = 45 + \frac{\phi}{2} \tag{4.7}$$

Table 4.5 shows the deviator stresses at two confining pressures (34.5 kPa and 69 kPa), and the values of friction angle (ϕ) and cohesion (c). Friction angles range from 32˚ – 50˚ where the range is close to the typical range for gravel with some sand (34˚– 48˚) [21]. It appears that friction angles at 65% optimal moisture content were higher than friction angles at 100% optimal moisture content except sample X, and the friction angles of CR 3 materials with RAP were higher than the friction angles of CR 3 materials of 100% aggregate for both 100% and 65% OMC specimens except for sample S. The orientation of the failure planes (θ) ranged from 58˚– 72˚ by actual measurement and from 61˚– 70˚ by calculation (Appendix D.5).

Table 4.5: Shear Strength Test Result.

Specimen ID	Description	Confining Pressure (kPa)	Deviator Stress (kPa)	ϕ (°)	c (kPa)
S_5.1_1	CR 3_Blend_65%OMC_1	69	906	32	207
S_5.1_2	CR 3_Blend_65%OMC_2	34	793		
S_7.8_1	CR 3_Blend_100%OMC_1	34	719	32	157
S_7.8_2	CR 3_Blend_100%OMC_2	69	830		
T_5.7_1	CR 3_100%A_65%OMC_1	69	917	46	115
T_5.7_2	CR 3_100%A_65%OMC_2	34	707		
T_8.8_1	CR 3_100%A_100%OMC_1	69	858	39	152
T_8.8_2	CR 3_100%A_100%OMC_2	34	710		
U_5.7_1	CR 3_75%A-25%R_65%OMC_1	69	1026	49	110
U_5.7_2	CR 3_75%A-25%R_65%OMC_2	34	775		
U_8.7_1	CR 3_75%A-25%R_100%OMC_1	69	820	47	85
U_8.7_2	CR 3_75%A-25%R_100%OMC_2	34	593		
V_5.2_1	CR 3_50%A-50%R_65%OMC_1	69	934	50	85
V_5.2_2	CR 3_50%A-50%R_65%OMC_2	34	667		
V_8_1	CR 3_50%A-50%R_100%OMC_1	69	834	45	104
V_8_2	CR 3_50%A-50%R_100%OMC_2	34	633		
W_4.7_1	CR 3_25%A-75%R_65%OMC_1	69	1005	48	113
W_4.7_2	CR 3_25%A-75%R_65%OMC_2	34	766		
W_7.2_1	CR 3_25%A-75%R_100%OMC_1	69	868	44	120
W_7.2_2	CR 3_25%A-75%R_100%OMC_2	34	680		
X_3.5_1	TH 23_Blend_65%OMC_1	69	750	39	125
X_3.5_2	TH 23_Blend_65%OMC_2	34	600		
X_5.4_1	TH 23_Blend_100%OMC_1	69	758	48	72
X_5.4_2	TH 23_Blend_100%OMC_2	34	529		
Y_3.7_1	TH 200_Blend_65%OMC_1	69	809	45	96
Y_3.7_2	TH 200_Blend_65%OMC_2	34	604		
Y_5.7_1	TH 200_Blend_100%OMC_1	69	778	42	110
Y_5.7_2	TH 200_Blend_100%OMC_2	34	602		

If it is assumed that the CR 3 specimens have a distinct friction angle dependent on density only, then the effect of moisture and RAP content can be estimated through the cohesion parameter. Thus, the values of cohesion were estimated assuming the constant friction angle of 45° (Table 4.6). Lower moisture content specimens had 5 – 50% higher values of cohesion than higher moisture content specimens.

Table 4.6: Estimated Cohesion (c) Assuming $\phi = 45^\circ$.

Specimen ID	Description	Confining Pressure (kPa)	Deviator Stress (kPa)	c (kPa)
T_5.7_1	CR 3_100%A_65%OMC_1	69	917	106
T_5.7_2	CR 3_100%A_65%OMC_2	34	707	
T_8.8_1	CR 3_100%A_100%OMC_1	69	858	100
T_8.8_2	CR 3_100%A_100%OMC_2	34	710	
U_5.7_1	CR 3_75%A-25%R_65%OMC_1	69	1026	124
U_5.7_2	CR 3_75%A-25%R_65%OMC_2	34	775	
U_8.7_1	CR 3_75%A-25%R_100%OMC_1	69	820	84
U_8.7_2	CR 3_75%A-25%R_100%OMC_2	34	593	
V_5.2_1	CR 3_50%A-50%R_65%OMC_1	69	934	103
V_5.2_2	CR 3_50%A-50%R_65%OMC_2	34	667	
V_8_1	CR 3_50%A-50%R_100%OMC_1	69	834	89
V_8_2	CR 3_50%A-50%R_100%OMC_2	34	633	
W_4.7_1	CR 3_25%A-75%R_65%OMC_1	69	1005	121
W_4.7_2	CR 3_25%A-75%R_65%OMC_2	34	766	
W_7.2_1	CR 3_25%A-75%R_100%OMC_1	69	868	98
W_7.2_2	CR 3_25%A-75%R_100%OMC_2	34	680	

4.3 Cyclic Triaxial Test Result

A total of 14 cyclic triaxial tests were conducted: seven different mixtures of RAP and aggregate at one density and moisture content at two different peak-stress ratios. A three dimensional pavement stress analysis, performed using layered linear elastic theory contained in Bitumen Stress Analysis in Roads (BISAR) software, showed that the cyclic triaxial stress state at 35% peak stress corresponded to a similar stress state for the following three layer system: 152 mm asphalt pavement (E = 552 MPa) on top, 152 mm base (E = 276 MPa) in the middle, and soil layer (E = 28 MPa) on the bottom; traffic load was assumed to be 758 kPa uniform stress on a 152 mm diameter area. Stresses were estimated at three points, top, middle and bottom of the base layer; all three points were below the center of the traffic load. The result is shown in Table 4.7. The stresses near the top of the base layer were close to the stresses of the 35% peak stress ratio (σ_1 = 203 kPa and σ_3 = 21 kPa).

Table 4.7: BISAR Pavement (3D) Stress Analysis.

	σ_1 (kPa)	σ_3 (kPa)
Top	203	21
Middle	87	46
Bottom	40	101

The stress-strain behavior of CR 3 mixtures at selected cycles are shown in Figs. 4.16 – 4.17. Notice that the material stiffened as the number of cycles increased; this was probably a result of the specimen compacting during loading, as indicated by the permanent deformation. Energy loss and permanent deformation decreased with continued loading.

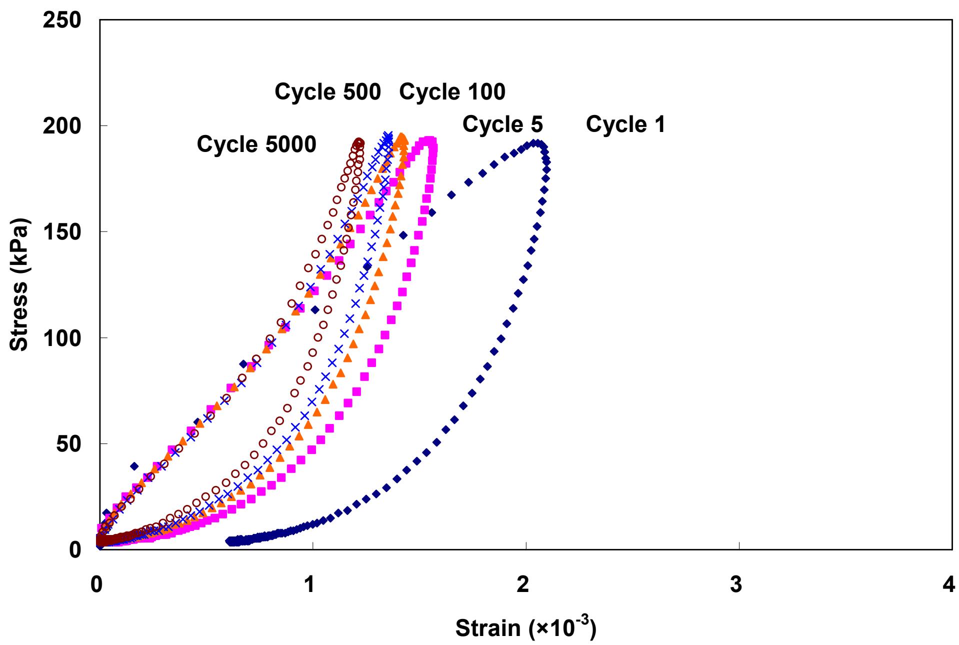

Figure 4.16: Stress-Strain Behavior by Cycle
(CR 3 100% Aggregate at 35% Peak Stress).

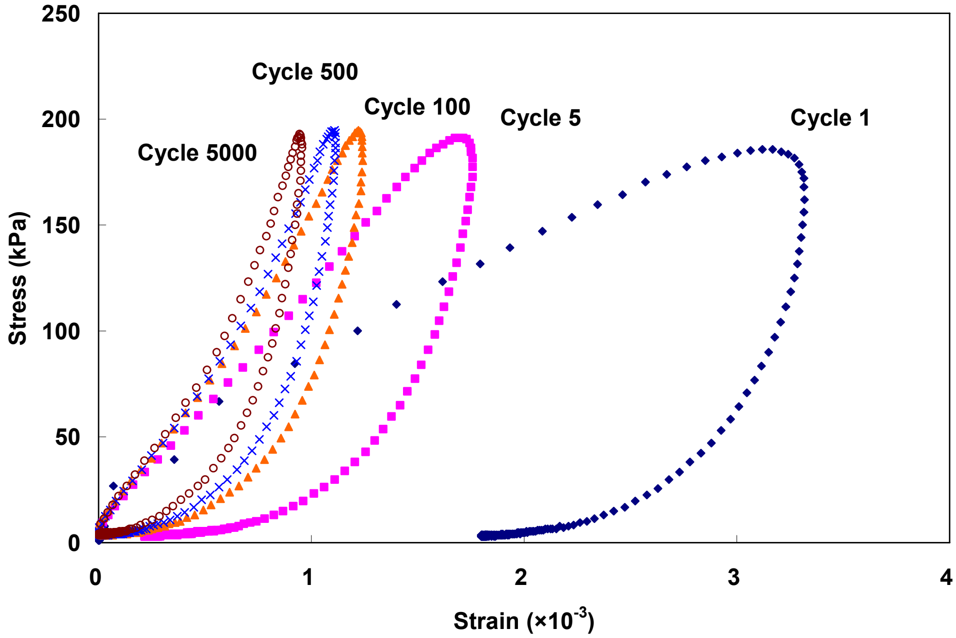

Figure 4.17: Stress-Strain Behavior by Cycle
(CR 3 25% Aggregate – 75% RAP at 35% Peak Stress).

Figures 4.18 – 4.19 show the cumulative permanent strain (ε_p) versus cycle number for CR 3 specimens at 50% and 35% peak stress ratios respectively. The cumulative permanent strain (ε_p) leveled off as cycles of loading increased. It is noted that the specimens containing RAP experienced higher cumulative permanent strain (ε_p) than the 100% aggregate specimens at both peak stress ratios. In addition, the specimens with more RAP usually had more cumulative permanent strain (ε_p). For example, the 100% aggregate specimen experienced $\varepsilon_p = 0.29\%$ while the 25% aggregate – 75% RAP specimen had $\varepsilon_p = 1.21\%$ at the peak stress ratio of 35%**.** From Figs 4.18 – 4.19, the cumulative permanent strains at the 50% peak stress ratio were approximately twice higher than cumulative permanent strains at the 35% peak stress ratio for the five different mixtures (also see Appendix D.6).

Figures 4.20 – 4.21 show the incremental permanent strain ($\Delta\varepsilon_p$) for the first five cycles. For the specimens containing RAP, the first cycle of loading resulted in a significant amount of permanent deformation (approximately 10% of cumulative permanent strain (ε_p)).

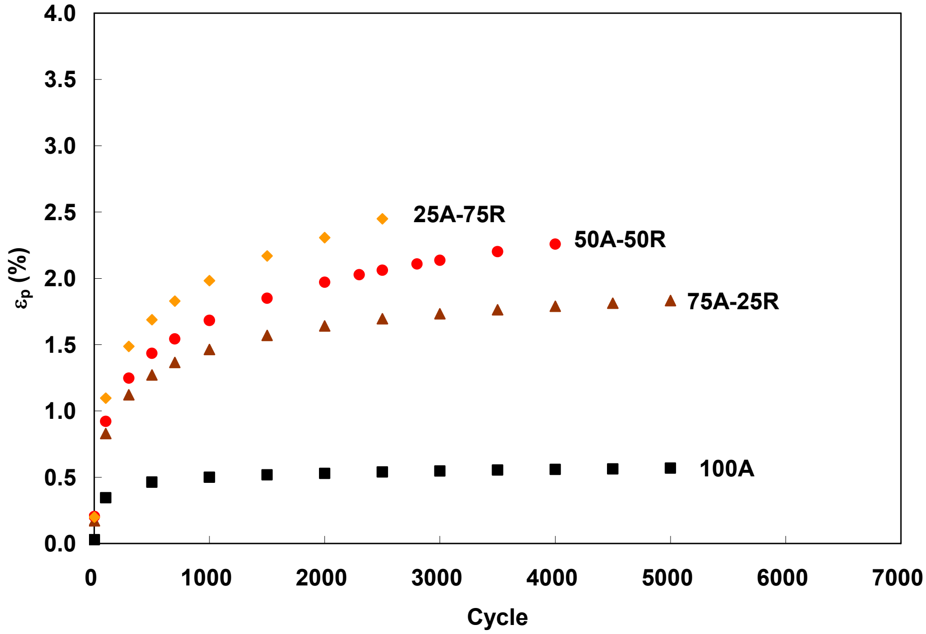

Figure 4.18: Cumulative Permanent Strain (ε_p) of CR 3 Materials at 50% Peak Stress.

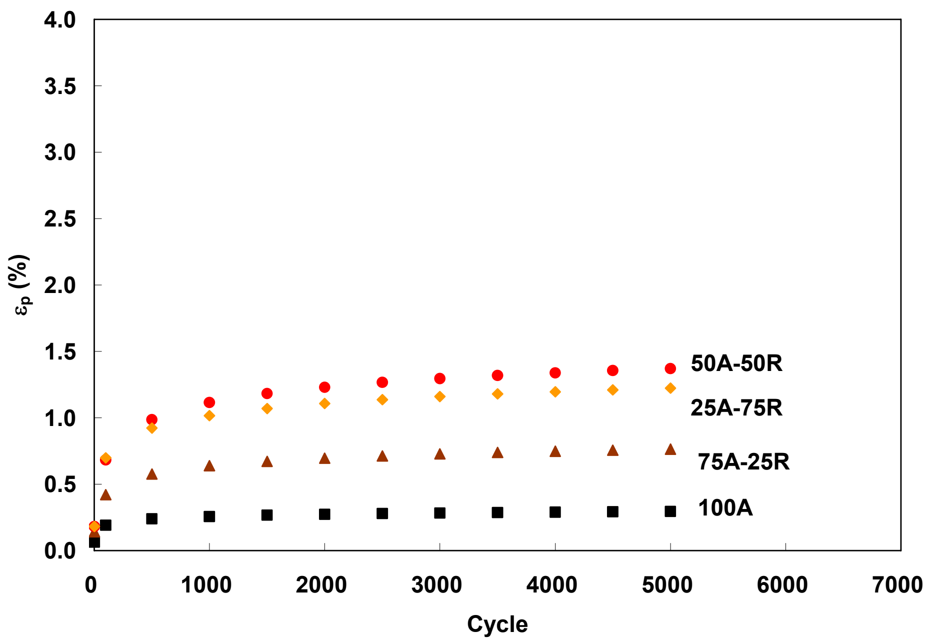

Figure 4.19: Cumulative Permanent Strain (ε_p) of CR 3 Materials at 35% Peak Stress.

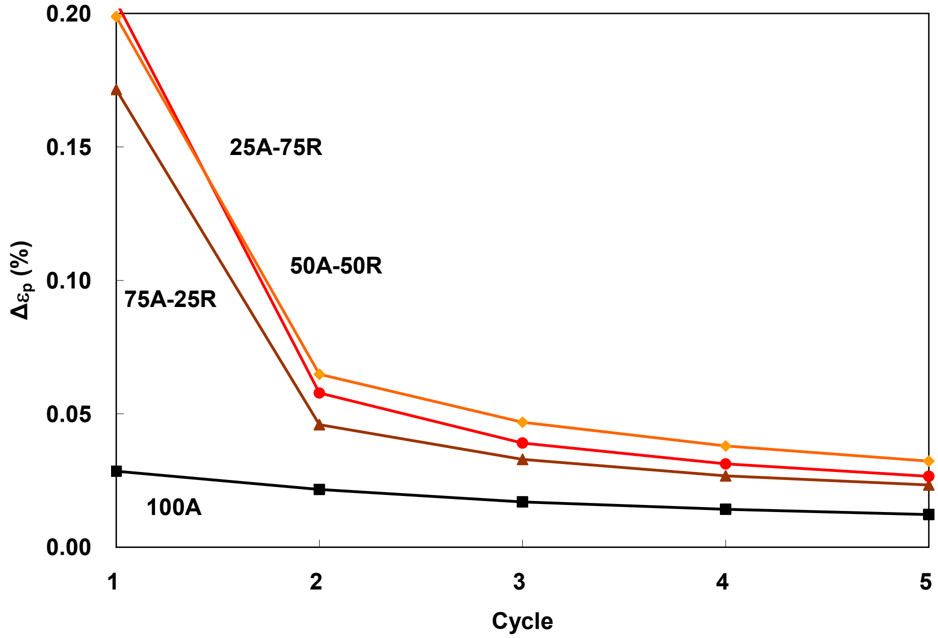

Figure 4.20: Incremental Permanent Strain ($\Delta\varepsilon_p$) of CR 3 Materials at 50% Peak Stress: First Five Cycles.

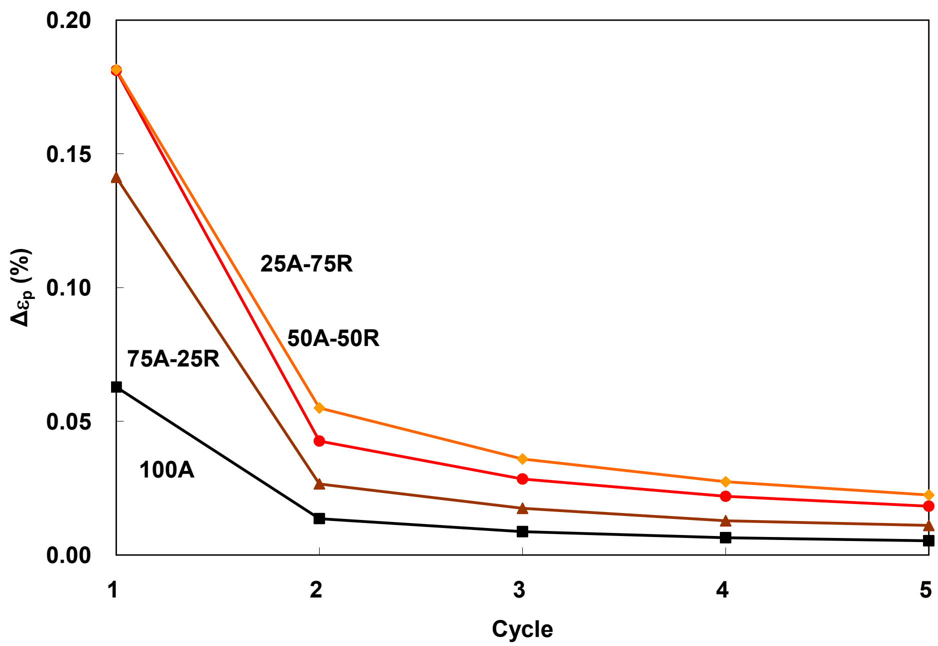

Figure 4.21: Incremental Permanent Strain ($\Delta\varepsilon_p$) of CR 3 Materials at 35% Peak Stress: First Five Cycles.

Figures 4.22 – 4.23 show the cumulative permanent strain (ε_p) versus cycle of in-situ blend specimens from CR 3, TH 23 and TH 200 at 50% and 35% peak stress ratios. TH 200 specimens experienced the highest cumulative permanent strain, and CR 3 and TH 23 specimens had similar cumulative permanent deformation at both peak stress ratios. The increase of cumulative permanent strain from 35% peak stress to 50% peak stress is also noticed (also see Appendix D.6).

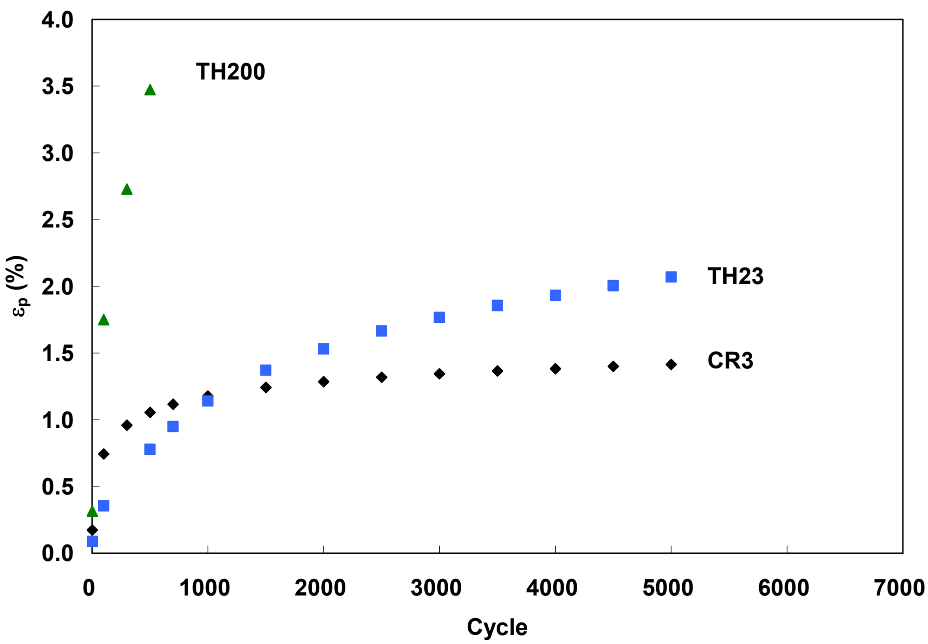

Figure 4.22: Cumulative Permanent Strain (ε_p) of Blend Materials at 50% Peak Stress.

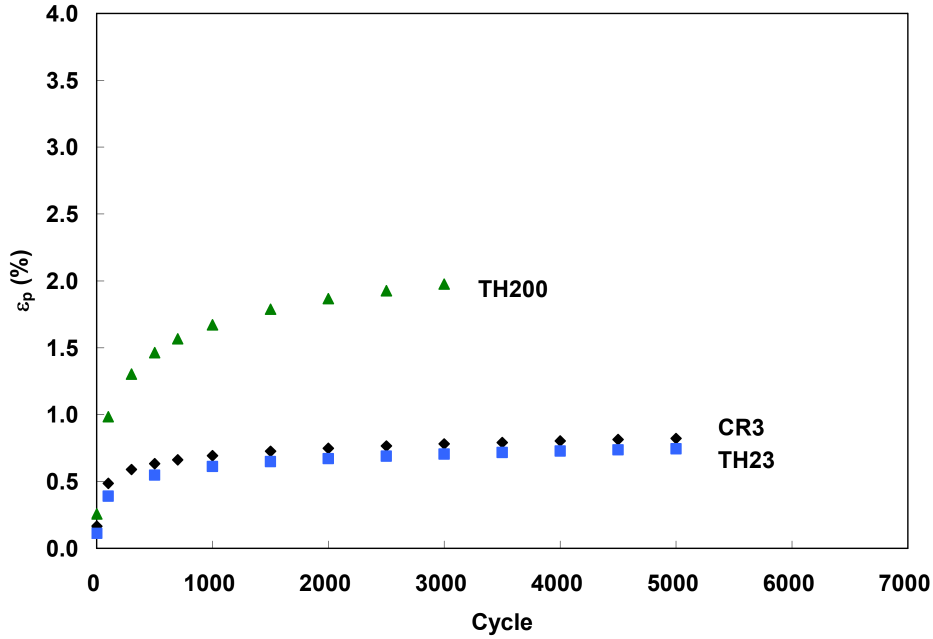

Figure 4.23: Cumulative Permanent Strain (ε_p) of Blend Materials at 35% Peak Stress.

Figures 4.24 – 4.25 illustrate the change in the secant Young's modulus (E_{secant}) with loading at 50% and 35% peak stresses, where E_{secant} is defined as (Fig. 1.2)

$$E_{secant} = \frac{\Delta\sigma_a}{\Delta\varepsilon^r{}_a} \tag{4.8}$$

$\Delta\sigma_a$ = cyclic axial (deviator) stress and $\Delta\varepsilon^r{}_a$ = recoverable axial strain. From both figures, it is noticed that the 25% aggregate – 75% RAP specimens had the highest E_{secant} values (185 – 200 MPa) at both peak stress ratios. The 100% aggregate specimens were very close or slightly stiffer (155 – 175 MPa) than 50% aggregate – 50% RAP and 75% aggregate – 25% RAP specimens at both peak stress ratios.

Young's modulus (E_{secant}) increased as cycle number increased, and leveled off gradually, probably because permanent strain leveled off. Young's modulus (E_{secant}) at the 50% peak stress ratio was higher than that at the 35% peak stress ratio, as the increased deviator stress induced more permanent deformation and thus more compaction (also see Appendix D.7).

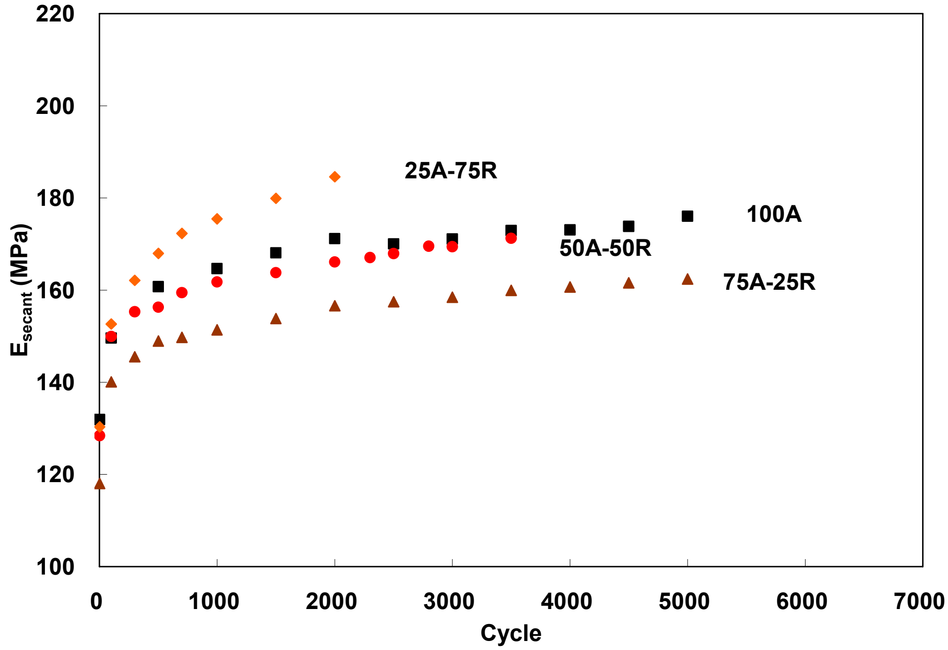

Figure 4.24: Young's Modulus (E_{secant}) of CR 3 Materials at 50% Peak Stress.

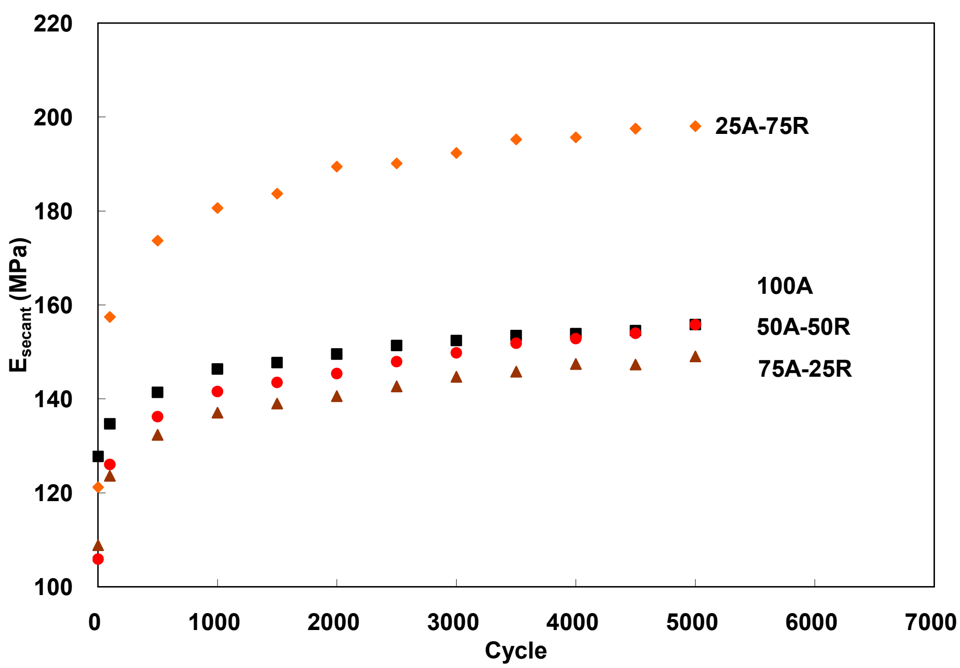

Figure 4.25: Young's Modulus (E_{secant}) of CR 3 Materials at 35% Peak Stress.

Figures 4.26 – 4.27 show Young's modulus (E_{secant}) for the first five cycles. The order of E_{secant} for the first five cycles did not follow the same order when considering 5000 cycles. The 100% aggregate specimen was the stiffest for the first five cycles whereas the 25% aggregate – 75% RAP specimen was the stiffest at the end of 5000 cycles. The RAP specimens experienced more permanent deformation than the 100% aggregate specimens due to more compaction (permanent deformation) through cycles.

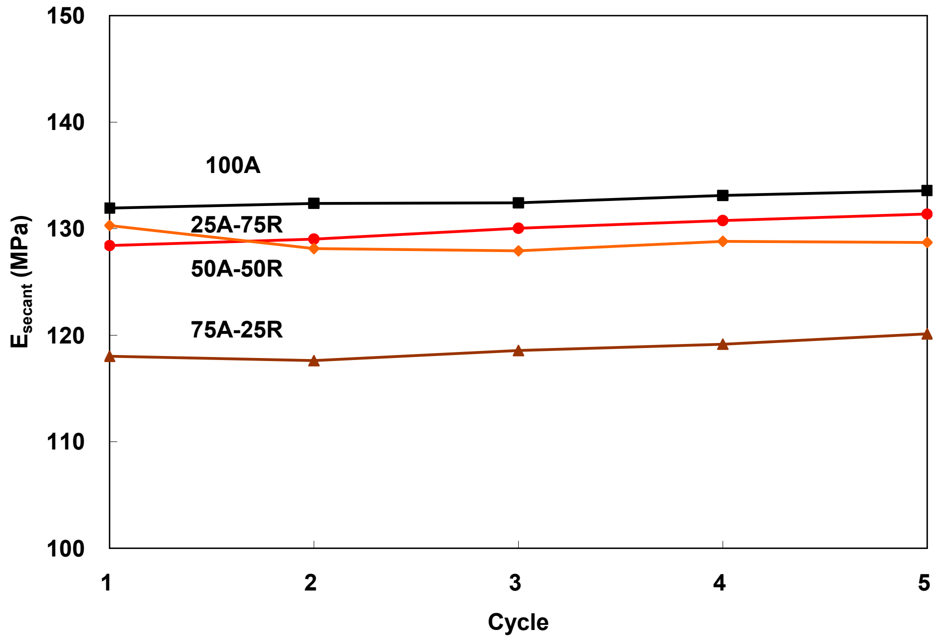

Figure 4.26: Young's Modulus of CR 3 Materials at 50% Stress Ratio: First Five Cycles.

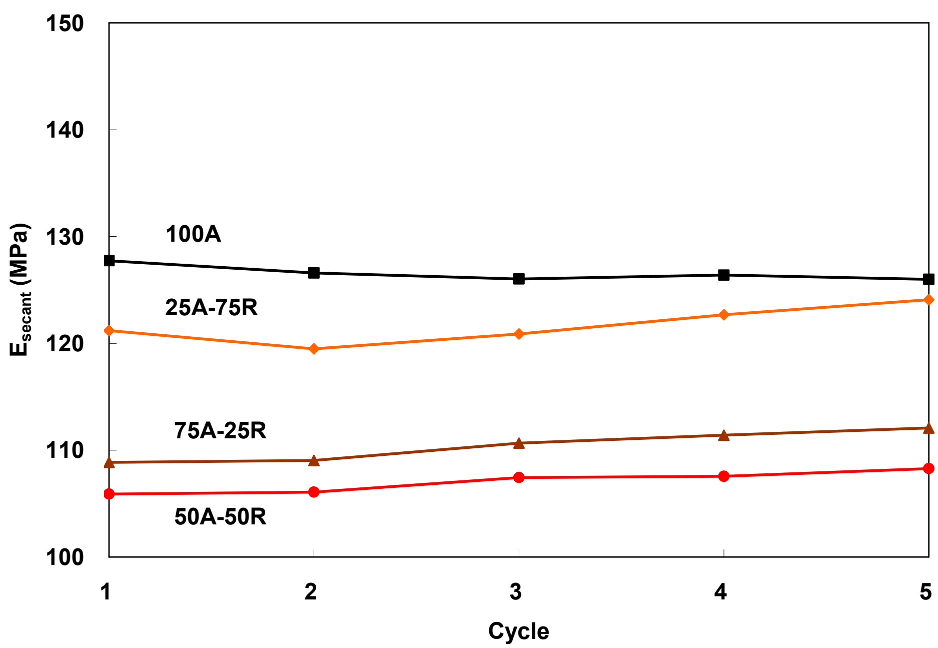

Figure 4.27: Young's Modulus of CR 3 Materials at 35% Stress Ratio: First Five Cycles.

Figures 4.28 – 4.29 show the Young's modulus (E_{secant}) versus cycle of in-situ blend materials at 50% and 35% peak stress ratios. From both figures, it is noticed that the TH 23 specimens had the highest Young's modulus (E_{secant}) values at both peak stress ratios. The Young's modulus (E_{secant}) increased as cycle increased, and leveled off gradually, probably because permanent strain leveled off. Opposite to the result from CR 3 materials, the Young's modulus (E_{secant}) at the 35% peak stress ratio was higher than that at the 50% peak stress ratio for TH 23 and TH 200 specimens (also see Appendix D.7).

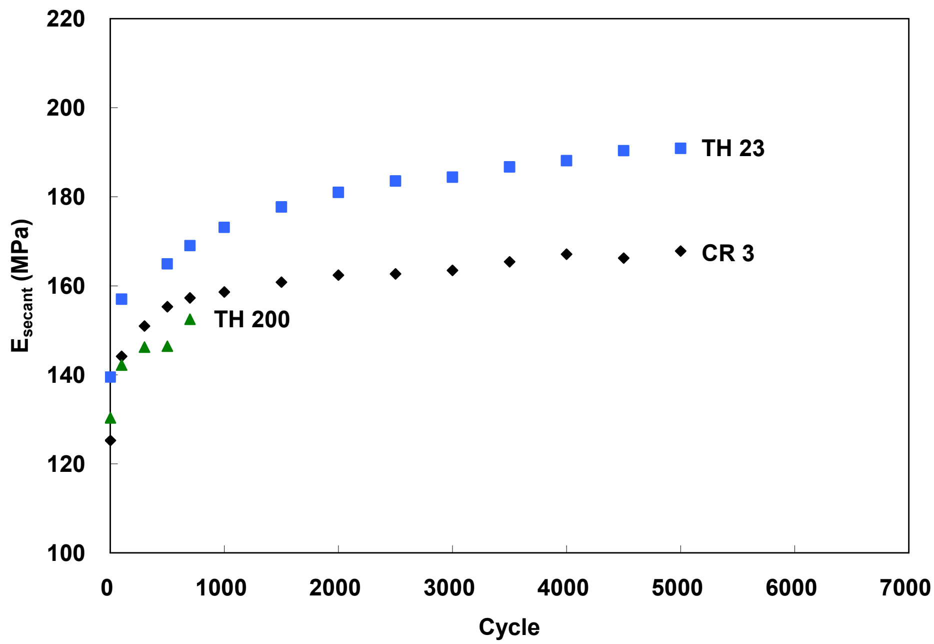

Figure 4.28: Young's Modulus (E_{secant}) of Blend Materials at 50% Peak Stress.

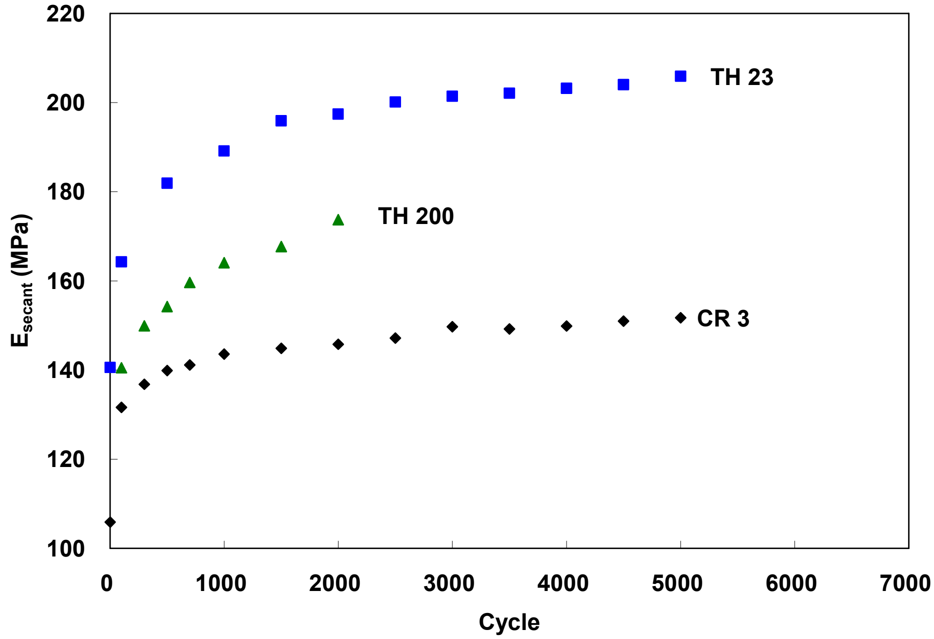

Figure 4.29: Young's Modulus (E_{secant}) of Blend Materials at 35% Peak Stress.

4.3.1 Test Data Interpretation

Several researchers [32-34] suggested a linear relation between the cumulative permanent strain (ε_p) and the logarithm of the number of load cycles:

$$\varepsilon_p = a + b(\log N) \tag{4.9}$$

where ε_p = cumulative permanent strain, N = number of loading cycles, and *a, b* = regression coefficients.

As seen from Figs. 4.30 – 4.31, the relation is close to linear. Therefore, (4.10) is modified from (4.9), and coefficient *a* and R^2 of the trend lines of 14 specimens were calculated and presented in Table 4.8.

$$\varepsilon_p = \varepsilon_{p(1)} + a(\log N) \tag{4.10}$$

where ε_p = cumulative permanent strain, $\varepsilon_{p(1)}$ = permanent strain at the first cycle, N = number of loading cycles, and *a* = regression coefficient.

From Table 4.8, coefficient *a* for the 50% peak stress specimens are 1.7 – 2.6 times higher than that for the 35% peak stress specimens for different mixtures (more permanent deformation). Also, increase of RAP contents results in an increase of coefficient *a* (more permanent deformation) from CR 3. The test results correlate with the model (most of the R^2 values > 0.9).

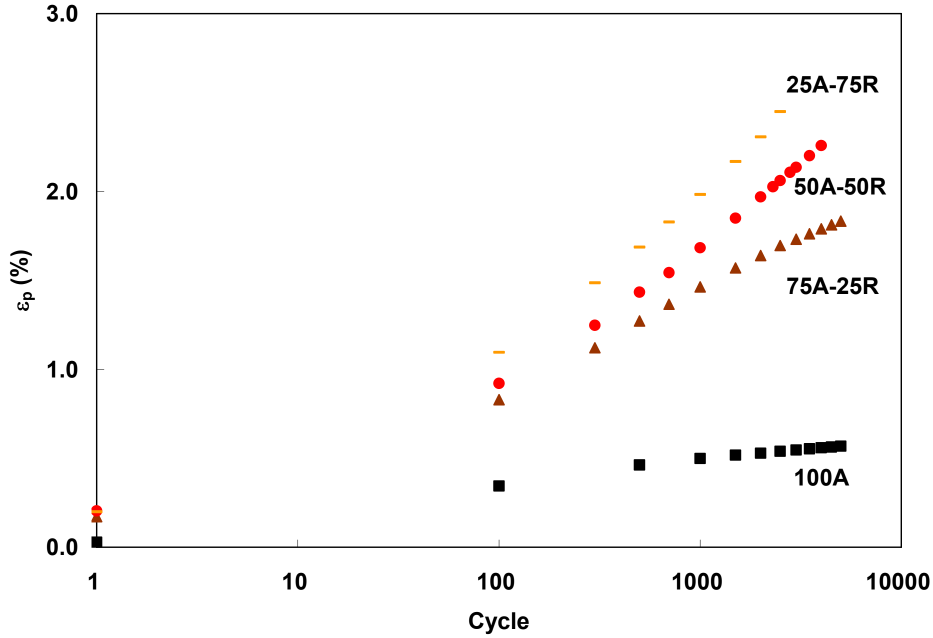

Figure 4.30: ε_p vs. Log (Cycle) of CR 3 Materials at 50% Peak Stress.

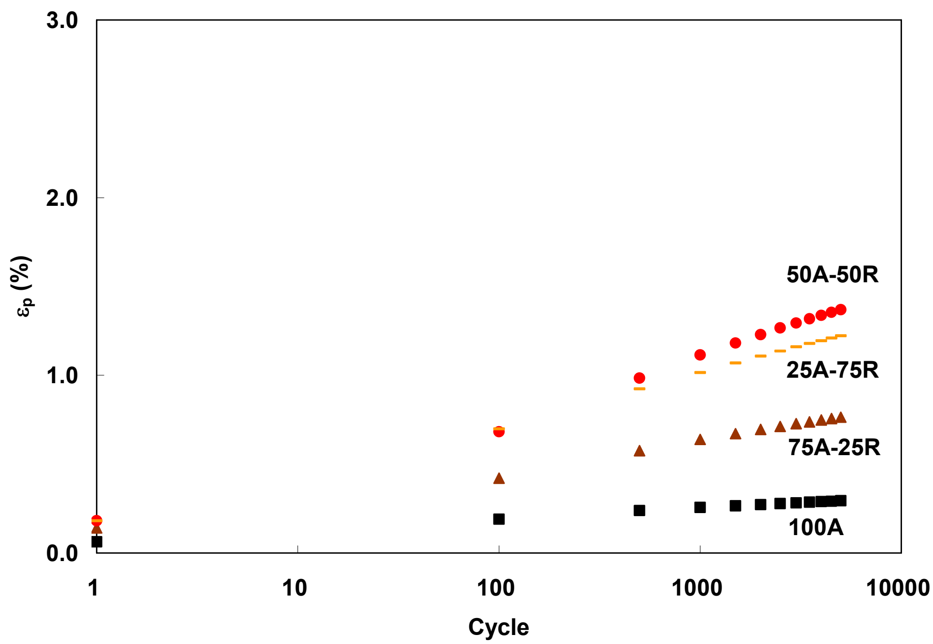

Figure 4.31: ε_p vs. Log (Cycle) of CR 3 Materials at 35% Peak Stress.

Table 4.8: Coefficient *a* and R^2.

Specimen ID	Description	*a*	R^2
S_50	CR 3_Blend_50% Peak Stress Ratio	0.33	0.99
T_50	CR 3_100%A_50% Peak Stress Ratio	0.15	0.99
U_50	CR 3_75%A-25%R_50% Peak Stress Ratio	0.44	0.97
V_50	CR 3_50%A-50%R_50% Peak Stress Ratio	0.52	0.93
W_50	CR 3_25%A-75%R_50% Peak Stress Ratio	0.59	0.94
X_50	TH 23_Blend_50% Peak Stress Ratio	0.44	0.75
Y_50	TH 200_Blend_50% Peak Stress Ratio	1.11	0.87
S_35	CR 3_Blend_35% Peak Stress Ratio	0.18	1.00
T_35	CR 3_100%A_35% Peak Stress Ratio	0.06	1.00
U_35	CR 3_75%A-25%R_35% Peak Stress Ratio	0.17	0.99
V_35	CR 3_50%A-50%R_35% Peak Stress Ratio	0.32	0.98
W_35	CR 3_25%A-75%R_35% Peak Stress Ratio	0.28	1.00
X_35	TH 23_Blend_35% Peak Stress Ratio	0.17	0.99
Y_35	TH 200_Blend_35% Peak Stress Ratio	0.47	0.97

As shown schematically in Fig. 4.32, energy dissipation during cyclic triaxial testing can be measured by the size of the hysteresis loop [35, 36], where the area enclosed by the loading-unloading response represents the loss of energy per unit volume. Previous work [36] showed that energy dissipation is the largest at the beginning of loading, decreases continuously, and becomes stable after a number of cycles. A concept of a total energy dissipation capacity for certain aggregate materials was suggested, and the remaining life of the base course was claimed to be predicted by comparing the cumulative energy dissipation with the total energy dissipation capacity [36]. The cumulative permanent deformation appeared to increase after further loading because the cumulative energy dissipation approached the total energy dissipation capacity [37, 38].

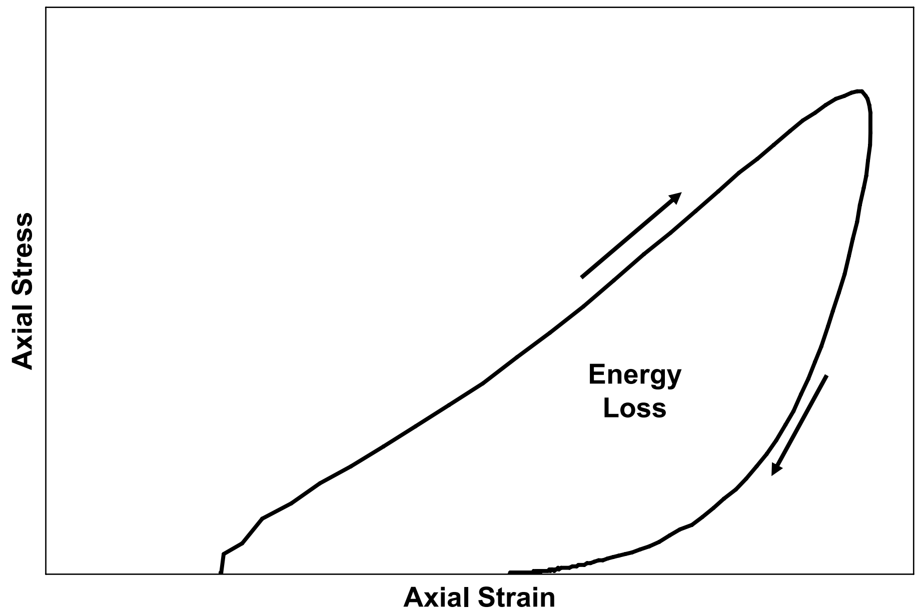

Figure 4.32: Energy Loss (Hysteresis Loop).

Energy loss (ΔW) was analyzed by calculating the size of the hysteresis loop (Fig. 4.32) for each cycle of CR 3 specimens at both 50% and 35% peak stress ratios and shown in Figs 4.33 – 4.34. Similar to the previous research, the energy loss is the largest at the beginning, decreases continuously, and becomes stable after a number of cycles. The energy loss plots from the 35% peak stress ratio specimens are very close to each other (Fig. 4.34). However, from the 50% peak stress ratio plots (Fig. 4.33), it is noticed that specimens with more RAP had more energy loss, and the order of energy loss is same as the order of permanent deformation. The energy loss from the 50% peak stress ratio specimens was higher than the energy loss from the 35% peak stress ratio (Appendix D.8). Figures 4.35 – 4.36 show the energy loss for the first five cycles. As the RAP content increased, the energy loss also increased.

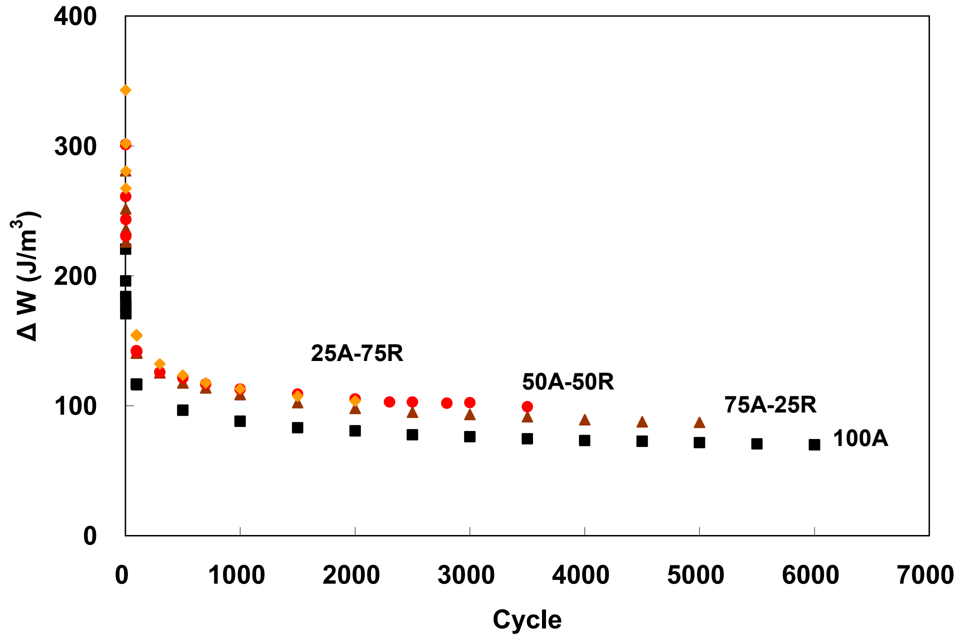

Figure 4.33: ΔEnergy Loss of CR 3 Materials at 50% Peak Stress.

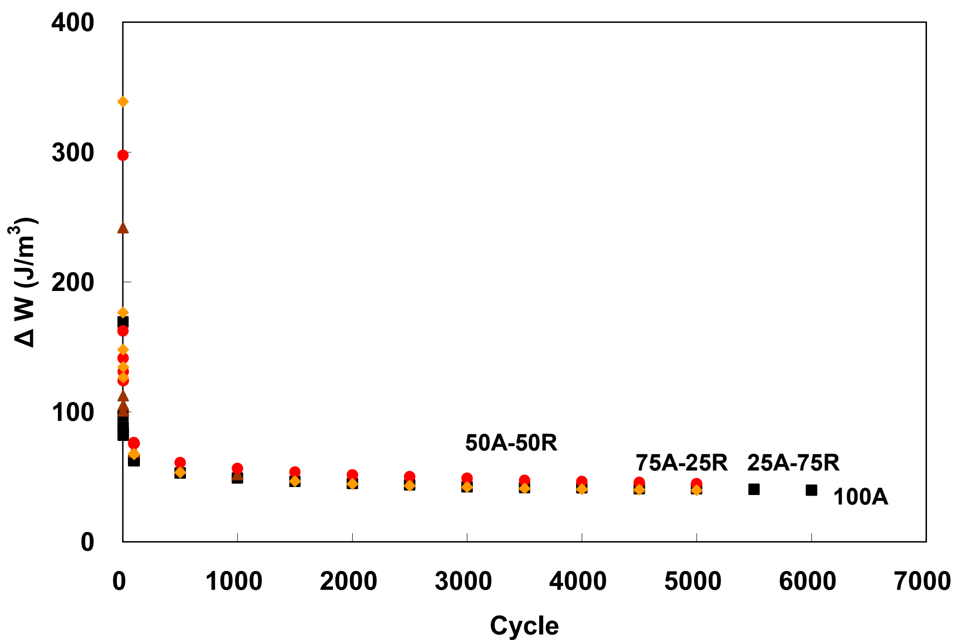

Figure 4.34: ΔEnergy Loss of CR 3 Materials at 35% Peak Stress.

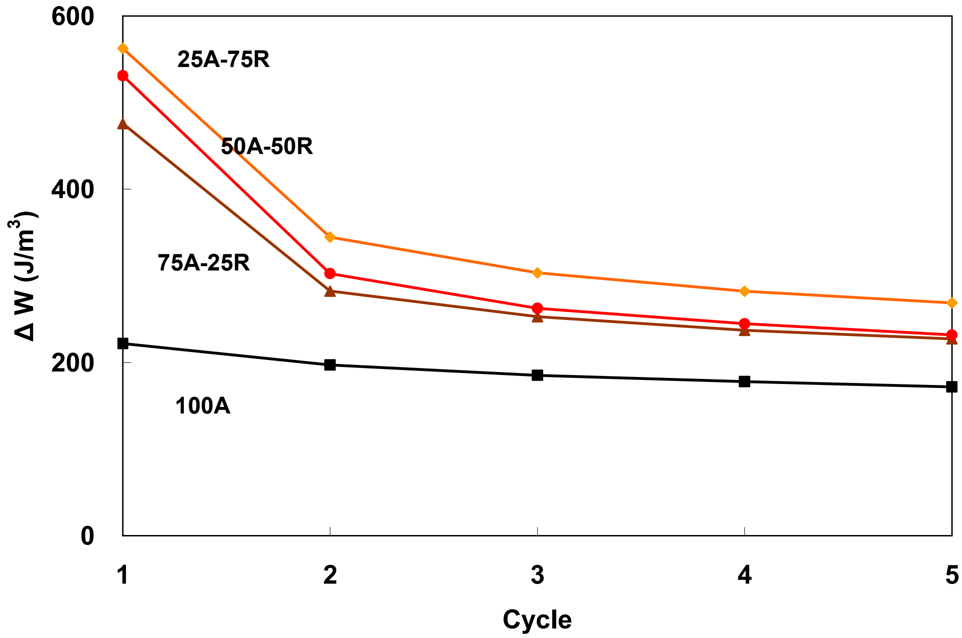

Figure 4.35: ΔEnergy Loss of CR 3 Materials at 50% Peak Stress: First Cycles.

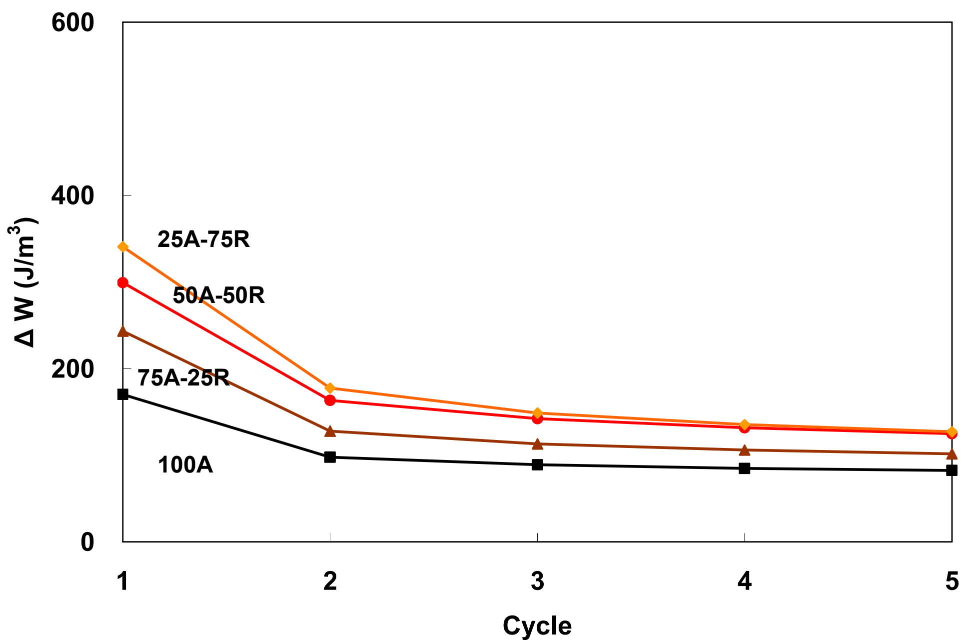

Figure 4.36: ΔEnergy Loss of CR 3 Materials at 35% Peak Stress: First Cycles.

The relation between loading cycle and ΔW is modeled as

$$\frac{\Delta W}{W_0} = b \cdot (N)^{\frac{1}{5}} \tag{4.11}$$

where N = number of loading cycles
W_0 = 1 J/m^3
ΔW = Energy loss / cycle
b = regression coefficient

The coefficient *b* and R^2 of the trend lines of 14 specimens are shown in Table 4.9. The coefficient *b* for the 50% peak stress ratio specimens were about two times higher than that of the 35% peak stress ratio specimens for different mixtures, indicating more energy loss. Also, increase of RAP content results in an increase of the coefficient *b* (more energy loss).

Table 4.9: Coefficient *b* and R^2.

Specimen ID	Description	b	R^2
S_50	CR 3_Blend_50% Peak Stress Ratio	103	0.99
T_50	CR 3_100%A_50% Peak Stress Ratio	83	0.97
U_50	CR 3_75%A-25%R_50% Peak Stress Ratio	107	0.99
V_50	CR 3_50%A-50%R_50% Peak Stress Ratio	111	0.97
W_50	CR 3_25%A-75%R_50% Peak Stress Ratio	122	0.96
X_50	TH 23_Blend_50% Peak Stress Ratio	85	0.59
Y_50	TH 200_Blend_50% Peak Stress Ratio	124	0.96
S_35	CR 3_Blend_35% Peak Stress Ratio	51	0.98
T_35	CR 3_100%A_35% Peak Stress Ratio	43	0.82
U_35	CR 3_75%A-25%R_35% Peak Stress Ratio	50	0.98
V_35	CR 3_50%A-50%R_35% Peak Stress Ratio	59	0.98
W_35	CR 3_25%A-75%R_35% Peak Stress Ratio	57	0.92
X_35	TH 23_Blend_35% Peak Stress Ratio	41	0.99
Y_35	TH 200_Blend_35% Peak Stress Ratio	58	0.88

In conclusion, permanent strain and energy loss leveled off as number of cycles increase, and the order of permanent strain and energy loss for the first five cycles was the same as the order for the entire cycling, indicating that more permanent strain and energy loss happened with more RAP content. However, the order of Young's modulus (E_{secant}) for the first five cycles did not follow the order of E_{secant} for 5000 cycles. The 100% aggregate specimen was the stiffest for the first five cycles whereas the 25% aggregate – 75% RAP specimen was the stiffest after 5000 cycles.

4.3.2 Quality Control / Quality Assurance

Cyclic triaxial test data were analyzed by angle of rotation (maximum limit of 0.04°), signal to noise ratio (minimum limit of 3 for LVDT displacements and 10 for loading cycles) and coefficient of variation (maximum limit of 10%). Table 4.10 shows the % passing rate for each criterion of sampled cycles of all 14 specimens. Cycles at the beginning usually had higher rotation.

Table 4.10: Quality Control / Quality Assurance of Cyclic Triaxial Test Data.

% Passing			
Rotation	SNR	SNR F	COV
<0.04°	>3	>10	<10%
95.7	100	100	100

Chapter 5
Summary and Conclusions

Resilient modulus (M_R), shear strength, and cyclic triaxial tests were conducted on various mixtures of recycled asphalt pavement (RAP) and aggregate. Eight different blended mixtures were prepared: four in-situ blends and four laboratory samples with different ratios of RAP and aggregate (%RAP/aggregate: 0/100, 25/75, 50/50, 75/25). As %RAP increased, the gradation curve shifted to coarse-grained and fine contents decreased. Specimens were prepared by a gyratory compactor because the density was closer to that measured in the field. As %RAP increased for gyratory compaction tests, the OMC decreased slightly, but the maximum dry density stayed the same.

A total of 28 resilient modulus and strength tests were conducted generally following the National Cooperative Highway Research Program (NCHRP) 1-28A test protocol; seven different blend types at one density (100% gyratory density), two moisture contents (100% and 65% OMC), and one set of replicates. M_R increased with increase of confining pressure, and the effect of deviator stress was not pronounced. The specimens with 65% OPM were 10 – 116% stiffer than the specimens with 100% OPM at all confining pressures with the effect increasing at higher confining pressures. As % RAP increased, a 0 – 65% increase in M_R occurred with the effect increasing at higher confining pressures. The in-situ blend produced during full-depth reclamation behaved similar to the 50% aggregate – 50% RAP specimens and the M_R of these materials were similar to 100% aggregate.

M_R data were evaluated with the universal model involving k_1, k_2, k_3 and a simplified model (k_2 = 0.5, k_3 = 0) and the values are reported in Table 4.2. The quality control / quality assurance criteria of angle of rotation, signal-to-noise ratio and coefficient of variance were evaluated and about 95% of the sequences passed the criteria. Strength parameters (cohesion and friction angle) for different mixtures were calculated from shear strength tests. By assuming a constant friction angle of 45° (specimen density remained constant), 65% OMC specimens had 5 – 50% larger values of cohesion than 100% OMC specimens, probably due to an increase in soil suction.

A total of 14 cyclic triaxial tests were conducted: seven different blend types at one density (100% gyratory density) and one moisture content (100% OMC) at two different peak stress ratios, 35% and 50% of the estimated deviator stress at failure (peak). Cumulative permanent deformation leveled off after approximately 1000 cycles. The specimens with RAP exhibited at least two times greater permanent deformation than the 100% aggregate material. As % RAP increased, 15 – 300% more permanent deformation occurred. The 25% aggregate – 75% RAP specimens exhibited the highest permanent deformation, and the 100% aggregate specimens exhibited the lowest permanent deformation. The Young's modulus (E_{secant}) increased as the number of cycles increased, and leveled off after approximately 1000 cycles as the permanent strain leveled off. The 25% aggregate – 75% RAP specimens had the highest Young's modulus (E_{secant}) values (185 – 200 MPa), and the 100% aggregate specimens were very close or slightly (3 – 8%) stiffer than 50% aggregate – 50% RAP specimens (155 – 175 MPa). A summary of the main conclusions follow.

- In terms of stiffness and strength, base course containing 50% aggregate – 50% RAP performed similar to 100% aggregate with proper compaction. For the field sites studied, the reclaimed material was coarser as %RAP increased, and the in-situ blend was equivalent to the 50-50 mix.
- To match densities measured in the field for bases containing aggregate with RAP, laboratory specimens were compacted using a gyratory process with compaction pressure of 600 kPa and 50 gyrations. Further research is needed to evaluate compaction effort and material behavior such as change in stiffness.
- The specimens with 65% OPM were stiffer and stronger (cohesion increased assuming friction angle remained constant) than the specimens with 100% OPM at the same density, probably due to the increase in soil suction and compaction energy with decrease in moisture.
- From triaxial tests with cyclic loading, specimens with RAP exhibited at least two times greater permanent deformation than the 100% aggregate material. Further research is needed to understand the mechanism of higher permanent deformation in RAP material.

References

[1] J. Aurstad, and I. Hoff. (2002). Crushed Asphalt and Concrete as Unbound Road Materials Comparisons of Field Measurements and Laboratory Investigations. *Bearing Capacity of Roads, Railways, and Airfields*, 967.

[2] U.S. Department of Transportation, Federal Highway Administration. (2001). *Basic Asphalt Recycling Manual*. U.S. Department of Transportation, Federal Highway Administration, PUB:NH101-022.

[3] P. R. Fleming. (1998). Recycled Bituminous as Unbound Granular Materials for Road Foundations in the UK. *Proceedings 5th International Conference of Bearing Capacity of Roads and Airfields*, 1581.

[4] D. Bloomquist, G. Diamond, M. Oden, B. Ruth, and M. Tia. (1993). *Engineering and Environmental Aspects of Recycled Materials for Highway Construction*, U.S. Department of Transportation, Federal Highway Administration and U.S. Environmental Protection Agency. FHWA-RD-93-088.

[5] K. W. Lee, and J. S. Davis. (1998). Structural Properties of New England Subbase Materials of Flexible Pavements. *Proceedings 5th International Conference of Bearing Capacity of Roads and Airfields*, 1641.

[6] W. H. Highter, J. A. Clary, and D. J. DeGroot. (1997). *Structural Numbers for Reclaimed Asphalt Pavement Base and Subbase Course Mixes*. Final Report, University of Massachusetts Amherst, Amherst, Massachusetts.

[7] W. J. Papp, A. Maher, T. Bennert, and N. Gucunski. (1998). Behavior of Construction and Demolition Debris in Base and Subbase Applications. *Recycled Materials in Geotechnical Applications. Vol. 79*, 122-136.

[8] National Cooperative Highway Research Program. (2002). *Recommended Standard Method for Routine Resilient Modulus Testing of Unbound Granular Base/Subbase Materials and Subgrade Soils, Protocol 1-28A*. National Cooperative Highway Research Program.

[9] R. P. Elliott, N. D. Dennis, and Y. Qiu. (1998). *Permanent Deformation of Subgrade soils: Phase I, A Test Protocol*. Mack-Blackwell Transportation Center, Fayetteville, Arkansas.

[10] G. Behzadi, and W. O. Yandell. (1996). A Determination of Elastic and Plastic Subgrade Soil Parameters for Asphalt Cracking and Rutting Prediction. *Transportation Research Record*, 97-104.

[11] T. Bennert, W. J. Papp, A. Maher, and N. Gucunski. (2000). Utilization of Construction and Demolition Debris under Traffic-Type Loading in Base and Subbase Applications. *Transportation Research Record, No. 1714*, Paper No. 00-1350., 33-39

[12] A. J. Puppala, S. Chomtid, and V. Bhadriraju. (2005). Using Repeated-Load Triaxial Tests to Evaluate Plastic Strain Potentials in Subgrade Soils. *Transportation Research Record, No. 1913*, 86-98.

[13] American Society for Testing and Materials Standards (ASTM Standard): C136-01. *Standard Test Method for Sieve Analysis of Fine and Coarse Aggregate.*

[14] Minnesota Department of Transportation Specification: 3138.3. 2000.

[15] American Association of State Highway and Transportation Officials (AASHTO):

T99. *The Moisture-Density Relations of Soils Using a 2.5 kg (5.5 lb) Rammer and a 305 mm (12 in) Drop.*
[16] American Society for Testing and Materials Standards (ASTM Standard): D698-00ae1. *Standard Test Method for Laboratory Compaction Characteristics Using Standard Effort.*
[17] American Association of State Highway and Transportation Officials (AASHTO): TP4. *Preparation of Compacted Specimens of Modified and Unmodified Hot Mix Asphalt by Means of the SHRP Gyratory Compactor.*
[18] Asphalt Institute (1996). *Superpave Mix Design.* Asphalt Institute Superpave Series No. 2 (SP-2).
[19] R. Mallich, P. Kandhal, E. Brown, R. Bradbury, and E. Kearney. (2002). *Development of a Rational and Practical Mix Design System for Full Depth Reclaimed (FDR) Mixes.* Final Report for a Project (Subcontract No. 00-373) Funded by the Recycled Materials Resource Center (RMRC) at the University of New Hampshire, New Hampshire.
[20] P. Davich, J. Labuz, B. Guzina, and A. Drescher. (2004). *Small Strain and Resilient Modulus Testing of Granular Soils.* Minnesota Department of Transportation Report, Final Report 2004-39.
[21] B. M. Das. (2000). *Fundamentals of Geotechnical Engineering*. Brooks/Cole.
[22] Federal Highway Administration Pavement Performance Division. (1996). *Resilient Modulus of Unbound Granular Base/Subbase Materials and Subgrade Soils*, *Long Term Pavement Performance, Protocol 46.*
[23] J. J. Tuma. (1987). *Engineering Mathematics Handbook*. McGraw-Hill, Inc, 3rd Ed.
[24] B. Chadbourn. (2005). Resilient Modulus Testing at Mn/DOT. Minnesota Department of Transportation Internal Report.
[25] F. Lekarp, U. Isacsson, and A. Dawson. (2000). State of the Art. I: Resilient Response of Unbound Aggregates. *Journal of Transportation Engineering, Jan/Feb 2000*, 66-75.
[26] W. A. Dunlap. (1963). *A Report on a Mathematical Model Describing the Deformation Characteristics of Granular Materials.* Texas Transp. Inst., Tech. Rep. No. 1, Proj. 2-8-62-27, Texas A&M University, College Station, Texas.
[27] C. L. Monismith, H. B. Seed, F. G. Mitry, and C. K. Chan. (1967). Prediction of Pavement Deflections from Laboratory Tests. *Proc., 2nd Int. Conf. Struct. Des. of Asphalt Pavements*, 109–140.
[28] H. B. Seed, F. G. Mitry, C. L. Monismith, and C. K. Chan. (1967). Prediction of Flexible Pavement Deflections from Laboratory Repeated Load Tests. *NCHRP Rep. No. 35*, National Cooperative Highway Research Program.
[29] R. G. Hicks. (1970). Factors Influencing the Resilient Properties of Granular Materials. Ph.D. thesis, University of California, Berkeley.
[30] J. Uzan. (1985). Characterization of granular material. *Transportation Research Record No.1022*, 52–59.
[31] F. E. Richard, R. D. Woods, and J. R. Hall. (1970). *Vibrations of Soils and Foundations.* Prentice-Hall.

[32] R. D. Barksdale. (1972). *Repeated Load Test Evaluation of Base Course Materials.* Georgia Highway Department Research Project 7002, Georgia Institute of Technology, Atlanta, Georgia.
[33] R. W. Lentz, and G. Y. Baladi. (1981). Constitutive Equation for Permanent Strain of Sand Subjected to Cyclic Loading. *Transportation Research Record, No. 810*, 50-54.
[34] R. W. Lentz. (1979). *Permanent Deformation of a Cohesionless Subgrade Material under Cyclic Loading.* Ph.D. Thesis, Michigan State University, East Lansing.
[35] M. Zytynski, M. F. Randolph, R. Nova, and C. P. Wroth. (1978). Short Communications on Modeling the Unloading-Reloading Behavior of Soils. *International Journal for Numerical and Analytical Methods in Geomechanics, Vol. 2*, 87-94.
[36] K. Sobhan, and R. J. Krizek. (1998). Resilient Properties and Fatigue Damage in Stabilized Recycled Aggregate Base Course Material. *Transportation Research Record, No. 1611*, 28-37.
[37] F. Lekarp, U. Isacsson, and A. Dawson. (2000). State of the Art. II: Permanent Strain Response of Unbound Aggregates. *Journal of Transportation Engineering, Jan/Feb 2000*, 76-83.

Appendix A

Index Properties

A.1 Gradation

Table A.1: Gradation.

Pecent Passing										
Sieve (mm)	CR 3 Blend	CR 3 Aggregate	CR 3 75%A-25%R	CR 3 50%A-50%R	CR 3 25%A-75%R	TH 23 Blend	TH 200 Blend	TH 5 Blend	Class 5 Max Band	Class 5 Min Band
63										
50										
37.5	100.0						100.0			
31.5	95.7		100.0	100.0	100.0	100.0	98.9	100.0		
25	90.8	100.0	99.6	98.7	99.6	99.6	96.3	98.4	100.0	100.0
19	84.6	98.7	97.6	94.3	95.5	99.4	91.0	96.0	100.0	90.0
16	80.8	97.0	95.4	92.3	93.6	98.4	89.1	92.8		
12.5	76.8	94.7	91.5	87.0	88.2	95.0	84.9	88.4		
9.5	71.8	92.2	87.6	81.3	81.8	89.8	79.6	82.6	90.0	50.0
4.75	59.9	81.7	72.6	64.2	59.8	73.4	65.9	67.8	80.0	35.0
2.36	29.4	57.3	44.4	31.5	23.9	59.6	54.9	56.1		
2	27.7	54.7	42.1	28.8	21.3	56.4	52.2	53.5	65.0	20.0
1.18	22.8	46.7	34.6	22.0	15.0	46.7	42.8	44.8		
0.6	16.7	36.2	25.4	15.0	8.9	29.1	28.2	30.8		
0.425	13.5	30.1	20.7	11.9	6.7	20.4	21.9	23.9	35.0	10.0
0.3	9.4	22.0	15.1	8.3	4.6	12.8	16.6	16.5		
0.15	4.9	11.4	8.1	4.6	2.4	5.3	8.6	8.7		
0.075	3.3	8.3	6.0	3.5	1.7	3.0	4.0	6.1	10.0	3.0

A.2 Proctor Compaction Test

Table A.2: Proctor Compaction Test Results.

	MC (%)	Dry Density (kg/m^3)	MC (%)	Dry Density (kg/m^3)
CR 3 Blend	3.5	1846	4.8	1922
	6.7	1916	6.6	1938
	8.8	1958	8.7	1994
	9.9	1983	10.4	1980
	11.2	1938		
CR 3 Aggregate	9.3	1979	4.2	1827
	12.0	1953	6.1	1899
	13.3	1889	8.2	1934
			9.7	2016
			12.2	1936
CR 3 75%A-25%R	6.3	1921		
	8.8	1964		
	9.8	2012		
	11.8	1927		
CR 3 50%A-50%R	4.1	1836	3.6	1816
	6.8	1900	5.6	1819
	10.2	1949	7.2	1903
	10.9	1942	8.7	1933
			10.3	1941
			10.6	1927
CR 3 25%A-75%R	4.8	1830		
	6.3	1897		
	8.0	1920		
	10.8	1907		

Table A.2: Proctor Compaction Test Results (Continued).

	MC (%)	Dry Density (kg/m^3)	MC (%)	Dry Density (kg/m^3)
TH 200 Blend	3.6	2004		
	4.9	2065		
	6.0	2099		
	8.0	2076		
TH 23 Blend	3.7	1907		
	5.1	1944		
	7.3	2004		
	8.6	1974		
TH 5 Blend	4.7	1952		
	7.1	1971		
	9.0	1992		
	10.1	1974		

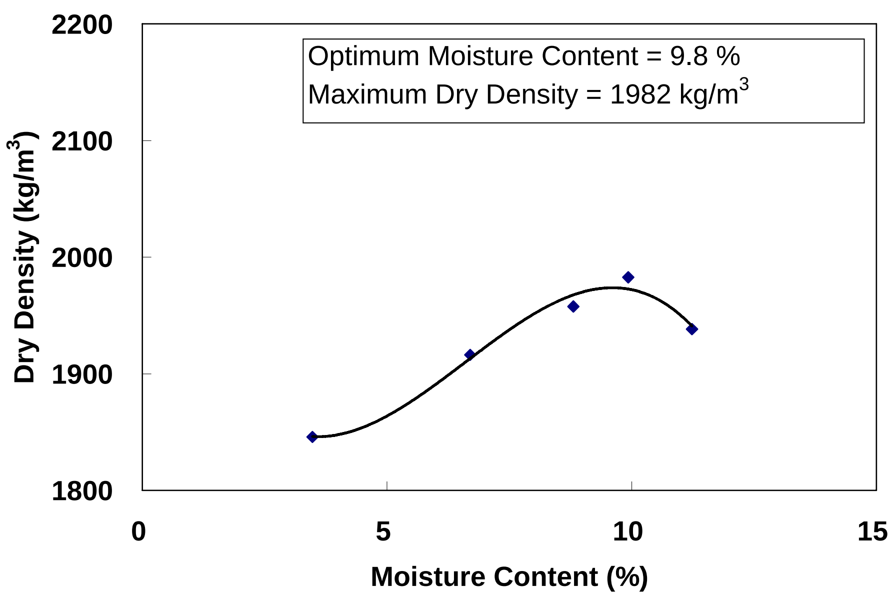

Figure A.1: Proctor Compaction Curve: CR 3 Blend: Test 1.

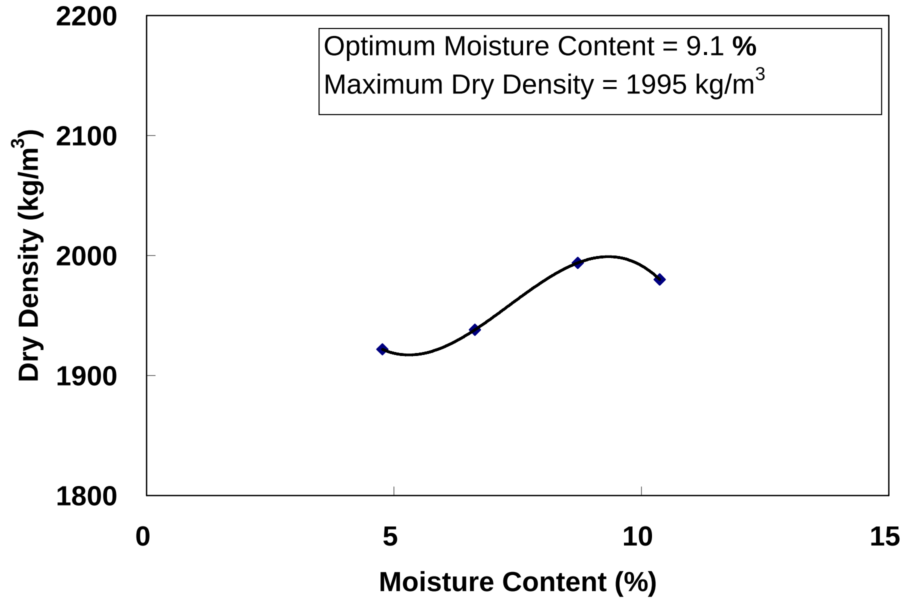

Figure A.2: Proctor Compaction Curve: CR 3 Blend: Test 2.

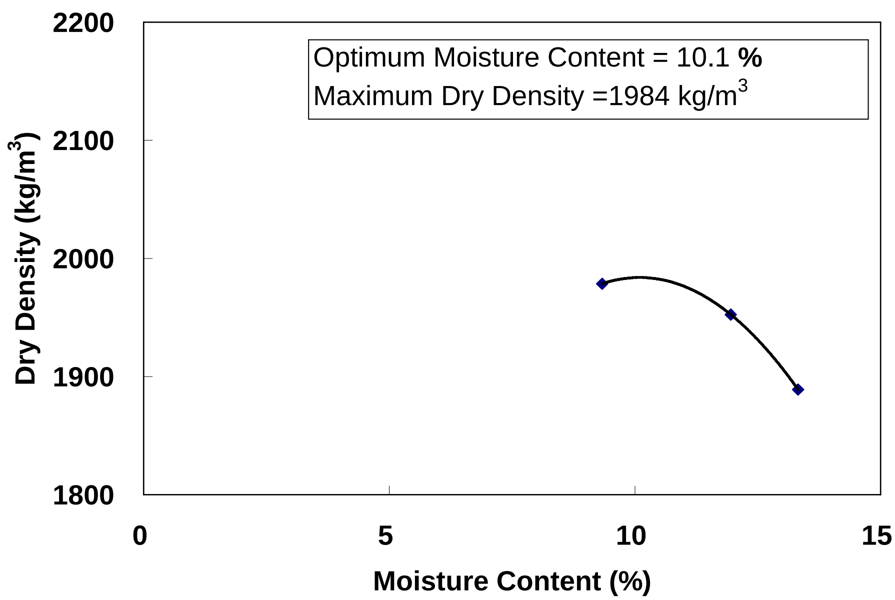

Figure A.3: Proctor Compaction Curve: CR 3 100% Aggregate: Test 1.

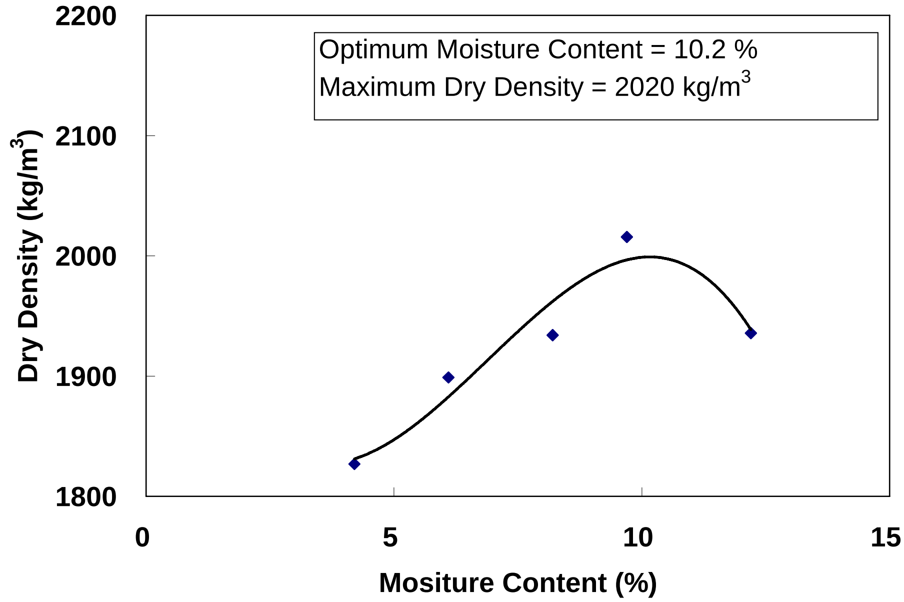

Figure A.4: Proctor Compaction Curve: CR 3 100% Aggregate: Test 2.

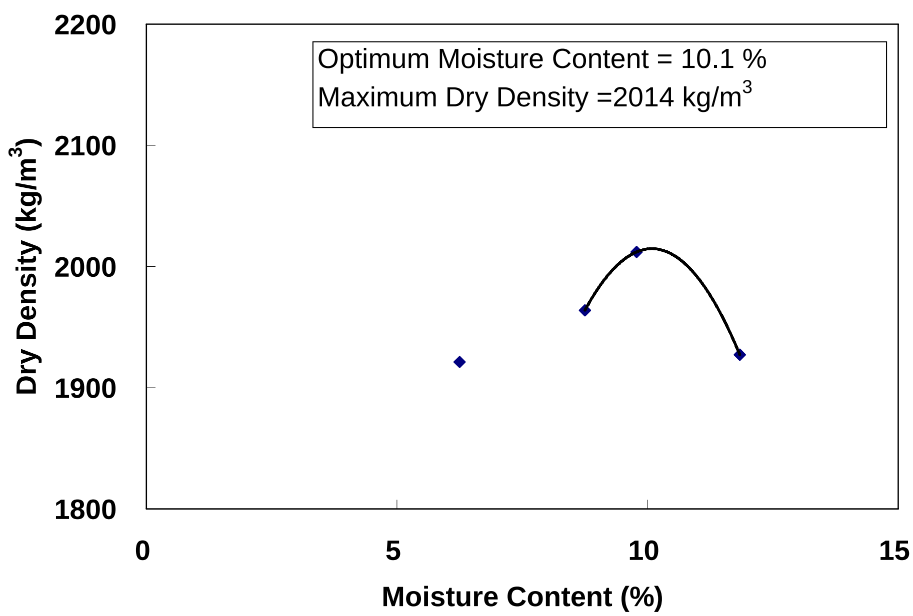

Figure A.5: Proctor Compaction Curve: CR 3 75% Aggregate – 25% RAP.

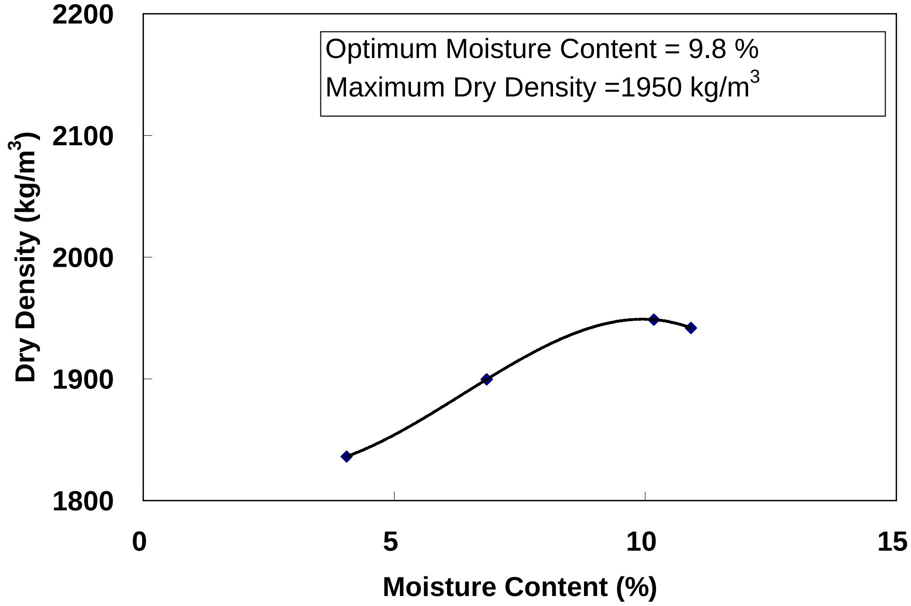

Figure A.6: Proctor Compaction Curve: CR 3 50% Aggregate – 50% RAP: Test 1.

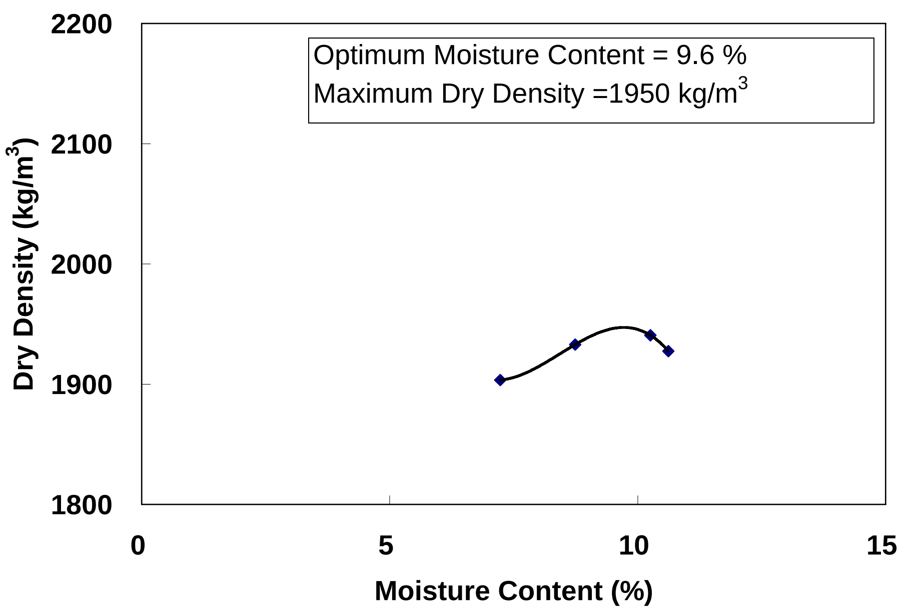

Figure A.7: Proctor Compaction Curve: CR 3 50% Aggregate – 50% RAP: Test 2.

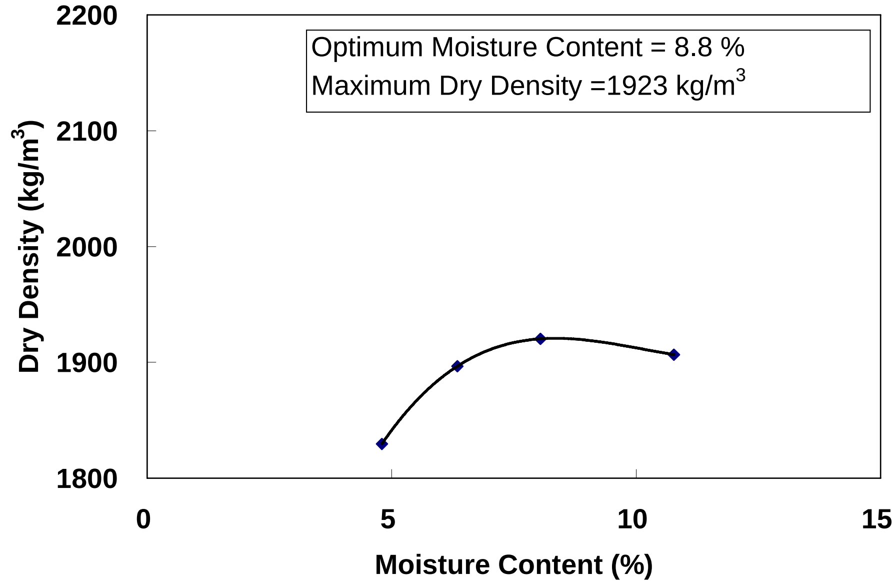

Figure A.8: Proctor Compaction Curve: CR 3 25% Aggregate – 75% RAP.

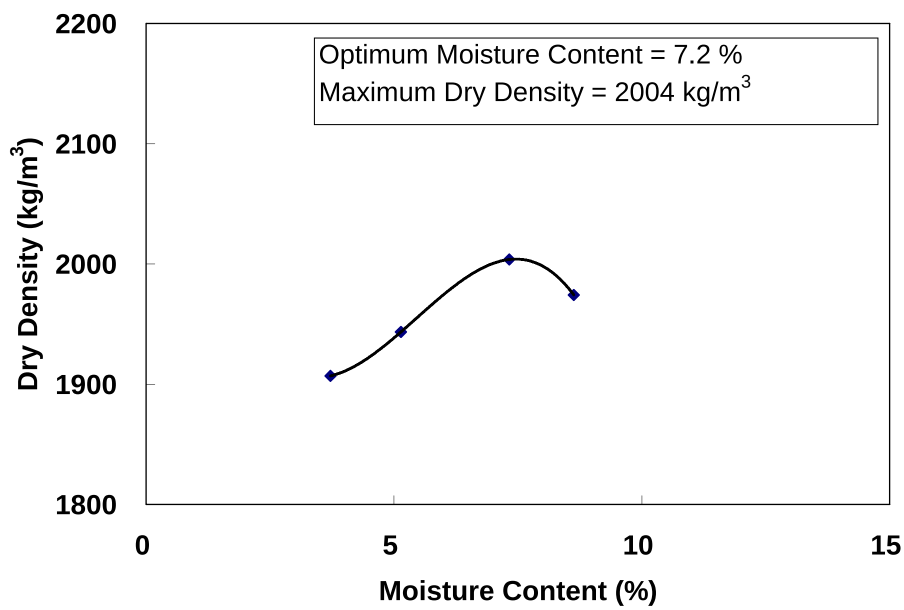

Figure A.9: Proctor Compaction Curve: TH 23 Blend.

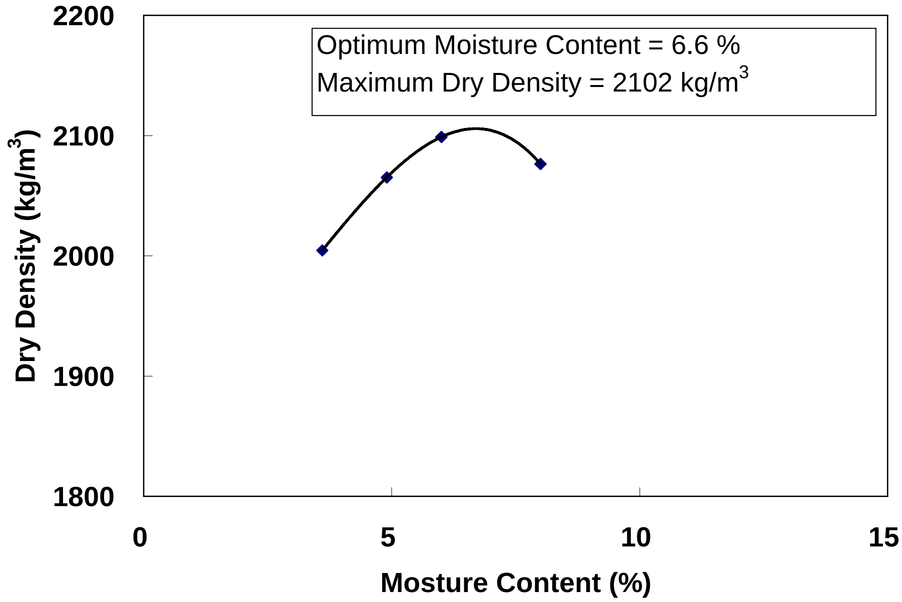

Figure A.10: Proctor Compaction Curve: TH 200 Blend.

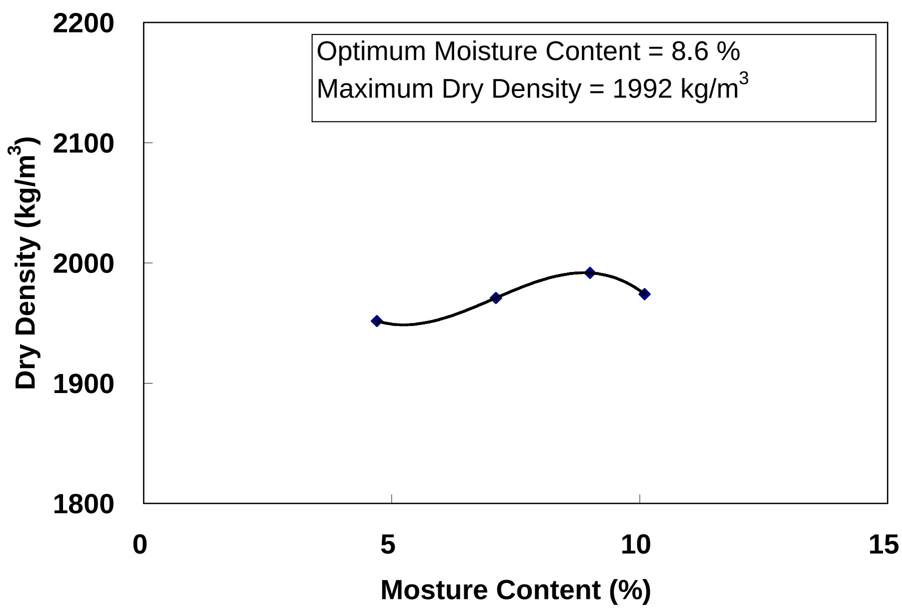

Figure A.11: Proctor Compaction Curve: TH 5 Blend.

ENGLISH UNITS

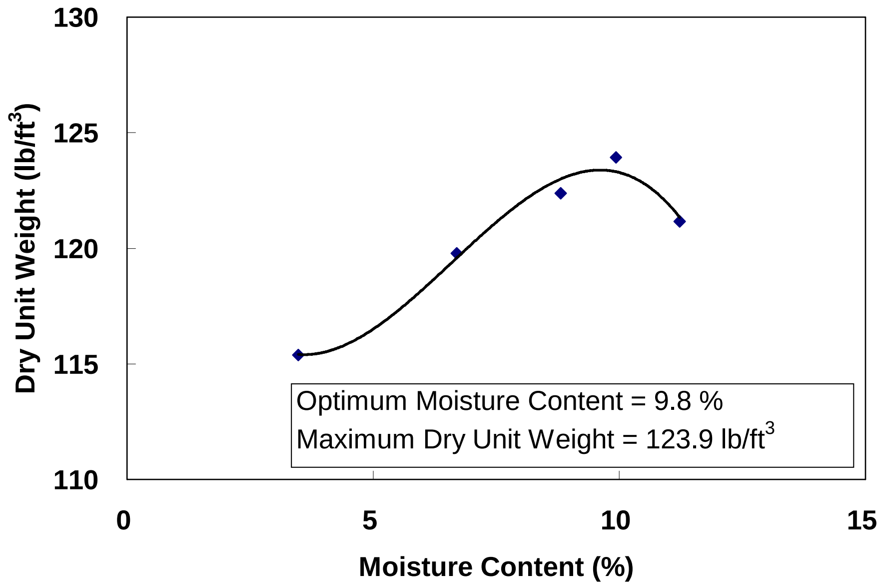

Figure A.12: Proctor Compaction Curve: CR 3 Blend: Test 1.

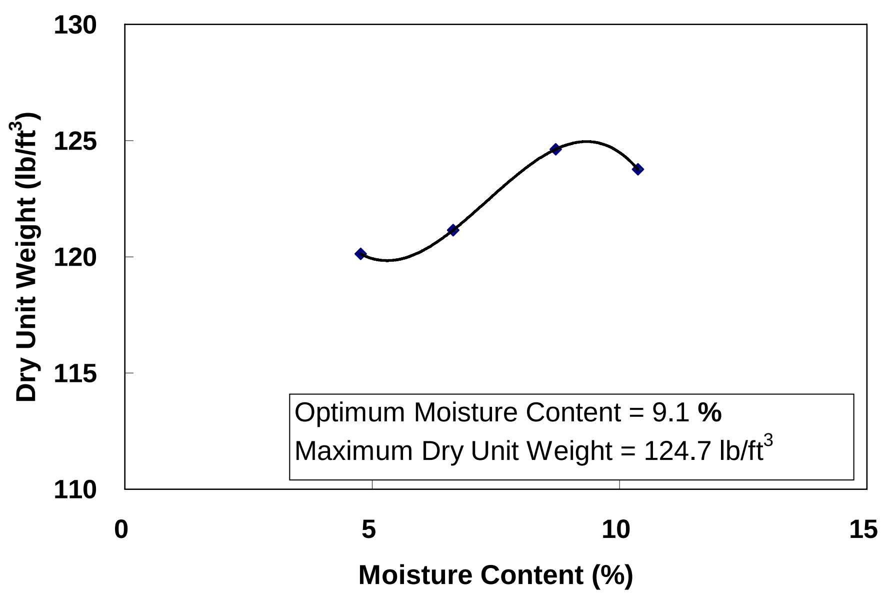

Figure A.13: Proctor Compaction Curve: CR 3 Blend: Test 2.

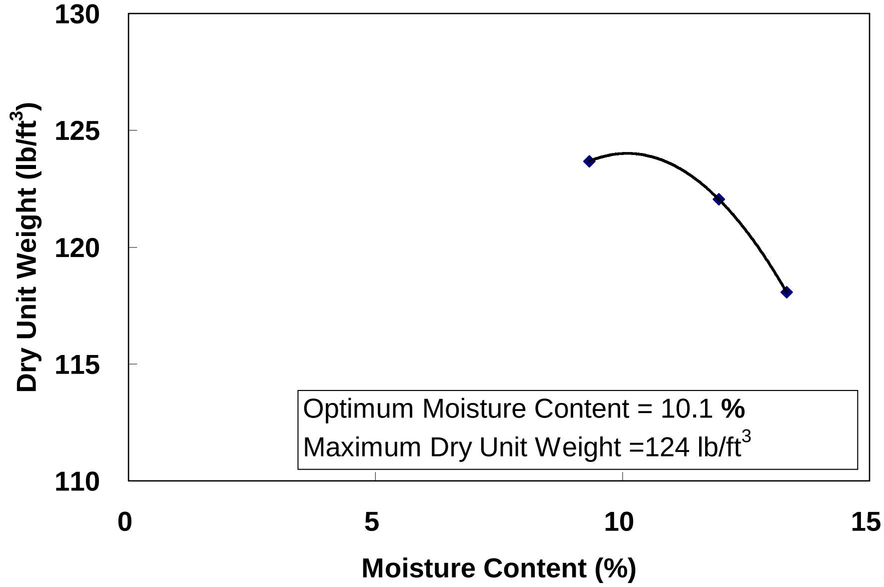

Figure A.14: Proctor Compaction Curve: CR 3 100% Aggregate: Test 1.

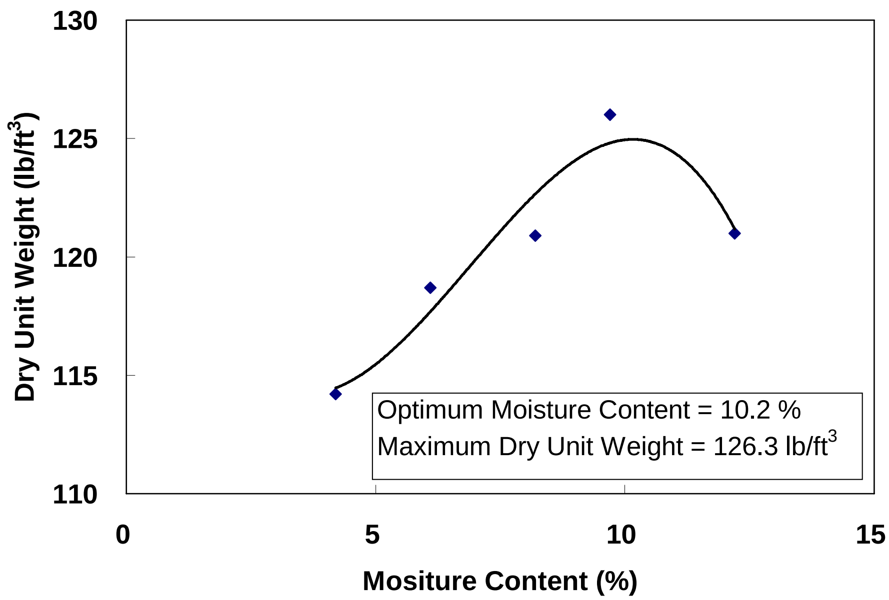

Figure A.15: Proctor Compaction Curve: CR 3 100% Aggregate: Test 2.

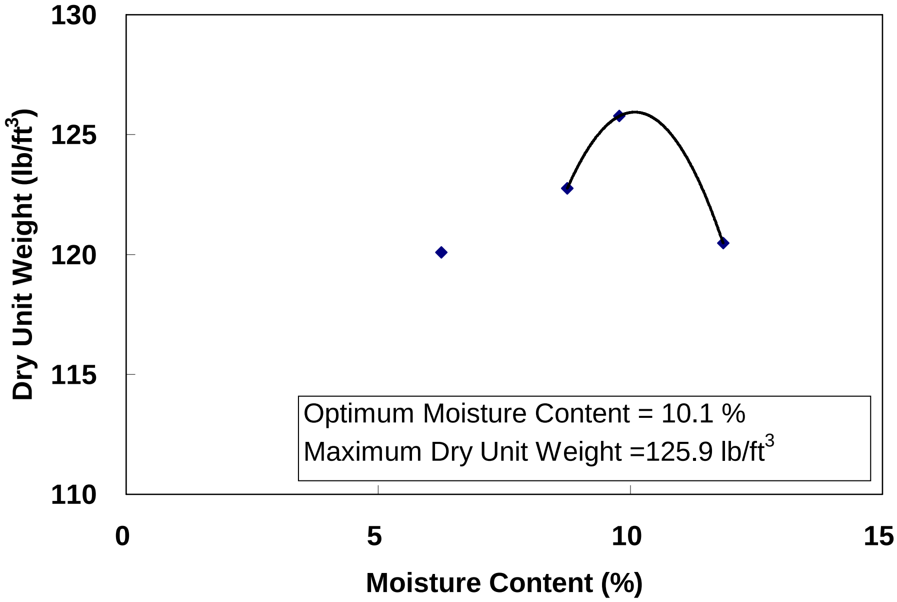

Figure A.16: Proctor Compaction Curve: CR 3 75% Aggregate – 25% RAP.

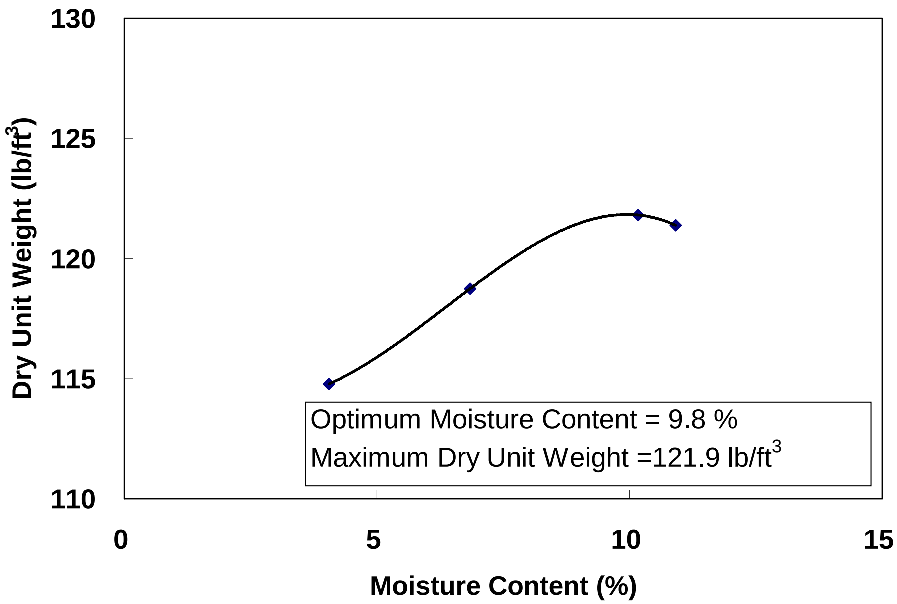

Figure A.17: Proctor Compaction Curve: CR 3 50% Aggregate – 50% RAP: Test 1.

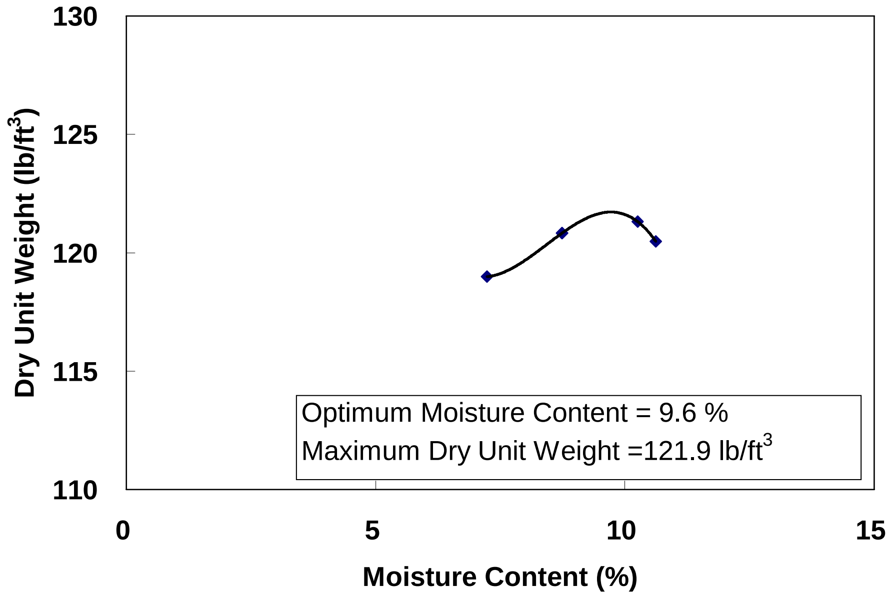

Figure A.18: Proctor Compaction Curve: CR 3 50% Aggregate – 50% RAP: Test 2.

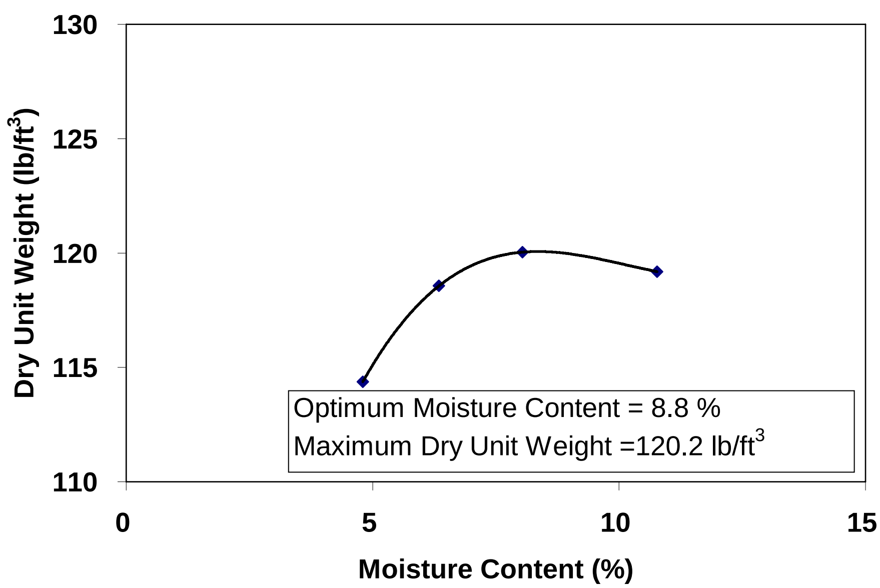

Figure A.19: Proctor Compaction Curve: CR 3 25% Aggregate – 75% RAP.

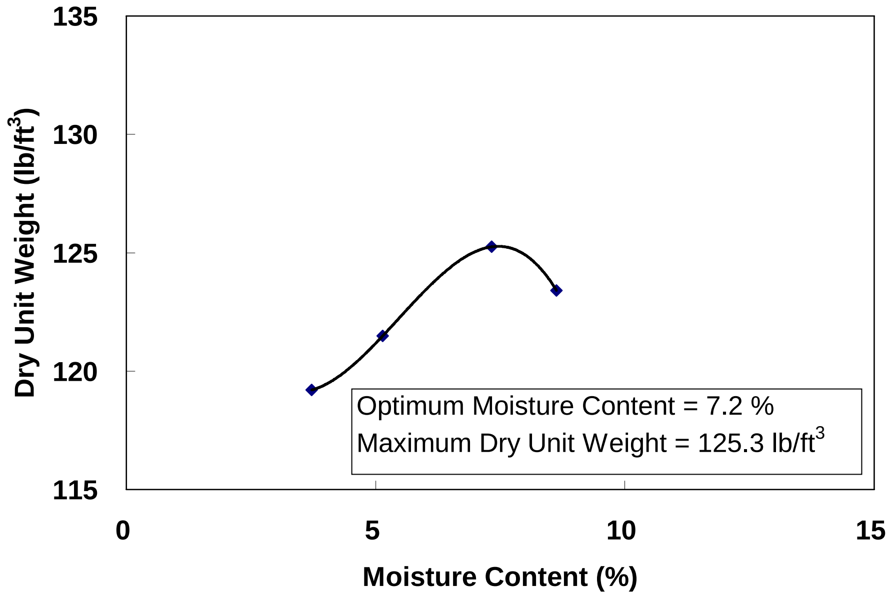

Figure A.20: Proctor Compaction Curve: TH 23 Blend.

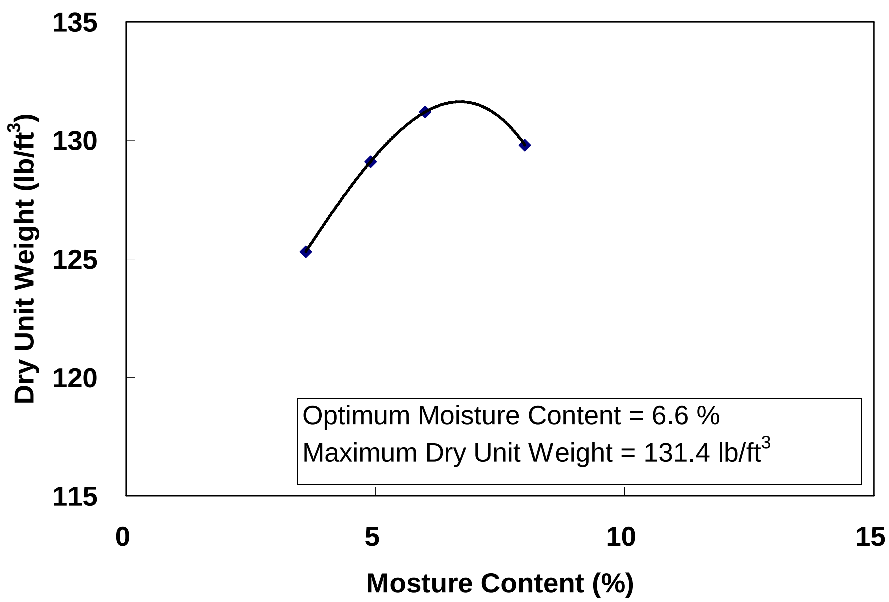

Figure A.21: Proctor Compaction Curve: TH 200 Blend.

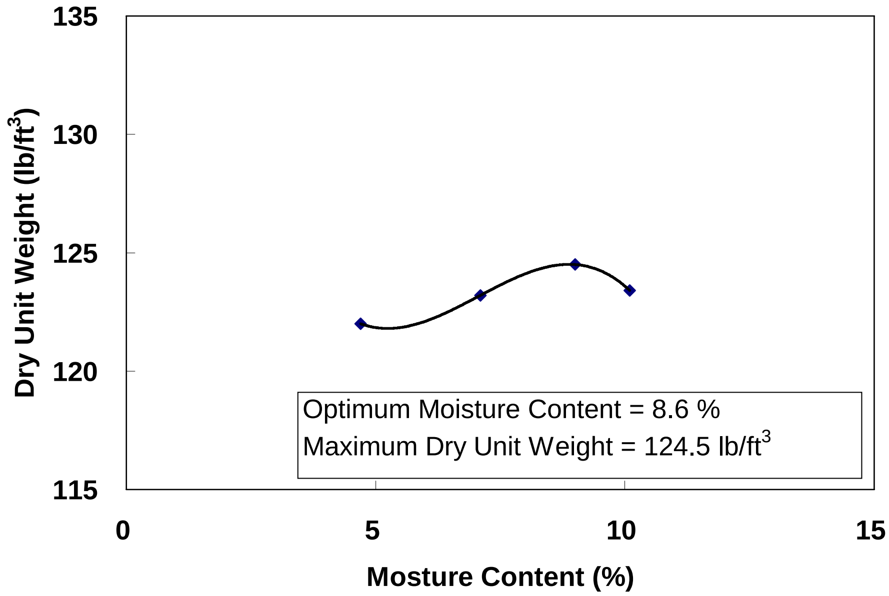

Figure A.22: Proctor Compaction Curve: TH 5 Blend.

A.3 Gyratory Compaction Test

Table A.3: Gyratory Compaction Test Results.

	MC (%)	Dry Density (kg/m^3)
CR 3 Blend	5.0	1968
	5.6	1982
	6.9	2025
	9.7	2006
CR 3 Aggregate	4.8	1902
	6.7	1987
	8.8	2030
	10.5	2004
CR 3 75%A-25%R	4.7	1917
	6.9	2003
	9.0	2036
	10.4	2006
CR 3 50%A-50%R	4.2	1944
	6.0	2001
	8.4	2033
	10.0	2004
CR 3 25%A-75%R	4.4	1947
	6.3	1982
	7.3	2032
	7.9	1995
TH 23 Blend	3.1	2062
	4.8	2091
	6.4	2088
	8.0	2078
TH 200 Blend	3.5	2110
	5.5	2152
	7.6	2123
TH 5 Blend	5.3	2065
	5.5	2081
	6.3	2118
	8.4	2023

ENGLISH UNITS

Table A.4: Gyratory Compaction Test Results.

	MC (%)	Dry Unit Weight (lb/ft^3)
CR 3 Blend	5.0	123.0
	5.6	123.9
	6.9	126.6
	9.7	125.4
CR 3 Aggregate	4.8	118.9
	6.7	124.2
	8.8	126.9
	10.5	125.3
CR 3 75%A-25%R	4.7	119.8
	6.9	125.2
	9.0	127.3
	10.4	125.4
CR 3 50%A-50%R	4.2	121.5
	6.0	125.1
	8.4	127.1
	10.0	125.3
CR 3 25%A-75%R	4.4	121.7
	6.3	123.9
	7.3	127.0
	7.9	124.7
TH 23 Blend	3.1	128.9
	4.8	130.7
	6.4	130.5
	8.0	129.9
TH 200 Blend	3.5	131.9
	5.5	134.5
	7.6	132.7
TH 5 Blend	5.3	129.1
	5.5	130.1
	6.3	132.4
	8.4	126.4

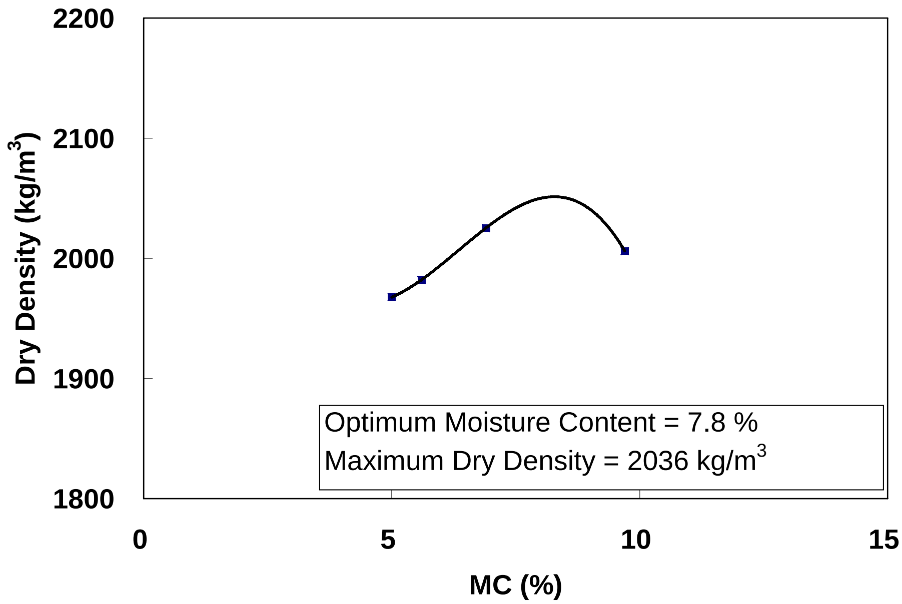

Figure A.23: Gyratory Compaction Curve: CR 3 Blend.

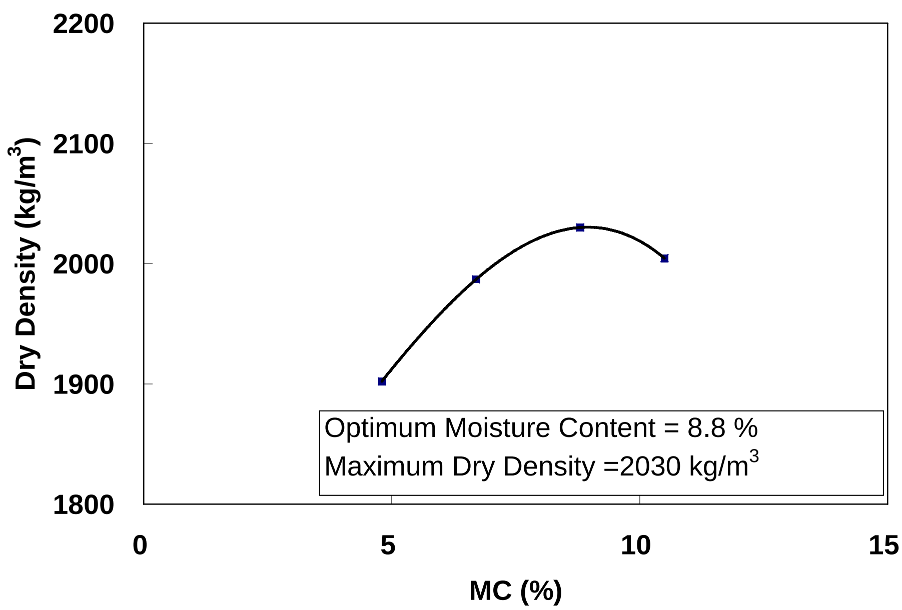

Figure A.24: Gyratory Compaction Curve: CR 3 100% Aggregate.

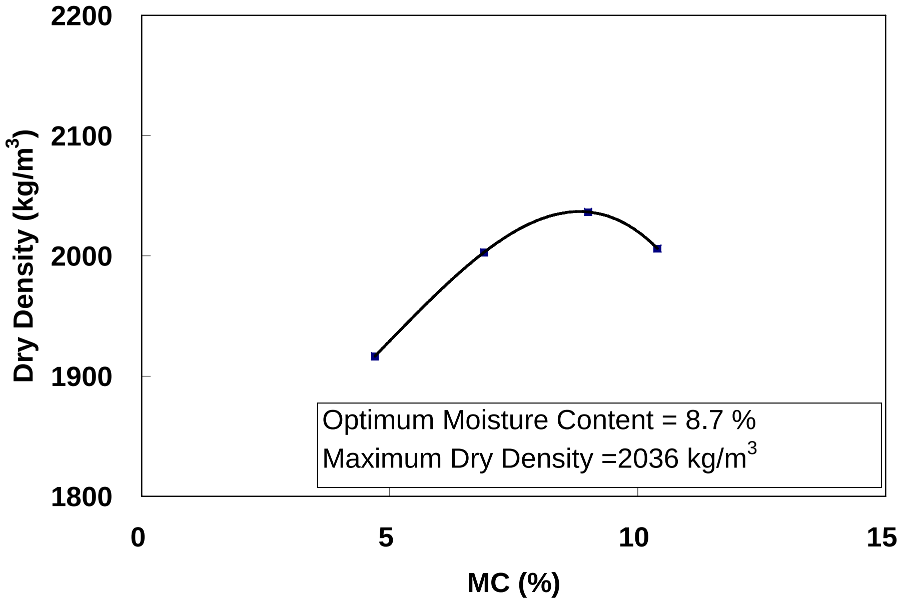

Figure A.25: Gyratory Compaction Curve: CR 3 75% Aggregate – 25% RAP.

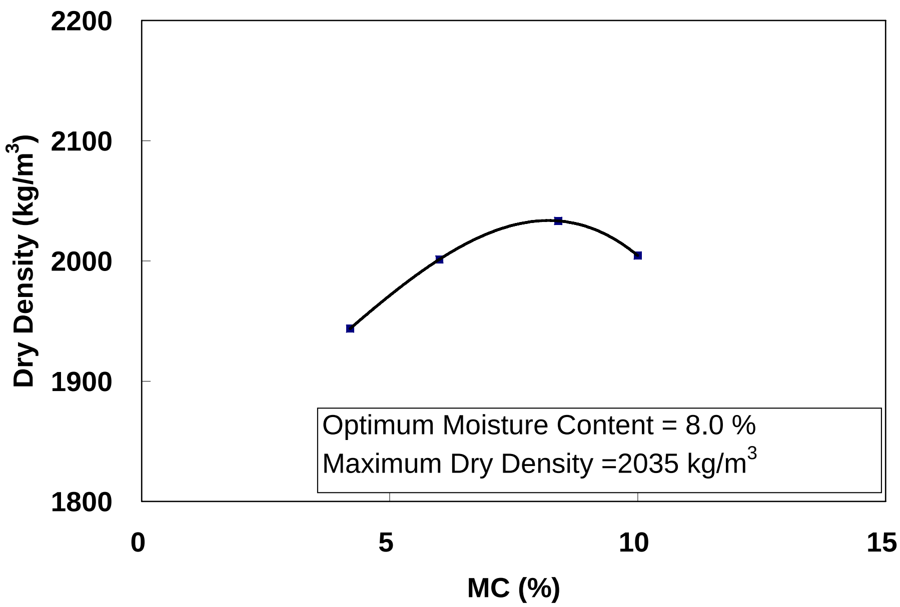

Figure A.26: Gyratory Compaction Curve: CR 3 50% Aggregate – 50% RAP.

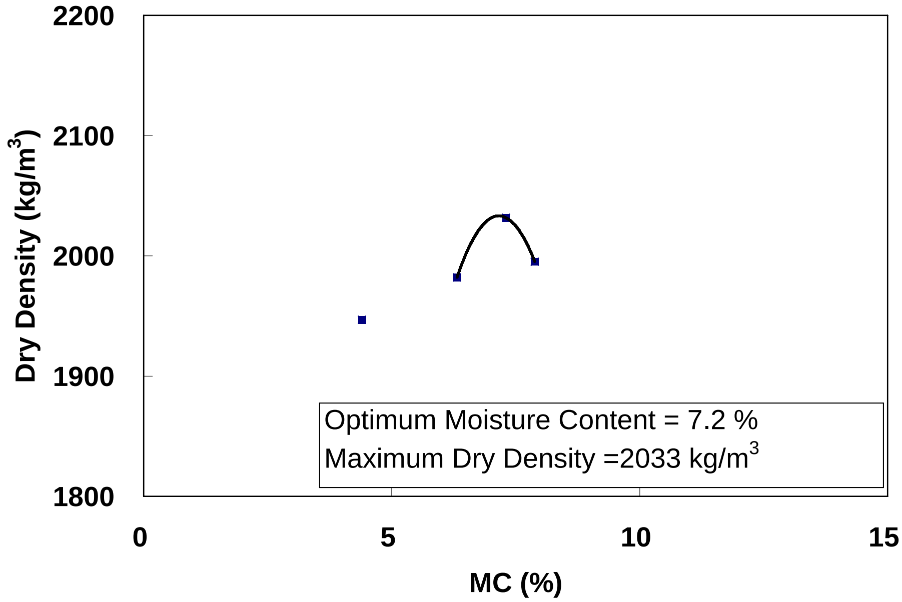

Figure A.27: Gyratory Compaction Curve: CR 3 25% Aggregate – 75% RAP.

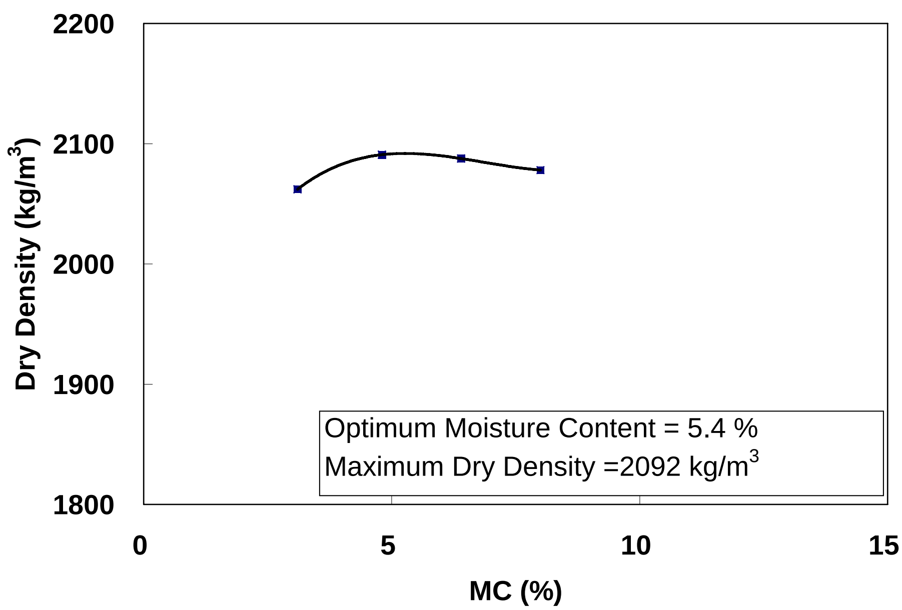

Figure A.28: Gyratory Compaction Curve: TH 23 Blend.

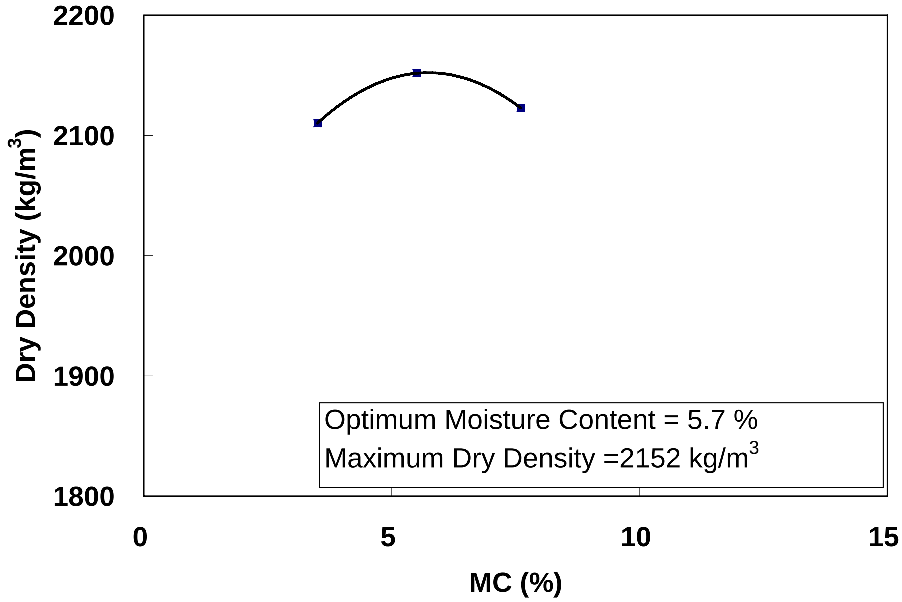

Figure A.29: Gyratory Compaction Curve: TH 200 Blend.

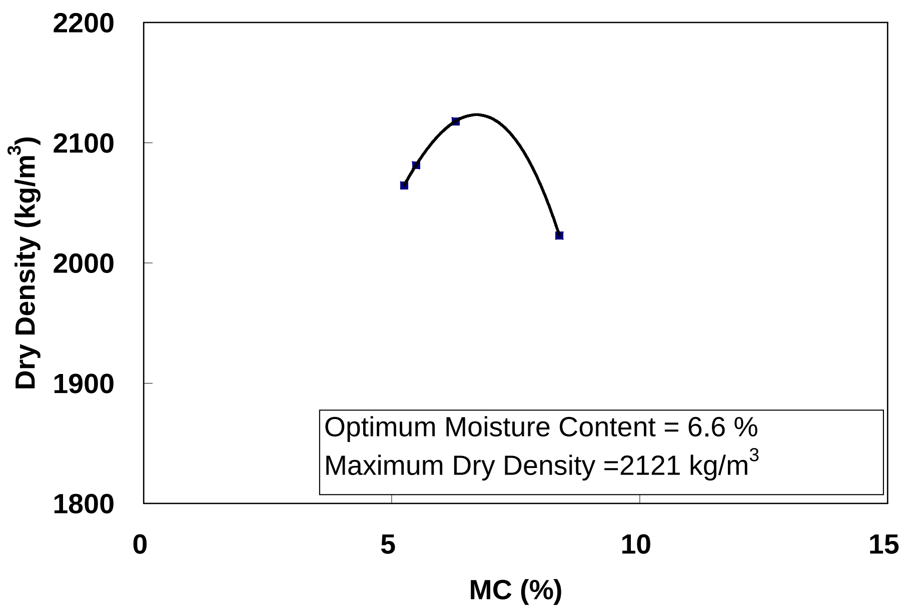

Figure A.30: Gyratory Compaction Curve: TH 5 Blend.

ENGLISH UNITS

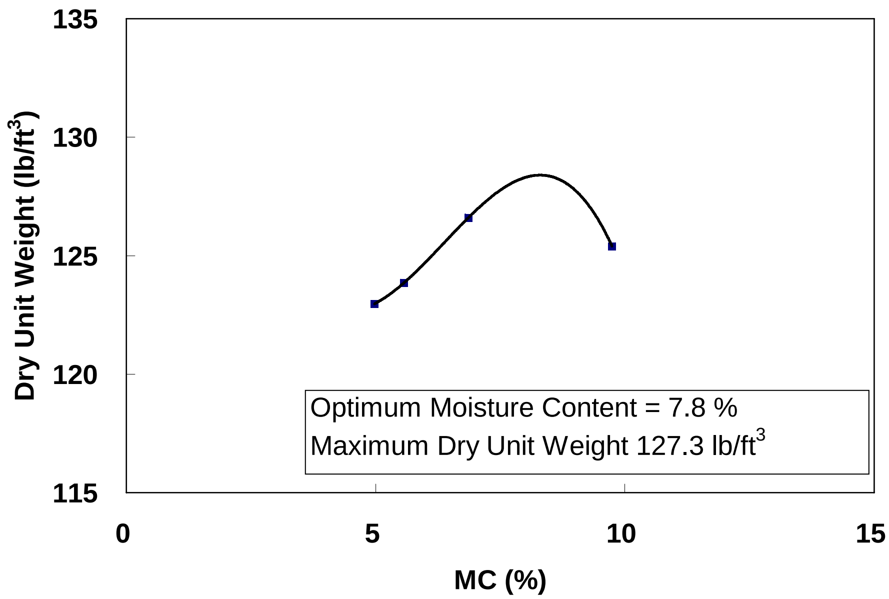

Figure A.31: Gyratory Compaction Curve: CR 3 Blend.

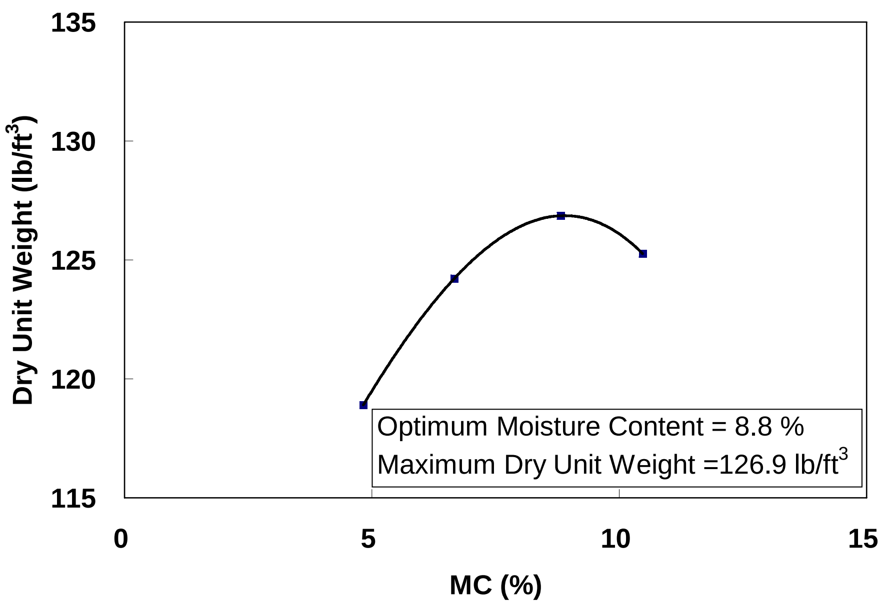

Figure A.32: Gyratory Compaction Curve: CR 3 100% Aggregate.

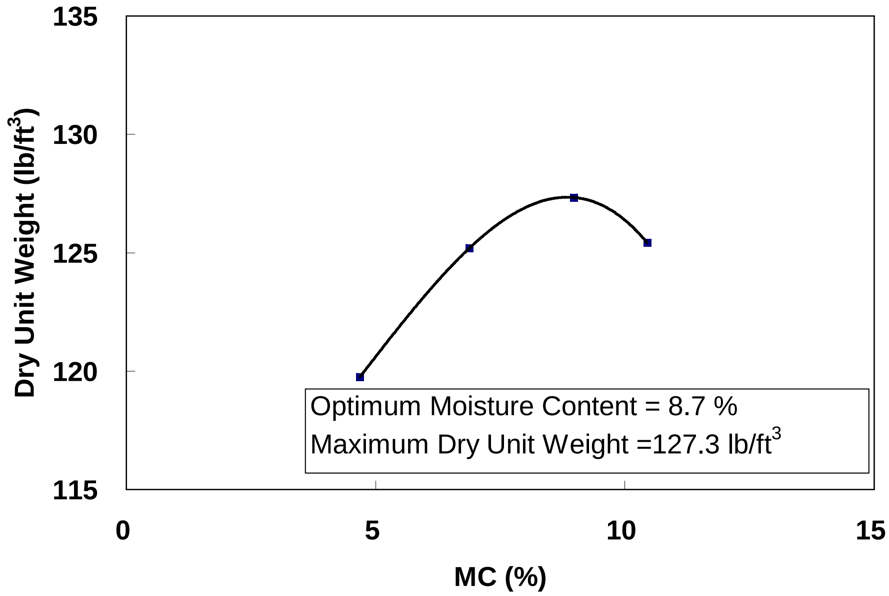

Figure A.33: Gyratory Compaction Curve: CR 3 75% Aggregate – 25% RAP.

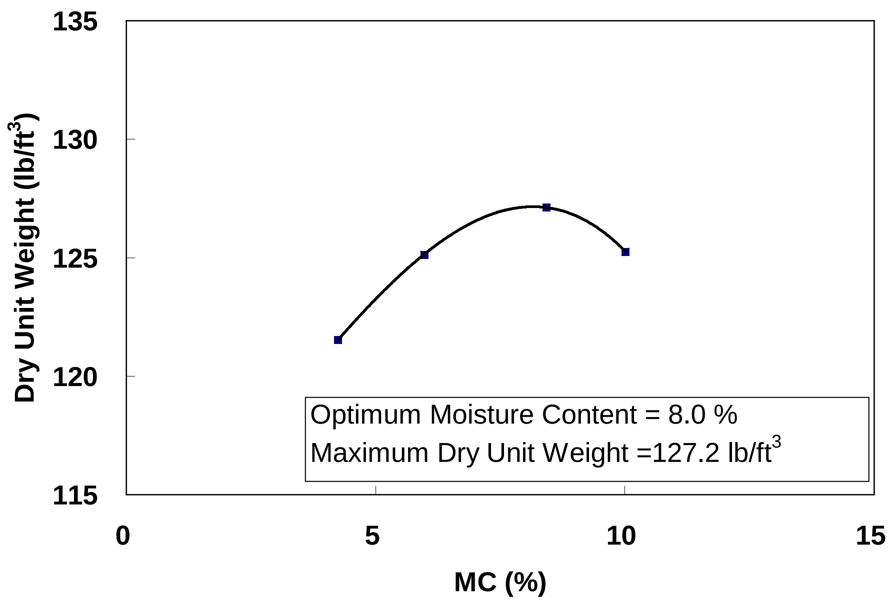

Figure A.34: Gyratory Compaction Curve: CR 3 50% Aggregate – 50% RAP.

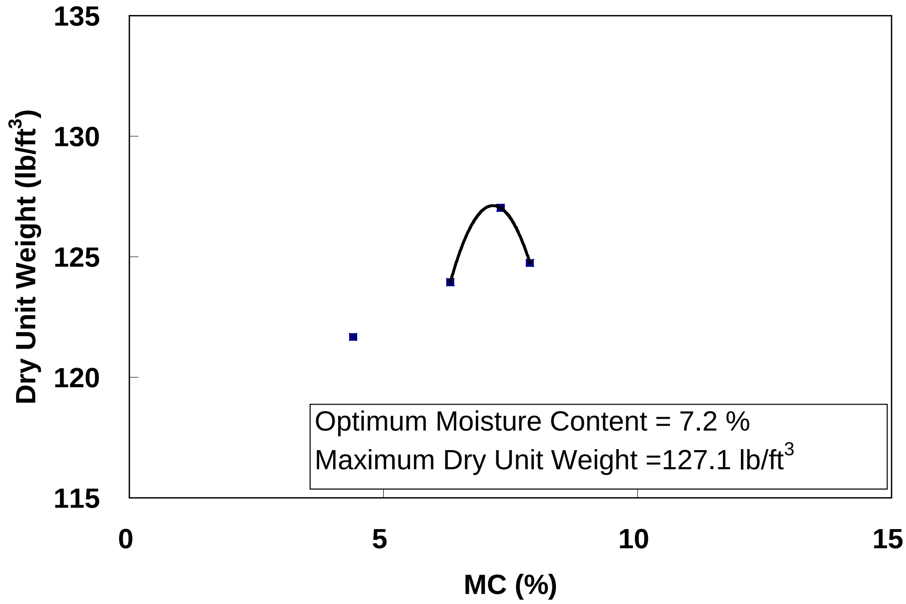

Figure A.35: Gyratory Compaction Curve: CR 3 25% Aggregate – 75% RAP.

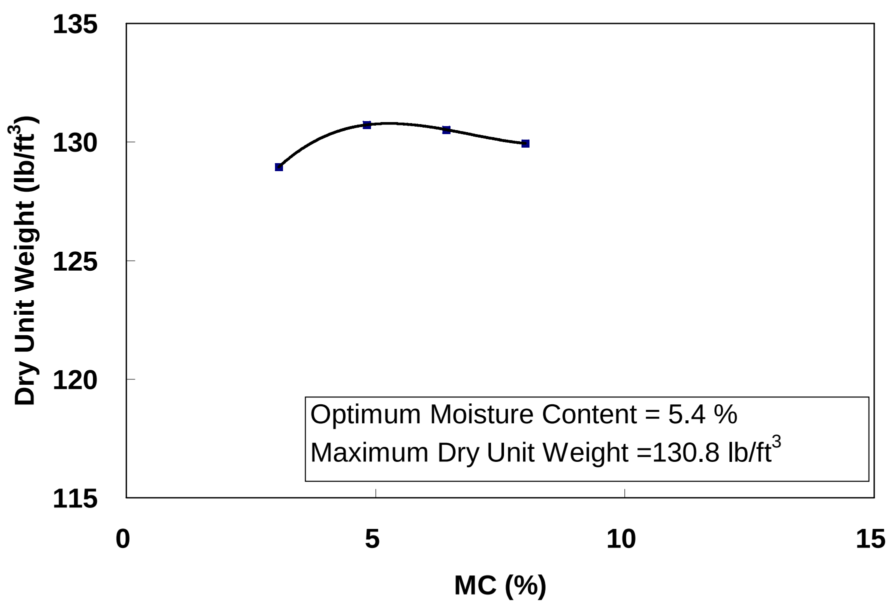

Figure A.36: Gyratory Compaction Curve: TH 23 Blend.

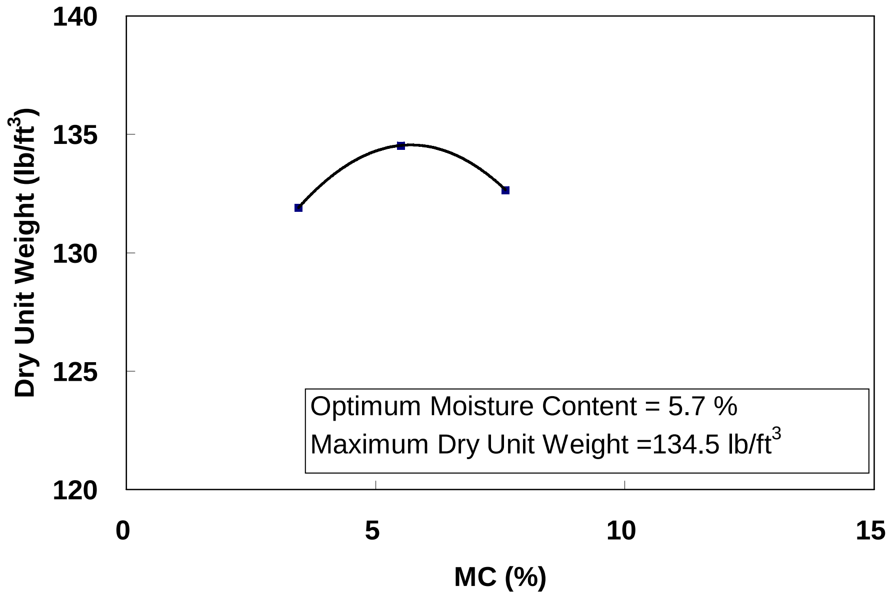

Figure A.37: Gyratory Compaction Curve: TH 200 Blend.

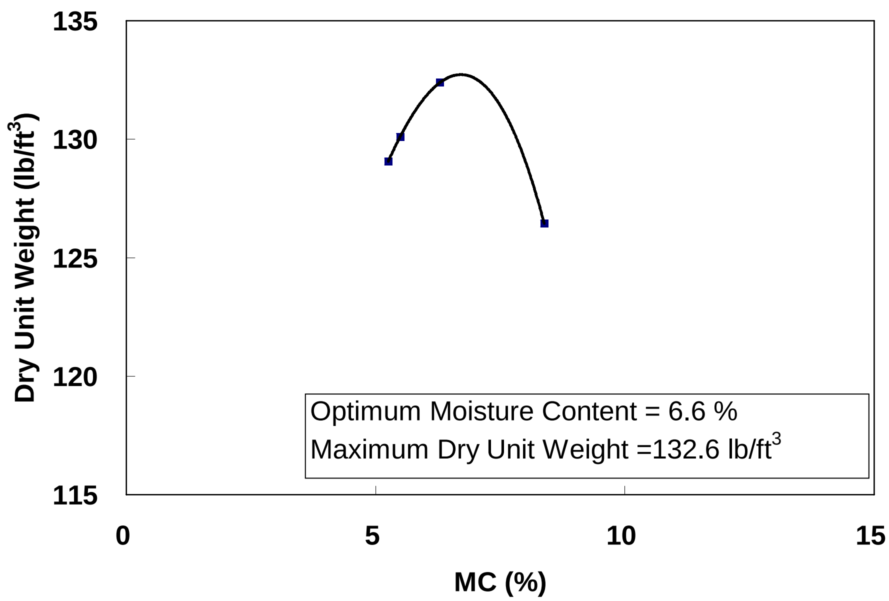

Figure A.38: Gyratory Compaction Curve: TH 5 Blend.

A.4 Zero Air Void Curve

Figures A.20 and A.21 compare the Proctor and gyratory compaction curves of all eight mixtures with the zero air void curve (100% saturation curve, G_s=2.7). As seen here, none of the compaction curves reaches the zero air void curve.

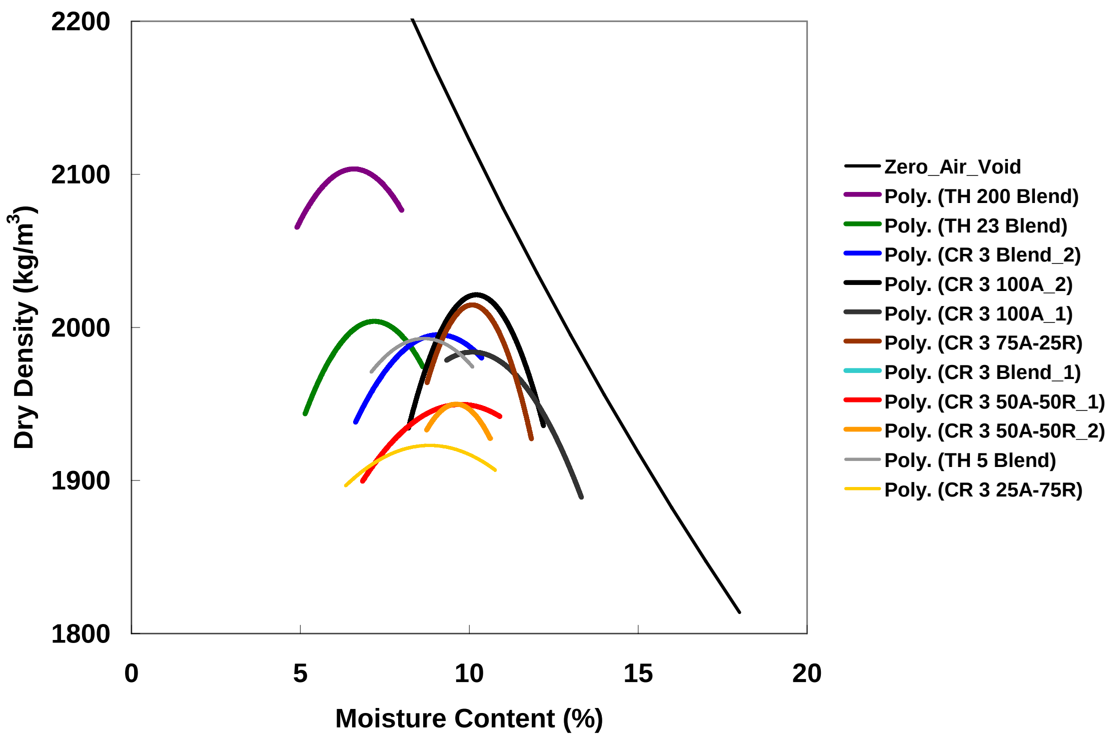

Figure A.39: Proctor Compaction Curves vs. Zero Air Void Curve.

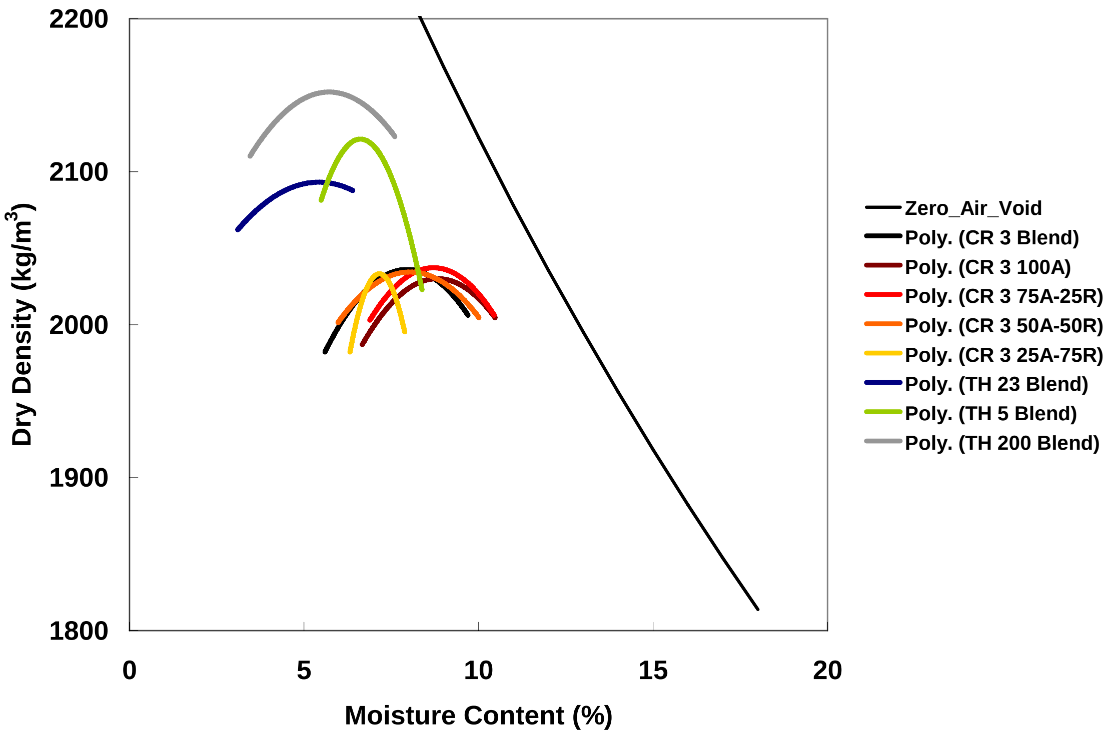

Figure A.40: Gyratory Compaction Curves vs. Zero Air Void Curve.

A.5 Gyratory Compaction Test Procedure

1. Prepare a sample following the procedure described in section 2.1. Dump RAP and aggregate materials into a splitter according to the specified ratio by mass, and mix several (4-6) times until the materials is visually well-mixed.
2. Replace +12.5 mm material with -12.5 mm , +4.75 mm material for material homogeneity.
3. Add water to have moisture content around 3.5%-4.5%.
4. Pour around 5400g of sample to the gyratory mold.
5. Act 50 gyrations at 600 kPa pressure for compaction.
6. Check and record height of the compacted specimen after compaction.
7. Calculate volume and density of the specimen based on the height.
8. Obtain about 200 g of material sample from the center of the mold and dry in an oven at 40^{o}C for 6 days.
9. Break the compacted specimen and pour back into the rest of the sample.
10. Add water to the sample to make the moisture content increase of 1.5%-2%.
11. Repeat steps 4-10 until the density of the compacted specimen decreases.
12. Measure the weight of the oven dried samples, and calculate moisture contents.
13. Calculate dry densities based on the densities and moisture contents.

A.6 Asphalt Extraction

Asphalt extraction tests were conducted by MnDOT on five different mixtures from CR 3 (Table A.4). The tests were done with the samples previously used for M_R and shear strength tests, therefore, aggregates larger than 12.5 mm were already removed. Therefore, the gradation results were less granular than the gradation test results in Appendix A.1. As percent of RAP increased, percent of asphalt extracted increased (Table A.4).

Table A.5: Asphalt Extraction Test Result.

Percent Passing					
Sieve (mm)	CR3 Blend	CR3 100%A	CR3 75%A-25%R	CR3 50%A-50%R	CR3 25%A-75%R
19	99	97	100	100	99
16	98	94	98	100	98
12.5	96	90	96	97	97
9.5	93	88	92	94	96
4.75	86	81	83	86	85
2.36	77	71	72	76	73
2	74	69	69	73	69
1.18	65	60	59	63	59
0.6	52	48	46	49	44
0.425	43	41	38	39	35
0.3	31	30	28	28	26
0.15	16	16	15	13	14
0.075	11.9	12.6	11.8	9.1	10.5
% AC Extracted	**4.5**	**2.3**	**3.6**	**4.4**	**6**

Appendix B

Calibrations

B.1 Load Cell Calibration

Load cell calibration was performed by two proving rings with different load calibration ranges. Table B.1 and Figure B.1 show the result. From Fig. B.1, the difference was less then one percent to each other, and which was less than within ±5 percent difference requirement from LTTP P46 protocol [22].

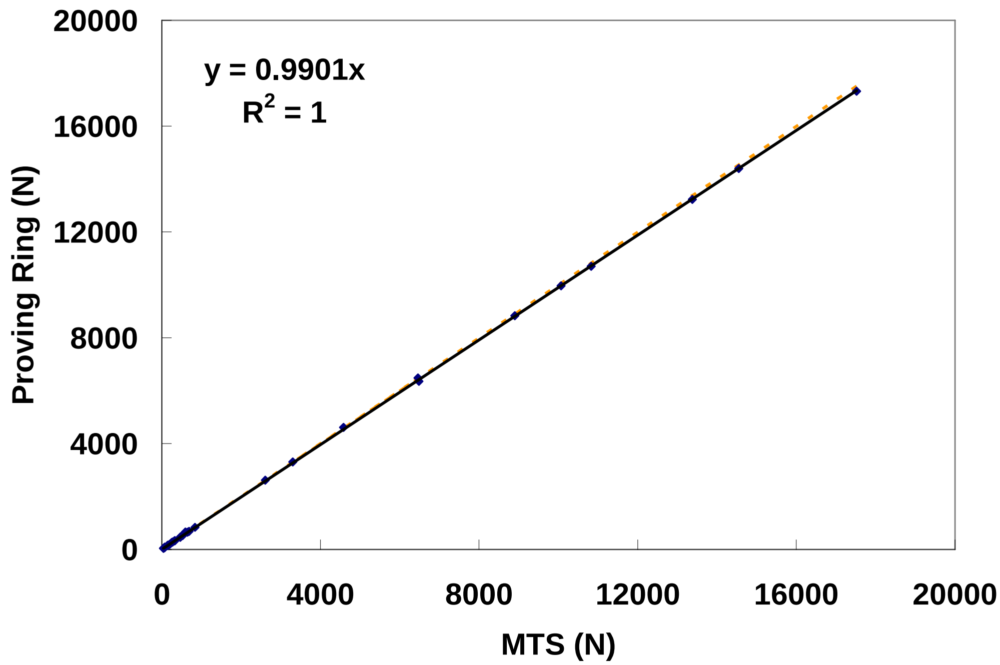

Figure B.1: Load Cell Calibration.

Table B.1: Load Cell Calibration.

MTS (N)	Proving Ring (Divisions)	Proving Ring (N)
42	10	42
155	35	149
277	66	280
467	107	454
688	161	684
44	11	47
69	14	59
72	19	81
72	19	81
146	36	153
170	38	161
205	47	200
255	62	263
324	76	323
333	78	331
480	113	480
526	124	527
651	153	650
840	197	837
592	15	653
2610	60	2611
4580	106	4612
6460	149	6483
17519	398	17317
14547	331	14402
13378	304	13227
10826	246	10704
10069	229	9964
8901	203	8833
6485	146	6353
3300	76	3307

B.2 Data Acquisition System Check

The data acquired from the data acquisition file in the Labview program was compared with the data displayed on the MTS computer. The results are shown in Table B.2 and Figs. B.2 and B.3.

Table B.2: MTS vs. Data Acquisition.

MTS (mm)	Data Acquisition (mm)	MTS (N)	Data Acquisition (N)
713	714	240	251
777	779	556	568
791	791	1263	1268
794	794	2548	2570
797	797	3550	3565
780	782	4970	4998
574	574		

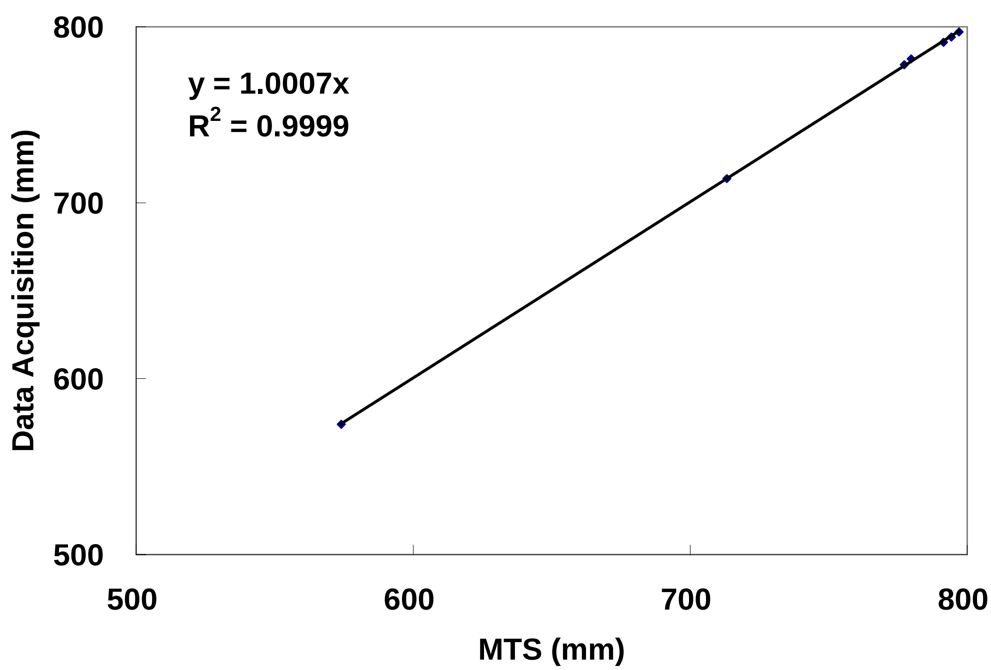

Figure B.2: MTS vs. Data Acquisition: Stroke.

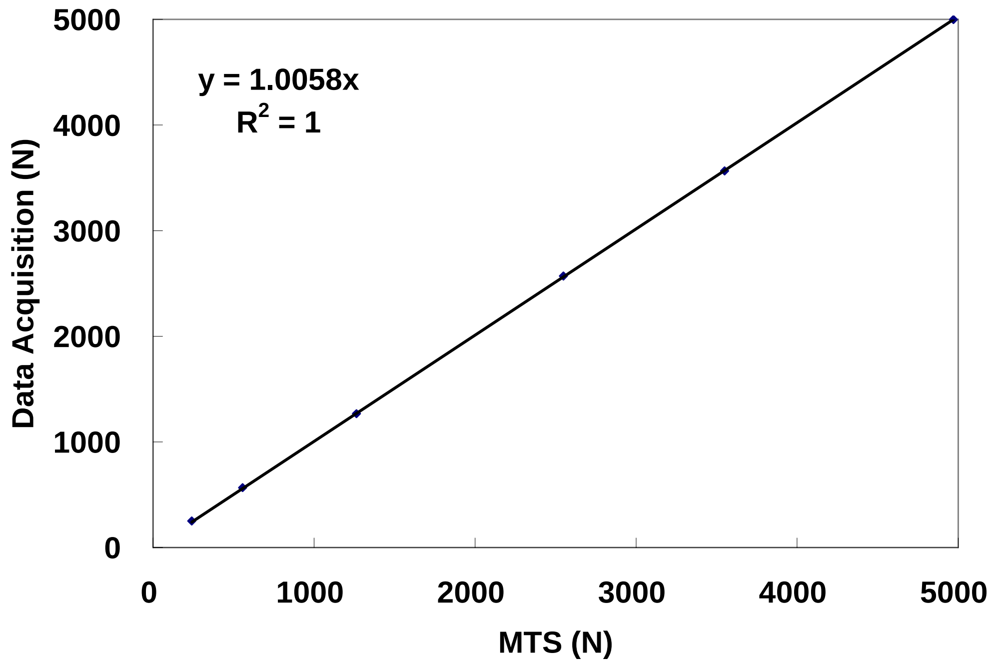

Figure B.3: MTS vs. Data Acquisition: Load.

B.3 LVDT Calibration

Sensitivities of three LVDTs were calibrated by the measurements shown in Fig. B.4. The voltage measurement measures voltage change per unit displacement of stroke measurement, and the sensitivity can be calculated by the slope of voltage change per unit displacement. Detail results are in Table B.3 and Fig. B.5.

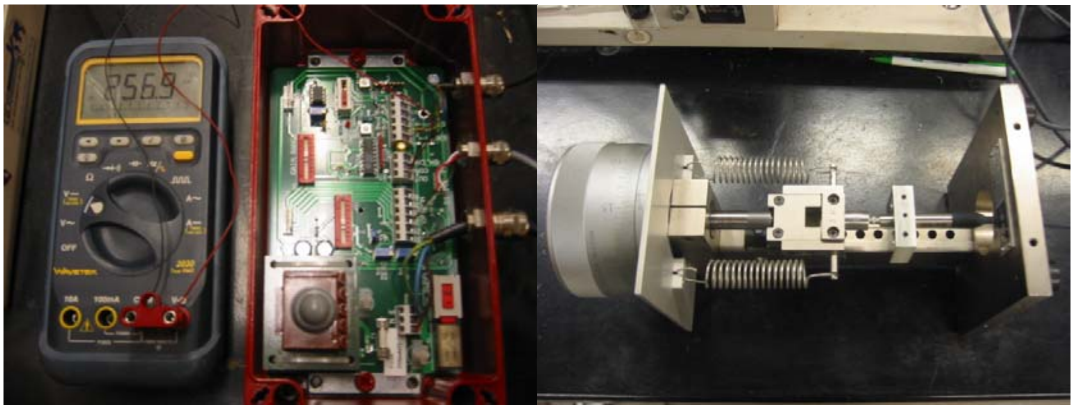

Figure B.4: Voltage Measurement, Conditioner (Left) and Stroke Measurement (Right).

Table B.3: Calibration Results.

Conditioner	**LVDT1**		**LVDT2**		**LVDT3**	
LVDT#	**81353**		**79028**		**78581**	
	V	mm	V	mm	V	mm
	-12.140	0.0	-10.080	0.0	-12.988	0.0
	-9.632	0.5	-7.835	0.5	-10.800	0.5
	-7.152	1.0	-5.616	1.0	-8.560	1.0
	-4.681	1.5	-3.405	1.5	-6.300	1.5
	-2.184	2.0	-1.170	2.0	-3.999	2.0
	0.348	2.5	1.096	2.5	-1.728	2.5
	2.958	3.0	3.431	3.0	0.500	3.0
	5.467	3.5	5.676	3.5	2.790	3.5
	7.991	4.0	7.935	4.0	5.016	4.0
			10.274	4.5	7.225	4.5
			12.538	5.0	9.446	5.0
			14.650	5.5	11.741	5.5
					14.165	6.0
Sensitivity	5.036	V/mm	4.519	V/mm	4.514	V/mm
± Range (mm)	2.5	mm	2.5	mm	2.5	mm
± Range (V)	15.1068	V	13.5567	V	13.5417	V
R^2	1		1		1	

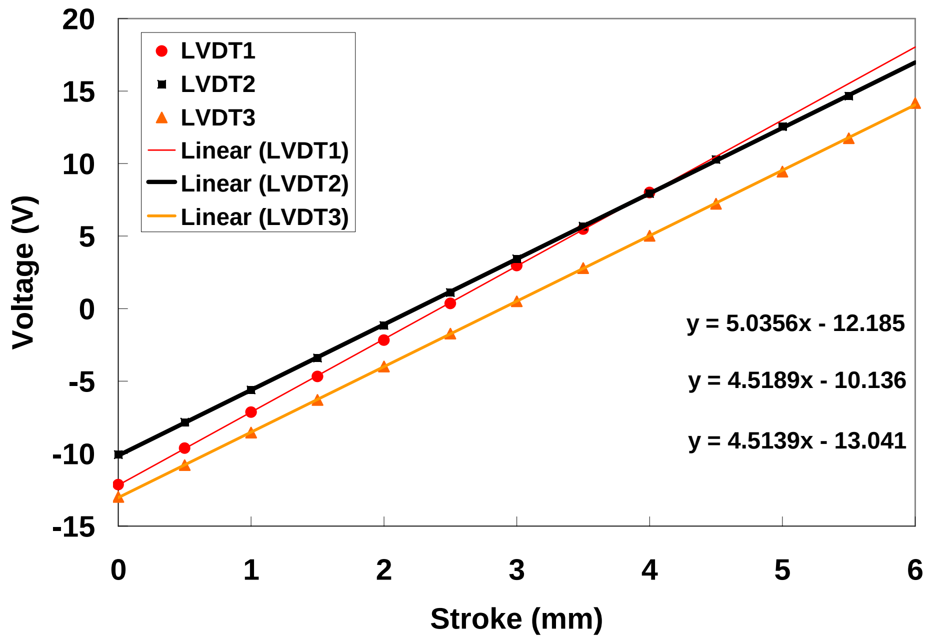

Figure B.5: Calibration Results.

B.4 LVDT Clamp Weight

From the NCHRP 1-28A testing protocol, the maximum LVDT clamp weight requirement for 152 mm diameter testing specimen is 2.4 N [8]. The upper clamp had 2.4 N weight, however, the lower clamp had its weight of 3.6 N, which exceeded the requirement.

B.5 Dynamic Response

This section presents the results of the system check performed on the resilient modulus testing equipment utilized by the Department of Civil Engineering of the University of Minnesota. The verification generally follows the procedure recommended by the LTPP Protocol 46 [11]. The main goals are to quantify the overall machine response by estimating the phase angle between load and displacement, as well as the attenuation in the load amplitude. The method followed is briefly described, results from a previous study analyzed, and results of the new system verification are presented and discussed.

Phase Angle Estimation

The approach follows the procedure described in [11]. In this approach, the phase angle introduced by the entire system (machine, electronics and sensors) is evaluated, in a least-square sense, from a series of measurements. The topic of attenuation of the load amplitude is not addressed in [11].

Procedure
As a reminder, the procedure in [11] is based a series of sweep sinusoidal loading experiments with:

- Use of a proving ring in place of the specimen, the load cell and 2 LVDTs usually utilized in the resilient modulus tests (LVDT1 and LVDT2).
- Application of 100 cycles of a sinusoidal load with a peak-to-peak amplitude of 1.33 kN and an average of 1.11 kN, using the resilient modulus testing system controls.
- Recording load and deformation measurements for the last 5 cycles.
- 3 frequencies: 1, 5 and 10 Hz with corresponding sampling frequencies of 200, 1,000 and 2,000 Hz.

Data Analysis
The analysis is based on the sole assumption that the system is linear. For such a system, it is well known that a steady-state sinusoidal input results in an output that is also sinusoidal, with identical frequency but possibly shifted in time and with a different amplitude (attenuated or amplified). In addition one can also include a shift in the base level (DC component). In other words, if the input is a sinusoidal signal of amplitude A_x and frequency $\omega = 2\pi f$, i.e.

$$x = A_x \sin(\omega t) \tag{B.1}$$

then the output can be written as

$$y = A_y \sin(\omega t + \varphi) + b \tag{B.2}$$

where φ is the phase angle, A_y the amplitude, and *b* a shift in the DC response. The amplification factor between input and output is

$$K = \frac{A_y}{Ax} \tag{B.3}$$

It can easily be shown that (B.2) is equivalent to

$$y = C\sin(\omega t) + D\sin(\omega t) + b \tag{B.4}$$

with

$$A_y = \sqrt{C^2 + D^2} \tag{B.5}$$

and

$$\varphi = a\tan\left(\frac{C}{D}\right) \tag{B.6}$$

Note that the temporal delay τ [s] is obtained from the phase angle φ [^{o}] using

$$\tau = \frac{\varphi}{360 f} \tag{B.7}$$

Defining new variables x_1 and x_2 as

$$m_1 = \sin(\omega t), \quad m_2 = \cos(\omega t) \tag{B.8}$$

allows one to rewrite (B.4) as

$$y = m_1 x_1 + m_2 x_2 \tag{B.9}$$

which can be solved for an unknown *y*, and known (measured) x_1 and x_2, in a least square sense.

More precisely, x_1 and x_2 are computed for each time step. The least square fitting is applied separately three times: to the load, the displacement measured by LVDT1, and that measured by LVDT2, which constitute the unknowns *y* for each data fitting. Resulting from each data set, one obtains phase angle, amplitude gain and DC offset pertaining to the load cell and to each LVDT, with respect to the digital input. Finally, phase angle between load cell and LVDTs is obtained by subtraction of the corresponding phase angle with respect to the digital input. Similarly to the procedure in [11], the program *Microsoft Excel* is used for this study to perform the calculations, the function *Linest* being utilized for the least-squares fitting.

Previous Results

Preliminary results were obtained in 2004 by Davich et al. [12]. However, to cater with the only data available at the time, the approach followed for the 2004 study did not strictly follow the protocol in [11]. Indeed, the driving (input) signal was a haversine constituted of 1/10th second (0.1 s duration load pulses and 0.9 s of rest) with a peak load of 276 kPa. The data were analyzed by assuming a sinusoidal input with frequency of 5 Hz and by using only the data corresponding to one loading period (i.e. 0.1 s) of the measured input.

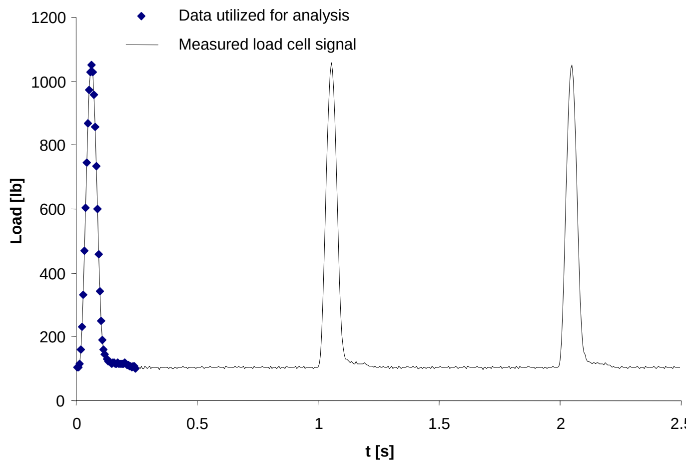

Figure B.6: Cycles Considered for The Analysis in [12] – Force Load Time History.

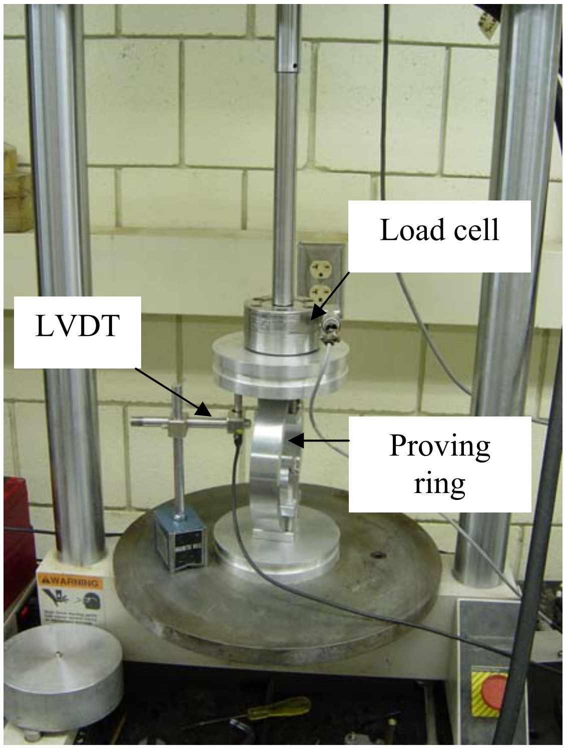

Figure B.7: Testing Setup.

New Phase Angle Verification

The present testing campaign was conducted according to the specifications in [11]. However, a few modifications were necessary to adapt the technique to the equipment utilized.

Test Setup

As shown in Fig. B.7, tests are performed on a proving ring. Load and displacement are measured using a load cell and a Linear Variable Differential Transformer (LVDT), respectively. Because the software of the control system allows only for forcing signal based on ramp, step and haversine segments, using a simple sine input was not possible. Therefore, haversine oscillations were utilized. Fortunately, the data analysis described for sine input can be directly applied to haversine signals. This can be readily shown using the superposition property of the linear system and the definition of haversine,:

$$hav(\theta) = \frac{1 - \cos(\theta)}{2} \tag{B.10}$$

Data Interpretation and Results

Three series of tests, each composed of one test at 1 Hz, one test at 5 Hz and one test at 10 Hz, were conducted. Series 1 includes tests 1 to 3, series 2 contains tests 4 to 6, and series 3 consists of tests 7 to 9. Each series corresponds to an independent test, as the location of the LVDT is changed from one test series to another. Also, the proving ring is removed and repositioned in-between each test series.

Figure B.8 illustrates how the five cycles considered in the fitting process were selected from the end of the recording of the measured data. For example, the first cycle is located between peaks number 1 and 2. The data analysis is performed on each of the five cycles.

Table B.4 shows the average results and maximum variation for the phase angle (in degrees) and corresponding average time delay (in milliseconds) between the load cell and the LVDT. Results for series 1 and 2 present phase angles smaller than 1.5 degrees. They also show a good consistency in the phase angle estimate, within approximately 0.5 degrees. Series 3 exhibits slightly higher values for the phase angle, up to about 2.29 in average and about 3.03 for the last cycle at 10 Hz. The outstanding deviation of 0.79 reported for test 9 in Table 1 is also due to this particular cycle. Disregarding the fifth cycle in test 9 would yield an average phase angle of - 2.11 +/- 0.61 degrees.

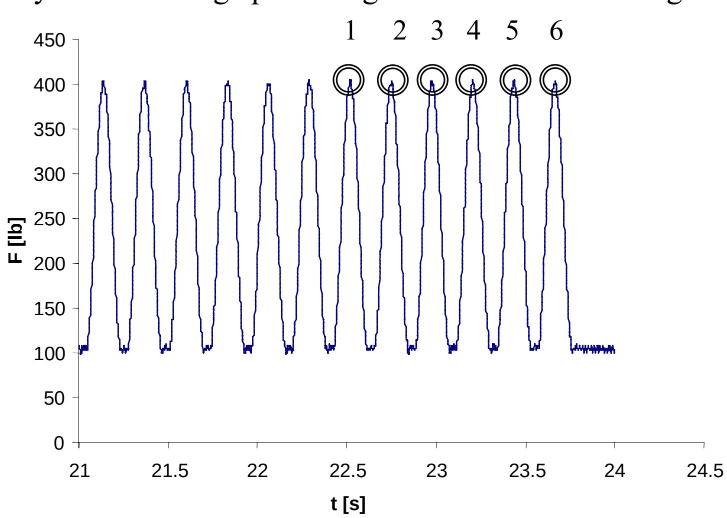

Figure B.8: Cycles Considered in The Present Work – Measured Load with 5 Hz Input.

Additional Results

Using the same series of data than for the phase angle verification, one can also extract some information pertaining to the reduction in amplitude between peak load specified as input in the system's controls and peak load measured by the load cell. The attenuation or gain in amplitude is given by

$$G = \frac{A_y + b}{A_{input}} \tag{B.11}$$

where A_{input} is the amplitude of the specified haversine oscillation (1.775 kN, i.e. 399 lb, as suggested in [11]). The values of A_y and b are those computed in the least squares fitting process. Table B.4 shows the average values for the gain over the five cycles for each test. It can be seen that the gain estimates in each series are consistent. These results exhibit an increase of the attenuation with increase test frequencies; the amplitude reduction reaches about 15% at 10 Hz.

Table B.4: Tests Results.

Input frequency	Sampling frequency	Test ID	Gain	Phase angle [^{o}]	Delay [ms]
1 Hz	200 Hz	Test 1	0.97	- 0.90 +/- 0.54	2.50
		Test 4	0.98	- 0.71 +/- 0.33	1.98
		Test 7	0.98	- 2.13 +/- 0.13	5.92
5 Hz	1 kHz	Test 2	0.91	-1.25 +/- 0.42	0.70
		Test 5	0.90	- 1.31 +/- 0.13	0.73
		Test 8	0.89	- 2.73 +/- 0.18	1.47
10 Hz	2 kHz	Test 3	0.82	-1.49 +/- 0.49	0.41
		Test 6	0.82	- 1.33 +/- 0.05	0.37
		Test 9	0.85	- 2.29 +/- 0.79	0.64

Table B.5: Additional Results Using the 5 Last Cycles Altogether.

Input frequency	Sampling frequency	Test ID	Gain	Phase angle [^{o}]	Delay [ms]
1 Hz	200 Hz	Test 1	0.96	- 0.88	2.43
		Test 4	0.97	- 0.70	1.93
		Test 7	0.97	- 2.11	5.85
5 Hz	1 kHz	Test 2	0.72	-1.01	0.56
		Test 5	0.71	- 0.89	0.49
		Test 8	0.68	- 2.23	1.24
10 Hz	2 kHz	Test 3	0.63	-1.52	0.42
		Test 6	0.62	- 1.11	0.31
		Test 9	0.63	- 2.57	0.71

To investigate further the data collected, a second method that considers the five last cycles altogether rather than individually, is employed. Table B.5 shows the results for gain, phase angle and time delay corresponding to fitting the last five cycles conjointly. Comparison between Table B.4 and Table B.5 shows that in general both approaches yield similar results for the estimation of phase angle and time delay. The results for the gain in Table B.5 follow the same trend than those in Table B.4. However, the magnitude of the amplification for test series 2 and 3 is much lower than that in Table B.4. With this method of analysis, the attenuation becomes very severe at 10 Hz with an amplitude diminution up to about 40%. The discrepancy between the results for the gain for series 1 and 3 can be due to the presence of high-frequency noise at the lower and upper peaks of the signals; fitting the five cycle altogether might results in filtering out the extreme values and therefore in a lower gain than if the cycles are fitted one by one.

Summary

The acceptance criteria in [12] are: (1) phase angle within +/- 0.5 degree in each series of five cycles; and (2) average phase angle less than 2.8 degrees. The second criterion is based on a tolerance for the electronics phase angle of 1.8 degrees, specific to the equipment used in [12], and a desired phase angle of 1 degree. No similar information for the equipment utilized in this study was found. Based on acceptance criteria similar than those in [12], verification tests results show that the equipment response is acceptable. The degradation in the goodness of the results observed in the last test series can be attributed to a mechanical misalignment. Tests show that the gain of the system decreases with frequency, and that the loss in amplitude can be significant. This frequency dependant attenuation can be due to the filters characteristics, but further work is needed to investigate this topic.

Equipment Utilized

Servo-hydraulic Load frame: MTS 858 Table Top System.
Control system software: MTS TestWare-SX 4.0D.
Load cell: Sensotec model 41/05 72-05, 5,000 lbs range, S/N 913573.
Proving ring: Humboldt MFG.CO, model H-4454.property of Mn/DOT.
LVDT: LVDT # 2 with conditioner # 52384.

Test Series Setup

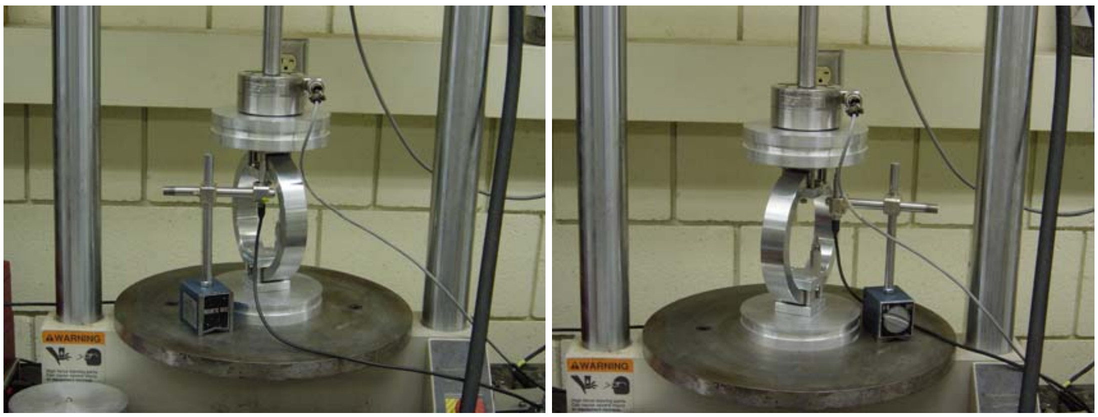

(*a*) (*b*)

Figuer B.9: Testing Setup for Test Series 2 and 3: (*a*) Series 2, and (*b*) Series 3.

Appendix C

Detailed Procedures

C.1 M_R and Shear Strength Tests

1. Weigh a large container.

2. Pour 13.6 kg of the sample to be tested into the large container through a 12.5 mm sieve.

3. Mix until sample materials are homogeneous.

4. Determine the amount of water to be added for the sample (assume the dry sample originally has 0.3 % moisture content).

5. Mix the correct amount of water and soil until the moisture content of the sample looks relatively homogeneous by color.

6. Take moisture contents from two different locations within the sample. Moisture contents samples should be more than 200 g.

7. Place the moisture content samples within an oven at approximately 60°C until moisture content does not change.

8. Seal the remainder of the sample in the airtight container and allow it to temper overnight.

9. Before compaction, compare the actual and target moisture contents of the sample, and adjust if necessary.

10. Calculate the mass for the target density, with height of 140 mm.

11. Pour the material into the gyratory compacter and turn on the compacter. Start with pressure = 500 kPa and gyrations up to 150.

12. Check to see if target height (density) was reached. If not, increase pressure by 100 kPa (pressure = 600 kPa) and repeat step 11.

13. Check to see if target height (density) was reached. If not, increase pressure by 100 kPa (pressure = 700 kPa) and repeat step 11.

14. If target height was not reached, use specimen as compacted. Repeat steps 10-13 one more time to get two specimens around 140 mm in height.

15. Inspect the base unit, mold, and top and bottom platens for damage and cleanliness.

16. Place the porous stone on top of the platen and bender element if not already in place.

17. Place a small amount of fine (Ottawa) sand around the lower bender element to protect it.

18. Place one specimen on the porous stone.

19. Attach a membrane to the lower bender element platen using two O-rings in the appropriate grooves. A third O-ring may be placed between the grooves if the vacuum mold does not seal properly without it.

20. Place the vacuum mold on top of the platen and tighten the ring supports; the upper ring support should be placed over the excess rubber membrane to hold it in place.

21. Open the blue vacuum valve. Apply a 10 in.-Hg vacuum supply and turn on the Vacuum button on the pressure panel. Connect the pressure panel to the mold by an air hose. Check to make certain that the vacuum is acting uniformly on the membrane.

22. Scratch the top surface of the specimen on the platen, and scratch the top surface of the other specimen also for better contact between them.

23. Place the second specimen on the first one inside the mold. Place it upside down.

24. Place the compaction plate into the vacuum mold. Make certain that they sit evenly on the specimens.

25. Compact two specimens using a 3000 beats-per-minute rotary hammer (AASHTO 307 specification). Make certain that the top of the specimen remains level and that only a small amount of soil escapes around the edges of the compaction plate. Compact around 10 seconds.

26. Use threaded rods to pull the compaction plate from the vacuum mold.

27. Place the upper porous stone on top of the specimen and put a small amount of fine (Ottawa) sand around the center hole of the porous stone to protect the upper bender element. Place the upper platen on the porous stone. Make certain that there is enough fine sand around the bender element to ensure a good contact.

28. Release vacuum and close the vacuum valve.

29. Remove the split mold and use O-rings to hold the membrane to the upper platen. The material used in this study will hold together due to apparent cohesion.

30. Record the height and weight of the specimen.

31. Pull a second membrane over the exterior of the first. After reaching the bottom, slide all but one O-ring from the surface of the first membrane over the surface of the second. Place four O-rings in the platens' grooves to seal the membrane.

32. Assemble the LVDT frame (LVDT 1-2-3 from right to left).

33. Check to make certain that the LVDTs have a sufficient stroke range (For example, set them to 80% of their negative range or 3.5mm of their range.).

34. Slide the LVDT holder into place over the membrane. Make certain that there is a good contact between the LVDT holder and the membrane.

35. Attach the LVDT holder with two elastic bands (o-rings). Use the smallest size o-rings for better contact.

36. Carefully place the specimen in the center of the triaxial cell. Clean all surfaces to ensure that the cell and specimen are airtight.

37. Attach the air hoses to the platens.

38. Check the cable orders of the triaxial cell (1-Bottom bender, 2-Blank, 3-LVDT1, 4-Load cell, 5-Top bender, 6-LVDT2, 7-LVDT3) and connect them.

39. Check that the LVDTs are resting evenly on top of their pedestals and that none of the lead wires in the cell are impeding their movement.

40. Connect the three LVDT lead wires, both of the bender element lead wires, and the load cell wire to their respective LEMO connectors.

41. Open the LabView program (on the Dell personal computer) named "M_R Data Acquisition".

42. Define the data channels in LabView (0-Load cell, 1-Stroke, 2-LVDT1, 3-LVDT2, 4-LVDT3) and make certain that it records data at a rate of 400 points per second.

43. Check the sensitivities of three LVDTs (go to tool and menu).

44. Check the range of the three LVDTs, and make sure all three LVDTs are in the correct range. Try several times until the best ranges are achieved.

45. Remove the spacers from the LVDT holder.

46. Connect the cables from the MTS load frame (Ground – Ground, LVDT – LVDT, Valve – Valve, Load cell – Load cell, HSM – HSM Solenoid).

47. Connect the cables in the back of the MTS computer (HSM – HSM Solenoid, long cable → left bottom).

48. Change the load cell cable connection of the MTS computer from J2 to J3.

49. Turn on the computer (Password: MTS).

50. Open Test Star2 -> Utility -> Test Star setup (Next, change hardware parameters -> next, next, next, no, 2 state, next, next, no, finish).

51. Open Test Star (ID: mts, Password: mts). Next, go to File -> Open -> Davich -> Soil Lab M_R.

52. Open the water supply (the yellow valve).

53. Turn on the pump (to low -> come back to middle automatically -> to high after 10s).

54. Open the air supply (the yellow valve).

55. Turn on the hydraulic system through the MTS pod (Reset -> low -> high). Always turn off the pod except when you move it.

56. Place the steel ball bearing on top of the upper platen and lower the plexiglass chamber around the outside of the specimen. Make certain that none of the wires are pinched.

57. Connect the cell with the load cell cable.

58. Place the top cap, and load cell on top of the cell and screw the load shafts together.

59. Press the top cap down into the plexiglass chamber. Make sure everything is aligned. The location of the cell may have to be shifted slightly to prevent lateral pressure on the shaft. Attach the top cap with the three bolts.

60. Lock the chamber by screwing down the circular plates on top of the top cap.

61. Attach all of the external wiring to the front of the cell and the air hose to the back of the cell. Connect the interior load cell lead wire.

62. Use the MTS pod to lower the actuator to make contact with the top of the specimen. Check that the load cell is reading a small value. Zero the load by using F2 and F1 on the pod.

63. Look over the entire system to make certain that everything is connected properly.

64. Open the Test Ware program on the MTS computer named "M_R Test – NCHRP_6in" (file, open, C, Winnt, Profiles, All users, Start Menu, Program, Test Star2, Test Ware program, Davich,). Then go to procedure, and execute.

65. Turn on pressure and external button on the pressure panel. Pressurize the cell by opening the air supply and pressure valve (Listen for leaks in the system).

66. Pressurize the cell to103 kPa.

67. Make certain that the system is in stroke control and turn off the pod.

68. Run the data collection. As soon as the data collection is running resume the M_R test.

69. Check the permanent strain of each LVDT after each sequence and stop the test whenever 5% strain is reached. When the LVDT reach its range, re-zero and proceed with testing.

70. After all 30 sequences are finished, stop the Test Ware program, release confining pressure, remove top cap and plexiglass chamber, remove LVDTs and LVDT holder, and reset the topcap and plexiglass chamber. Open the Test Ware program on the MTS computer named "M_R Test – NCHRP_6in_shear." Use 69 kPa confining pressure for trial 1 and 34.5 kPa for trial 2. Run the test and record the data using the LabVIEW program (200 points per second). The specimen will be loaded in stroke control.

71. After finishing the test, relief confining pressure, remove top cap and plexiglass chamber, turn off TestWare and TestStar, close air valve, close hydraulic pump and valve, remove air hoses, remove wires and take out the specimen from the triaxial cell.

72. Take soil samples from the top and bottom of the failed specimen for moisture contents.

C.2 M_R and Shear Strength Tests: Hammering Compaction

When a specimen was compacted by a vibratory hammer instead of a gyratory compactor, test steps 10 – 30 in Appendix C.1 were replaced by the steps 10 – 29 listed below.

10. Inspect the base unit, mold, and top and bottom platens for damage and cleanliness.

11. Place the porous stone on top of the platen and bender element if not already in place.

12. Attach a membrane to the lower bender element platen using two O-rings in the appropriate grooves. A third O-ring may be placed between the grooves if the vacuum mold does not seal properly without it.

13. Place the vacuum mold on top of the platen and tighten the ring supports; the upper ring support should be placed over the excess rubber membrane to hold it in place.

14. Open the blue vacuum valve. Apply a 10 in.-Hg vacuum supply and turn on the Vacuum button on the pressure panel. Connect the pressure panel to the mold by an air hose. Check to make certain that the vacuum is acting uniformly on the membrane.

15. Weigh the split mold assembly with ring supports in place. Record the weight.

16. Record the initial height of the mold from top to bottom at three different points.

17. Calculate the amount of soil needed for a 51 mm lift.

18. Place a small amount of fine (Ottawa) sand around the lower bender element to protect it.

19. Pour the soil into the vacuum mold on the scale until the right amount achieved. Use a trowel to give the soil a relatively flat surface.

20. Lower a plastic spacer and the compaction plate into the vacuum mold. Make certain that they sit evenly on the sample.

21. Compact each lift using a 3000 beats-per-minute rotary hammer (spec. AASHTO 307). Make certain that the top of the specimen remains level and that only a small amount of soil escapes around the edges of the compaction plate. The length of compaction varies between soil types (10 to 20 seconds).

22. Use threaded rods to pull the plate and spacer from the vacuum mold.

23. Record the height and weight of the specimen and check to see that the correct dry density was achieved.

24. Scratch the top surface for better contact between layers.

25. Repeat steps 19-24 five times.

26. Release vacuum and close the vacuum valve.

27. Place a wire mesh over the top of the specimen to protect the upper bender element. Cover this mesh with approximately ¼ in. of fine (Ottawa) sand and compact using a short burst from the rotary hammer.

28. Place the upper platen and porous stone on top of the specimen. Make certain that there is enough fine sand around the bender element to ensure a good contact.

29. Remove the split mold and use ones O-ring to hold the membrane to the upper platen. The materials used in this study will hold together due to apparent cohesion.

C.3 Cyclic Triaxial Tests

The cyclic triaxial tests were conducted with the steps in Appendix C.1 with replacing steps 64 – 72 with steps 64 – 71 listed below.

64. Open the Test Ware program on the MTS computer named "Cyclic Triaxial _6in" (file, open, C, Winnt, Profiles, All users, Start Menu, Program, Test Star2, Test Ware program). Then go to procedure, and execute.

65. Turn on pressure and external button on the pressure panel. Pressurize the cell by opening the air supply and pressure valve (Listen for leaks in the system).

66. Pressurize the cell to 21 kPa.

67. Make certain that the system is in stroke control and turn off the pod.

68. Run the data collection. As soon as the data collection is running resume the cyclic triaxial test.

69. Check the permanent strain of each LVDT frequently and stop the test whenever 5% strain is reached.

70. After finishing the test, stop the Test Ware program, release confining pressure, remove top cap and plexiglass chamber, turn off TestStar, close air valve, close hydraulic pump and valve, remove air hoses, remove LVDTs and LVDT holder, remove wires and take out the specimen from the triaxial cell.

71. Take soil samples from the top and bottom of the failed specimen for moisture contents.

C.4 Cyclic Triaxial Test Design

Because base material is located immediately below a pavement, other researchers [9] have used a confining pressure of 21 kPa in cyclic triaxial testing.

From the shear strength tests, the average friction angle (ϕ) and cohesion (c) of the various materials were about $\phi = 45°$ and $c = 103$ kPa. Based on the values, using equations (C.1) and (C.2), the major principal stresses (σ_{1f}) at a given confining pressures (σ_3) can be calculated for all 30 sequences of the National Cooperative Highway Research Program (NCHRP) 1-28A testing protocol for base/sub-base materials [8] (Table C.1).

$$\sigma_{1f} = 2c\sqrt{K_p} + K_p\sigma_3 \tag{C.1}$$

$$K_p = \frac{1+\sin\phi}{1-\sin\phi} \tag{C.2}$$

where σ_3 = confining pressure
σ_{1P} = confining pressure + deviator stress at peak stress (failure)
ϕ = friction angle
c = cohesion

Also, the peak stress ratio, defined as confining pressure plus deviator stress for each sequence divided by σ_{1P} (C.3), can be computed for each sequence (Table C.1).

$$\text{Peak Stress Ratio}(\%) = \frac{\sigma_a}{\sigma_{1P}} \tag{C.3}$$

where $\sigma_a = \sigma_3$ + deviator stress

Table C.1: Stress Ratio of NCHRP 1–28A Testing Sequences.

Sq	σ_3 (kPa)	Deviator Stress (kPa)	σ_a (kPa)	Estimated σ_{1P} (kPa)	Peak Stress Ratio (%)
0	103	228	331	1102	30.0
1	21	14	35	620	5.7
2	41	29	70	741	9.5
3	69	48	117	901	13.0
4	103	72	176	1102	16.0
5	138	97	234	1303	18.0
6	21	25	46	620	7.3
7	41	50	91	741	12.3
8	69	83	152	901	16.8
9	103	124	228	1102	20.6
10	138	165	303	1303	23.3
11	21	46	66	620	10.7
12	41	91	132	741	17.9
13	69	152	221	901	24.5
14	103	228	331	1102	30.0
15	138	303	441	1303	33.9
16	21	66	87	620	14.0
17	41	132	174	741	23.5
18	69	221	290	901	32.1
19	103	331	434	1102	39.4
20	138	441	579	1303	44.4
21	21	108	128	620	20.7
22	41	215	256	741	34.6
23	69	359	427	901	47.4
24	103	538	641	1102	58.2
25	138	717	855	1303	65.6
26	21	149	170	620	27.4
27	41	298	339	741	45.8
28	69	496	565	901	62.7
29	103	745	848	1102	76.9
30	138	993	1131	1303	86.8

From the M_R tests on four specimens (100% OMC) from CR 3, recoverable and permanent deformations were calculated from the 100 cycles of each sequence with a stress ratio from 30 – 80%, as shown in Fig. C.1. The relations between permanent deformation and stress ratio were approximately linear, and very little permanent deformation occurred at a peak stress ratio less than 30% (Figs C.2 – C.5). Also, if the peak stress ratio was above 60%, there was a possibility of specimen failure with cyclic loading based on the failure angle calculated from shear strength test (32˚ – 50˚). Therefore, the two peak stress ratios for cyclic triaxial tests were recommended to be 35% and 50%.

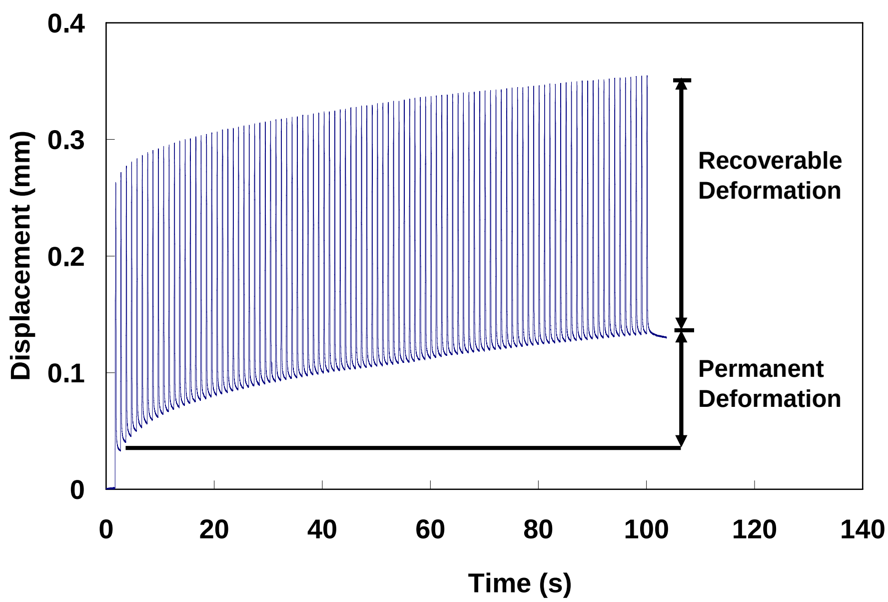

Figure C.1: Permanent Deformation of CR 3 In-situ Blend: Sequence 28 (S_7.8_2, 100% Gyratory, 100% OMC (γ_d = 2043 kg/m^3, MC = 7.7%)).

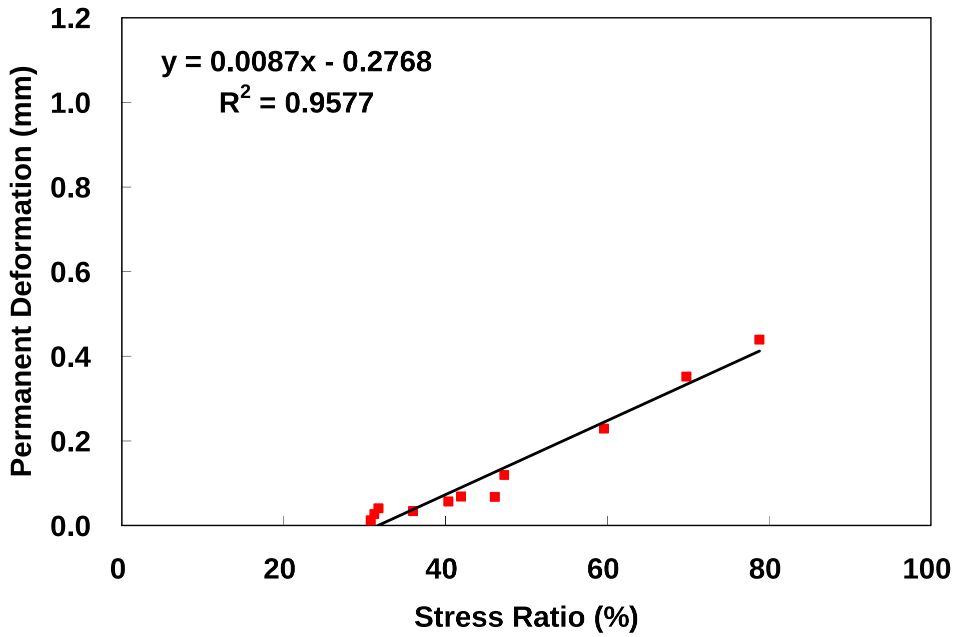

Figure C.2: Deformation vs. Peak Stress Ratio: CR 3 100% Aggregate (T_8.8_2, 100% Gyratory, 100% OMC (γ_d = 2035 kg/m^3, MC = 9.1%)).

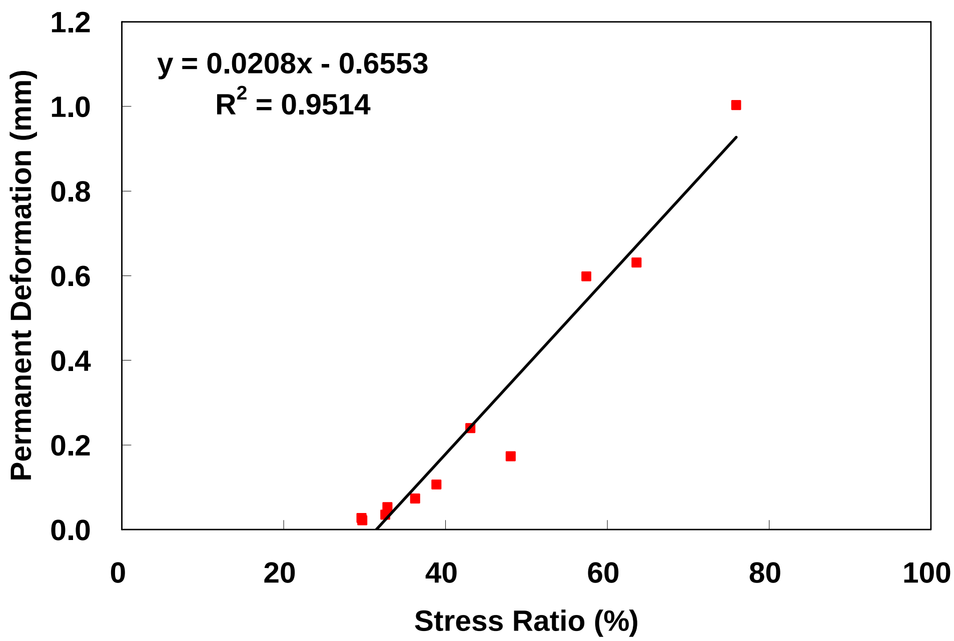

Figure C.3: Deformation vs. Peak Stress Ratio: CR 3 75% Aggregate – 25% RAP (U_8.7_2, 100% Gyratory, 100% OMC (γ_d = 2049 kg/m^3, MC = 8.8%)).

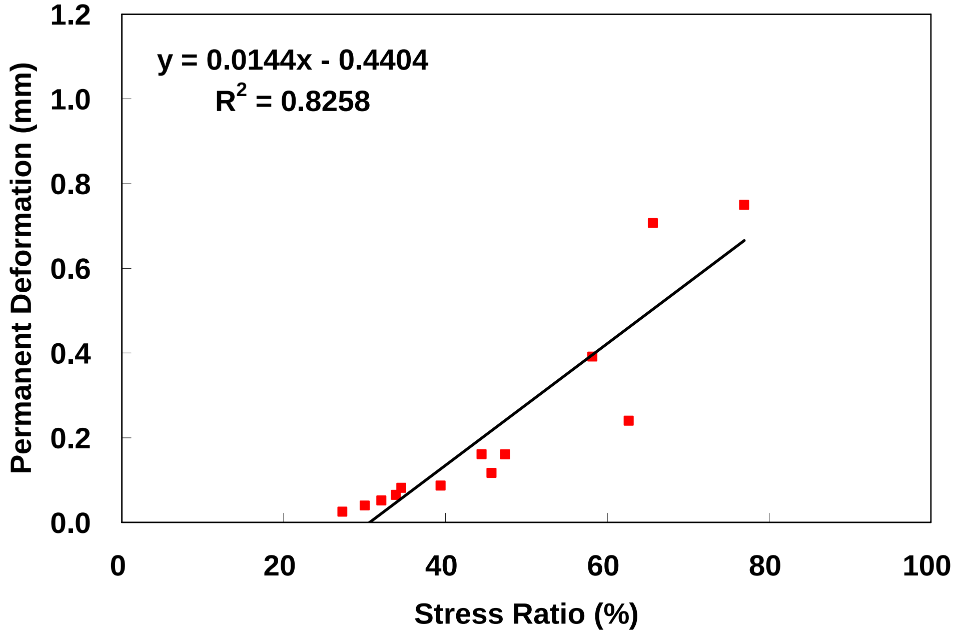

Figure C.4: Deformation vs. Peak Stress Ratio: CR 3 50% Aggregate – 50% RAP (V_8_2, 100% Gyratory, 100% OMC (γ_d = 2049 kg/m^3, MC = 8.0%)).

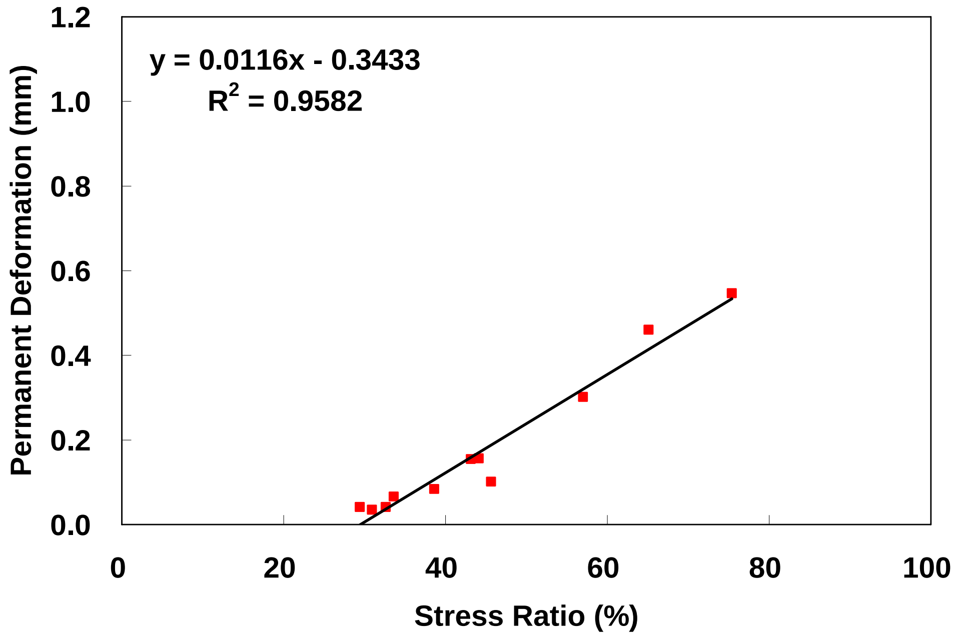

Figure C.5: Deformation vs. Peak Stress Ratio: CR 3 25% Aggregate – 75% RAP (W_7.2_2, 100% Gyratory, 100% OMC (γ_d = 2032 kg/m^3, MC = 7.7%)).

For 21 kPa confining pressure, the axial stresses were estimated to be 197 kPa for the 35% peak stress ratio and 290 kPa for the 50% peak stress ratio. Axial stress is the sum of contact stress and cyclic stress, where contact stress is axial stress applied to a specimen to maintain a positive contact between the specimen cap and specimen, and cyclic stress is a repeated haversine axial stress applied to a test specimen. From the NCHRP 1–28A protocol, contact stress is set to maintain a constant (contact stress + confining pressure)/confining pressure = 1.2 [8]. In conclusion, following the NCHRP 1–28A protocol, cyclic triaxial tests were performed with 21 kPa confining pressure, 4 kPa contact stress and 193 kPa and 286 kPa cyclic stresses.

From preliminary tests, no significant changes in permanent deformation were noticed after 2,000 cycles. Thus, the 5,000 repeated cycles of axial stress was decided. Each cycle was 1 s in duration, consisting of a 0.1 s haversine pulse followed by a 0.9 s rest period, following the M_R protocol for base materials [8]; this loading was also used by previous researchers [9]. Specimens dimension (152 mm diameter and 280 mm height) were the same as for the M_R tests.

Appendix D

Detailed Results

D.1 Resilient Modulus (M_R) Tables

Tables D.1 – D.14 show confining pressure, deviator stress and M_R values at each sequence of all 28 specimens. The sequences that failed to pass the quality control / quality assurance criteria do not have M_R values listed (the cell is blank).

Table D.1: Resilient Modulus of CR 3 Blend

(S_5.1_1 and S_5.1_2, 98% Gyratory = 1991 kg/m^3, 65% OMC = 5.1%).

Sq	Confining kPa	Deviator kPa	M_R MPa	Sq	Confining kPa	Deviator kPa	M_R MPa	Difrerence (%)
1	21	10.3	286	1	21	10.3		
2	41	19.7	342	2	41	19.8		
3	69	33.7	432	3	69	33.8	624	31
4	103	50.5	529	4	103	50.6	722	27
5	138	67.4	614	5	138	67.2	770	20
6	21	20.6	270	6	21	20.4	345	22
7	41	40.6	306	7	41	40.4	402	24
8	69	67.4	391	8	69	67.4	465	16
9	103	101.1	480	9	103	100.9	538	11
10	138	135.5	560	10	138	135.3	600	7
11	21	40.5	238	11	21	40.6	294	19
12	41	81.0	292	12	41	81.0	330	12
13	69	136.0	370	13	69	135.7	392	6
14	103	203.5	458	14	103	202.7	460	0
15	138	271.4	524	15	138	269.9	512	2
16	21	61.3	223	16	21	60.9	267	17
17	41	122.0	279	17	41	121.5	300	7
18	69	203.2	362	18	69	202.6	367	1
19	103	305.0	447	19	103	303.7	433	3
20	138	407.5	510	20	138	404.4	482	5
21	21	101.3	213	21	21	101.2	239	11
22	41	203.9	283	22	41	202.6	286	1
23	69	339.1	370	23	69	337.0	359	3
24	103	508.6	438	24	103	504.3	413	6
25	138	680.0	500	25	138	669.2	469	6
26	21	142.2	208	26	21	142.2	232	11
27	41	284.7	277	27	41	283.7	291	5
28	69	476.1	369	28	69	471.4	369	0
29	103	713.6	451	29	103	703.8	432	4
30	138	945.5		30	138	924.7	466	

Table D.2: Resilient Modulus of CR 3 Blend

(S_7.8_1 and S_7.8_2, 100% Gyratory = 2032 kg/m^3, 100% OMC = 7.8%).

Sq	Confining kPa	Deviator kPa	M_R MPa	Sq	Confining kPa	Deviator kPa	M_R MPa	Difrerence (%)
1	21	10.1		1	21	10.2	183	
2	41	19.5	249	2	41	19.6	263	6
3	69	33.6	313	3	69	33.8	345	9
4	103	50.3	396	4	103	50.7	448	12
5	138	67.8	497	5	138	67.8	542	8
6	21	19.8		6	21	20.1	163	
7	41	40.5	228	7	41	40.4	225	1
8	69	67.8	300	8	69	67.9	320	6
9	103	101.8	389	9	103	101.8	423	8
10	138	135.1	479	10	138	135.9	537	11
11	21	40.6		11	21	40.5	149	
12	41	81.0	221	12	41	81.6	221	0
13	69	135.4	301	13	69	135.9	314	4
14	103	202.9	390	14	103	204.0	432	10
15	138	271.2	455	15	138	272.5	513	11
16	21	60.6	154	16	21	61.3	143	7
17	41	121.5	217	17	41	122.2	221	2
18	69	202.7	302	18	69	204.1	324	7
19	103	304.8	382	19	103	305.7	420	9
20	138	406.2	438	20	138	407.6	492	11
21	21	101.1	152	21	21	101.7	145	4
22	41	202.8	225	22	41	203.9	232	3
23	69	338.9	311	23	69	338.9	324	4
24	103	505.2	378	24	103	508.9	394	4
25	138	671.8	446	25	138	678.2	454	2
26	21	141.4	149	26	21	142.3	140	6
27	41	283.9	228	27	41	283.9	230	0
28	69	472.3	323	28	69	474.1	329	2
29	103	705.8	406	29	103	710.3	388	4
30	138	937.3	476	30	138	945.3		

Table D.3: Resilient Modulus of CR 3 100% Aggregate

(T_5.7_1 and T_5.7_2, 98% Gyratory = 1991 kg/m^3, 65% OMC = 5.7%).

Sq	Confining kPa	Deviator kPa	M_R MPa	Sq	Confining kPa	Deviator kPa	M_R MPa	Difrerence (%)
1	21	10.2	242	1	21	10.2	230	5
2	41	19.7	292	2	41	19.6	292	0
3	69	32.5	347	3	69	33.7	348	0
4	103	51.1	418	4	103	50.6	421	1
5	138	68.2	501	5	138	67.5	507	1
6	21	20.5	236	6	21	19.8	215	9
7	41	40.7	278	7	41	40.1	255	8
8	69	67.9	329	8	69	67.4	311	5
9	103	101.9	396	9	103	101.5	386	2
10	138	136.3	468	10	138	135.5	468	0
11	21	40.6	214	11	21	40.6	195	9
12	41	81.7	256	12	41	81.2	237	7
13	69	136.3	314	13	69	135.7	302	4
14	103	204.9	394	14	103	203.5	386	2
15	138	272.8	457	15	138	270.3	453	1
16	21	61.4	203	16	21	60.9	181	11
17	41	122.9	251	17	41	121.8	231	8
18	69	204.8	317	18	69	200.8	306	4
19	103	306.9	388	19	103	303.2	384	1
20	138	409.1	442	20	138	405.2	440	0
21	21	99.4	196	21	21	99.6	175	11
22	41	203.7	249	22	41	202.6	236	5
23	69	342.3	322	23	69	339.6	317	2
24	103	511.9	386	24	103	507.6	378	2
25	138	679.1	444	25	138	676.6	433	2
26	21	143.4	190	26	21	141.9	172	9
27	41	287.0	246	27	41	284.8	233	5
28	69	477.0	325	28	69	473.1	316	3
29	103	711.2	395	29	103	707.4	389	1
30	138	946.1	435	30	138	940.5	434	0

Table D.4: Resilient Modulus of CR 3 100% Aggregate

(T_8.8_1 and T_8.8_2, 100% Gyratory = 2032 kg/m^3, 100% OMC = 8.8%).

Sq	Confining kPa	Deviator kPa	M_R MPa	Sq	Confining kPa	Deviator kPa	M_R MPa	Difrerence (%)
1	21	10.1	108	1	21	9.8		
2	41	19.6	169	2	41	19.3		
3	69	33.7	231	3	69	33.8	277	16
4	103	50.6	310	4	103	51.0	353	12
5	138	67.7	396	5	138	67.7	439	10
6	21	19.8	111	6	21	20.1	159	30
7	41	40.5	163	7	41	40.7	196	17
8	69	67.6	228	8	69	68.0	255	11
9	103	101.4	306	9	103	102.2	340	10
10	138	135.6	376	10	138	136.3	424	11
11	21	40.0	104	11	21	40.6	137	24
12	41	81.3	161	12	41	81.7	188	14
13	69	135.8	230	13	69	136.0	258	11
14	103	203.4	315	14	103	204.4	350	10
15	138	271.6	372	15	138	272.1	419	11
16	21	58.1	105	16	21	60.9	131	19
17	41	119.2	164	17	41	122.1	186	12
18	69	200.7	242	18	69	204.3	267	9
19	103	303.6	308	19	103	306.5	345	11
20	138	407.4	352	20	138	407.3	399	12
21	21	99.3	110	21	21	101.4	128	14
22	41	201.2	177	22	41	203.6	194	9
23	69	340.1	250	23	69	339.9	274	9
24	103	509.1	296	24	103	509.3		
25	138	677.2	335	25	138	679.2		
26	21	141.1	108	26	21	142.3	124	13
27	41	285.1	176	27	41	285.1	187	6
28	69	475.9	255	28	69	475.8	274	7
29	103	710.6	298	29	103	711.9	332	10
30	138	942.1		30	138	944.7	369	

Table D.5: Resilient Modulus of CR 3 75% Aggregate – 25% RAP

(U_5.7_1 and U_5.7_2, 98% Gyratory = 1991 kg/m^3, 65% OMC = 5.7%).

Sq	Confining kPa	Deviator kPa	M_R MPa	Sq	Confining kPa	Deviator kPa	M_R MPa	Difrerence (%)
1	21	10.6	268	1	21	9.5		
2	41	19.7	329	2	41	19.7		
3	69	34.0	412	3	69	34.1		
4	103	51.1	522	4	103	50.8	643	19
5	138	68.3	605	5	138	67.8	727	17
6	21	20.4	251	6	21	20.3		
7	41	40.5	296	7	41	40.6	373	21
8	69	67.9	381	8	69	68.0	436	13
9	103	101.9	473	9	103	101.9	525	10
10	138	136.5	563	10	138	136.1	619	9
11	21	40.6	222	11	21	41.1	274	19
12	41	81.5	286	12	41	82.0	316	9
13	69	136.5	371	13	69	136.3	393	6
14	103	204.9	468	14	103	204.5	486	4
15	138	273.8	534	15	138	272.2	548	3
16	21	61.3	216	16	21	61.3	244	12
17	41	123.0	283	17	41	122.7	297	5
18	69	205.0	366	18	69	204.1	376	3
19	103	307.2	456	19	103	306.3	459	0
20	138	408.4	513	20	138	408.3	511	0
21	21	101.1	209	21	21	102.4	216	3
22	41	204.8	282	22	41	204.1	282	0
23	69	342.3	372	23	69	339.8	369	1
24	103	510.9	438	24	103	509.3	437	0
25	138	680.1	480	25	138	677.3	501	4
26	21	143.9	198	26	21	142.7	202	2
27	41	286.6	270	27	41	285.4	273	1
28	69	478.0	365	28	69	475.3	370	1
29	103	711.8	428	29	103	710.3		
30	138	944.5	452	30	138	944.6		

Table D.6: Resilient Modulus of CR 3 75% Aggregate – 25% RAP

(U_8.7_1 and U_8.7_2, 100% Gyratory = 2032 kg/m^3, 100% OMC = 8.7%).

Sq	Confining kPa	Deviator kPa	M_R MPa	Sq	Confining kPa	Deviator kPa	M_R MPa	Difrerence (%)
1	21	10.1	148	1	21	9.9	76	49
2	41	19.6	211	2	41	19.2	139	34
3	69	33.5	289	3	69	33.4	214	26
4	103	50.6	378	4	103	50.2	295	22
5	138	67.3	456	5	138	67.2	366	20
6	21	20.1	135	6	21	19.2	70	48
7	41	40.4	190	7	41	40.0	137	28
8	69	67.3	267	8	69	67.3	219	18
9	103	101.3	356	9	103	101.2	304	15
10	138	135.0	443	10	138	135.2	368	17
11	21	40.0	126	11	21	40.0	76	39
12	41	81.3	194	12	41	81.1	148	24
13	69	132.7	279	13	69	135.6	236	15
14	103	200.8	368	14	103	202.9	315	14
15	138	270.3	429	15	138	270.1	357	17
16	21	60.8	129	16	21	60.6	82	37
17	41	122.9	201	17	41	121.5	160	20
18	69	204.2	285	18	69	203.3	244	14
19	103	306.6	362	19	103	303.6	301	17
20	138	407.0	413	20	138	404.6	332	19
21	21	101.3	130	21	21	100.7	91	30
22	41	203.8	208	22	41	203.0	169	19
23	69	338.8	288	23	69	334.7	238	18
24	103	507.2	347	24	103	503.0	283	18
25	138	674.6	398	25	138	672.4	338	15
26	21	141.9	125	26	21	138.7	91	27
27	41	284.5	202	27	41	280.2	173	14
28	69	473.4	289	28	69	471.9	253	13
29	103	707.4	349	29	103	703.8	291	17
30	138	939.0		30	138	932.1		

Table D.7: Resilient Modulus of CR 3 50% Aggregate – 50% RAP

(V_5.2_1 and V_5.2_2, 98% Gyratory = 1991 kg/m^3, 65% OMC = 5.2%).

Sq	Confining kPa	Deviator kPa	M_R MPa	Sq	Confining kPa	Deviator kPa	M_R MPa	Difrerence (%)
1	21	10.4	231	1	21	10.7	234	1
2	41	19.8	324	2	41	19.7	290	11
3	69	34.1	412	3	69	34.0	387	6
4	103	50.9	528	4	103	50.9	508	4
5	138	67.8	625	5	138	67.8	605	3
6	21	20.5	239	6	21	20.5	216	9
7	41	40.7	310	7	41	40.6	283	9
8	69	67.8	403	8	69	67.9	373	7
9	103	101.9	511	9	103	101.9	473	8
10	138	136.6	609	10	138	136.1	567	7
11	21	40.4	217	11	21	40.4	202	7
12	41	81.3	296	12	41	81.6	274	7
13	69	136.3	398	13	69	136.4	370	7
14	103	204.6	502	14	103	205.2	469	7
15	138	273.5	578	15	138	273.1	539	7
16	21	61.3	209	16	21	61.4	189	9
17	41	122.9	296	17	41	122.6	271	8
18	69	204.3	398	18	69	204.2	367	8
19	103	307.3	494	19	103	306.9	455	8
20	138	409.1	558	20	138	408.4	514	8
21	21	102.0	209	21	21	102.1	188	10
22	41	204.2	302	22	41	204.1	273	10
23	69	340.8	408	23	69	340.5	367	10
24	103	509.8	485	24	103	509.9	428	12
25	138	677.7	547	25	138	679.2	487	11
26	21	142.7	203	26	21	142.5	179	12
27	41	285.9	297	27	41	285.8	266	10
28	69	476.1	408	28	69	475.7	365	11
29	103	712.3	491	29	103	713.2	426	13
30	138	946.3	539	30	138	946.0	491	9

Table D.8: Resilient Modulus of CR 3 50% Aggregate – 50% RAP

(V_8_1 and V_8_2, 100% Gyratory = 2032 kg/m^3, 100% OMC = 8%).

Sq	Confining kPa	Deviator kPa	M_R MPa	Sq	Confining kPa	Deviator kPa	M_R MPa	Difrerence (%)
1	21	10.0	88	1	21	10.0	70	21
2	41	19.6	171	2	41	19.5	153	11
3	69	33.9	273	3	69	33.6	255	7
4	103	50.9	383	4	103	50.9	379	1
5	138	67.8	487	5	138	67.8	473	3
6	21	20.2	98	6	21	19.8	76	23
7	41	40.7	182	7	41	40.7	164	10
8	69	67.9	280	8	69	67.7	266	5
9	103	101.9	387	9	103	101.6	376	3
10	138	135.6	475	10	138	135.9	473	0
11	21	40.6	106	11	21	40.4	88	17
12	41	81.7	198	12	41	81.7	178	11
13	69	135.7	297	13	69	136.1	285	4
14	103	203.9	389	14	103	204.2	377	3
15	138	272.1	457	15	138	271.8	447	2
16	21	61.4	115	16	21	61.4	95	17
17	41	122.5	206	17	41	122.4	185	10
18	69	204.1	299	18	69	204.1	283	5
19	103	305.9	377	19	103	305.5	362	4
20	138	408.0	434	20	138	408.0	426	2
21	21	101.7	124	21	21	101.5	105	15
22	41	203.6	214	22	41	203.5	196	8
23	69	339.0	295	23	69	339.3	280	5
24	103	508.3	350	24	103	508.7	343	2
25	138	677.1	410	25	138	672.2	402	2
26	21	142.3	119	26	21	141.3	105	12
27	41	285.4	214	27	41	283.1	199	7
28	69	475.3	300	28	69	471.3	284	5
29	103	711.9	355	29	103	706.2		
30	138	945.9		30	138	937.3		

Table D.9: Resilient Modulus of CR 3 25% Aggregate – 75% RAP

(W_4.7_1 and W_4.7_2, 98% Gyratory = 1991 kg/m^3, 65% OMC = 4.7%).

Sq	Confining kPa	Deviator kPa	M_R MPa	Sq	Confining kPa	Deviator kPa	M_R MPa	Difrerence (%)
1	21	10.7		1	21	10.4	264	
2	41	19.7	407	2	41	19.6	396	3
3	69	34.1	570	3	69	34.0	560	2
4	103	51.0	699	4	103	50.8	766	9
5	138	68.1	853	5	138	67.8	864	1
6	21	20.6	281	6	21	20.6	257	9
7	41	40.8	396	7	41	40.5	375	5
8	69	68.0	533	8	69	67.9	512	4
9	103	101.9	670	9	103	101.8	651	3
10	138	136.8	813	10	138	136.1	760	6
11	21	40.8	260	11	21	40.6	245	6
12	41	81.3	386	12	41	81.3	362	6
13	69	135.9	520	13	69	136.3	492	5
14	103	204.3	655	14	103	204.8	620	5
15	138	273.8	718	15	138	273.4	696	3
16	21	60.2	254	16	21	61.5	238	6
17	41	119.8	367	17	41	122.8	351	4
18	69	205.7	504	18	69	204.2	480	5
19	103	307.7	616	19	103	307.3	593	4
20	138	450.6	681	20	138	408.9	649	5
21	21	102.5	241	21	21	102.5	232	4
22	41	204.6	367	22	41	204.1	352	4
23	69	341.7	496	23	69	340.2	477	4
24	103	511.6	586	24	103	509.6	558	5
25	138	685.3	651	25	138	679.3	620	5
26	21	143.3	231	26	21	142.5	225	3
27	41	286.3	358	27	41	285.3	348	3
28	69	476.7	495	28	69	475.5	476	4
29	103	711.8	578	29	103	713.0	558	4
30	138	945.7	635	30	138	946.3	611	4

Table D.10: Resilient Modulus of CR 3 25% Aggregate – 75% RAP

(W_7.2_1 and W_7.2_2, 100% Gyratory = 2032 kg/m^3, 100% OMC = 7.2%).

Sq	Confining kPa	Deviator kPa	M_R MPa	Sq	Confining kPa	Deviator kPa	M_R MPa	Difrerence (%)
1	21	10.3	148	1	21	10.3		
2	41	19.5	250	2	41	19.6		
3	69	34.1	362	3	69	33.8	400	9
4	103	51.0	501	4	103	50.7	518	3
5	138	68.0	609	5	138	67.8	624	2
6	21	20.0	148	6	21	20.1	180	18
7	41	40.6	253	7	41	40.6	268	6
8	69	67.8	370	8	69	67.8	378	2
9	103	101.9	492	9	103	101.5	490	0
10	138	135.8	589	10	138	136.0	583	1
11	21	40.5	151	11	21	40.5	172	12
12	41	81.5	259	12	41	81.1	274	6
13	69	136.3	376	13	69	135.8	378	0
14	103	204.7	485	14	103	204.2	478	1
15	138	273.6	557	15	138	272.5	548	2
16	21	61.5	152	16	21	61.4	176	13
17	41	123.0	262	17	41	122.6	272	4
18	69	204.3	373	18	69	204.0	379	2
19	103	306.9	469	19	103	306.0	472	1
20	138	408.5	531	20	138	407.1	532	0
21	21	102.0	163	21	21	101.7	176	8
22	41	204.0	270	22	41	204.1	282	4
23	69	340.4	373	23	69	339.4	379	2
24	103	509.6	443	24	103	508.7	449	1
25	138	679.1	507	25	138	676.5	517	2
26	21	142.5	157	26	21	142.3	169	7
27	41	285.6	274	27	41	285.2	270	1
28	69	475.7	380	28	69	475.5	369	3
29	103	711.8	446	29	103	711.3	441	1
30	138	945.3	504	30	138	944.8	498	1

Table D.11: Resilient Modulus of TH 23 Blend

(X_3.5_1 and X_3.5_2, 100% Gyratory = 2080 kg/m^3, 65% OMC = 3.5%).

Sq	Confining kPa	Deviator kPa	M_R MPa	Sq	Confining kPa	Deviator kPa	M_R MPa	Difrerence (%)
1	21	10.2		1	21	10.3	187	
2	41	19.6	290	2	41	19.6	257	12
3	69	33.6	380	3	69	33.6	336	12
4	103	50.4	485	4	103	50.4	431	11
5	138	67.2	584	5	138	67.2	520	11
6	21	20.0	197	6	21	20.0	163	17
7	41	40.3	266	7	41	40.2	237	11
8	69	67.4	364	8	69	67.4	326	11
9	103	101.0	464	9	103	101.4	427	8
10	138	135.0	564	10	138	135.1	519	8
11	21	40.1	180	11	21	40.0	158	12
12	41	81.0	265	12	41	81.1	244	8
13	69	135.4	363	13	69	135.7	340	6
14	103	203.2	468	14	103	203.3	440	6
15	138	271.2	540	15	138	271.0	508	6
16	21	61.0	177	16	21	61.0	161	9
17	41	121.9	270	17	41	121.8	251	7
18	69	203.2	366	18	69	202.9	350	4
19	103	304.6	451	19	103	304.3	434	4
20	138	406.3	514	20	138	405.9	500	3
21	21	101.5	178	21	21	101.4	171	4
22	41	202.7	272	22	41	203.1	269	1
23	69	338.1	360	23	69	337.7	358	1
24	103	507.0	437	24	103	505.8	429	2
25	138	674.2	512	25	138	673.3	509	1
26	21	141.9	178	26	21	142.0	179	0
27	41	284.1	284	27	41	283.7	281	1
28	69	473.1	391	28	69	472.7	391	0
29	103	708.4		29	103	707.3	449	
30	138			30	138	938.3		

Table D.12: Resilient Modulus of TH 23 Blend

(X_5.4_1 and X_5.4_2, 100% Gyratory = 2080 kg/m^3, 100% OMC = 5.4%).

Sq	Confining kPa	Deviator kPa	M_R MPa	Sq	Confining kPa	Deviator kPa	M_R MPa	Difrerence (%)
1	21	10.4	155	1	21	10.3	169	8
2	41	19.5	224	2	41	19.6	240	7
3	69	33.8	317	3	69	33.6	315	1
4	103	50.8	410	4	103	50.5	411	0
5	138	67.7	506	5	138	67.1	497	2
6	21	20.1	143	6	21	19.8	129	10
7	41	40.6	219	7	41	40.3	226	3
8	69	67.7	306	8	69	67.3	304	1
9	103	101.8	413	9	103	101.3	405	2
10	138	136.1	502	10	138	135.4	478	5
11	21	40.4	146	11	21	40.1	143	2
12	41	81.4	230	12	41	81.1	224	2
13	69	136.1	324	13	69	135.7	316	2
14	103	204.2	427	14	103	203.0	407	5
15	138	272.4	497	15	138	271.0	476	4
16	21	61.3	148	16	21	60.8	143	4
17	41	122.5	237	17	41	121.6	230	3
18	69	204.1	335	18	69	202.9	321	4
19	103	306.6	415	19	103	304.3	404	3
20	138	408.0	473	20	138	405.5	464	2
21	21	101.8	156	21	21	101.2	150	4
22	41	203.9	251	22	41	203.0	242	3
23	69	339.7	330	23	69	337.8	333	1
24	103	509.1	393	24	103	505.8	434	9
25	138	678.8	467	25	138	674.1	492	5
26	21	142.7	159	26	21	141.7	152	4
27	41	283.5	257	27	41	283.9	255	1
28	69	472.5	350	28	69	472.7	359	2
29	103	708.1	395	29	103	707.6		
30	138	940.8	453	30	138	940.9		

Table D.13: Resilient Modulus of TH 200 Blend

(Y_3.7_1 and Y_3.7_2, 100% Gyratory = 2144 kg/m^3, 65% OMC = 3.7%).

Sq	Confining kPa	Deviator kPa	M_R MPa	Sq	Confining kPa	Deviator kPa	M_R MPa	Difrerence (%)
1	21	10.3	172	1	21	10.1	196	12
2	41	20.0	274	2	41	19.8	274	0
3	69	34.1	369	3	69	33.6	362	2
4	103	51.2	496	4	103	50.9	488	2
5	138	68.1	610	5	138	68.0	619	2
6	21	20.4	172	6	21	20.0	161	7
7	41	40.9	272	7	41	40.5	255	6
8	69	68.0	372	8	69	67.6	365	2
9	103	102.3	495	9	103	101.1	496	0
10	138	136.3	608	10	138	134.6	610	0
11	21	41.1	176	11	21	40.4	157	11
12	41	81.6	279	12	41	80.7	256	8
13	69	136.4	399	13	69	135.1	384	4
14	103	203.9	515	14	103	202.7	511	1
15	138	275.8	582	15	138	269.6	596	2
16	21	61.4	177	16	21	60.6	161	9
17	41	122.6	283	17	41	121.4	264	7
18	69	204.4	400	18	69	202.0	393	2
19	103	305.6	492	19	103	303.5	504	2
20	138	409.3	557	20	138	404.5	576	3
21	21	102.3	184	21	21	100.7	169	8
22	41	203.8	298	22	41	201.4	287	4
23	69	340.6	399	23	69	336.0	401	1
24	103	509.3	475	24	103	503.2	490	3
25	138	677.8	555	25	138	671.2	576	4
26	21	142.7	188	26	21	140.9		
27	41	285.2	308	27	41	282.0	297	3
28	69	475.5	425	28	69	469.5	421	1
29	103	711.2	485	29	103	701.5	502	3
30	138	945.9		30	138	931.7	570	

Table D.14: Resilient Modulus of TH 200 Blend

(Y_5.7_1 and Y_5.7_2, 100% Gyratory = 2144 kg/m^3, 100% OMC = 5.7%).

Sq	Confining kPa	Deviator kPa	M_R MPa	Sq	Confining kPa	Deviator kPa	M_R MPa	Difrerence (%)
1	21	10.1	76	1	21	10.0	75	0
2	41	19.7	172	2	41	19.5	172	0
3	69	33.6	277	3	69	33.5	274	1
4	103	50.8	398	4	103	50.6	401	1
5	138	67.4	498	5	138	67.6	507	2
6	21	20.0	83	6	21	20.0	92	9
7	41	40.3	182	7	41	40.6	178	2
8	69	67.7	293	8	69	67.7	300	2
9	103	101.3	405	9	103	101.3	419	3
10	138	135.3	504	10	138	135.3	519	3
11	21	40.6	100	11	21	40.6	110	9
12	41	81.2	201	12	41	81.3	216	7
13	69	135.5	318	13	69	135.1	327	3
14	103	202.8	415	14	103	202.8	430	4
15	138	270.5	487	15	138	269.5	502	3
16	21	60.9	109	16	21	60.7	124	13
17	41	121.7	216	17	41	121.0	227	5
18	69	202.2	315	18	69	202.0	329	4
19	103	303.6	400	19	103	302.4	414	3
20	138	403.8	464	20	138	402.2	480	3
21	21	101.0	126	21	21	100.8	135	7
22	41	202.2	227	22	41	201.5	239	5
23	69	336.5	305	23	69	335.6	316	3
24	103	503.9	380	24	103	502.3	389	2
25	138	670.5	460	25	138	668.6	472	3
26	21	141.3	126	26	21	141.1	148	14
27	41	283.9	243	27	41	282.1	252	3
28	69	471.9	325	28	69	468.7	330	2
29	103	706.2	389	29	103	701.0	396	2
30	138	937.0		30	138	927.9		

ENGLISH UNITS

Table D.15: Resilient Modulus of CR 3 Blend

(S_5.1_1 and S_5.1_2, 98% Gyratory = 124.29 lb/ft^3, 65% OMC = 5.1%).

Sq	Confining	Deviator	Mr	Sq	Confining	Deviator	Mr	Difference
	psi	psi	psi		psi	psi	psi	(%)
1	3	1.5	41416	1	3	1.5		
2	6	2.9	49652	2	6	2.9		
3	10	4.9	62654	3	10	4.9	90446	31
4	15	7.3	76771	4	15	7.3	104762	27
5	20	9.8	89120	5	20	9.7	111656	20
6	3	3.0	39152	6	3	3.0	50005	22
7	6	5.9	44360	7	6	5.9	58364	24
8	10	9.8	56684	8	10	9.8	67477	16
9	15	14.7	69566	9	15	14.6	78021	11
10	20	19.7	81233	10	20	19.6	87010	7
11	3	5.9	34588	11	3	5.9	42637	19
12	6	11.8	42313	12	6	11.7	47831	12
13	10	19.7	53636	13	10	19.7	56924	6
14	15	29.5	66476	14	15	29.4	66722	0
15	20	39.4	76011	15	20	39.1	74319	2
16	3	8.9	32349	16	3	8.8	38749	17
17	6	17.7	40508	17	6	17.6	43441	7
18	10	29.5	52560	18	10	29.4	53261	1
19	15	44.2	64765	19	15	44.1	62775	3
20	20	59.1	73926	20	20	58.6	69879	6
21	3	14.7	30853	21	3	14.7	34653	11
22	6	29.6	41024	22	6	29.4	41546	1
23	10	49.2	53608	23	10	48.9	52014	3
24	15	73.8	63571	24	15	73.1	59906	6
25	20	98.6	72582	25	20	97.1	68027	7
26	3	20.6	30105	26	3	20.6	33651	11
27	6	41.3	40154	27	6	41.1	42191	5
28	10	69.1	53568	28	10	68.4	53493	0
29	15	103.5	65424	29	15	102.1	62586	5
30	20	137.1		30	20	134.1	67621	

Table D.16: Resilient Modulus of CR 3 Blend

(S_7.8_1 and S_7.8_2, 100% Gyratory = 126.85 lb/ft^3, 100% OMC = 7.8%).

Sq	Confining	Deviator	Mr	Sq	Confining	Deviator	Mr	Difference
	psi	psi	psi		psi	psi	psi	(%)
1	3	1.5		1	3	1.5	26566	
2	6	2.8	36052	2	6	2.8	38156	6
3	10	4.9	45403	3	10	4.9	50094	9
4	15	7.3	57463	4	15	7.4	65036	12
5	20	9.8	72015	5	20	9.8	78650	8
6	3	2.9		6	3	2.9	23575	
7	6	5.9	33038	7	6	5.9	32664	1
8	10	9.8	43545	8	10	9.8	46389	6
9	15	14.8	56400	9	15	14.8	61289	8
10	20	19.6	69405	10	20	19.7	77848	11
11	3	5.9		11	3	5.9	21577	
12	6	11.8	32056	12	6	11.8	32067	0
13	10	19.6	43643	13	10	19.7	45611	4
14	15	29.4	56631	14	15	29.6	62593	10
15	20	39.3	66004	15	20	39.5	74444	11
16	3	8.8	22296	16	3	8.9	20782	7
17	6	17.6	31434	17	6	17.7	32107	2
18	10	29.4	43782	18	10	29.6	46973	7
19	15	44.2	55373	19	15	44.3	60947	9
20	20	58.9	63520	20	20	59.1	71372	11
21	3	14.7	22023	21	3	14.8	21068	5
22	6	29.4	32688	22	6	29.6	33615	3
23	10	49.1	45115	23	10	49.1	47011	4
24	15	73.3	54802	24	15	73.8	57091	4
25	20	97.4	64652	25	20	98.4	65806	2
26	3	20.5	21660	26	3	20.6	20374	6
27	6	41.2	33127	27	6	41.2	33289	0
28	10	68.5	46917	28	10	68.8	47759	2
29	15	102.4	58812	29	15	103.0	56218	5
30	20	135.9	69050	30	20	137.1		

Table D.17: Resilient Modulus of CR 3 100% Aggregate

(T_5.7_1 and T_5.7_2, 98% Gyratory = 124.29 lb/ft^3, 65% OMC = 5.7%).

Sq	Confining	Deviator	Mr	Sq	Confining	Deviator	Mr	Difference
	psi	psi	psi		psi	psi	psi	(%)
1	3	1.5	35167	1	3	1.5	33403	5
2	6	2.9	42357	2	6	2.8	42411	0
3	10	4.7	50374	3	10	4.9	50535	0
4	15	7.4	60574	4	15	7.3	61030	1
5	20	9.9	72693	5	20	9.8	73466	1
6	3	3.0	34253	6	3	2.9	31150	10
7	6	5.9	40331	7	6	5.8	36933	9
8	10	9.8	47698	8	10	9.8	45161	6
9	15	14.8	57362	9	15	14.7	56051	2
10	20	19.8	67828	10	20	19.7	67896	0
11	3	5.9	31000	11	3	5.9	28346	9
12	6	11.8	37058	12	6	11.8	34303	8
13	10	19.8	45611	13	10	19.7	43821	4
14	15	29.7	57200	14	15	29.5	56028	2
15	20	39.6	66307	15	20	39.2	65666	1
16	3	8.9	29471	16	3	8.8	26256	12
17	6	17.8	36343	17	6	17.7	33532	8
18	10	29.7	46009	18	10	29.1	44363	4
19	15	44.5	56245	19	15	44.0	55653	1
20	20	59.3	64096	20	20	58.8	63781	0
21	3	14.4	28370	21	3	14.4	25356	12
22	6	29.5	36130	22	6	29.4	34168	6
23	10	49.6	46710	23	10	49.3	45905	2
24	15	74.2	56036	24	15	73.6	54852	2
25	20	98.5	64379	25	20	98.1	62815	2
26	3	20.8	27498	26	3	20.6	24904	10
27	6	41.6	35725	27	6	41.3	33779	6
28	10	69.2	47109	28	10	68.6	45855	3
29	15	103.1	57226	29	15	102.6	56468	1
30	20	137.2	63156	30	20	136.4	63001	0

Table D.18: Resilient Modulus of CR 3 100% Aggregate

(T_8.8_1 and T_8.8_2, 100% Gyratory = 126.85 lb/ft^3, 100% OMC = 8.8%).

Sq	Confining	Deviator	Mr	Sq	Confining	Deviator	Mr	Difference
	psi	psi	psi		psi	psi	psi	(%)
1	3	1.5	15599	1	3	1.4		
2	6	2.8	24510	2	6	2.8		
3	10	4.9	33518	3	10	4.9	40119	16
4	15	7.3	45012	4	15	7.4	51178	12
5	20	9.8	57431	5	20	9.8	63682	10
6	3	2.9	16058	6	3	2.9	23001	30
7	6	5.9	23672	7	6	5.9	28472	17
8	10	9.8	33022	8	10	9.9	36982	11
9	15	14.7	44409	9	15	14.8	49333	10
10	20	19.7	54590	10	20	19.8	61458	11
11	3	5.8	15048	11	3	5.9	19857	24
12	6	11.8	23303	12	6	11.8	27224	14
13	10	19.7	33349	13	10	19.7	37377	11
14	15	29.5	45715	14	15	29.6	50808	10
15	20	39.4	54018	15	20	39.5	60746	11
16	3	8.4	15297	16	3	8.8	18965	19
17	6	17.3	23763	17	6	17.7	26991	12
18	10	29.1	35152	18	10	29.6	38681	9
19	15	44.0	44706	19	15	44.4	50091	11
20	20	59.1	51103	20	20	59.1	57861	12
21	3	14.4	15978	21	3	14.7	18551	14
22	6	29.2	25609	22	6	29.5	28097	9
23	10	49.3	36307	23	10	49.3	39718	9
24	15	73.8	42913	24	15	73.9		
25	20	98.2	48601	25	20	98.5		
26	3	20.5	15678	26	3	20.6	17935	13
27	6	41.4	25523	27	6	41.3	27107	6
28	10	69.0	37016	28	10	69.0	39800	7
29	15	103.1	43211	29	15	103.2	48118	10
30	20	136.6		30	20	137.0	53572	

Table D.19: Resilient Modulus of CR 3 75% Aggregate – 25% RAP

(U_5.7_1 and U_5.7_2, 98% Gyratory = 124.29 lb/ft^3, 65% OMC = 5.7%).

Sq	Confining	Deviator	Mr	Sq	Confining	Deviator	Mr	Difference
	psi	psi	psi		psi	psi	psi	(%)
1	3	1.5	38870	1	3	1.4		
2	6	2.9	47662	2	6	2.9		
3	10	4.9	59799	3	10	4.9		
4	15	7.4	75660	4	15	7.4	93248	19
5	20	9.9	87815	5	20	9.8	105367	17
6	3	3.0	36343	6	3	2.9		
7	6	5.9	42870	7	6	5.9	54164	21
8	10	9.8	55222	8	10	9.9	63303	13
9	15	14.8	68635	9	15	14.8	76152	10
10	20	19.8	81638	10	20	19.7	89802	9
11	3	5.9	32135	11	3	6.0	39693	19
12	6	11.8	41527	12	6	11.9	45860	9
13	10	19.8	53759	13	10	19.8	56932	6
14	15	29.7	67818	14	15	29.7	70425	4
15	20	39.7	77454	15	20	39.5	79480	3
16	3	8.9	31256	16	3	8.9	35337	12
17	6	17.8	41081	17	6	17.8	43099	5
18	10	29.7	53016	18	10	29.6	54529	3
19	15	44.5	66180	19	15	44.4	66502	0
20	20	59.2	74417	20	20	59.2	74126	0
21	3	14.7	30255	21	3	14.8	31352	3
22	6	29.7	40945	22	6	29.6	40943	0
23	10	49.6	53906	23	10	49.3	53458	1
24	15	74.1	63532	24	15	73.9	63388	0
25	20	98.6	69635	25	20	98.2	72649	4
26	3	20.9	28720	26	3	20.7	29307	2
27	6	41.6	39119	27	6	41.4	39560	1
28	10	69.3	52975	28	10	68.9	53631	1
29	15	103.2	62133	29	15	103.0		
30	20	137.0	65567	30	20	137.0		

Table D.20: Resilient Modulus of CR 3 75% Aggregate – 25% RAP

(U_8.7_1 and U_8.7_2, 100% Gyratory = 126.85 lb/ft^3, 100% OMC = 8.7%).

Sq	Confining	Deviator	Mr	Sq	Confining	Deviator	Mr	Difference
	psi	psi	psi		psi	psi	psi	(%)
1	3	1.5	21411	1	3	1.4	10987	49
2	6	2.8	30575	2	6	2.8	20125	34
3	10	4.9	41887	3	10	4.8	31047	26
4	15	7.3	54838	4	15	7.3	42840	22
5	20	9.8	66100	5	20	9.7	53124	20
6	3	2.9	19597	6	3	2.8	10165	48
7	6	5.9	27624	7	6	5.8	19854	28
8	10	9.8	38769	8	10	9.8	31822	18
9	15	14.7	51668	9	15	14.7	44036	15
10	20	19.6	64194	10	20	19.6	53300	17
11	3	5.8	18208	11	3	5.8	11018	39
12	6	11.8	28126	12	6	11.8	21415	24
13	10	19.3	40475	13	10	19.7	34226	15
14	15	29.1	53387	14	15	29.4	45708	14
15	20	39.2	62174	15	20	39.2	51772	17
16	3	8.8	18720	16	3	8.8	11858	37
17	6	17.8	29154	17	6	17.6	23266	20
18	10	29.6	41301	18	10	29.5	35389	14
19	15	44.5	52438	19	15	44.0	43620	17
20	20	59.0	59871	20	20	58.7	48207	19
21	3	14.7	18916	21	3	14.6	13200	30
22	6	29.6	30207	22	6	29.4	24560	19
23	10	49.1	41800	23	10	48.5	34465	18
24	15	73.6	50279	24	15	72.9	41024	18
25	20	97.8	57744	25	20	97.5	49050	15
26	3	20.6	18126	26	3	20.1	13142	27
27	6	41.3	29251	27	6	40.6	25094	14
28	10	68.7	41976	28	10	68.4	36723	13
29	15	102.6	50610	29	15	102.1	42198	17
30	20	136.2		30	20	135.2		

Table D.21: Resilient Modulus of CR 3 50% Aggregate – 50% RAP

(V_5.2_1 and V_5.2_2, 98% Gyratory = 124.29 lb/ft^3, 65% OMC = 5.2%).

Sq	Confining	Deviator	Mr	Sq	Confining	Deviator	Mr	Difference
	psi	psi	psi		psi	psi	psi	(%)
1	3	1.5	33454	1	3	1.5	33889	1
2	6	2.9	47032	2	6	2.9	42075	11
3	10	4.9	59791	3	10	4.9	56099	6
4	15	7.4	76529	4	15	7.4	73727	4
5	20	9.8	90701	5	20	9.8	87812	3
6	3	3.0	34634	6	3	3.0	31360	9
7	6	5.9	45019	7	6	5.9	41046	9
8	10	9.8	58407	8	10	9.8	54140	7
9	15	14.8	74167	9	15	14.8	68543	8
10	20	19.8	88365	10	20	19.7	82251	7
11	3	5.9	31540	11	3	5.9	29297	7
12	6	11.8	42962	12	6	11.8	39755	7
13	10	19.8	57789	13	10	19.8	53721	7
14	15	29.7	72847	14	15	29.8	68063	7
15	20	39.7	83819	15	20	39.6	78204	7
16	3	8.9	30287	16	3	8.9	27465	9
17	6	17.8	42930	17	6	17.8	39364	8
18	10	29.6	57695	18	10	29.6	53245	8
19	15	44.6	71624	19	15	44.5	65934	8
20	20	59.3	80964	20	20	59.2	74570	8
21	3	14.8	30365	21	3	14.8	27195	10
22	6	29.6	43836	22	6	29.6	39660	10
23	10	49.4	59106	23	10	49.4	53182	10
24	15	73.9	70300	24	15	73.9	62124	12
25	20	98.3	79309	25	20	98.5	70696	11
26	3	20.7	29502	26	3	20.7	25893	12
27	6	41.5	43025	27	6	41.5	38604	10
28	10	69.0	59219	28	10	69.0	52977	11
29	15	103.3	71143	29	15	103.4	61851	13
30	20	137.2	78205	30	20	137.2	71171	9

Table D.22: Resilient Modulus of CR 3 50% Aggregate – 50% RAP

(V_8_1 and V_8_2, 100% Gyratory = 126.85 lb/ft^3, 100% OMC = 8%).

Sq	Confining	Deviator	Mr	Sq	Confining	Deviator	Mr	Difference
	psi	psi	psi		psi	psi	psi	(%)
1	3	1.5	12812	1	3	1.5	10136	21
2	6	2.8	24839	2	6	2.8	22127	11
3	10	4.9	39649	3	10	4.9	36972	7
4	15	7.4	55518	4	15	7.4	54948	1
5	20	9.8	70647	5	20	9.8	68628	3
6	3	2.9	14234	6	3	2.9	11022	23
7	6	5.9	26379	7	6	5.9	23728	10
8	10	9.8	40675	8	10	9.8	38582	5
9	15	14.8	56181	9	15	14.7	54502	3
10	20	19.7	68823	10	20	19.7	68575	0
11	3	5.9	15334	11	3	5.9	12715	17
12	6	11.8	28779	12	6	11.8	25746	11
13	10	19.7	43127	13	10	19.7	41331	4
14	15	29.6	56397	14	15	29.6	54706	3
15	20	39.5	66245	15	20	39.4	64777	2
16	3	8.9	16649	16	3	8.9	13782	17
17	6	17.8	29895	17	6	17.8	26833	10
18	10	29.6	43362	18	10	29.6	41052	5
19	15	44.4	54624	19	15	44.3	52519	4
20	20	59.2	62968	20	20	59.2	61815	2
21	3	14.7	17919	21	3	14.7	15231	15
22	6	29.5	31030	22	6	29.5	28455	8
23	10	49.2	42719	23	10	49.2	40598	5
24	15	73.7	50731	24	15	73.8	49736	2
25	20	98.2	59469	25	20	97.5	58332	2
26	3	20.6	17280	26	3	20.5	15262	12
27	6	41.4	31022	27	6	41.1	28840	7
28	10	68.9	43500	28	10	68.4	41195	5
29	15	103.2	51558	29	15	102.4		
30	20	137.2		30	20	135.9		

Table D.23: Resilient Modulus of CR 3 25% Aggregate – 75% RAP

(W_4.7_1 and W_4.7_2, 98% Gyratory = 124.29 lb/ft^3, 65% OMC = 4.7%).

Sq	Confining	Deviator	Mr	Sq	Confining	Deviator	Mr	Difference
	psi	psi	psi		psi	psi	psi	(%)
1	3	1.5		1	3	1.5	38246	
2	6	2.9	58990	2	6	2.8	57447	3
3	10	5.0	82681	3	10	4.9	81228	2
4	15	7.4	101390	4	15	7.4	111123	10
5	20	9.9	123715	5	20	9.8	125378	1
6	3	3.0	40820	6	3	3.0	37203	9
7	6	5.9	57437	7	6	5.9	54395	5
8	10	9.9	77358	8	10	9.8	74232	4
9	15	14.8	97102	9	15	14.8	94397	3
10	20	19.8	117845	10	20	19.7	110274	6
11	3	5.9	37650	11	3	5.9	35547	6
12	6	11.8	55995	12	6	11.8	52559	6
13	10	19.7	75412	13	10	19.8	71333	5
14	15	29.6	95046	14	15	29.7	89871	5
15	20	39.7	104187	15	20	39.7	100965	3
16	3	8.7	36820	16	3	8.9	34580	6
17	6	17.4	53162	17	6	17.8	50908	4
18	10	29.8	73034	18	10	29.6	69662	5
19	15	44.6	89284	19	15	44.6	85982	4
20	20	65.3	98715	20	20	59.3	94091	5
21	3	14.9	34972	21	3	14.9	33718	4
22	6	29.7	53290	22	6	29.6	51045	4
23	10	49.6	71991	23	10	49.3	69137	4
24	15	74.2	84959	24	15	73.9	80862	5
25	20	99.4	94396	25	20	98.5	89978	5
26	3	20.8	33560	26	3	20.7	32666	3
27	6	41.5	51858	27	6	41.4	50543	3
28	10	69.1	71758	28	10	69.0	69013	4
29	15	103.2	83871	29	15	103.4	80895	4
30	20	137.2	92156	30	20	137.2	88585	4

Table D.24: Resilient Modulus of CR 3 25% Aggregate – 75% RAP

(W_7.2_1 and W_7.2_2, 100% Gyratory = 126.85 lb/ft^3, 100% OMC = 7.2%).

Sq	Confining	Deviator	Mr	Sq	Confining	Deviator	Mr	Difference
	psi	psi	psi		psi	psi	psi	(%)
1	3	1.5	21415	1	3	1.5		
2	6	2.8	36316	2	6	2.8		
3	10	4.9	52553	3	10	4.9	58026	10
4	15	7.4	72727	4	15	7.4	75091	3
5	20	9.9	88270	5	20	9.8	90486	3
6	3	2.9	21403	6	3	2.9	26041	22
7	6	5.9	36753	7	6	5.9	38915	6
8	10	9.8	53704	8	10	9.8	54820	2
9	15	14.8	71413	9	15	14.7	71096	0
10	20	19.7	85487	10	20	19.7	84582	1
11	3	5.9	21935	11	3	5.9	24985	14
12	6	11.8	37562	12	6	11.8	39765	6
13	10	19.8	54596	13	10	19.7	54864	0
14	15	29.7	70295	14	15	29.6	69315	1
15	20	39.7	80762	15	20	39.5	79513	2
16	3	8.9	22103	16	3	8.9	25469	15
17	6	17.8	38050	17	6	17.8	39511	4
18	10	29.6	54127	18	10	29.6	55035	2
19	15	44.5	68025	19	15	44.4	68492	1
20	20	59.2	76997	20	20	59.0	77186	0
21	3	14.8	23571	21	3	14.8	25560	8
22	6	29.6	39129	22	6	29.6	40891	5
23	10	49.4	54065	23	10	49.2	55017	2
24	15	73.9	64221	24	15	73.8	65144	1
25	20	98.5	73537	25	20	98.1	74986	2
26	3	20.7	22742	26	3	20.6	24443	7
27	6	41.4	39714	27	6	41.4	39152	1
28	10	69.0	55081	28	10	69.0	53521	3
29	15	103.2	64668	29	15	103.2	63934	1
30	20	137.1	73071	30	20	137.0	72294	1

Table D.25: Resilient Modulus of TH 23 Blend

(X_3.5_1 and X_3.5_2, 100% Gyratory = 129.85 lb/ft^3, 65% OMC = 3.5%).

Sq	Confining	Deviator	Mr	Sq	Confining	Deviator	Mr	Difference
	psi	psi	psi		psi	psi	psi	(%)
1	3	1.5		1	3	1.5	27092	
2	6	2.8	42109	2	6	2.8	37235	12
3	10	4.9	55119	3	10	4.9	48661	12
4	15	7.3	70301	4	15	7.3	62519	11
5	20	9.7	84645	5	20	9.7	75404	11
6	3	2.9	28541	6	3	2.9	23660	17
7	6	5.8	38568	7	6	5.8	34437	11
8	10	9.8	52825	8	10	9.8	47215	11
9	15	14.6	67357	9	15	14.7	61957	8
10	20	19.6	81728	10	20	19.6	75253	8
11	3	5.8	26035	11	3	5.8	22900	12
12	6	11.7	38466	12	6	11.8	35395	8
13	10	19.6	52692	13	10	19.7	49293	6
14	15	29.5	67859	14	15	29.5	63813	6
15	20	39.3	78337	15	20	39.3	73656	6
16	3	8.9	25660	16	3	8.9	23378	9
17	6	17.7	39100	17	6	17.7	36468	7
18	10	29.5	53082	18	10	29.4	50703	4
19	15	44.2	65424	19	15	44.1	62960	4
20	20	58.9	74561	20	20	58.9	72528	3
21	3	14.7	25831	21	3	14.7	24855	4
22	6	29.4	39472	22	6	29.5	38944	1
23	10	49.0	52186	23	10	49.0	51881	1
24	15	73.5	63327	24	15	73.4	62247	2
25	20	97.8	74283	25	20	97.6	73824	1
26	3	20.6	25847	26	3	20.6	25973	0
27	6	41.2	41219	27	6	41.1	40798	1
28	10	68.6	56660	28	10	68.6	56651	0
29	15	102.7		29	15	102.6	65073	
30	20			30	20	136.1		

Table D.26: Resilient Modulus of TH 23 Blend

(X_5.4_1 and X_5.4_2, 100% Gyratory = 129.85 lb/ft^3, 100% OMC = 5.4%).

Sq	Confining	Deviator	Mr	Sq	Confining	Deviator	Mr	Difference
	psi	psi	psi		psi	psi	psi	(%)
1	3	1.5	22459	1	3	1.5	24501	9
2	6	2.8	32463	2	6	2.8	34871	7
3	10	4.9	46007	3	10	4.9	45693	1
4	15	7.4	59491	4	15	7.3	59619	0
5	20	9.8	73420	5	20	9.7	72028	2
6	3	2.9	20745	6	3	2.9	18773	10
7	6	5.9	31728	7	6	5.8	32810	3
8	10	9.8	44373	8	10	9.8	44118	1
9	15	14.8	59934	9	15	14.7	58807	2
10	20	19.7	72835	10	20	19.6	69351	5
11	3	5.9	21197	11	3	5.8	20755	2
12	6	11.8	33295	12	6	11.8	32534	2
13	10	19.7	46947	13	10	19.7	45882	2
14	15	29.6	61969	14	15	29.4	59032	5
15	20	39.5	72124	15	20	39.3	68976	4
16	3	8.9	21491	16	3	8.8	20668	4
17	6	17.8	34419	17	6	17.6	33323	3
18	10	29.6	48607	18	10	29.4	46623	4
19	15	44.5	60235	19	15	44.1	58652	3
20	20	59.2	68630	20	20	58.8	67345	2
21	3	14.8	22657	21	3	14.7	21694	4
22	6	29.6	36340	22	6	29.4	35097	3
23	10	49.3	47879	23	10	49.0	48253	1
24	15	73.8	57036	24	15	73.4	62904	10
25	20	98.4	67729	25	20	97.8	71292	5
26	3	20.7	23045	26	3	20.6	22082	4
27	6	41.1	37342	27	6	41.2	36930	1
28	10	68.5	50791	28	10	68.5	52042	2
29	15	102.7	57317	29	15	102.6		
30	20	136.5	65765	30	20	136.5		

Table D.27: Resilient Modulus of TH 200 Blend

(Y_3.7_1 and Y_3.7_2, 100% Gyratory = 133.84 lb/ft^3, 65% OMC = 3.7%).

Sq	Confining	Deviator	Mr	Sq	Confining	Deviator	Mr	Difference
	psi	psi	psi		psi	psi	psi	(%)
1	3	1.5	24883	1	3	1.5	28430	12
2	6	2.9	39751	2	6	2.9	39722	0
3	10	4.9	53527	3	10	4.9	52571	2
4	15	7.4	71926	4	15	7.4	70711	2
5	20	9.9	88478	5	20	9.9	89847	2
6	3	3.0	24957	6	3	2.9	23309	7
7	6	5.9	39409	7	6	5.9	36928	7
8	10	9.9	53963	8	10	9.8	52925	2
9	15	14.8	71852	9	15	14.7	71980	0
10	20	19.8	88198	10	20	19.5	88533	0
11	3	6.0	25577	11	3	5.9	22761	12
12	6	11.8	40450	12	6	11.7	37169	9
13	10	19.8	57853	13	10	19.6	55654	4
14	15	29.6	74667	14	15	29.4	74132	1
15	20	40.0	84396	15	20	39.1	86509	2
16	3	8.9	25610	16	3	8.8	23392	9
17	6	17.8	41059	17	6	17.6	38246	7
18	10	29.7	58001	18	10	29.3	56926	2
19	15	44.3	71301	19	15	44.0	73090	2
20	20	59.4	80814	20	20	58.7	83590	3
21	3	14.8	26664	21	3	14.6	24546	9
22	6	29.6	43192	22	6	29.2	41661	4
23	10	49.4	57914	23	10	48.7	58212	1
24	15	73.9	68888	24	15	73.0	71039	3
25	20	98.3	80482	25	20	97.3	83487	4
26	3	20.7	27335	26	3	20.4		
27	6	41.4	44646	27	6	40.9	43098	4
28	10	69.0	61580	28	10	68.1	61101	1
29	15	103.2	70372	29	15	101.7	72805	3
30	20	137.2		30	20	135.1	82642	

Table D.28: Resilient Modulus of TH 200 Blend

(Y_5.7_1 and Y_5.7_2, 100% Gyratory = 133.84 lb/ft^3, 100% OMC = 5.7%).

Sq	Confining	Deviator	Mr	Sq	Confining	Deviator	Mr	Difference
	psi	psi	psi		psi	psi	psi	(%)
1	3	1.5	10953	1	3	1.4	10903	0
2	6	2.9	24905	2	6	2.8	24924	0
3	10	4.9	40212	3	10	4.9	39689	1
4	15	7.4	57750	4	15	7.3	58180	1
5	20	9.8	72279	5	20	9.8	73548	2
6	3	2.9	12090	6	3	2.9	13354	9
7	6	5.8	26405	7	6	5.9	25833	2
8	10	9.8	42469	8	10	9.8	43478	2
9	15	14.7	58725	9	15	14.7	60756	3
10	20	19.6	73146	10	20	19.6	75272	3
11	3	5.9	14538	11	3	5.9	15998	9
12	6	11.8	29122	12	6	11.8	31299	7
13	10	19.7	46131	13	10	19.6	47432	3
14	15	29.4	60127	14	15	29.4	62418	4
15	20	39.2	70603	15	20	39.1	72757	3
16	3	8.8	15751	16	3	8.8	18050	13
17	6	17.7	31322	17	6	17.6	32893	5
18	10	29.3	45668	18	10	29.3	47718	4
19	15	44.0	58011	19	15	43.9	60082	3
20	20	58.6	67258	20	20	58.3	69600	3
21	3	14.7	18210	21	3	14.6	19556	7
22	6	29.3	32953	22	6	29.2	34702	5
23	10	48.8	44281	23	10	48.7	45876	3
24	15	73.1	55053	24	15	72.8	56394	2
25	20	97.3	66677	25	20	97.0	68528	3
26	3	20.5	18346	26	3	20.5	21409	14
27	6	41.2	35236	27	6	40.9	36496	3
28	10	68.4	47113	28	10	68.0	47845	2
29	15	102.4	56443	29	15	101.7	57411	2
30	20	135.9		30	20	134.6		

D.2 Resilient Modulus (M_R) versus Deviator Stress

Figures D.1 – D.28 show M_R versus deviator stress at different confining pressures of all 28 soil specimens. M_R consistently increased as confining pressure increased. However, deviator stress effect on M_R was less pronounced than confining pressure effect on M_R. Generally, as deviator stress increased, M_R decreased. However, for higher moisture content specimens at lower confining pressures (21 kPa and 41 kPa), M_R values increasing as deviator stress increased were also noticed.

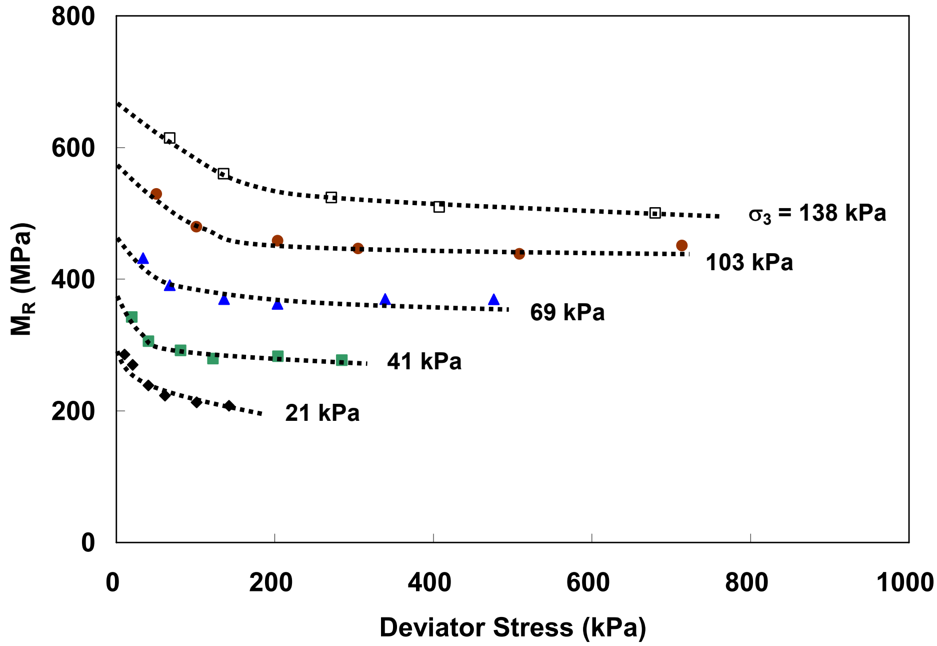

Figure D.1: Resilient Modulus of CR 3 Blend

(S_5.1_1, 98% Gyratory, 65% OMC (γ_d = 1966 kg/m^3, MC = 5.1%)).

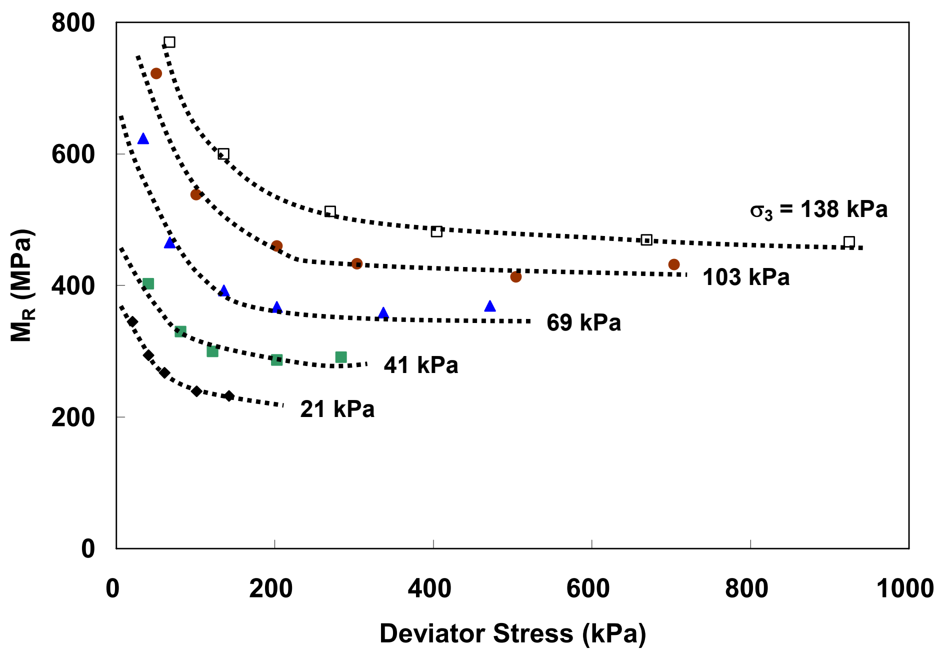

Figure D.2: Resilient Modulus of CR 3 Blend

(S_5.1_2, 98% Gyratory, 65% OMC (γ_d = 1995 kg/m^3, MC = 4.9%)).

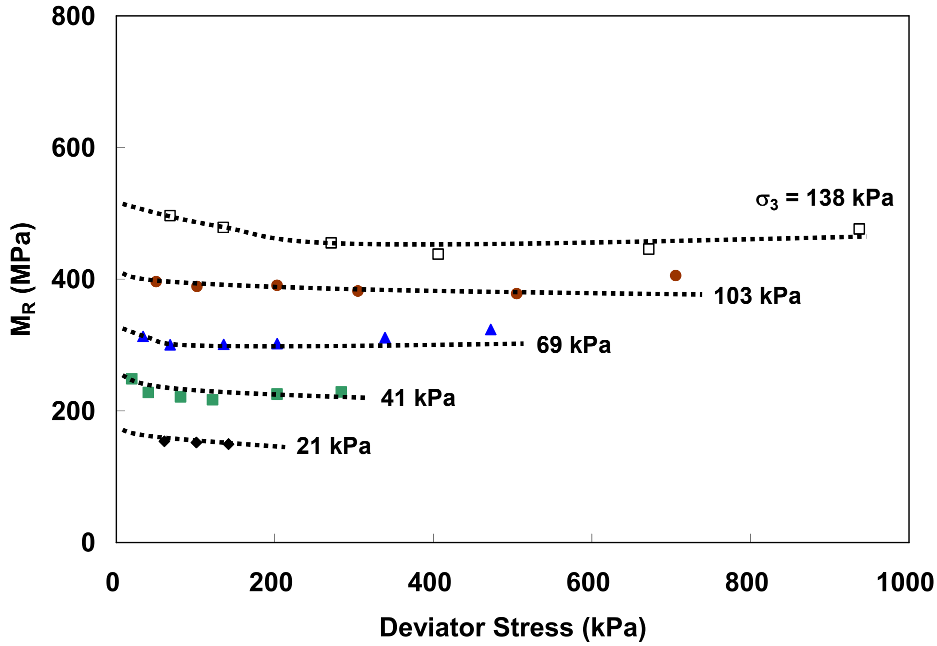

Figure D.3: Resilient Modulus of CR 3 Blend

(S_7.8_1, 100% Gyratory, 100% OMC (γ_d = 2032 kg/m^3, MC = 7.4%)).

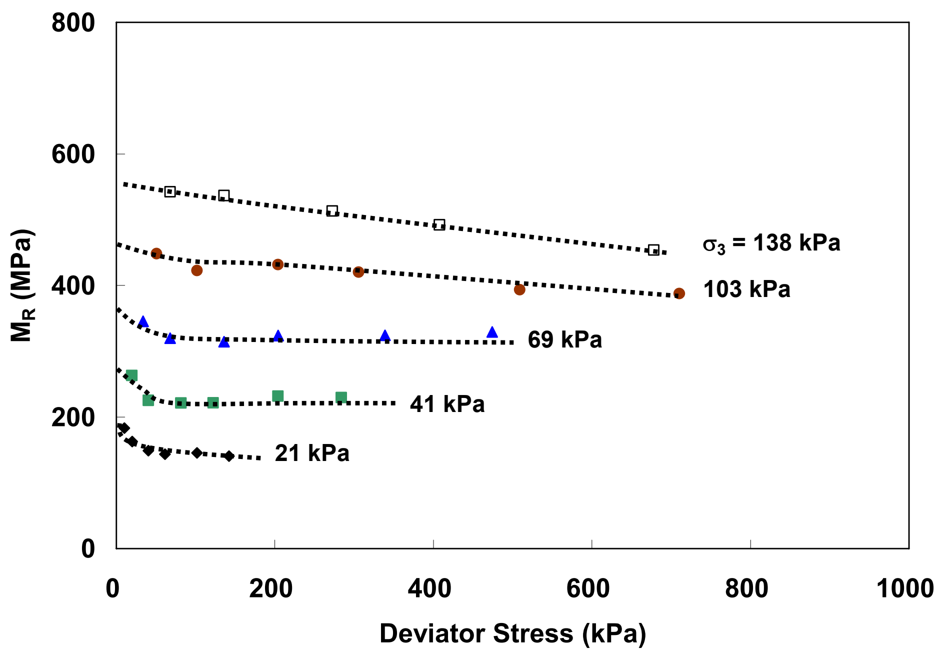

Figure D.4: Resilient Modulus of CR 3 Blend

(S_7.8_2, 100% Gyratory, 100% OMC (γ_d = 2043 kg/m^3, MC = 7.7%)).

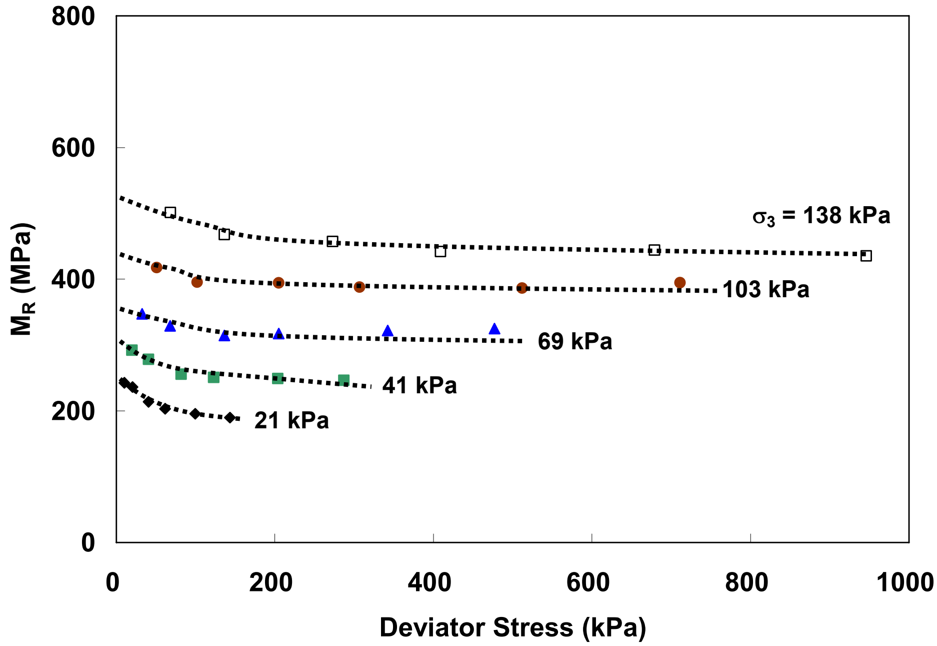

Figure D.5: Resilient Modulus of CR 3 100% Aggregate

(T_5.7_1, 98% Gyratory, 65% OMC (γ_d = 1963 kg/m^3, MC = 6.0%)).

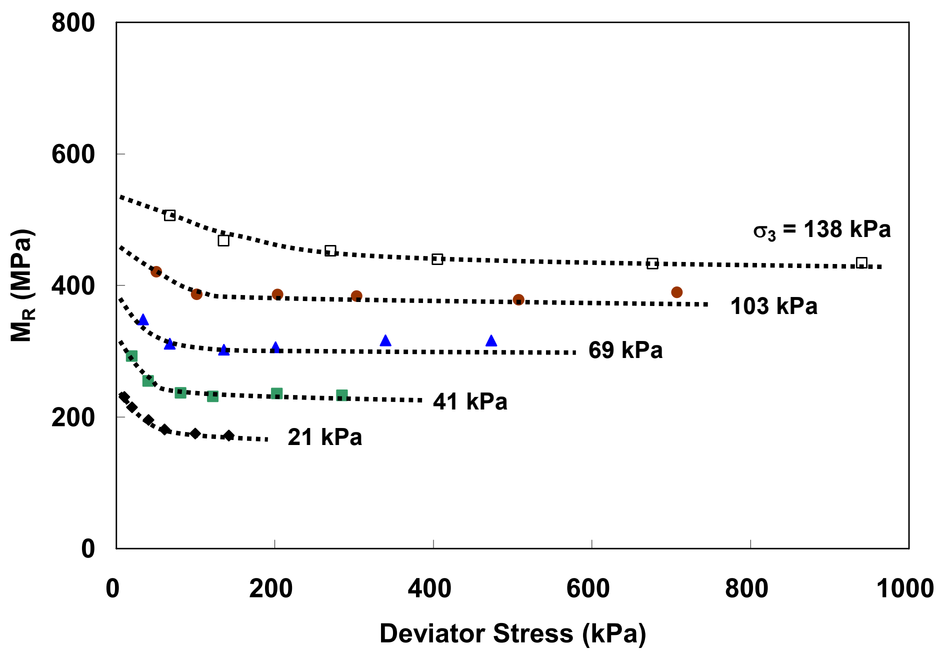

Figure D.6: Resilient Modulus of CR 3 100% Aggregate

(T_5.7_2, 98% Gyratory, 65% OMC (γ_d = 1961 kg/m^3, MC = 6.2%)).

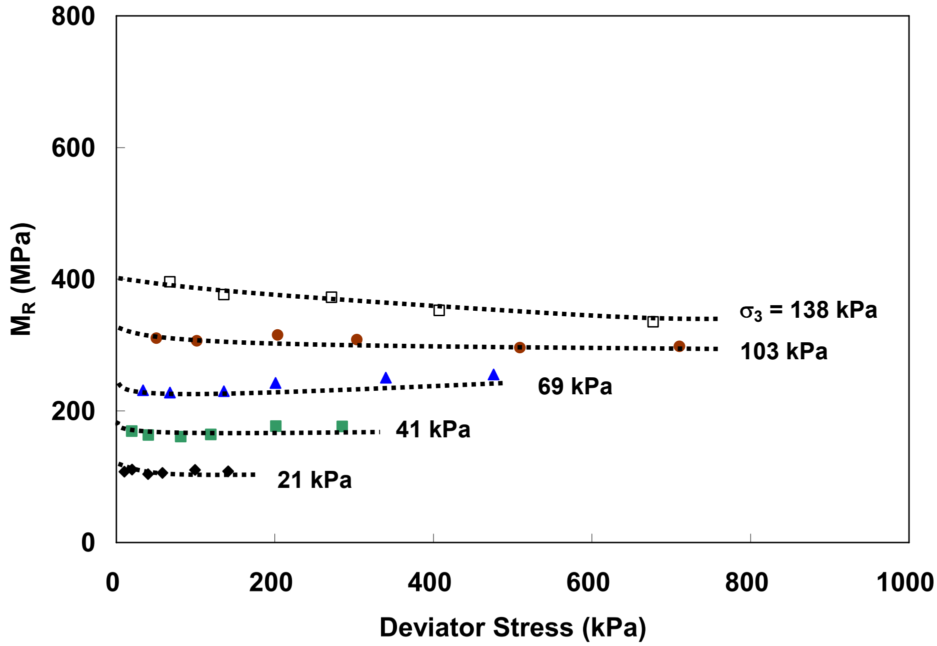

Figure D.7: Resilient Modulus of CR 3 100% Aggregate
(T_8.8_1, 100% Gyratory, 100% OMC (γ_d = 2041 kg/m^3, MC = 9.1%)).

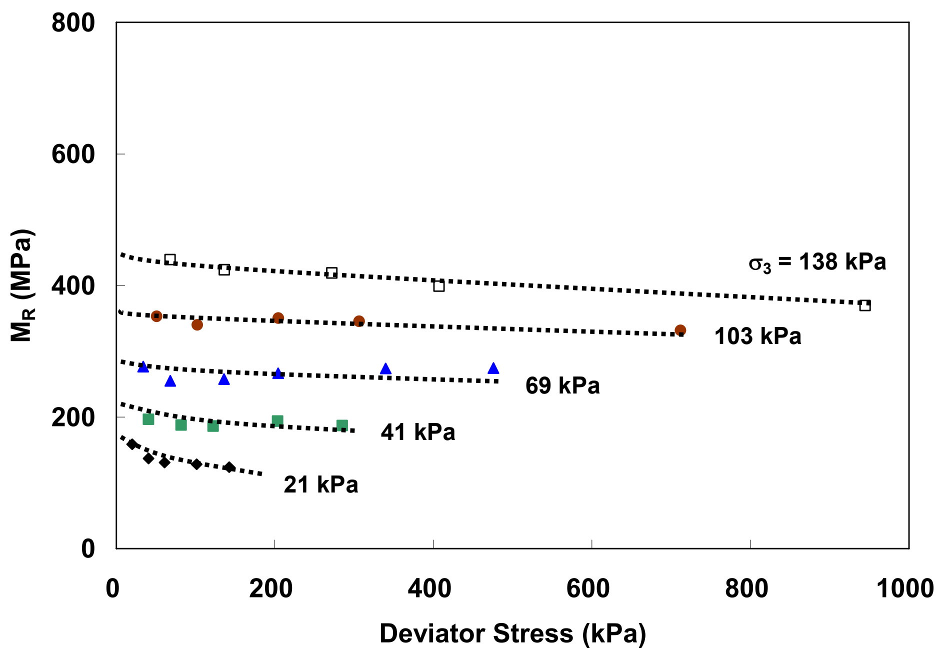

Figure D.8: Resilient Modulus of CR 3 100% Aggregate
(T_8.8_2, 100% Gyratory, 100% OMC (γ_d = 2035 kg/m^3, MC = 9.1%)).

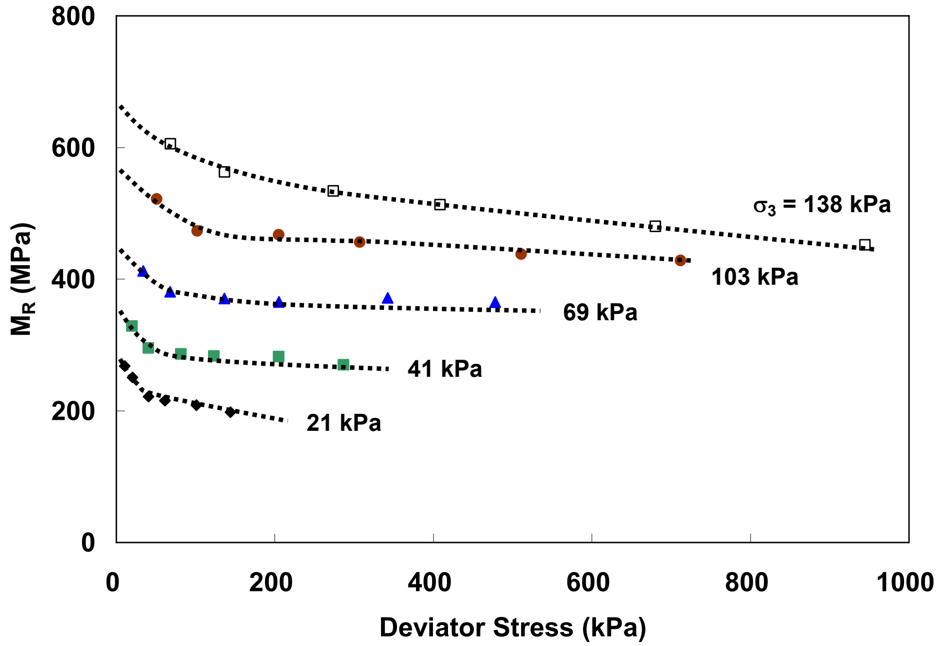

Figure D.9: Resilient Modulus of CR 3 75% Aggregate – 25% RAP (U_5.7_1, 98% Gyratory, 65% OMC (γ_d = 2001 kg/m^3, MC = 6.1%)).

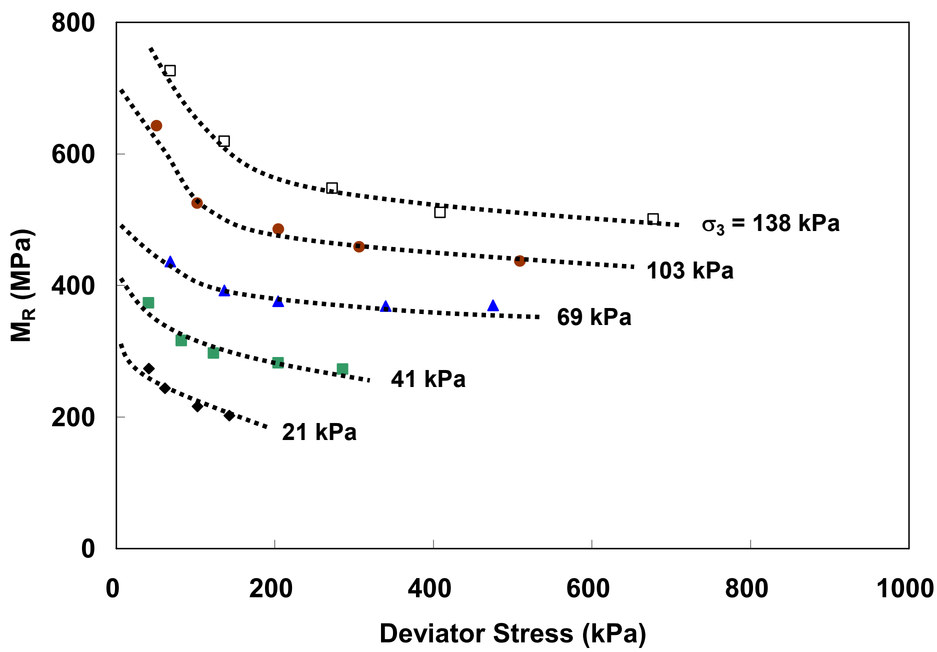

Figure D.10: Resilient Modulus of CR 3 75% Aggregate – 25% RAP (U_5.7_2, 98% Gyratory, 65% OMC (γ_d = 1958 kg/m^3, MC = 6.0%)).

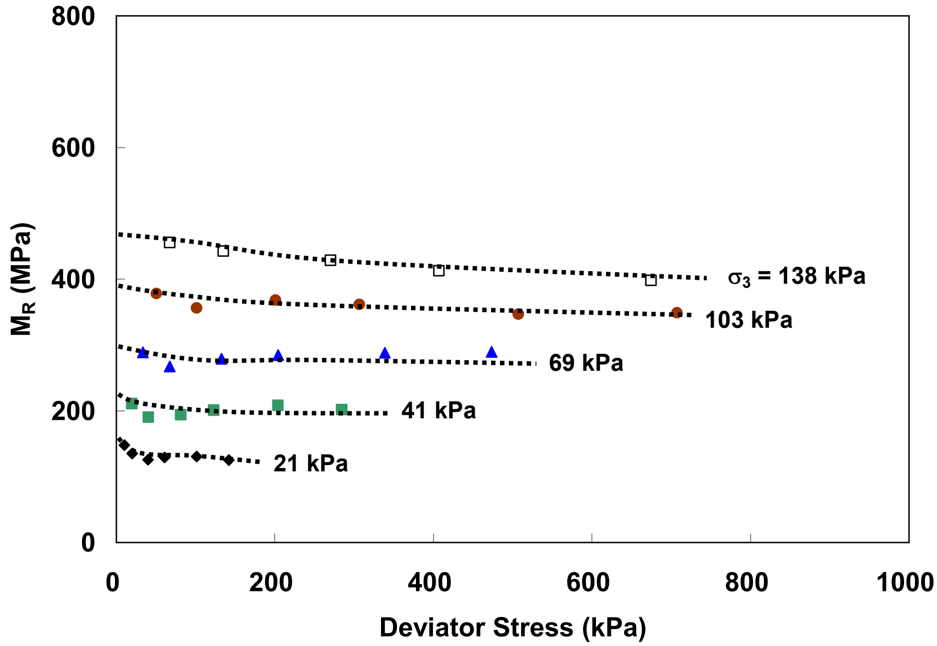

Figure D.11: Resilient Modulus of CR 3 75% Aggregate – 25% RAP (U_8.7_1, 100% Gyratory, 100% OMC (γ_d = 2051 kg/m^3, MC = 8.3%)).

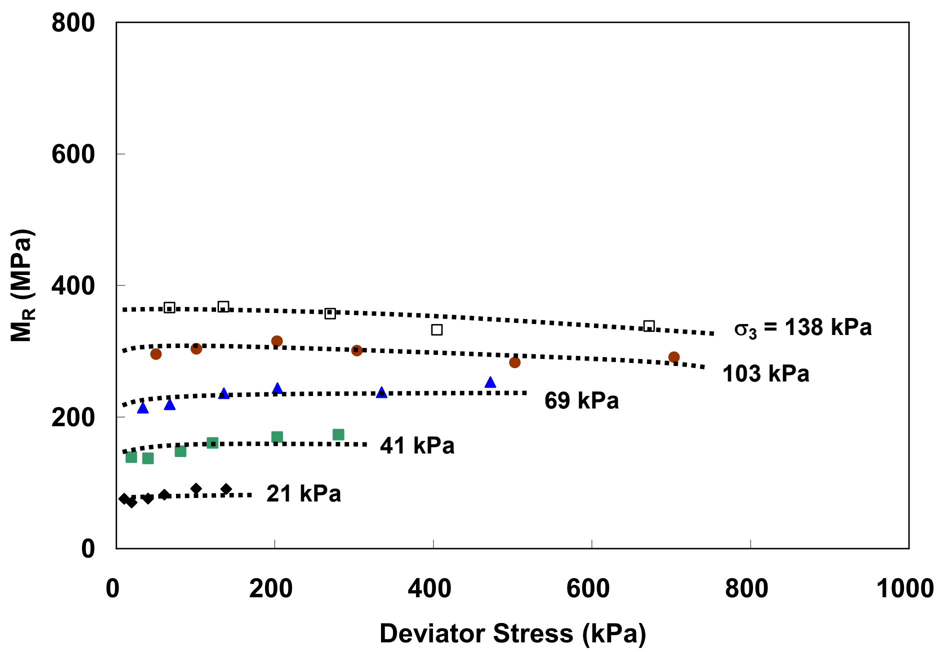

Figure D.12: Resilient Modulus of CR 3 75% Aggregate – 25% RAP (U_8.7_2, 100% Gyratory, 100% OMC (γ_d = 2049 kg/m^3, MC = 8.8%)).

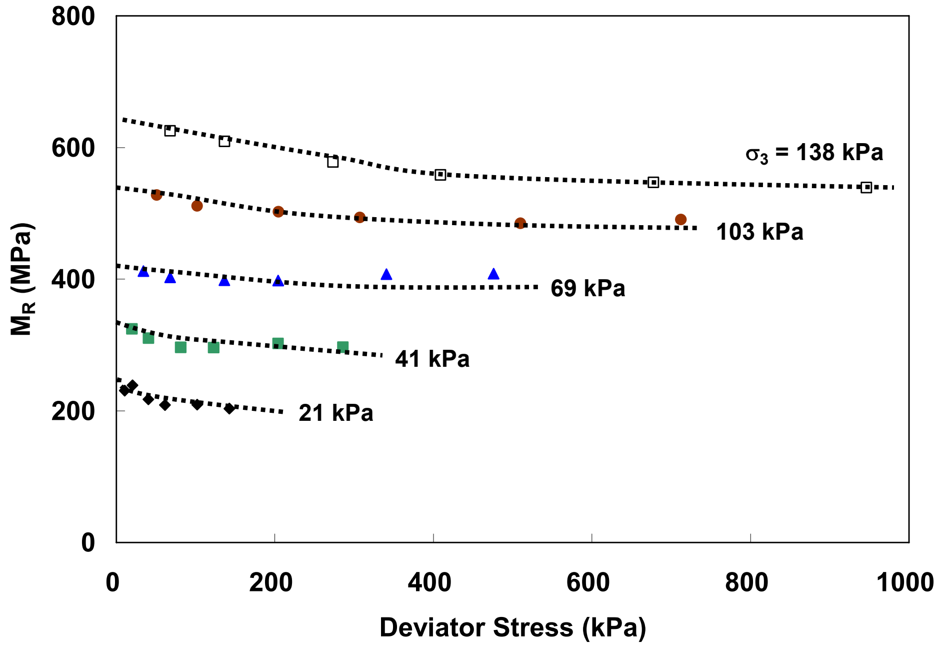

Figure D.13: Resilient Modulus of CR 3 50% Aggregate – 50% RAP (V_5.2_1, 98% Gyratory, 65% OMC (γ_d = 1996 kg/m^3, MC = 5.1%)).

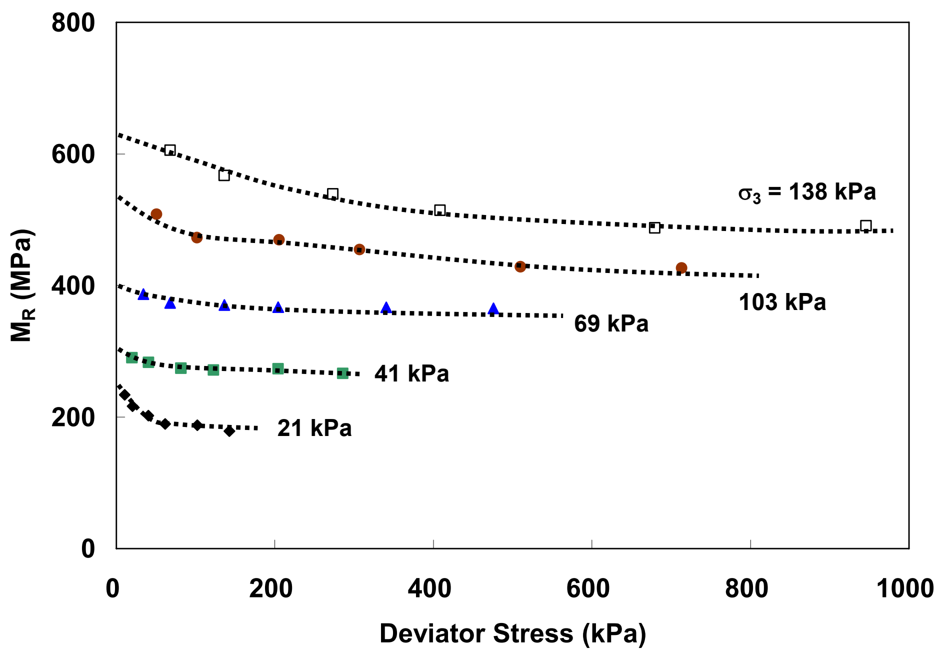

Figure D.14: Resilient Modulus of CR 3 50% Aggregate – 50% RAP (V_5.2_2, 98% Gyratory, 65% OMC (γ_d = 1964 kg/m^3, MC = 5.7%)).

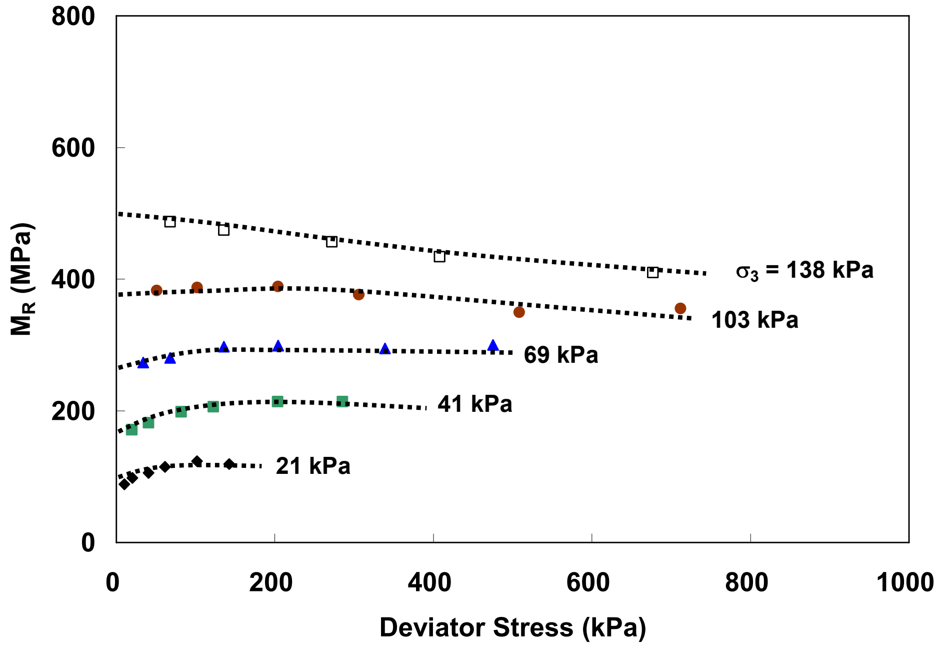

Figure D.15: Resilient Modulus of CR 3 50% Aggregate – 50% RAP (V_8_1, 100% Gyratory, 100% OMC (γ_d = 2048 kg/m^3, MC = 8.4%)).

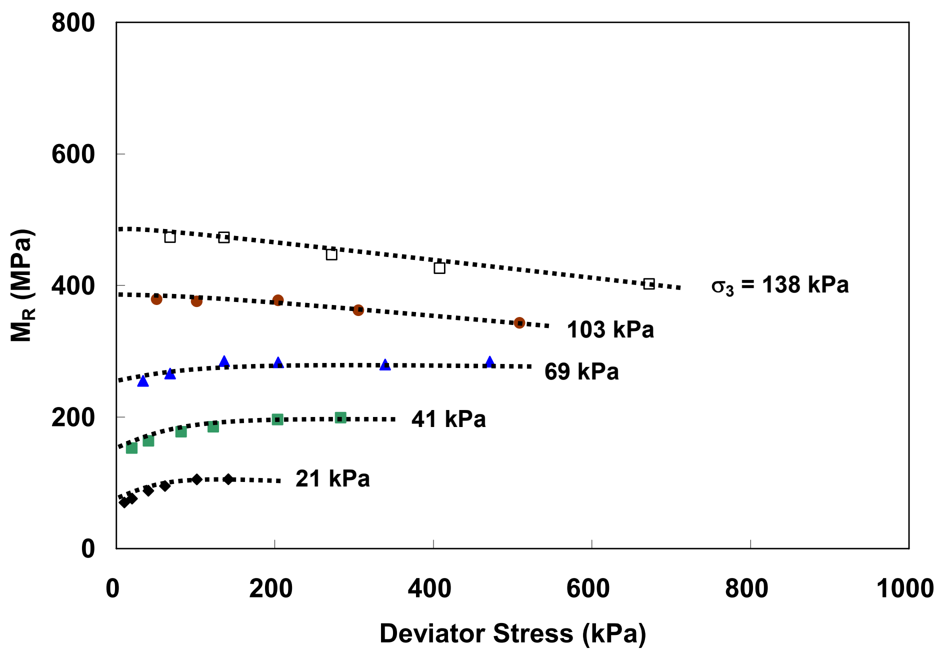

Figure D.16: Resilient Modulus of CR 3 50% Aggregate – 50% RAP (V_8_2, 100% Gyratory, 100% OMC (γ_d = 2049 kg/m^3, MC = 8.0%)).

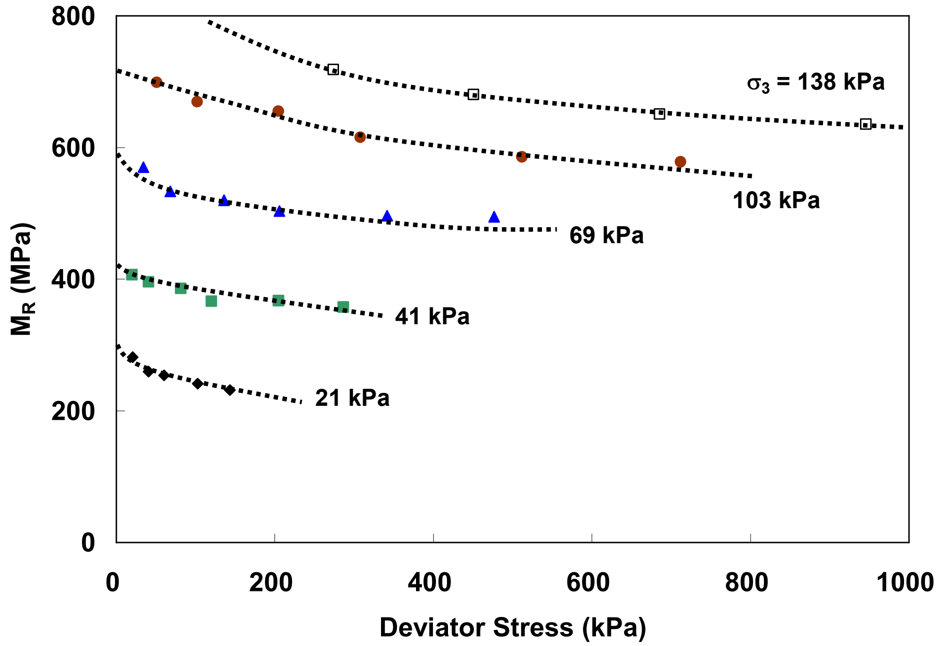

Figure D.17: Resilient Modulus of CR 3 25% Aggregate – 75% RAP (W_4.7_1, 98% Gyratory, 65% OMC (γ_d = 2000 kg/m^3, MC = 4.5%)).

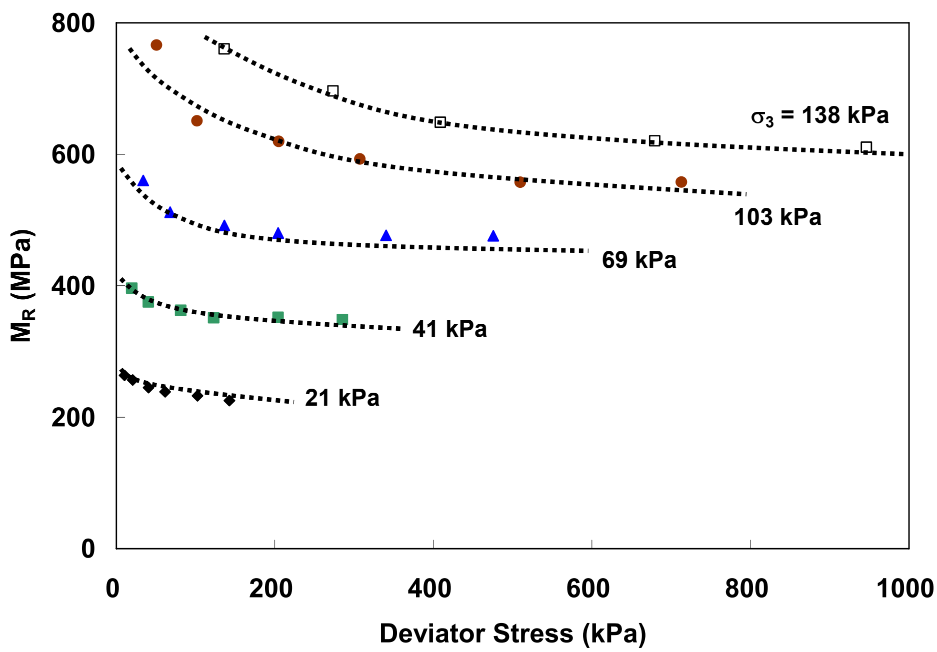

Figure D.18: Resilient Modulus of CR 3 25% Aggregate – 75% RAP (W_4.7_2, 98% Gyratory, 65% OMC (γ_d = 1987 kg/m^3, MC = 4.3%)).

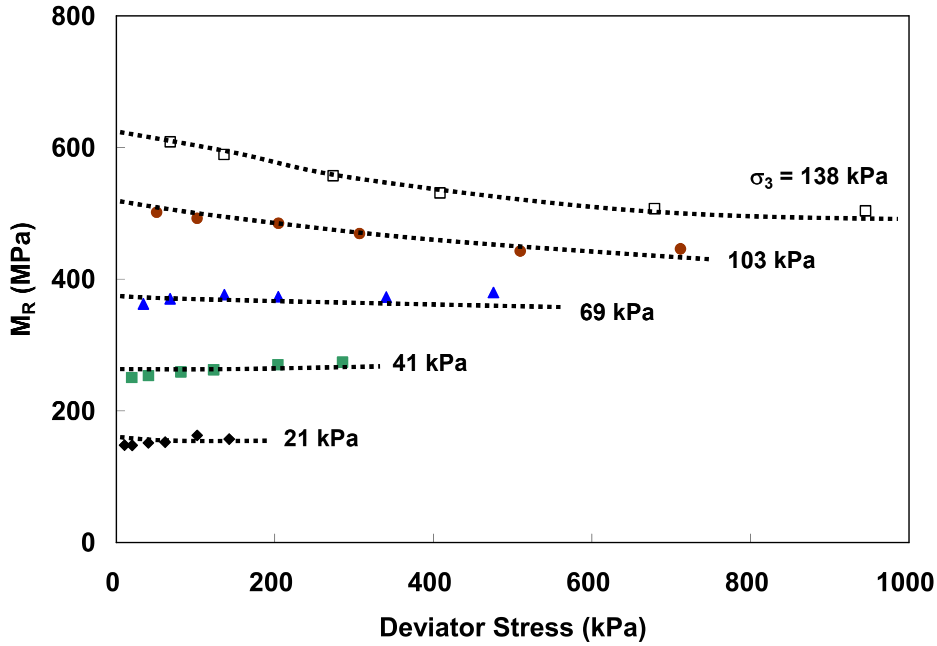

Figure D.19: Resilient Modulus of CR 3 25% Aggregate – 75% RAP (W_7.2_1, 100% Gyratory, 100% OMC (γ_d = 2052 kg/m^3, MC = 7.3%)).

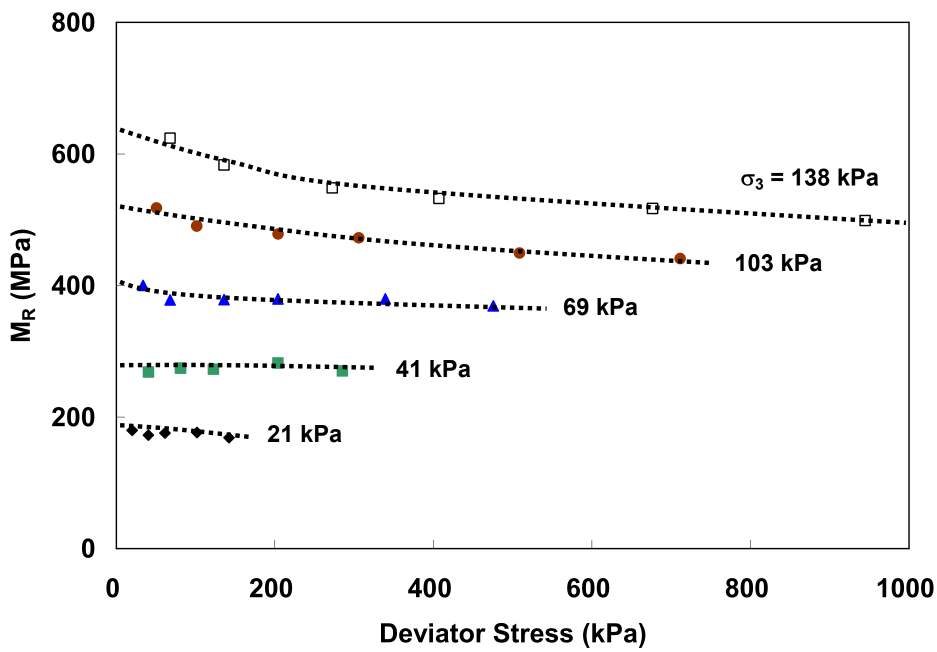

Figure D.20: Resilient Modulus of CR 3 25% Aggregate – 75% RAP (W_7.2_2, 100% Gyratory, 100% OMC (γ_d = 2032 kg/m^3, MC = 7.7%)).

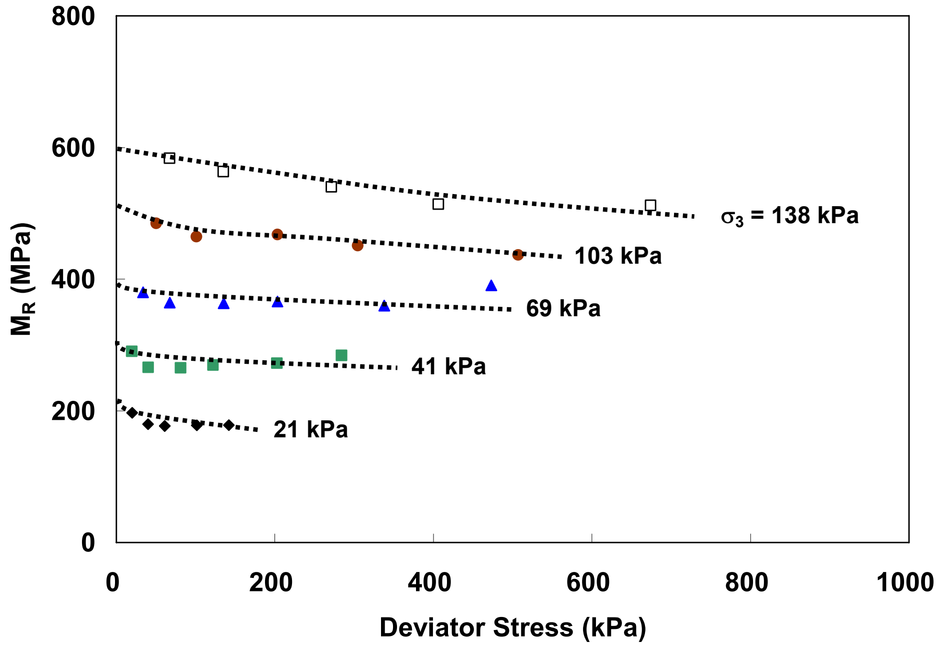

Figure D.21: Resilient Modulus of TH 23 Blend

(X_3.5_1, 100% Gyratory, 65% OMC (γ_d = 2097 kg/m^3, MC = 3.6%)).

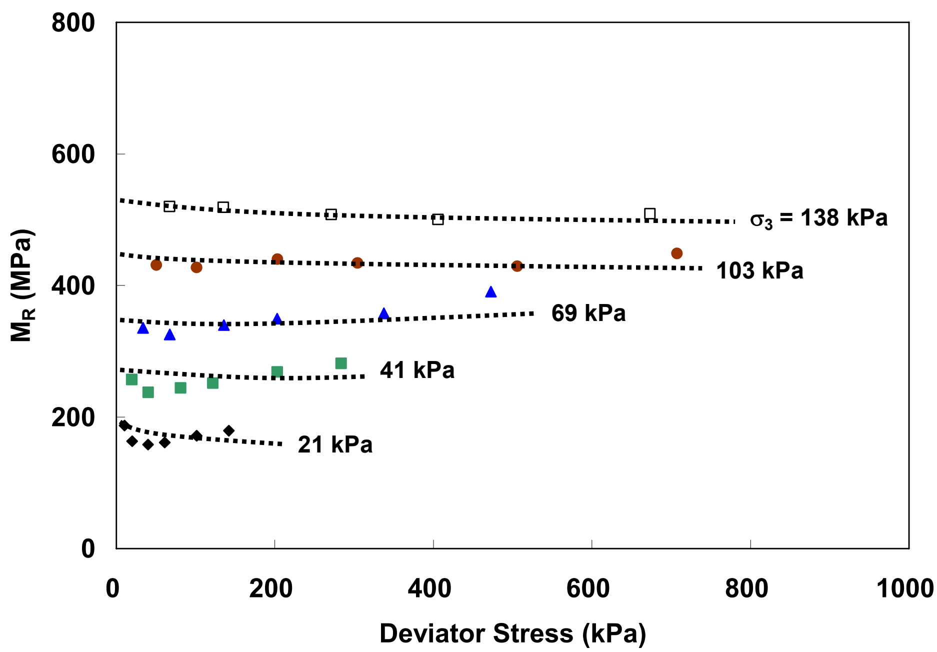

Figure D.22: Resilient Modulus of TH 23 Blend

(X_3.5_2, 100% Gyratory, 65% OMC (γ_d = 2094 kg/m^3, MC = 3.6%)).

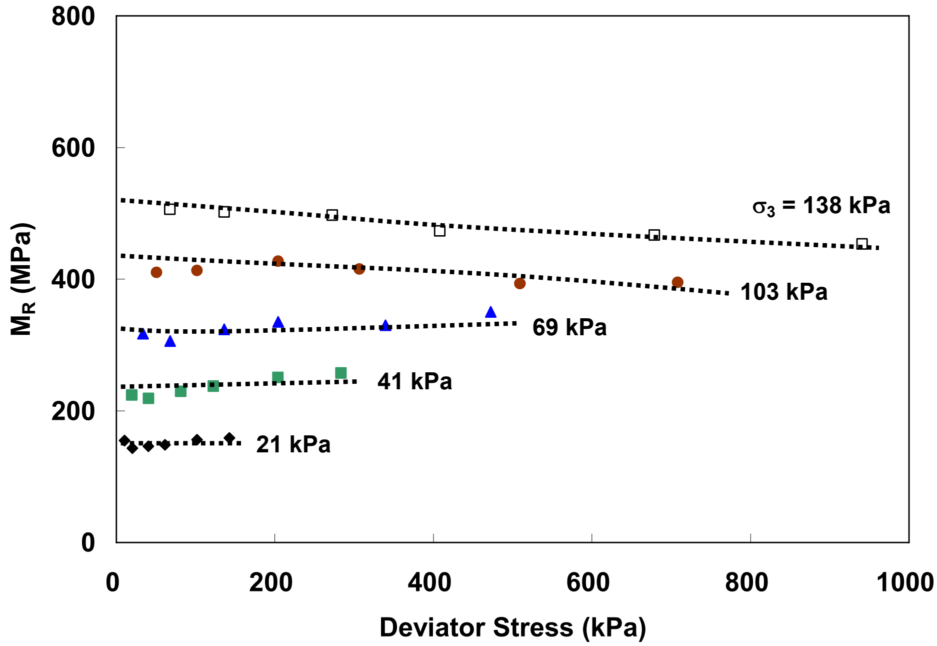

Figure D.23: Resilient Modulus of TH 23 Blend

(X_5.4_1, 100% Gyratory, 100% OMC ($\gamma_d = 2100$ kg/m^3, MC = 5.4%)).

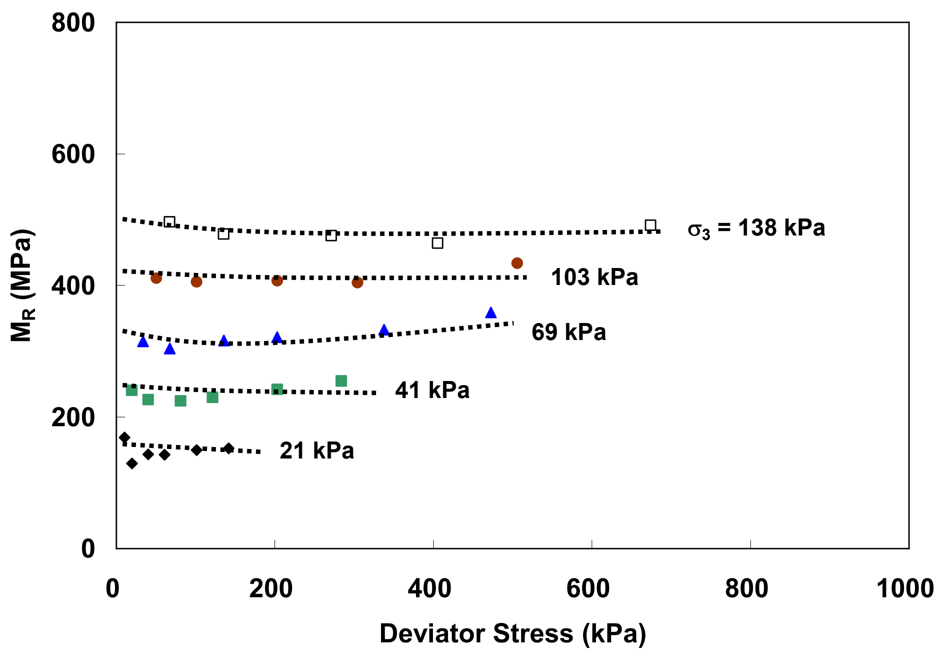

Figure D.24: Resilient Modulus of TH 23 Blend

(X_5.4_2, 100% Gyratory, 100% OMC ($\gamma_d = 2091$ kg/m^3, MC = 5.6%)).

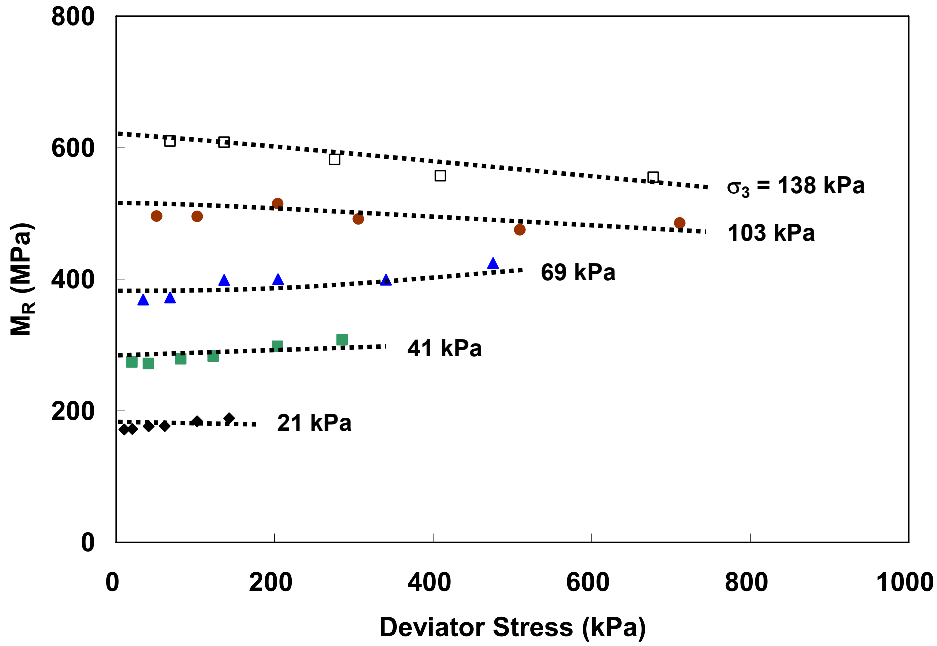

Figure D.25: Resilient Modulus of TH 200 Blend

(Y_3.7_1, 100% Gyratory, 65% OMC (γ_d = 2140 kg/m^3, MC = 4.0%)).

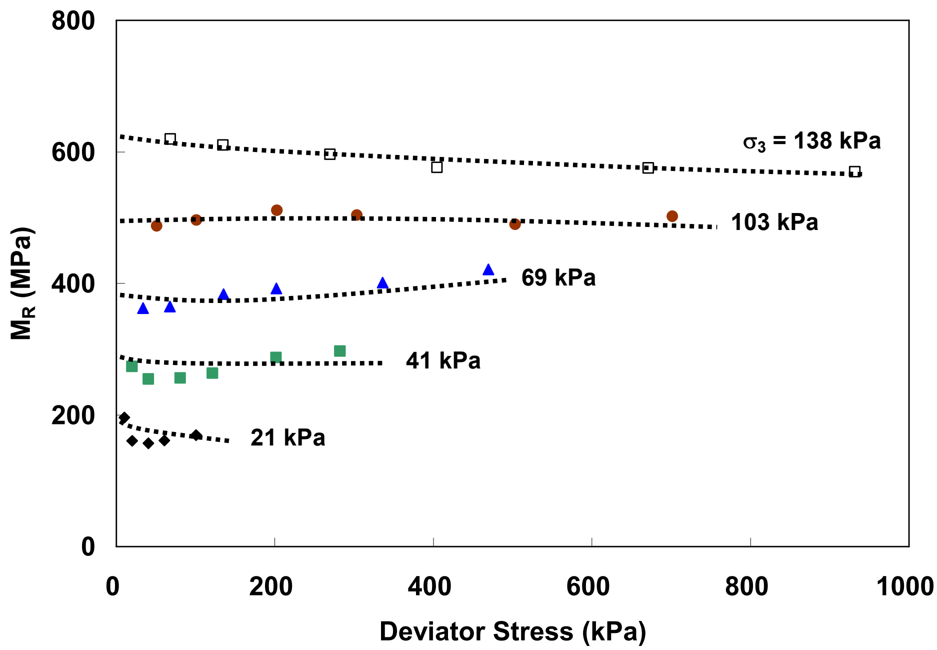

Figure D.26: Resilient Modulus of TH 200 Blend

(Y_3.7_2, 100% Gyratory, 65% OMC (γ_d = 2145 kg/m^3, MC = 3.9%)).

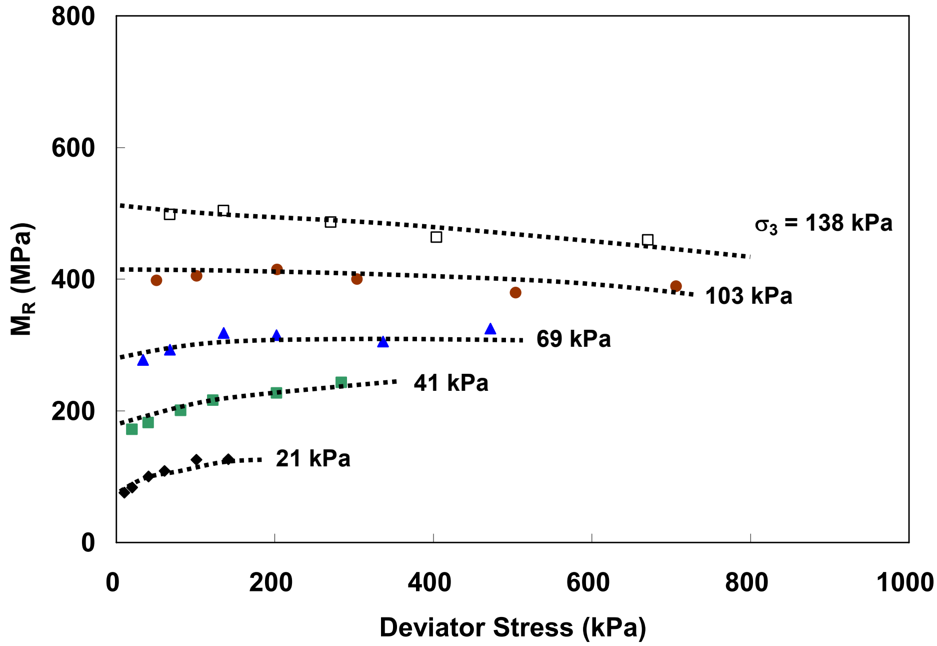

Figure D.27: Resilient Modulus of TH 200 Blend
(Y_5.7_1, 100% Gyratory, 100% OMC (γ_d = 2161 kg/m^3, MC = 5.6%)).

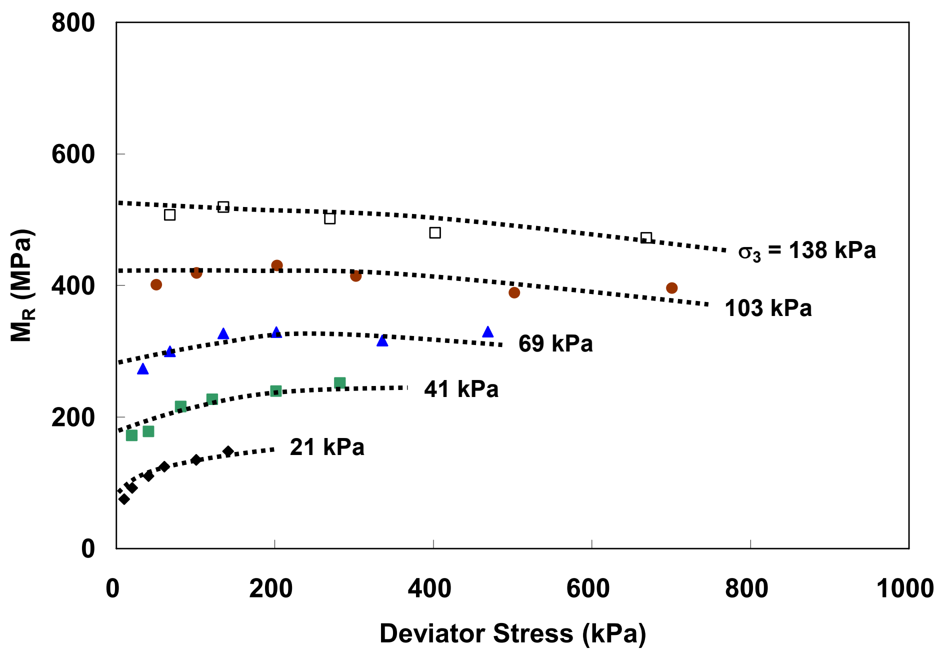

Figure D.28: Resilient Modulus of TH 200 Blend
(Y_5.7_2, 100% Gyratory, 100% OMC (γ_d = 2153 kg/m^3, MC = 5.9%)).

ENGLISH UNITS

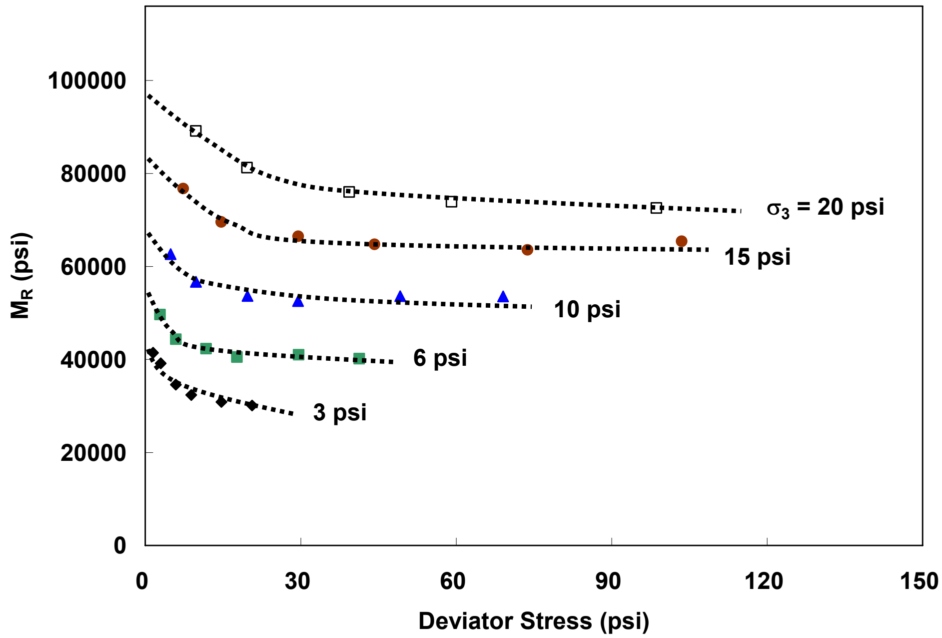

Figure D.29: Resilient Modulus of CR 3 Blend

(S_5.1_1, 98% Gyratory, 65% OMC (γ_d = 122.73 lb/ft^3, MC = 5.1%)).

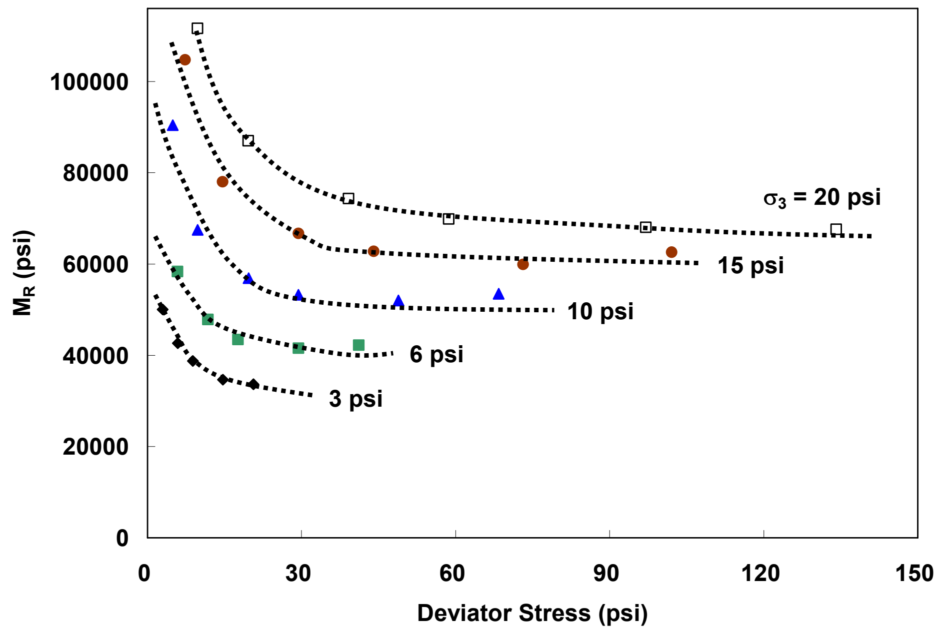

Figure D.30: Resilient Modulus of CR 3 Blend

(S_5.1_2, 98% Gyratory, 65% OMC (γ_d = 124.54 lb/ft^3, MC = 4.9%)).

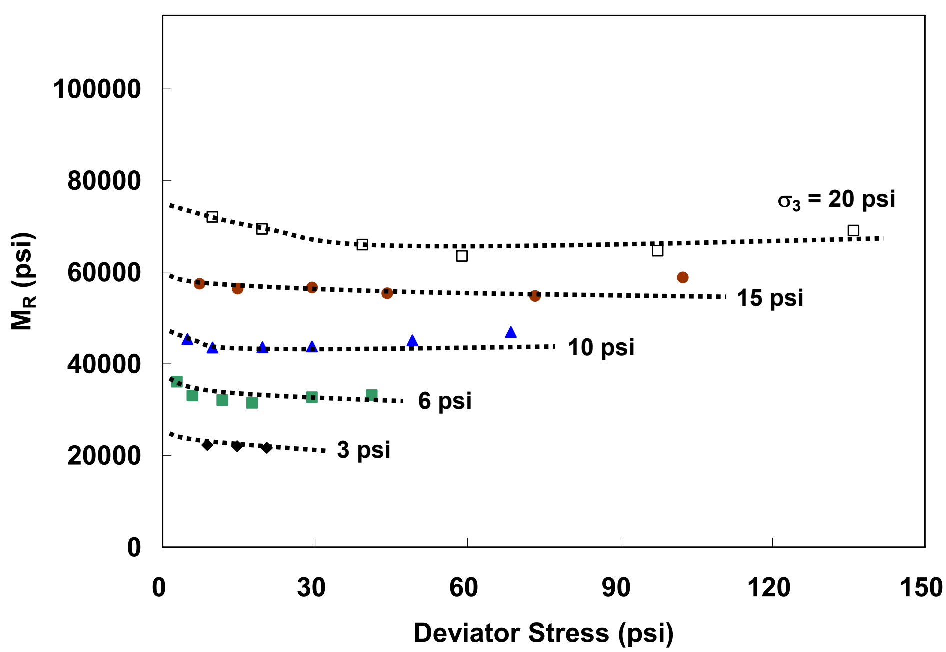

Figure D.31: Resilient Modulus of CR 3 Blend

(S_7.8_1, 100% Gyratory, 100% OMC (γ_d = 126.85 lb/ft^3, MC = 7.4%)).

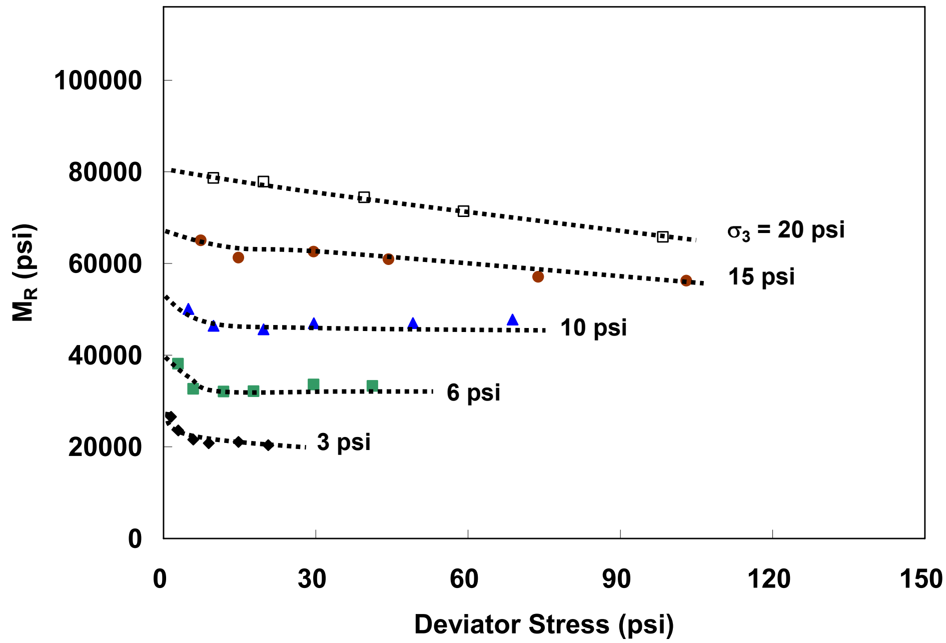

Figure D.32: Resilient Modulus of CR 3 Blend

(S_7.8_2, 100% Gyratory, 100% OMC (γ_d = 127.54 lb/ft^3, MC = 7.7%)).

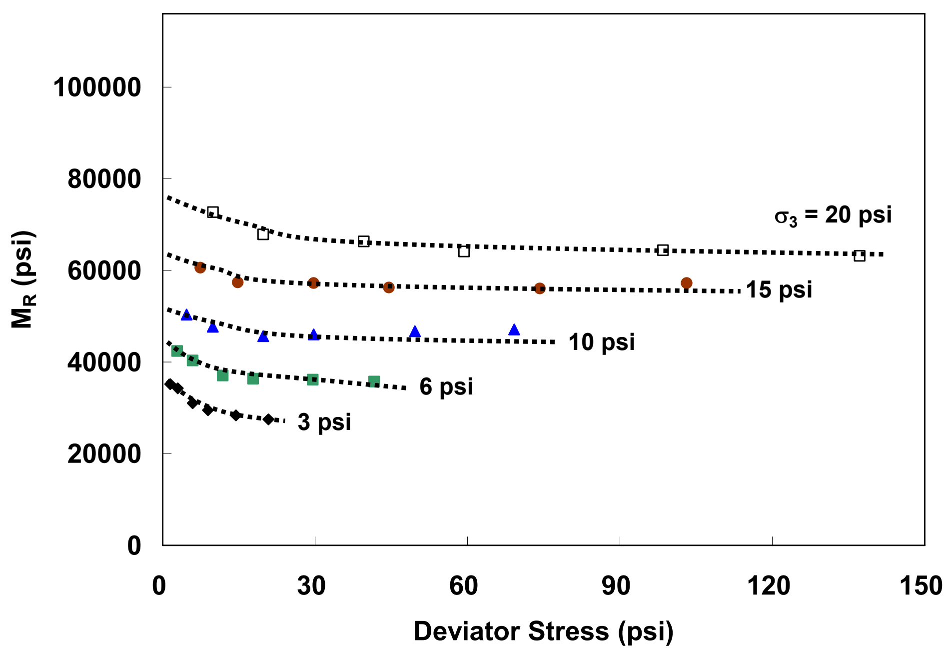

Figure D.33: Resilient Modulus of CR 3 100% Aggregate

(T_5.7_1, 98% Gyratory, 65% OMC (γ_d = 122.55 lb/ft^3, MC = 6.0%)).

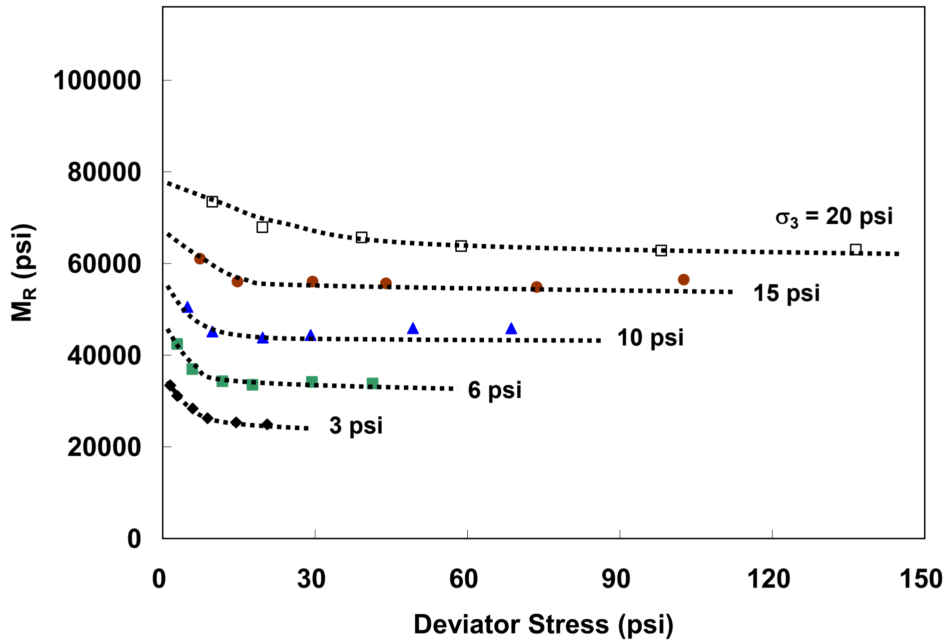

Figure D.34: Resilient Modulus of CR 3 100% Aggregate
(T_5.7_2, 98% Gyratory, 65% OMC (γ_d = 122.42 lb/ft^3, MC = 6.2%)).

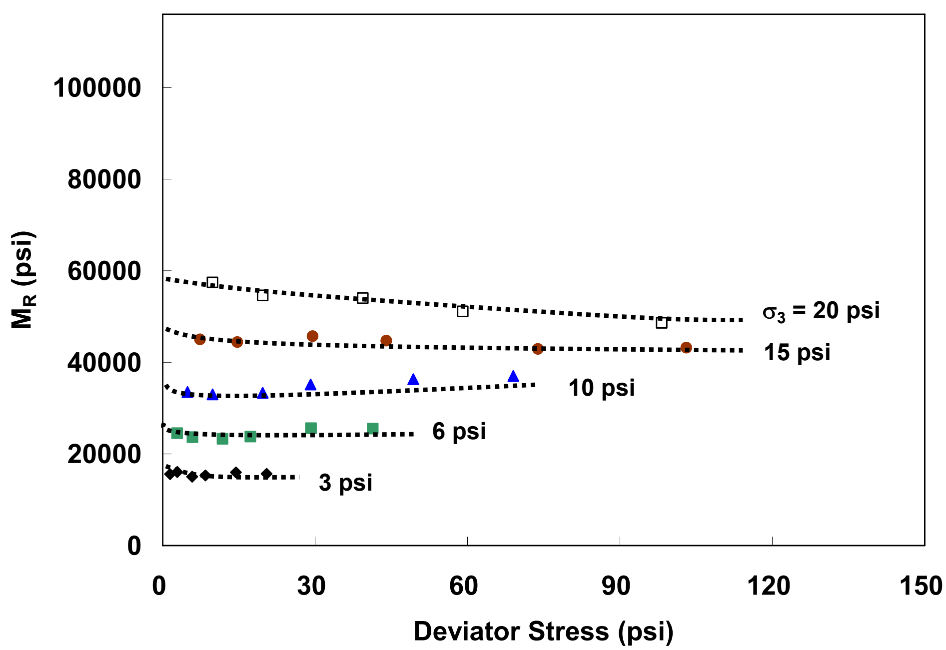

Figure D.35: Resilient Modulus of CR 3 100% Aggregate
(T_8.8_1, 100% Gyratory, 100% OMC (γ_d = 127.35 lb/ft^3, MC = 9.1%)).

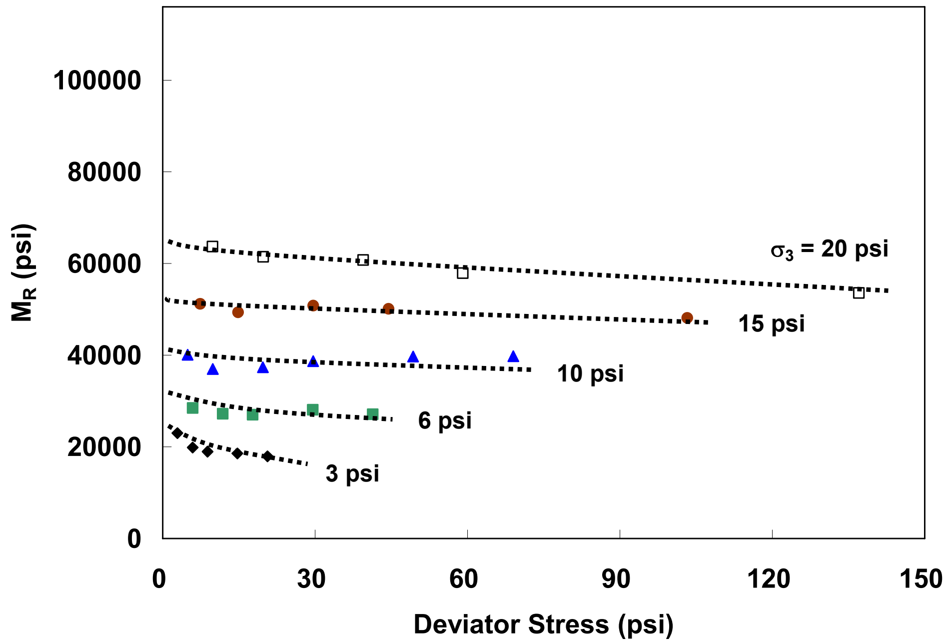

Figure D.36: Resilient Modulus of CR 3 100% Aggregate

(T_8.8_2, 100% Gyratory, 100% OMC (γ_d = 127.04 lb/ft^3, MC = 9.1%)).

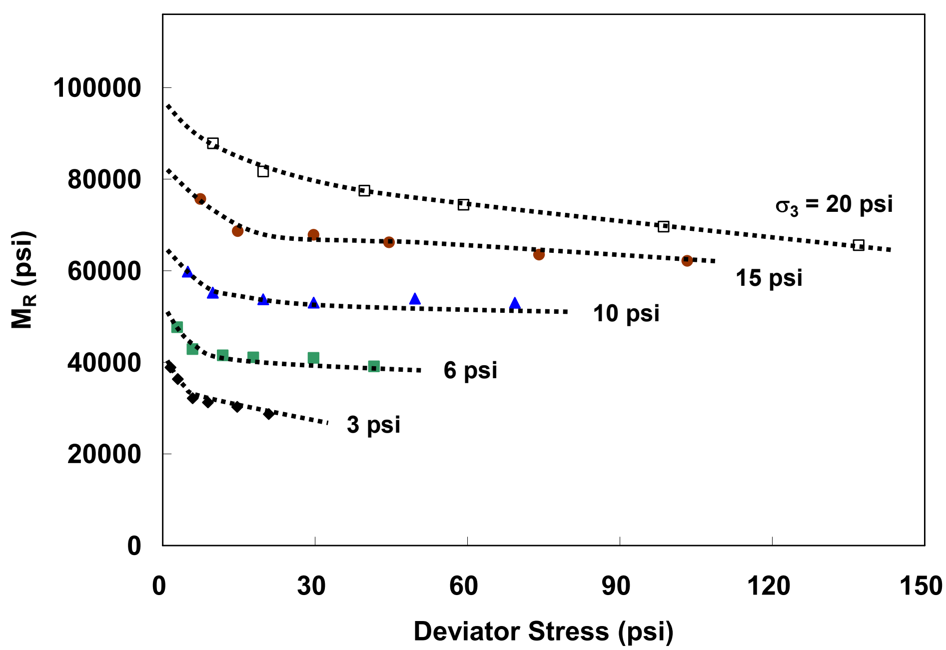

Figure D.37: Resilient Modulus of CR 3 75% Aggregate – 25% RAP

(U_5.7_1, 98% Gyratory, 65% OMC (γ_d = 124.98 lb/ft^3, MC = 6.1%)).

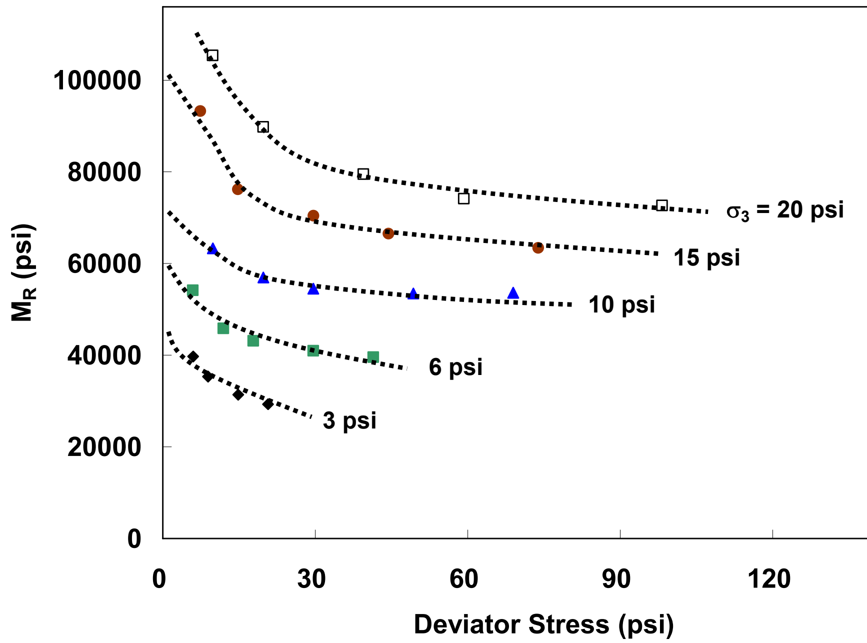

Figure D.38: Resilient Modulus of CR 3 75% Aggregate – 25% RAP (U_5.7_2, 98% Gyratory, 65% OMC (γ_d = 122.23 lb/ft^3, MC = 6.0%)).

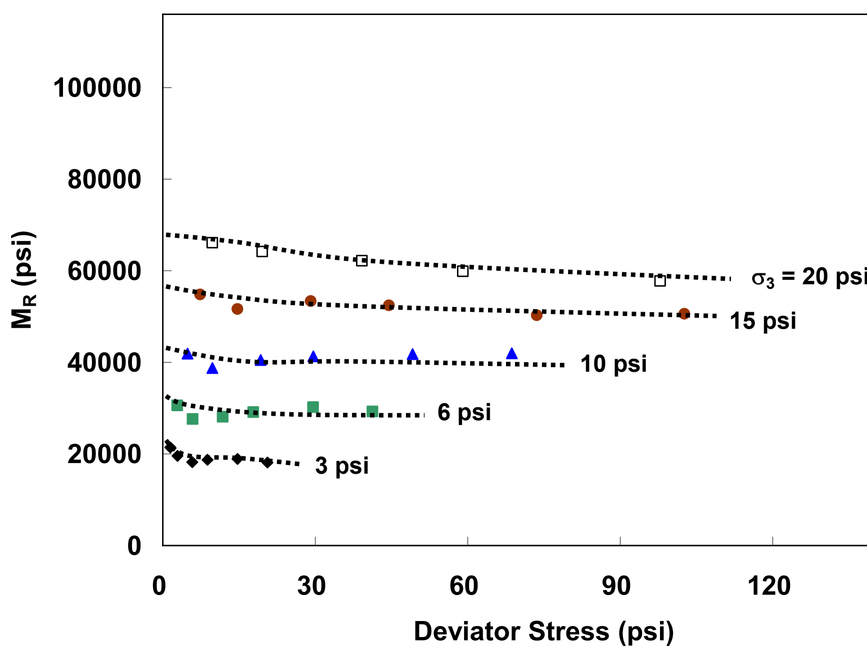

Figure D.39: Resilient Modulus of CR 3 75% Aggregate – 25% RAP (U_8.7_1, 100% Gyratory, 100% OMC (γ_d = 128.04 lb/ft^3, MC = 8.3%)).

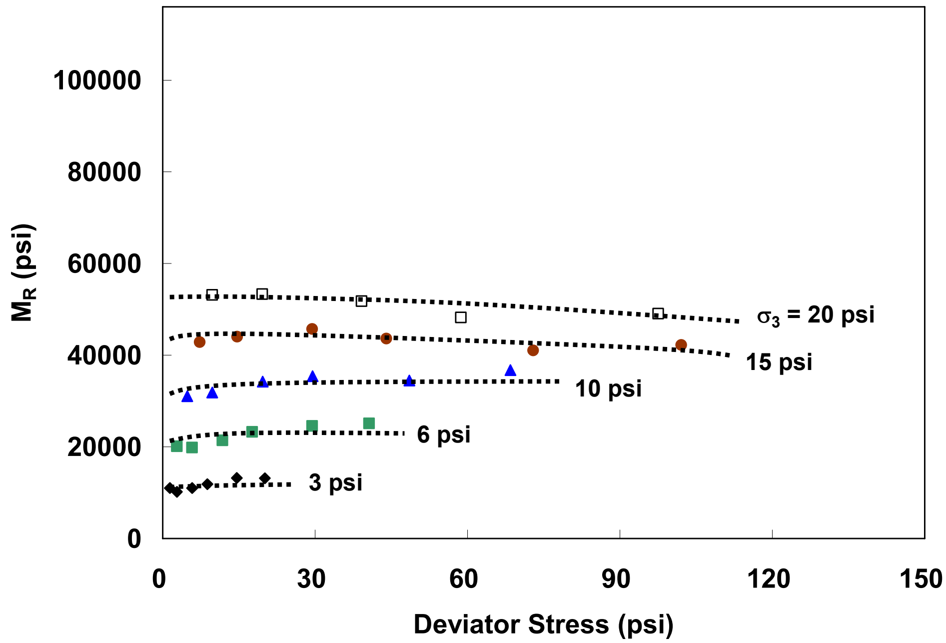

Figure D.40: Resilient Modulus of CR 3 75% Aggregate – 25% RAP (U_8.7_2, 100% Gyratory, 100% OMC (γ_d = 127.91 lb/ft^3, MC = 8.8%)).

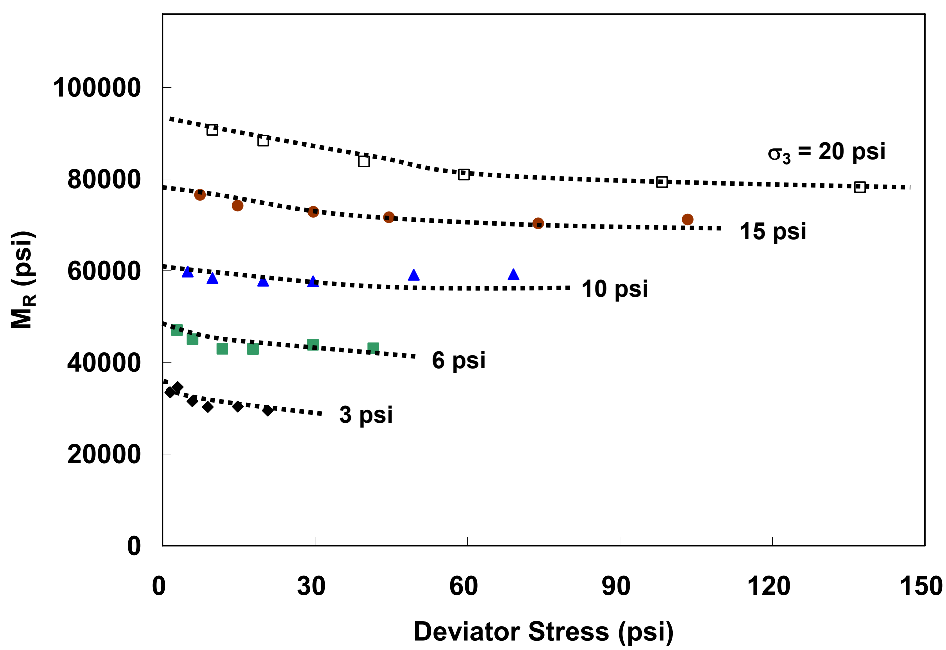

Figure D.41: Resilient Modulus of CR 3 50% Aggregate – 50% RAP (V_5.2_1, 98% Gyratory, 65% OMC (γ_d = 124.61 lb/ft^3, MC = 5.1%)).

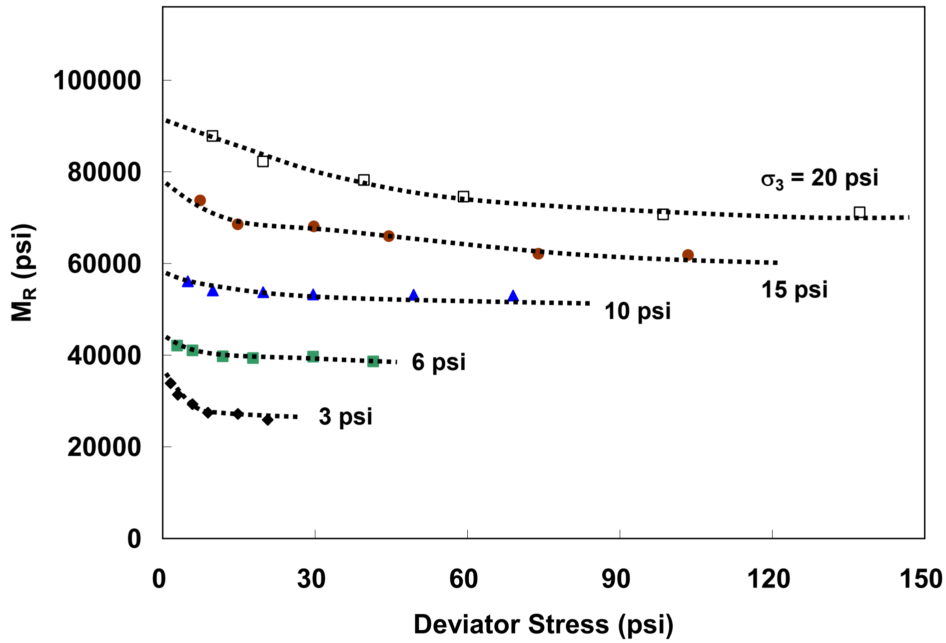

Figure D.42: Resilient Modulus of CR 3 50% Aggregate – 50% RAP (V_5.2_2, 98% Gyratory, 65% OMC (γ_d = 122.61 lb/ft^3, MC = 5.7%)).

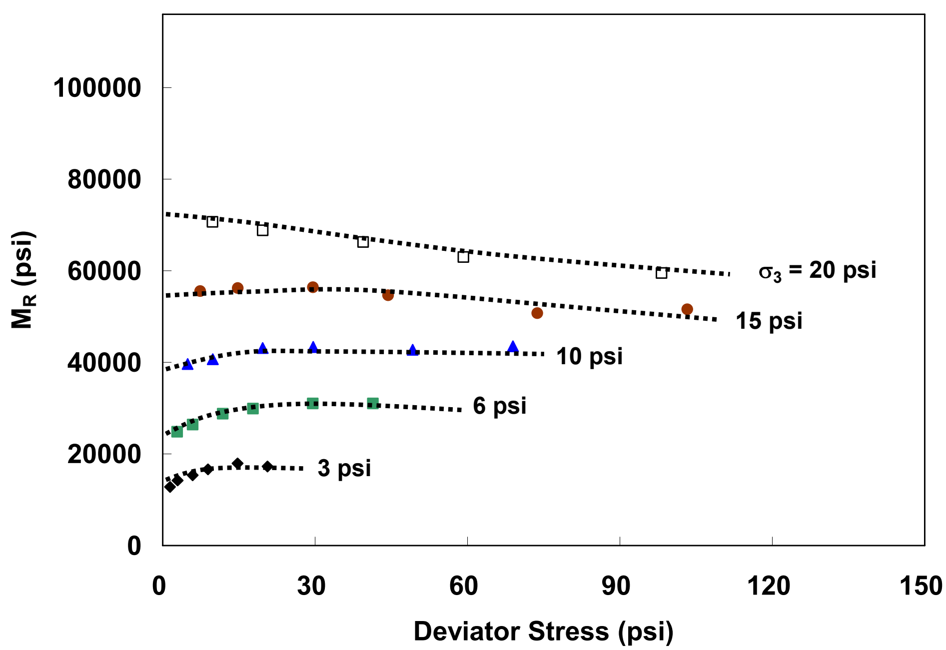

Figure D.43: Resilient Modulus of CR 3 50% Aggregate – 50% RAP (V_8_1, 100% Gyratory, 100% OMC (γ_d = 127.85 lb/ft^3, MC = 8.4%)).

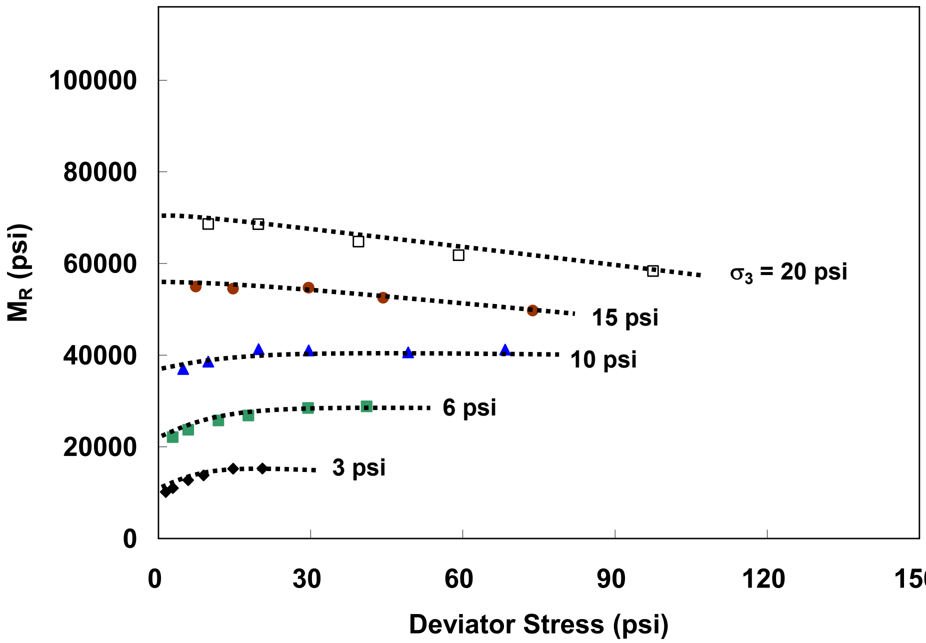

Figure D.44: Resilient Modulus of CR 3 50% Aggregate – 50% RAP (V_8_2, 100% Gyratory, 100% OMC (γ_d = 127.91 lb/ft^3, MC = 8.0%)).

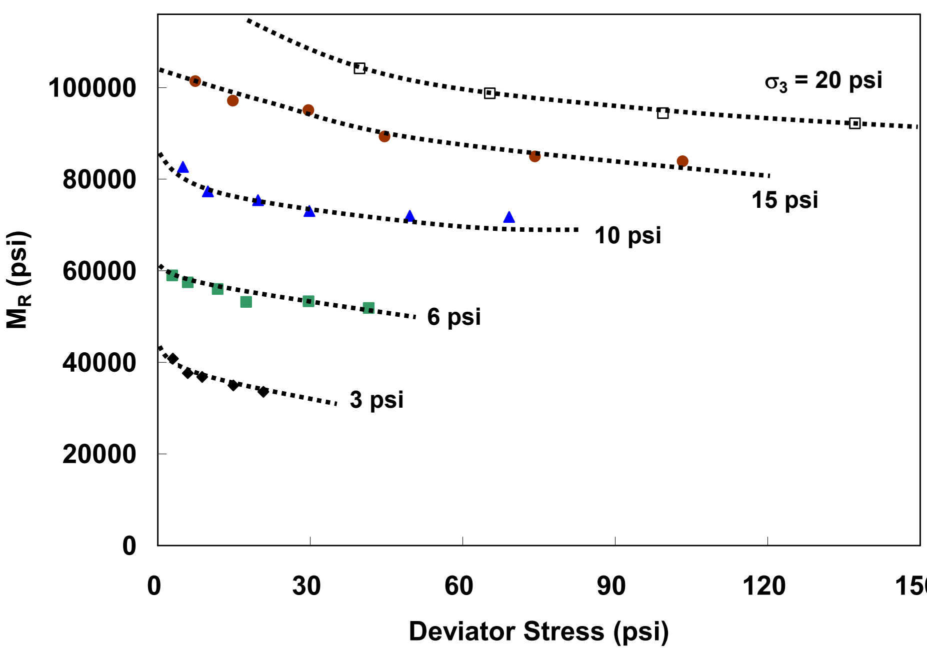

Figure D.45: Resilient Modulus of CR 3 25% Aggregate – 75% RAP (W_4.7_1, 98% Gyratory, 65% OMC (γ_d = 124.86 lb/ft^3, MC = 4.5%)).

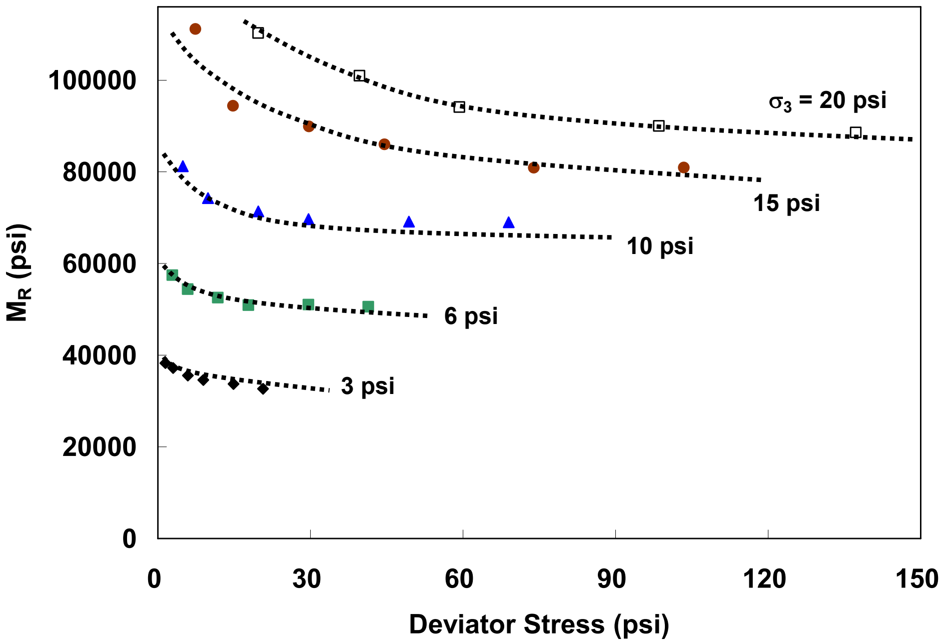

Figure D.46: Resilient Modulus of CR 3 25% Aggregate – 75% RAP (W_4.7_2, 98% Gyratory, 65% OMC (γ_d = 124.04 lb/ft^3, MC = 4.3%)).

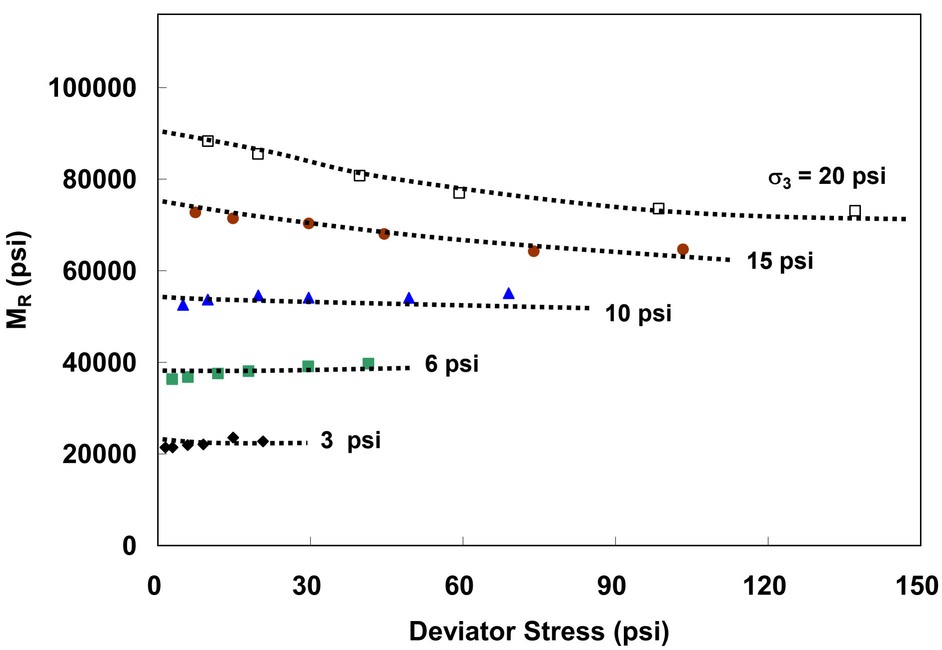

Figure D.47: Resilient Modulus of CR 3 25% Aggregate – 75% RAP (W_7.2_1, 100% Gyratory, 100% OMC (γ_d = 128.10 lb/ft^3, MC = 7.3%)).

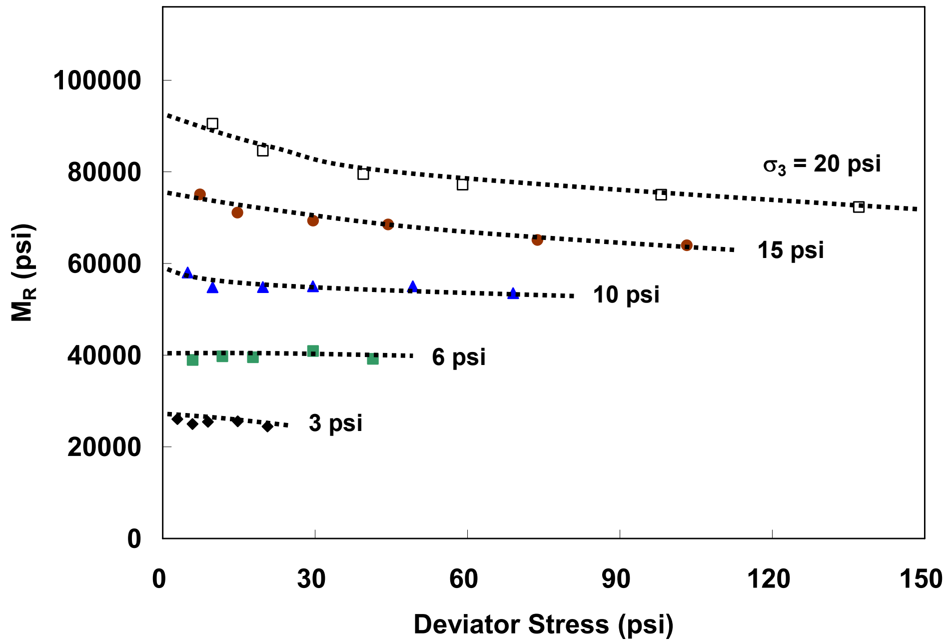

Figure D.48: Resilient Modulus of CR 3 25% Aggregate – 75% RAP (W_7.2_2, 100% Gyratory, 100% OMC (γ_d = 126.85 lb/ft^3, MC = 7.7%)).

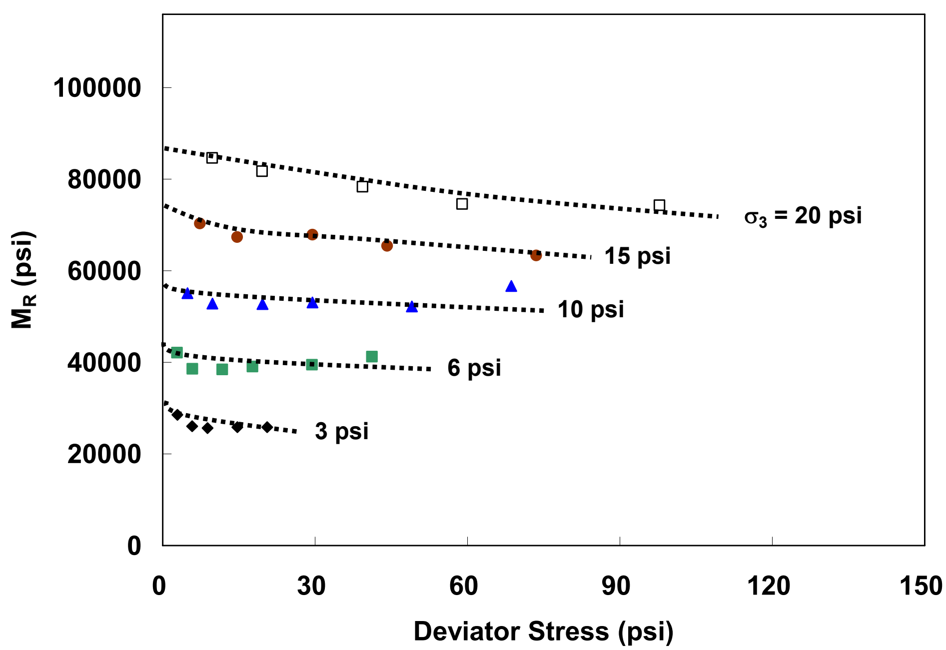

Figure D.49: Resilient Modulus of TH 23 Blend (X_3.5_1, 100% Gyratory, 65% OMC (γ_d = 130.91 lb/ft^3, MC = 3.6%)).

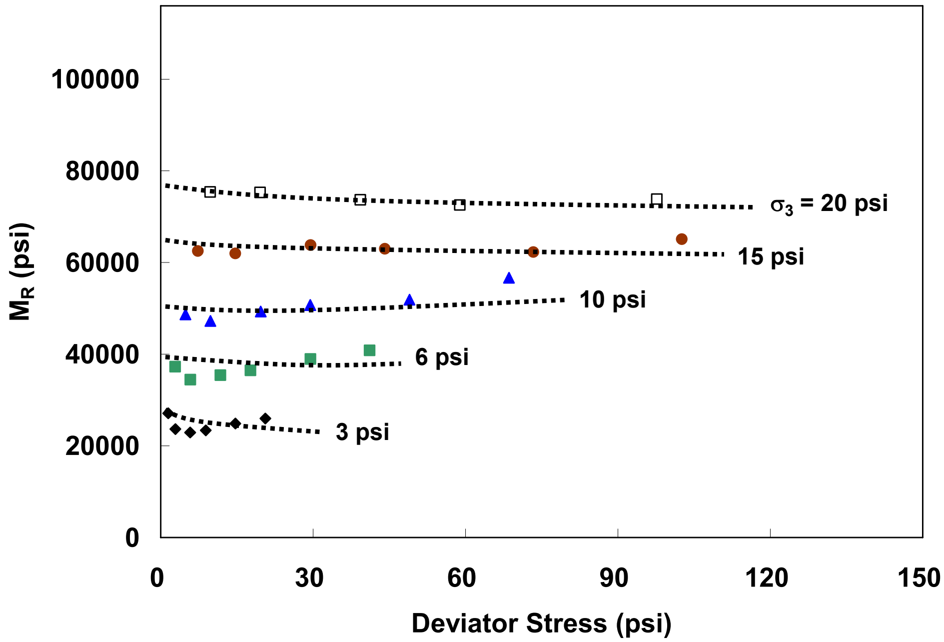

Figure D.50: Resilient Modulus of TH 23 Blend
(X_3.5_2, 100% Gyratory, 65% OMC (γ_d = 130.72 lb/ft^3, MC = 3.6%)).

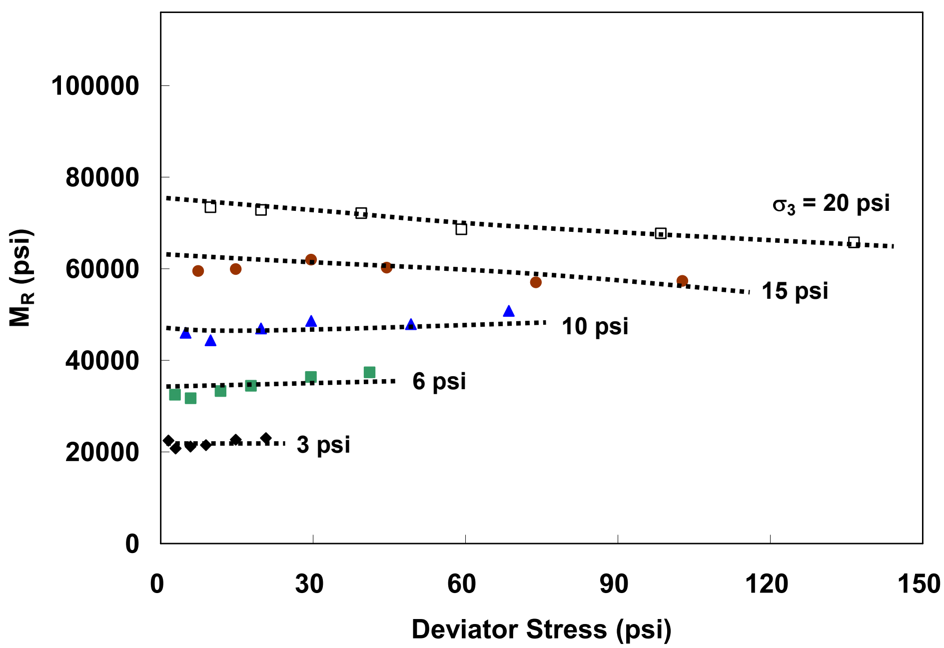

Figure D.51: Resilient Modulus of TH 23 Blend
(X_5.4_1, 100% Gyratory, 100% OMC (γ_d = 131.10 lb/ft^3, MC = 5.4%)).

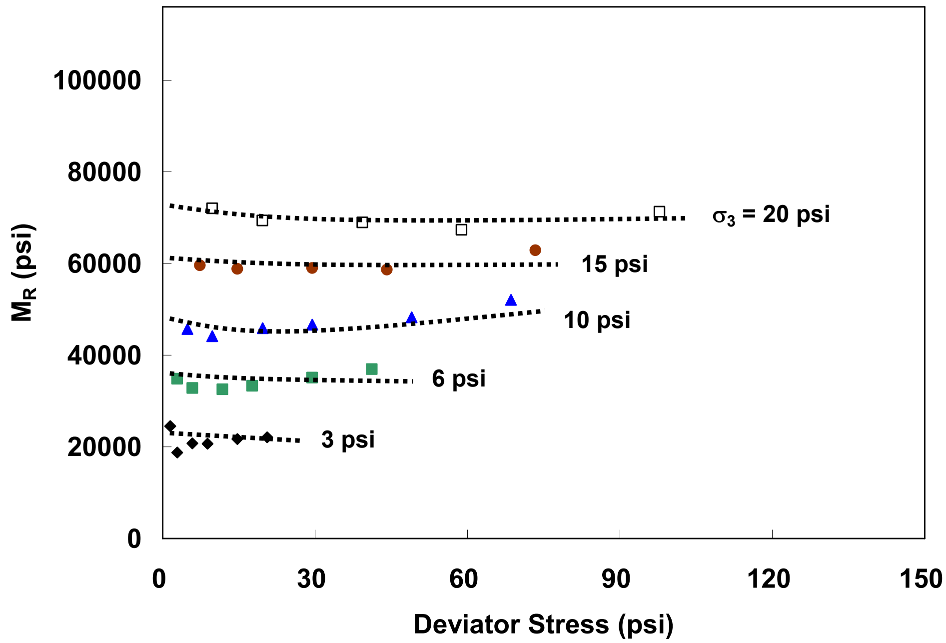

Figure D.52: Resilient Modulus of TH 23 Blend

(X_5.4_2, 100% Gyratory, 100% OMC (γ_d = 130.54 lb/ft^3, MC = 5.6%)).

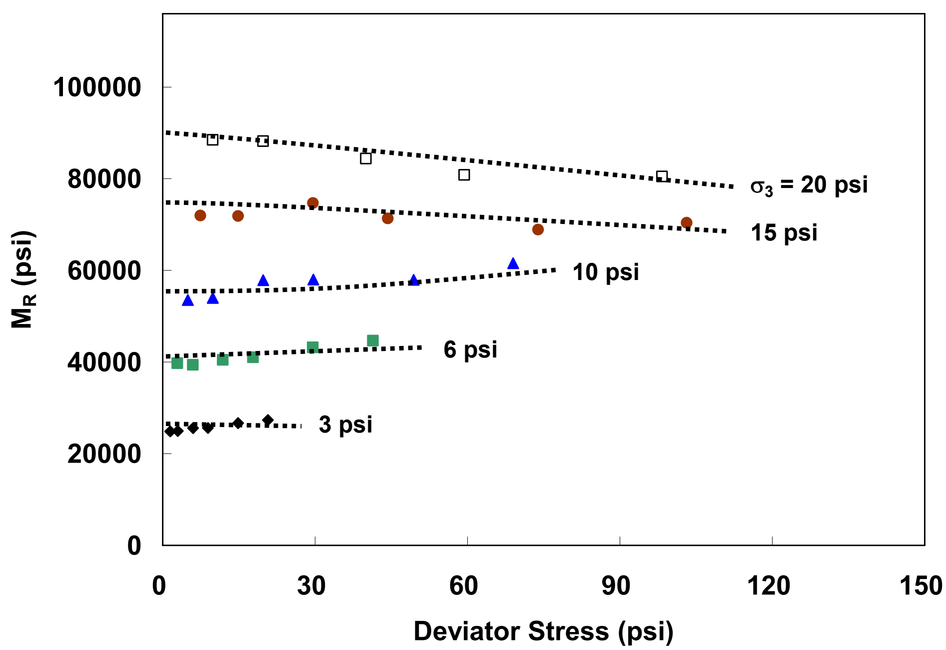

Figure D.53: Resilient Modulus of TH 200 Blend

(Y_3.7_1, 100% Gyratory, 65% OMC (γ_d = 133.60 lb/ft^3, MC = 4.0%)).

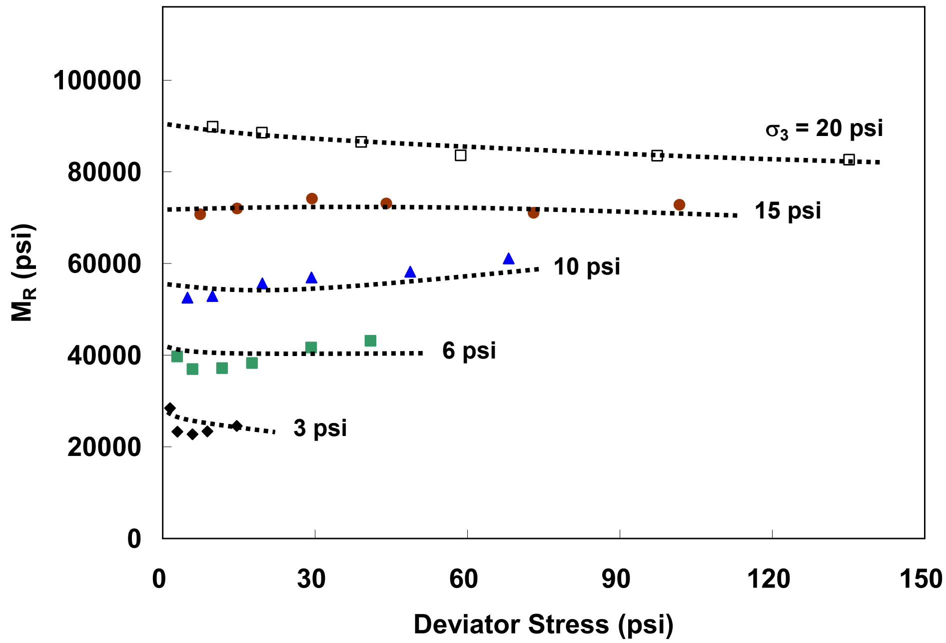

Figure D.54: Resilient Modulus of TH 200 Blend

(Y_3.7_2, 100% Gyratory, 65% OMC (γ_d = 133.91 lb/ft^3, MC = 3.9%)).

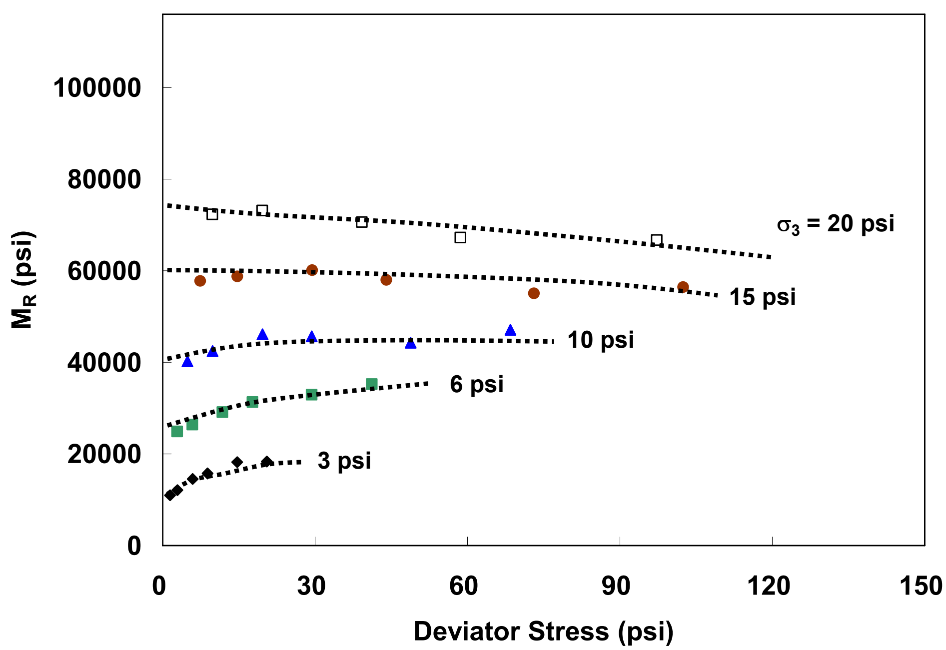

Figure D.55: Resilient Modulus of TH 200 Blend

(Y_5.7_1, 100% Gyratory, 100% OMC (γ_d = 134.91 lb/ft^3, MC = 5.6%)).

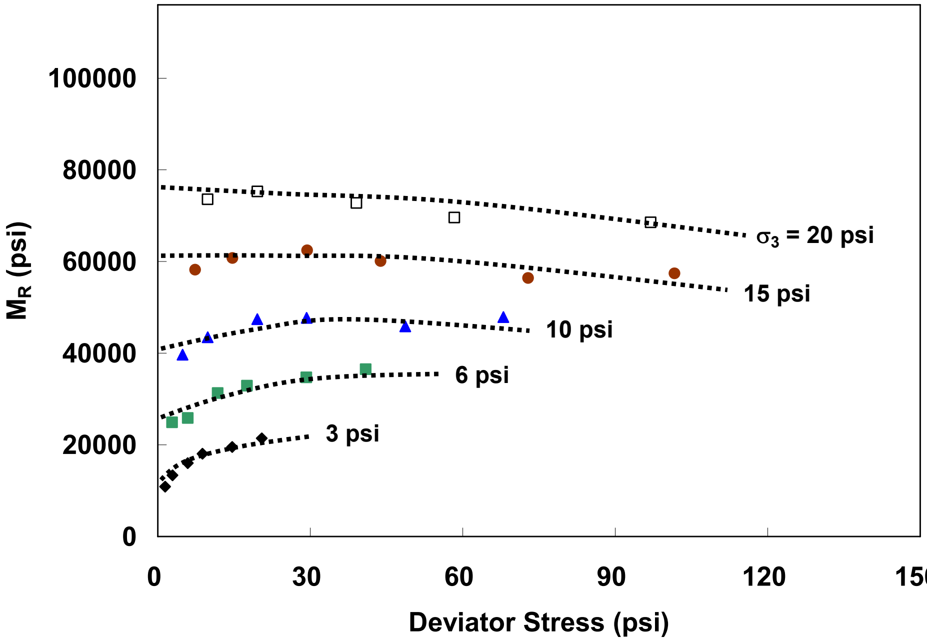

Figure D.56: Resilient Modulus of TH 200 Blend

(Y_5.7_2, 100% Gyratory, 100% OMC (γ_d = 134.51 lb/ft^3, MC = 5.9%)).

D.3 Resilient Modulus (M_R) vs. Deviator Stress vs. Confining Pressure

Figures D.29 – D.37 show M_R versus deviator stress versus confining pressure plots for the seven different mixtures at two different moisture contents. From the Figures, it is noticed that deviator stress effect on M_R was less pronounced than confining pressure effect on M_R

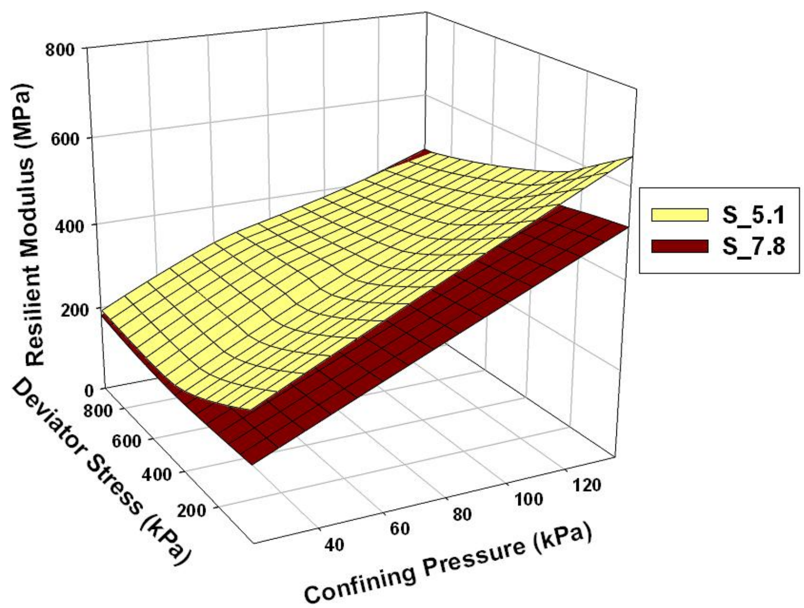

Figure D.57: Resilient Modulus of CR 3 Blend

(100% Gyratory = 2032 kg/m^3, 100% OMC = 7.8%, 65% OMC = 5.1%).

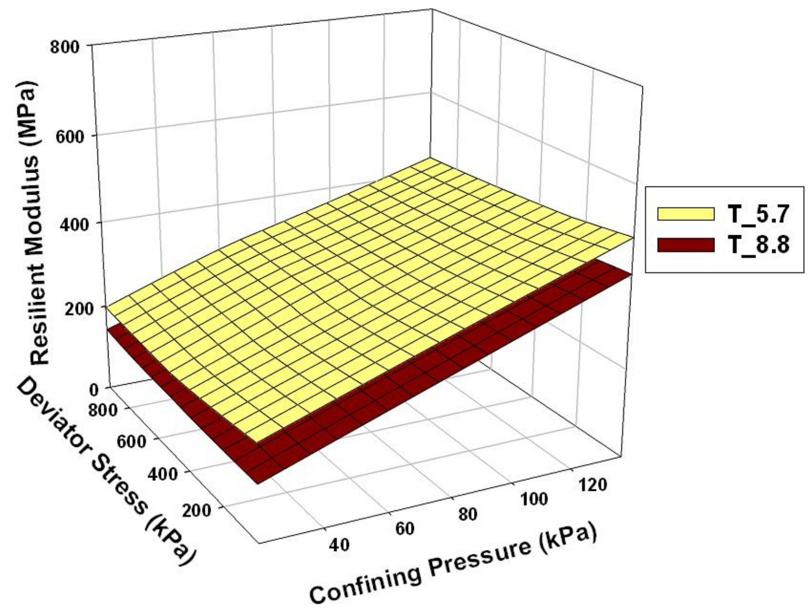

Figure D.58: Resilient Modulus of CR 3 100% Aggregate
(100% Gyratory = 2032 kg/m^3, 100% OMC = 8.8%, 65% OMC = 5.7%).

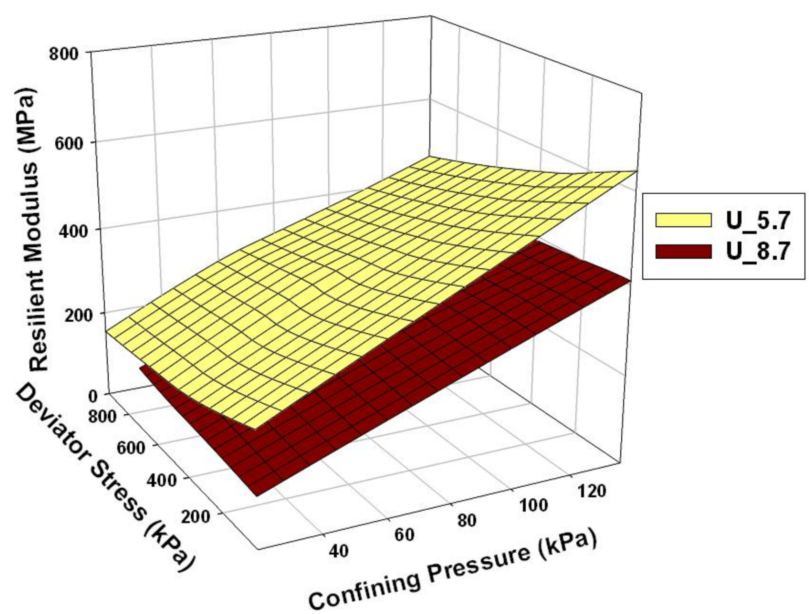

Figure D.59: Resilient Modulus of CR 3 75% Aggregate – 25% RAP
(100% Gyratory = 2032 kg/m^3, 100% OMC = 8.7%, 65% OMC = 5.7%).

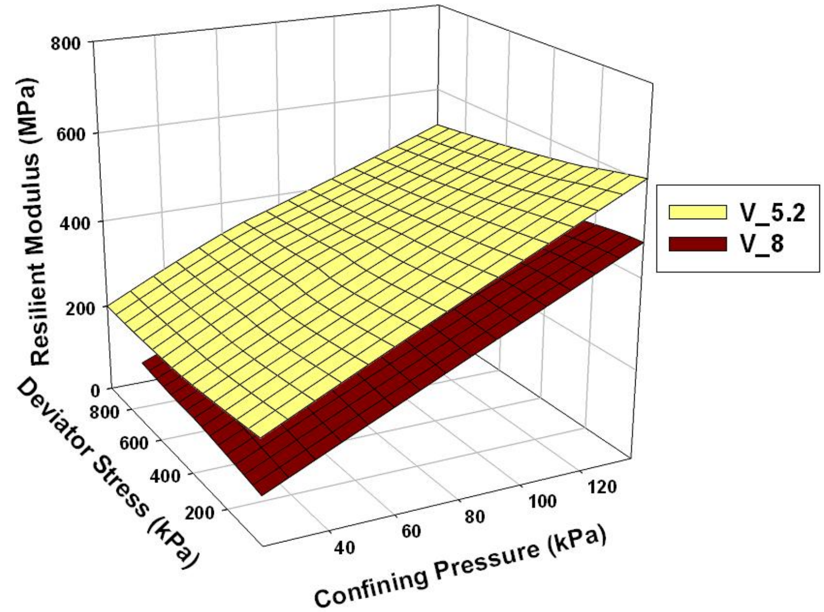

Figure D.60: Resilient Modulus of CR 3 50% Aggregate – 50% RAP
(100% Gyratory = 2032 kg/m^3, 100% OMC = 8%, 65% OMC = 5.2%).

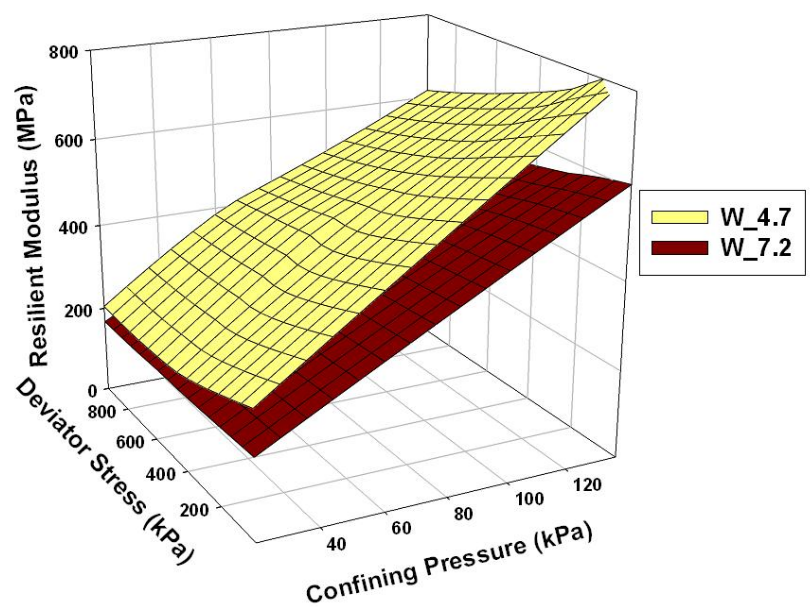

Figure D.61: Resilient Modulus of CR 3 25% Aggregate – 75% RAP
(100% Gyratory = 2032 kg/m^3, 100% OMC = 7.2%, 65% OMC = 4.7%).

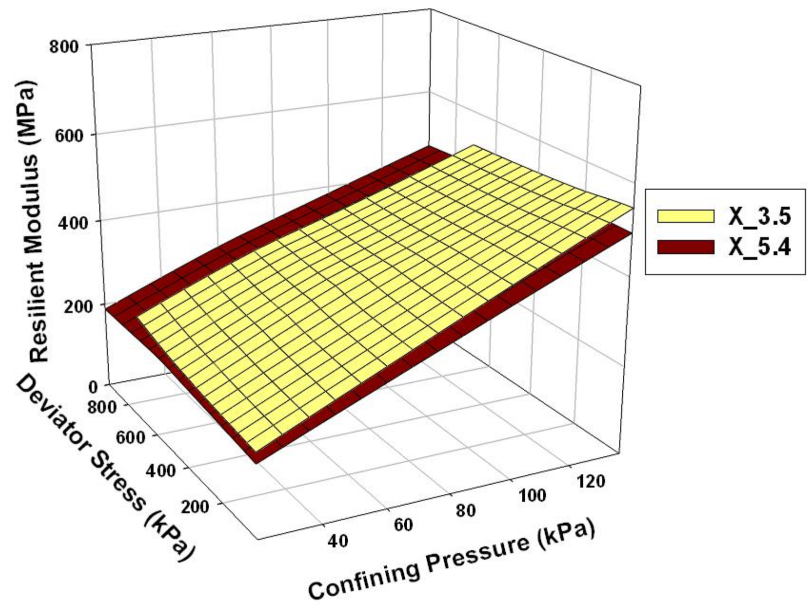

Figure D.62: Resilient Modulus of TH 23 Blend

(100% Gyratory = 2080 kg/m^3, 100% OMC = 5.4%, 65% OMC = 3.5%).

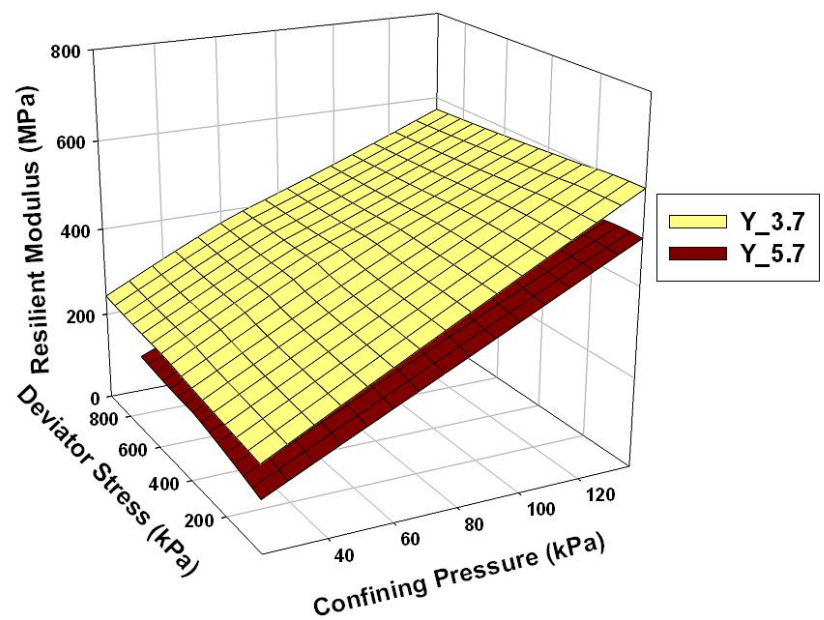

Figure D.63: Resilient Modulus of TH 200 Blend

(100% Gyratory = 2144 kg/m^3, 100% OMC = 5.7%, 65% OMC = 3.7%).

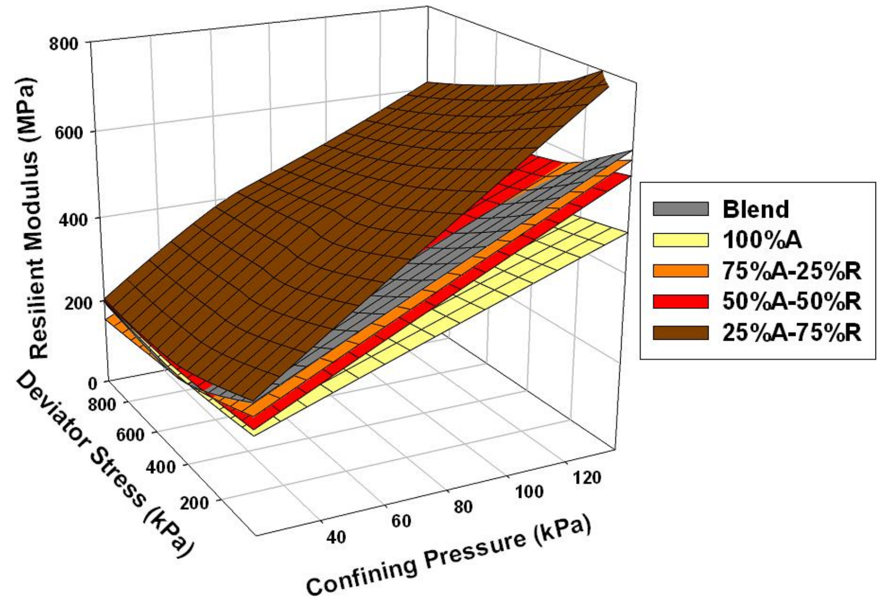

Figure D.64: Resilient Modulus of CR 3 Materials at 98% Gyratory and 65% OMC.

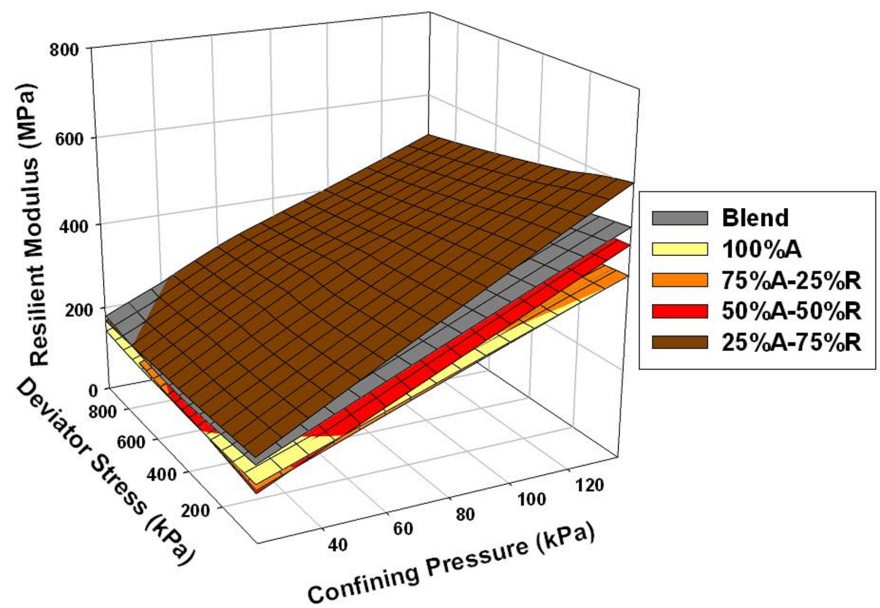

Figure D.65: Resilient Modulus of CR 3 Materials at 100% Gyratory and 100% OMC.

ENGLISH UNITS

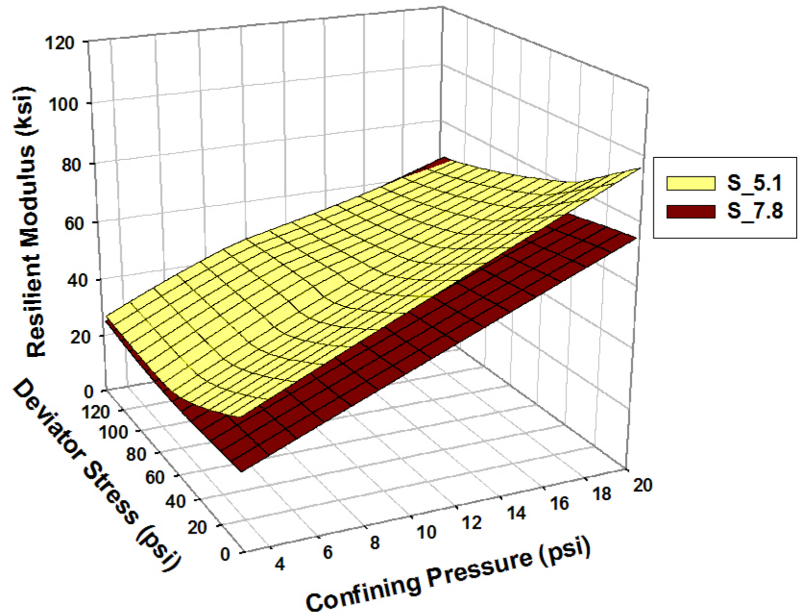

Figure D.66: Resilient Modulus of CR 3 Blend

(100% Gyratory = 2032 kg/m^3, 100% OMC = 7.8%, 65% OMC = 5.1%).

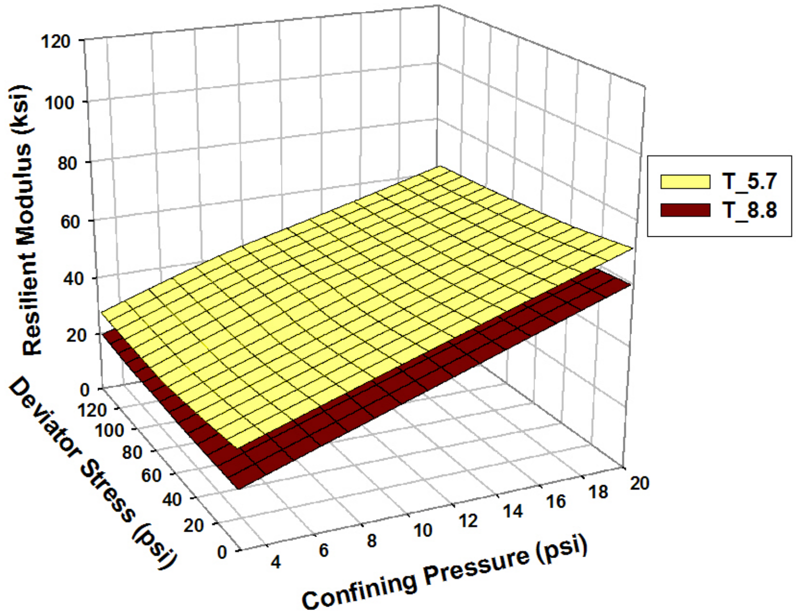

Figure D.67: Resilient Modulus of CR 3 100% Aggregate
(100% Gyratory = 2032 kg/m^3, 100% OMC = 8.8%, 65% OMC = 5.7%).

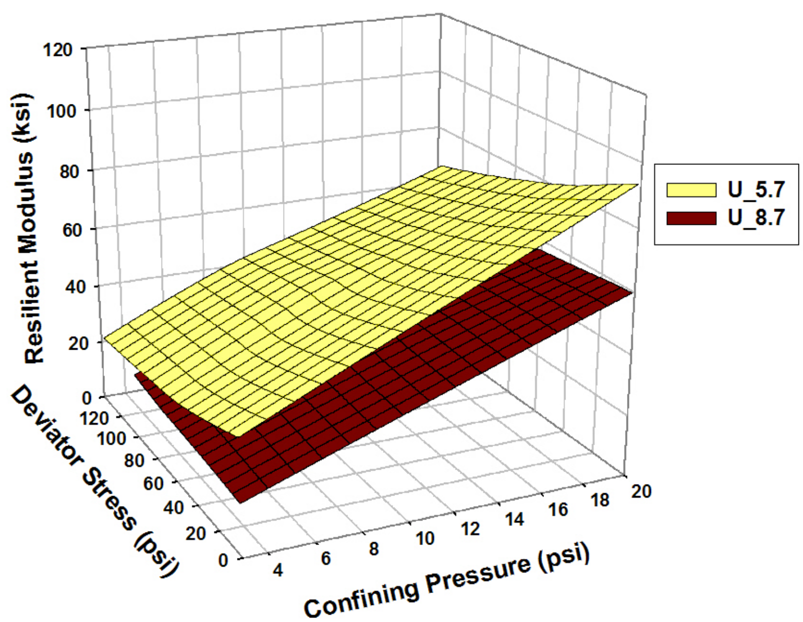

Figure D.68: Resilient Modulus of CR 3 75% Aggregate – 25% RAP
(100% Gyratory = 2032 kg/m^3, 100% OMC = 8.7%, 65% OMC = 5.7%).

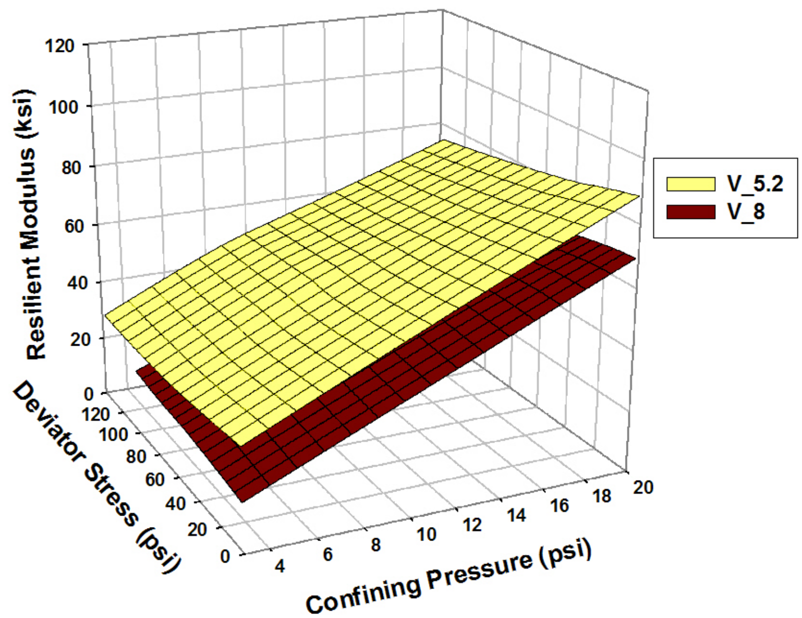

Figure D.69: Resilient Modulus of CR 3 50% Aggregate – 50% RAP (100% Gyratory = 2032 kg/m^3, 100% OMC = 8%, 65% OMC = 5.2%).

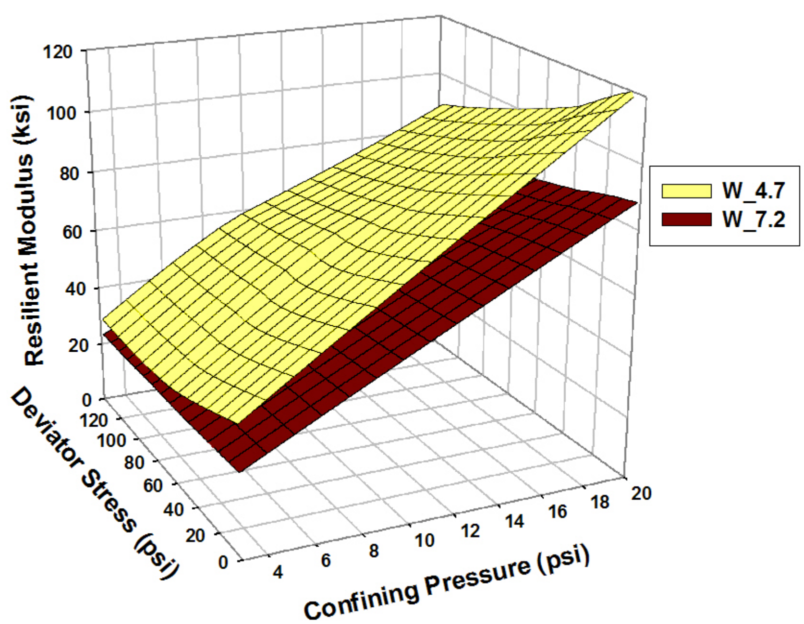

Figure D.70: Resilient Modulus of CR 3 25% Aggregate – 75% RAP (100% Gyratory = 2032 kg/m^3, 100% OMC = 7.2%, 65% OMC = 4.7%).

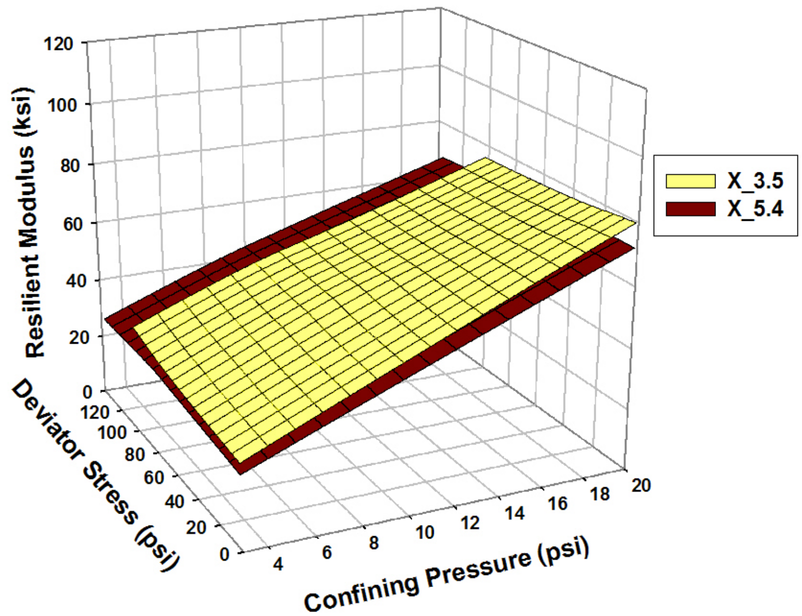

Figure D.71: Resilient Modulus of TH 23 Blend

(100% Gyratory = 2080 kg/m^3, 100% OMC = 5.4%, 65% OMC = 3.5%).

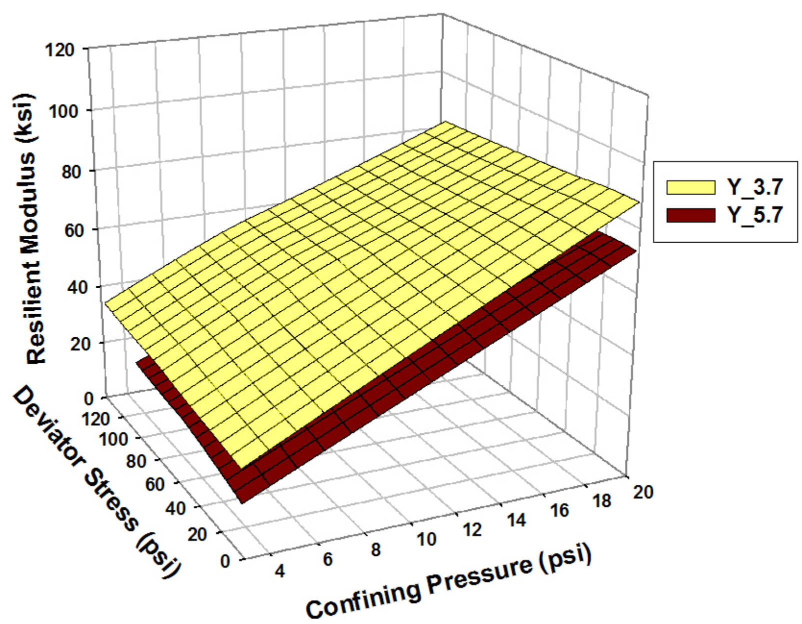

Figure D.72: Resilient Modulus of TH 200 Blend

(100% Gyratory = 2144 kg/m^3, 100% OMC = 5.7%, 65% OMC = 3.7%).

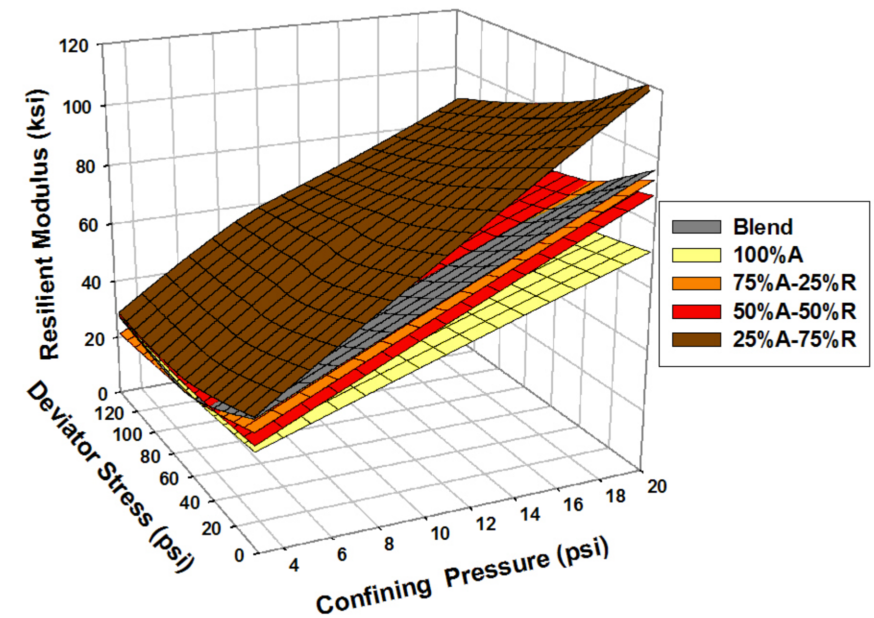

Figure D.73: Resilient Modulus of CR 3 Materials at 98% Gyratory and 65% OMC.

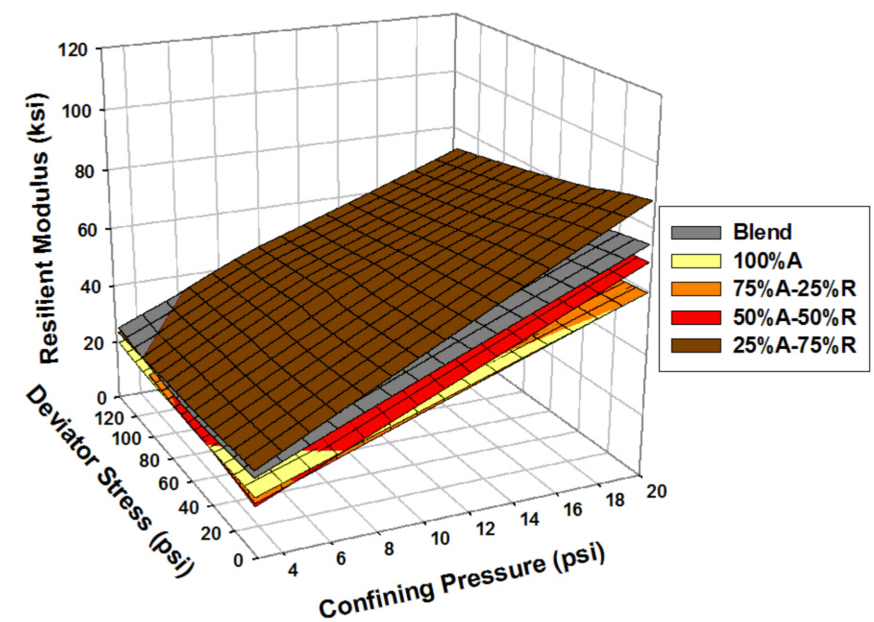

Figure D.74: Resilient Modulus of CR 3 Materials at 100% Gyratory and 100% OMC.

D.4 Strain at Maximum Stress

Table D.15 shows the strain at maximum stress from 28 shear strength tests. Machine stiffness was estimated to be 37.6 kN/mm. Test results from 100% optimum moisture content specimens usually had higher strain values compared to test results from 65% optimum moisture content specimens. For CR 3 samples, specimens with RAP had higher strain at maximum stress than 100% aggregate specimens for both 100% and 65% optimal moisture content samples.

Table D.29: Strain at Maximum Stress.

Specimen ID	Description	Confining Pressure (kPa)	Deviator Stress (kPa)	ϕ (°)	c (kPa)	Strain at Maximum Stress
S_5.1_1	CR 3_Blend_65%OMC_1	69	906	32	207	0.0093
S_5.1_2	CR 3_Blend_65%OMC_2	34	793			0.0057
S_7.8_1	CR 3_Blend_100%OMC_1	34	719	32	157	0.0048
S_7.8_2	CR 3_Blend_100%OMC_2	69	830			0.0064
T_5.7_1	CR 3_100%A_65%OMC_1	69	917	46	115	0.0044
T_5.7_2	CR 3_100%A_65%OMC_2	34	707			0.0062
T_8.8_1	CR 3_100%A_100%OMC_1	69	858	39	152	0.0089
T_8.8_2	CR 3_100%A_100%OMC_2	34	710			0.0076
U_5.7_1	CR 3_75%A-25%R_65%OMC_1	69	1026	49	110	0.0068
U_5.7_2	CR 3_75%A-25%R_65%OMC_2	34	775			0.0058
U_8.7_1	CR 3_75%A-25%R_100%OMC_1	69	820	47	85	0.0090
U_8.7_2	CR 3_75%A-25%R_100%OMC_2	34	593			0.0142
V_5.2_1	CR 3_50%A-50%R_65%OMC_1	69	934	50	85	0.0067
V_5.2_2	CR 3_50%A-50%R_65%OMC_2	34	667			0.0065
V_8_1	CR 3_50%A-50%R_100%OMC_1	69	834	45	104	0.0110
V_8_2	CR 3_50%A-50%R_100%OMC_2	34	633			0.0141
W_4.7_1	CR 3_25%A-75%R_65%OMC_1	69	1005	48	113	0.0088
W_4.7_2	CR 3_25%A-75%R_65%OMC_2	34	766			0.0073
W_7.2_1	CR 3_25%A-75%R_100%OMC_1	69	868	44	120	0.0097
W_7.2_2	CR 3_25%A-75%R_100%OMC_2	34	680			0.0086
X_3.5_1	TH 23_Blend_65%OMC_1	69	750	39	125	0.0069
X_3.5_2	TH 23_Blend_65%OMC_2	34	600			0.0056
X_5.4_1	TH 23_Blend_100%OMC_1	69	758	48	72	0.0066
X_5.4_2	TH 23_Blend_100%OMC_2	34	529			0.0058
Y_3.7_1	TH 200_Blend_65%OMC_1	69	809	45	96	0.0049
Y_3.7_2	TH 200_Blend_65%OMC_2	34	604			0.0060
Y_5.7_1	TH 200_Blend_100%OMC_1	69	778	42	110	0.0108
Y_5.7_2	TH 200_Blend_100%OMC_2	34	602			0.0093

ENGLISH UNITS

Table D.30: Strain at Maximum Stress.

Specimen ID	Description	Confining Pressure (psi)	Deviator Stress (psi)	ϕ (°)	c (psi)	Strain at Maximum Stress
S_5.1_1	CR 3_Blend_65%OMC_1	10.0	131.4	32	30.0	0.0093
S_5.1_2	CR 3_Blend_65%OMC_2	4.9	115.0			0.0057
S_7.8_1	CR 3_Blend_100%OMC_1	4.9	104.3	32	22.8	0.0048
S_7.8_2	CR 3_Blend_100%OMC_2	10.0	120.4			0.0064
T_5.7_1	CR 3_100%A_65%OMC_1	10.0	133.0	46	16.7	0.0044
T_5.7_2	CR 3_100%A_65%OMC_2	4.9	102.5			0.0062
T_8.8_1	CR 3_100%A_100%OMC_1	10.0	124.4	39	22.0	0.0089
T_8.8_2	CR 3_100%A_100%OMC_2	4.9	103.0			0.0076
U_5.7_1	CR 3_75%A-25%R_65%OMC_1	10.0	148.8	49	16.0	0.0068
U_5.7_2	CR 3_75%A-25%R_65%OMC_2	4.9	112.4			0.0058
U_8.7_1	CR 3_75%A-25%R_100%OMC_1	10.0	118.9	47	12.3	0.009
U_8.7_2	CR 3_75%A-25%R_100%OMC_2	4.9	86.0			0.0142
V_5.2_1	CR 3_50%A-50%R_65%OMC_1	10.0	135.5	50	12.3	0.0067
V_5.2_2	CR 3_50%A-50%R_65%OMC_2	4.9	96.7			0.0065
V_8_1	CR 3_50%A-50%R_100%OMC_1	10.0	121.0	45	15.1	0.011
V_8_2	CR 3_50%A-50%R_100%OMC_2	4.9	91.8			0.0141
W_4.7_1	CR 3_25%A-75%R_65%OMC_1	10.0	145.8	48	16.4	0.0088
W_4.7_2	CR 3_25%A-75%R_65%OMC_2	4.9	111.1			0.0073
W_7.2_1	CR 3_25%A-75%R_100%OMC_1	10.0	125.9	44	17.4	0.0097
W_7.2_2	CR 3_25%A-75%R_100%OMC_2	4.9	98.6			0.0086
X_3.5_1	TH 23_Blend_65%OMC_1	10.0	108.8	39	18.1	0.0069
X_3.5_2	TH 23_Blend_65%OMC_2	4.9	87.0			0.0056
X_5.4_1	TH 23_Blend_100%OMC_1	10.0	109.9	48	10.4	0.0066
X_5.4_2	TH 23_Blend_100%OMC_2	4.9	76.7			0.0058
Y_3.7_1	TH 200_Blend_65%OMC_1	10.0	117.3	45	13.9	0.0049
Y_3.7_2	TH 200_Blend_65%OMC_2	4.9	87.6			0.006
Y_5.7_1	TH 200_Blend_100%OMC_1	10.0	112.8	42	16.0	0.0108
Y_5.7_2	TH 200_Blend_100%OMC_2	4.9	87.3			0.0093

D.5 Orientation of Failure Plane (θ)

Table D.16 compares the failure plane orientation calculated from the shear strength test results and the actual failure plane orientation measured. Pictures of the failed specimens are shown in Figs. D.38 – D.61.

Table D.31: Orientation of Failure Plane.

Specimen ID	Description	θ from calculation	θ from specimen	
S_5.1_1	CR 3_Blend_65%OMC_1	61.0	58	
S_5.1_2	CR 3_Blend_65%OMC_2			
S_7.8_1	CR 3_Blend_100%OMC_1	60.9	68	
S_7.8_2	CR 3_Blend_100%OMC_2		63	68
T_5.7_1	CR 3_100%A_65%OMC_1	68.0	68	65
T_5.7_2	CR 3_100%A_65%OMC_2		68	72
T_8.8_1	CR 3_100%A_100%OMC_1	64.3	67	63
T_8.8_2	CR 3_100%A_100%OMC_2		68	68
U_5.7_1	CR 3_75%A-25%R_65%OMC_1	69.7	63	70
U_5.7_2	CR 3_75%A-25%R_65%OMC_2		68	67
U_8.7_1	CR 3_75%A-25%R_100%OMC_1	68.7	60	
U_8.7_2	CR 3_75%A-25%R_100%OMC_2			
V_5.2_1	CR 3_50%A-50%R_65%OMC_1	70.2	63	58
V_5.2_2	CR 3_50%A-50%R_65%OMC_2		72	66
V_8_1	CR 3_50%A-50%R_100%OMC_1	67.5	58	58
V_8_2	CR 3_50%A-50%R_100%OMC_2		65	58
W_4.7_1	CR 3_25%A-75%R_65%OMC_1	69.2		
W_4.7_2	CR 3_25%A-75%R_65%OMC_2			
W_7.2_1	CR 3_25%A-75%R_100%OMC_1	66.8		
W_7.2_2	CR 3_25%A-75%R_100%OMC_2			
X_3.5_1	TH 23_Blend_65%OMC_1	64.3		
X_3.5_2	TH 23_Blend_65%OMC_2		62	63
X_5.4_1	TH 23_Blend_100%OMC_1	68.8	68	
X_5.4_2	TH 23_Blend_100%OMC_2			
Y_3.7_1	TH 200_Blend_65%OMC_1	67.7	58	61
Y_3.7_2	TH 200_Blend_65%OMC_2		64	62
Y_5.7_1	TH 200_Blend_100%OMC_1	66.1		
Y_5.7_2	TH 200_Blend_100%OMC_2			

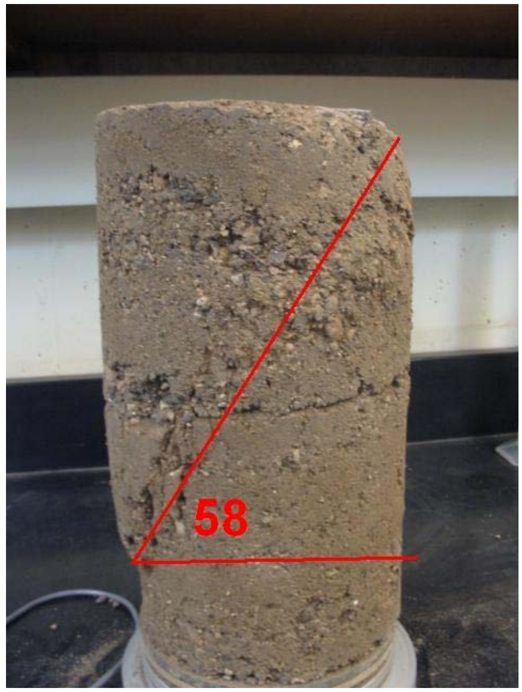

Figure D.75: S_5.1_1.

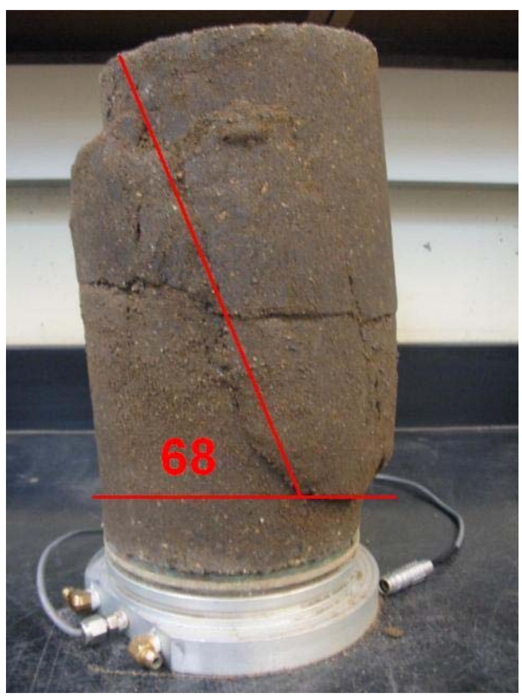

Figure D.76: S_7.8_1.

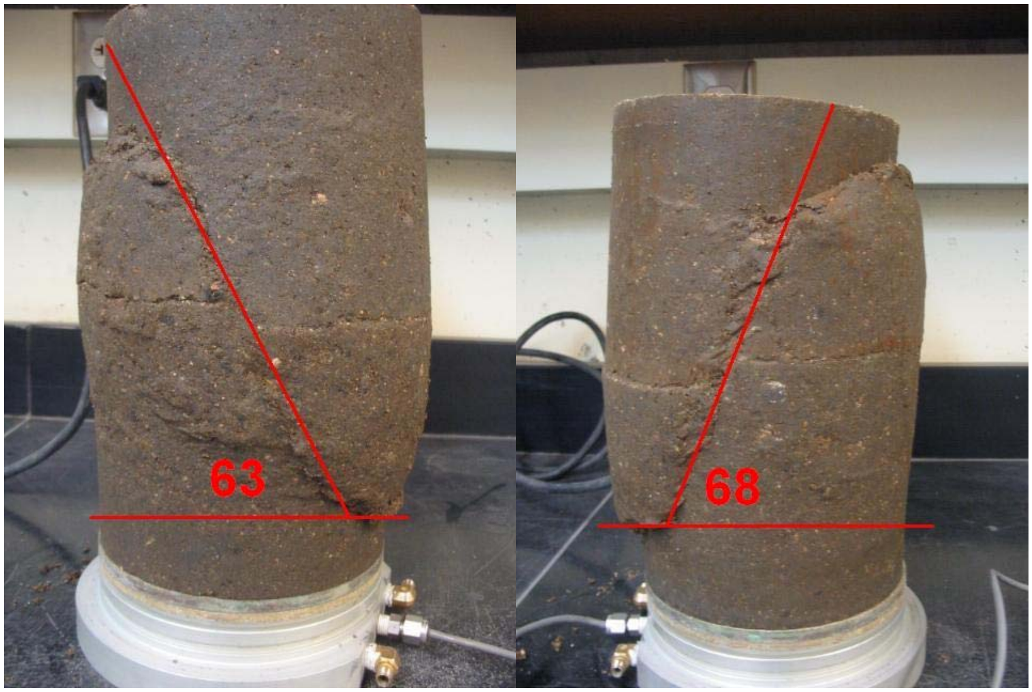

Figure D.77: S_7.8_2.

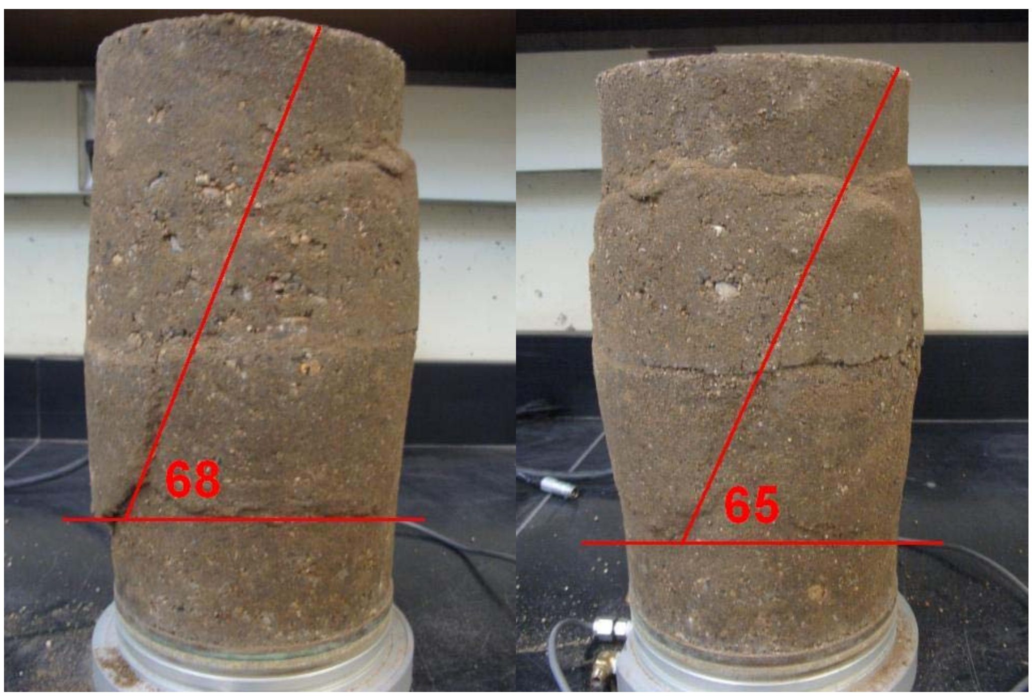

Figure D.78: T_5.7_1.

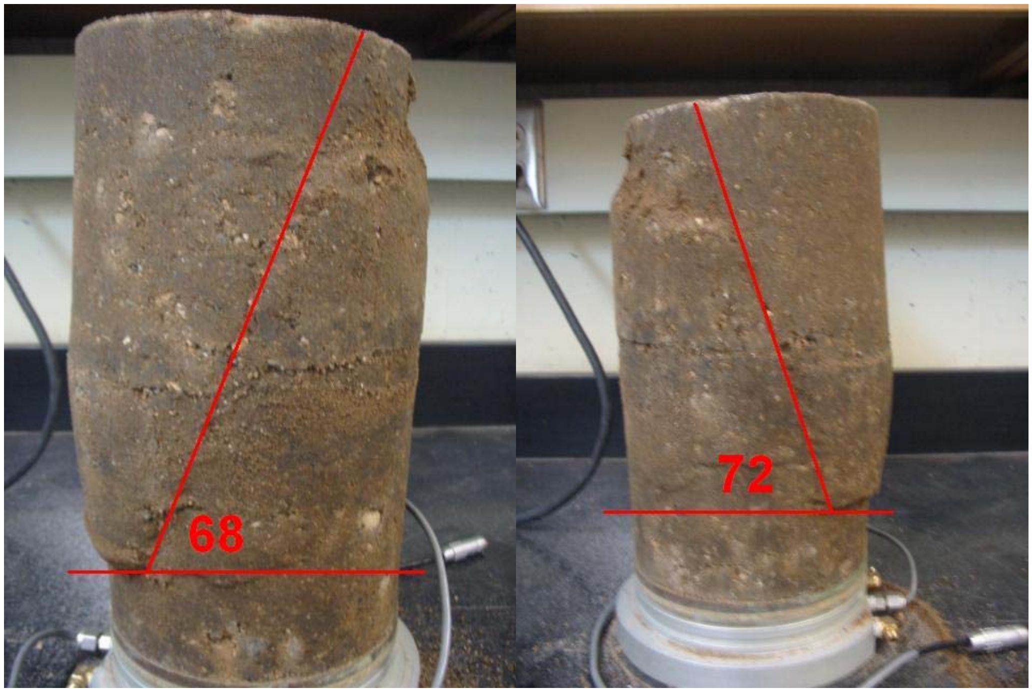

Figure D.79: T_5.7_2.

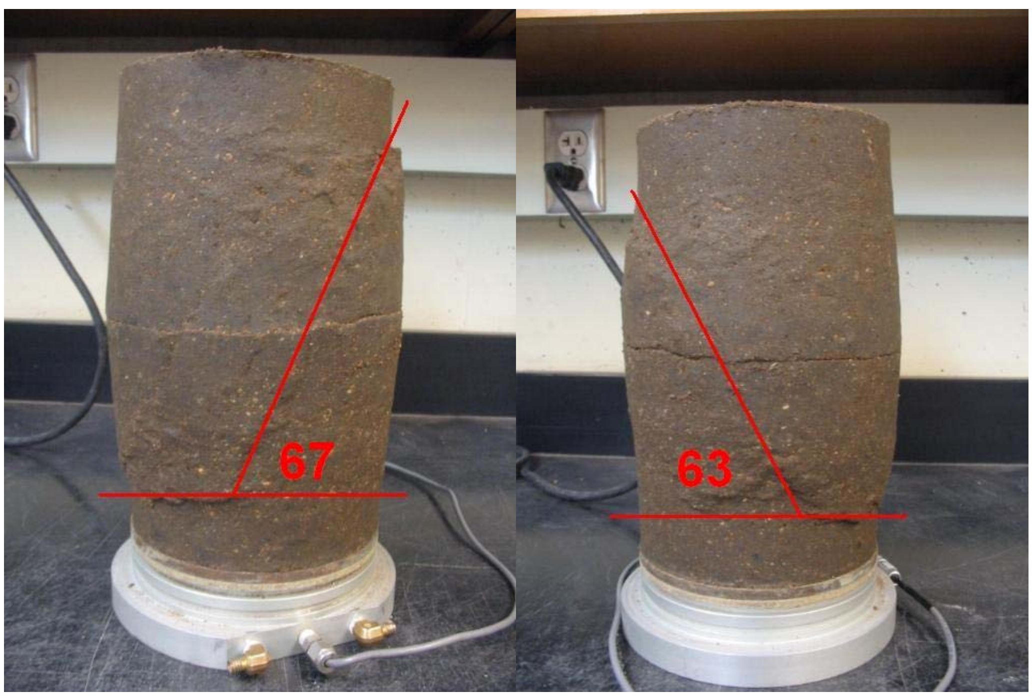

Figure D.80: T_8.8_1.

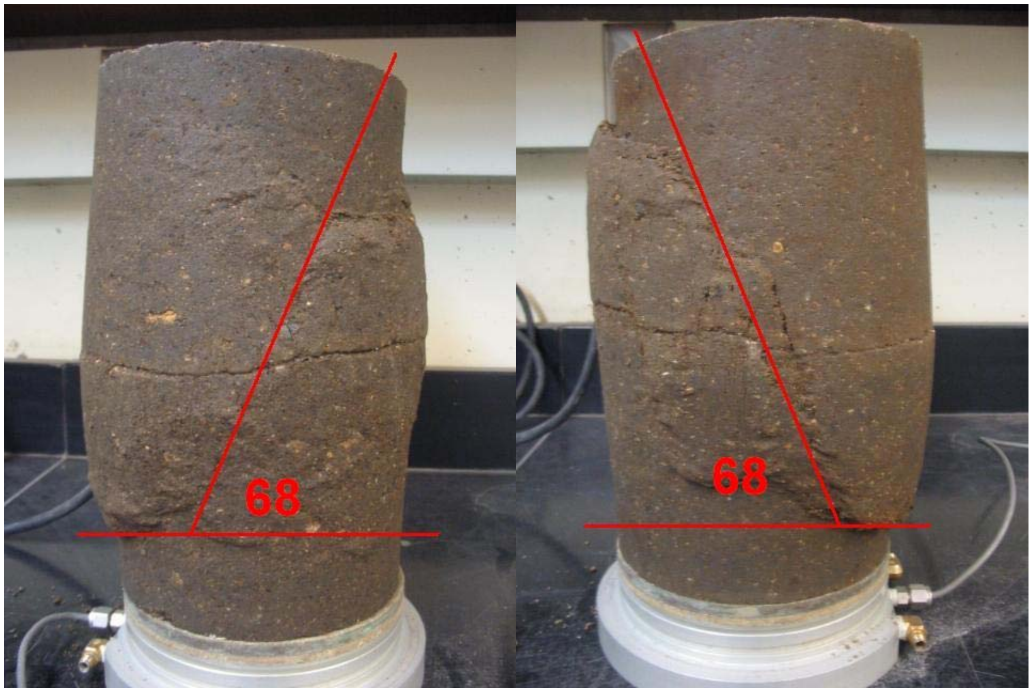

Figure D.81: T_8.8_2.

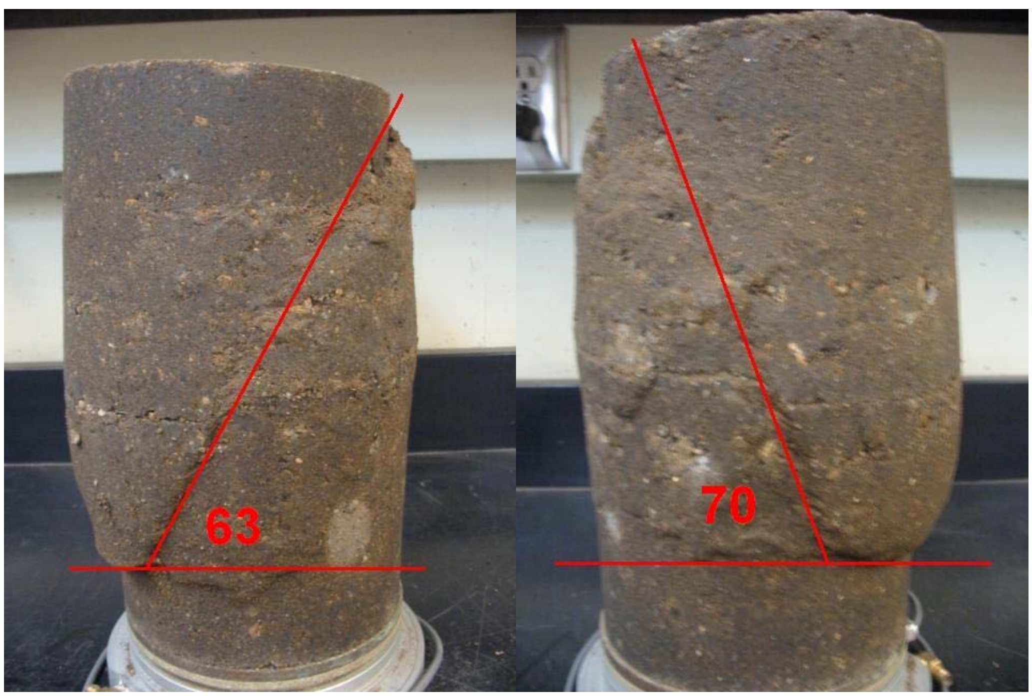

Figure D.82: U_5.7_1.

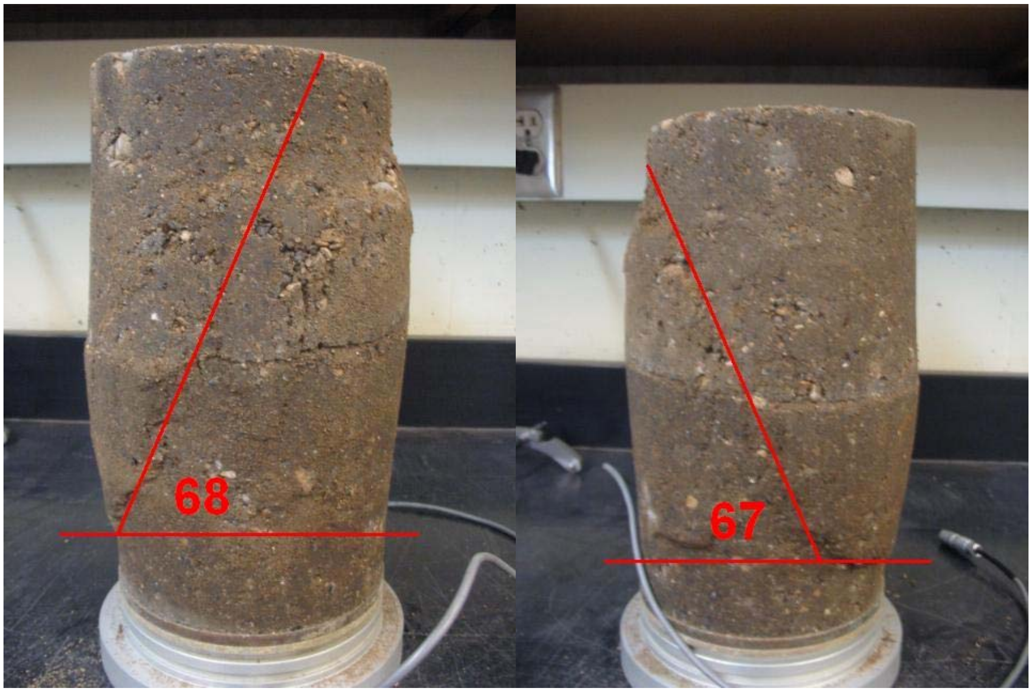

Figure D.83: U_5.7_2.

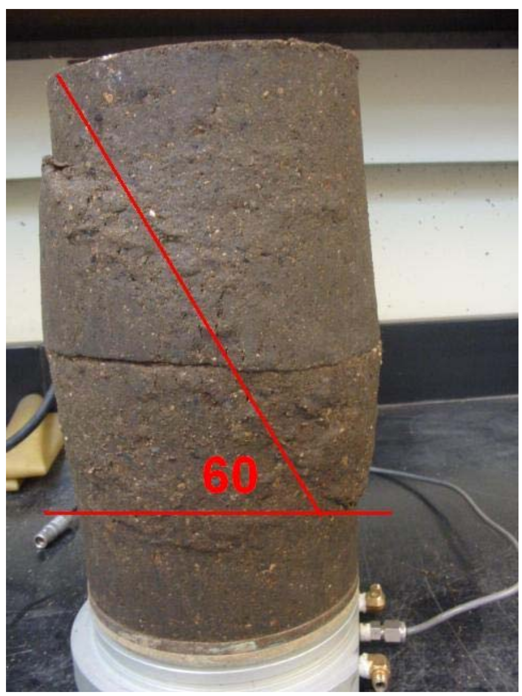

Figure D.84: U_8.7_1.

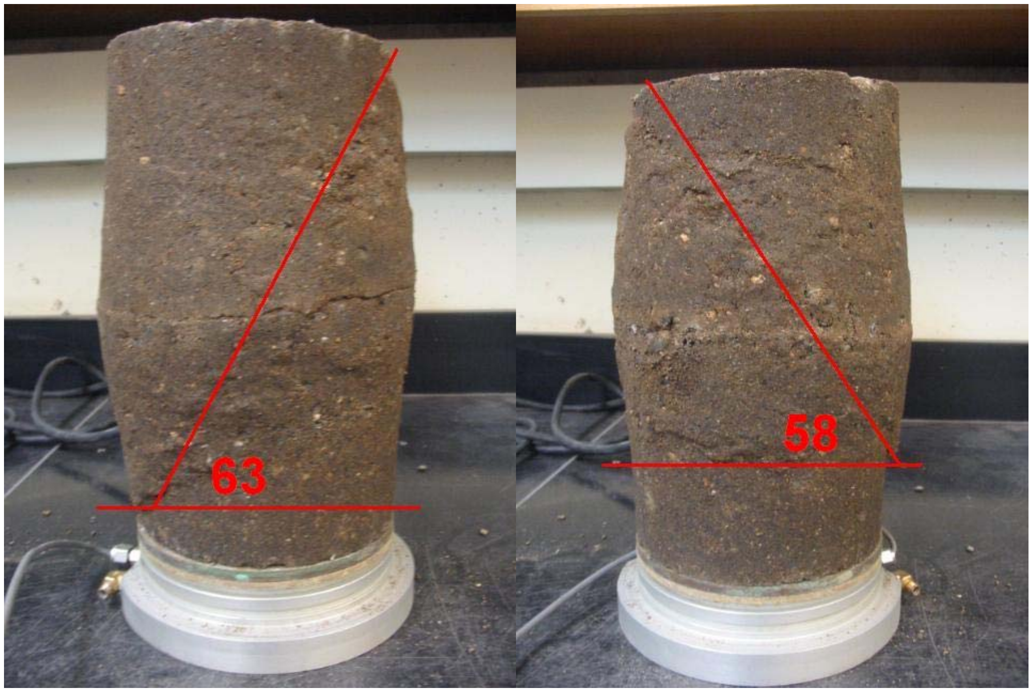

Figure D.85: V_5.2_1.

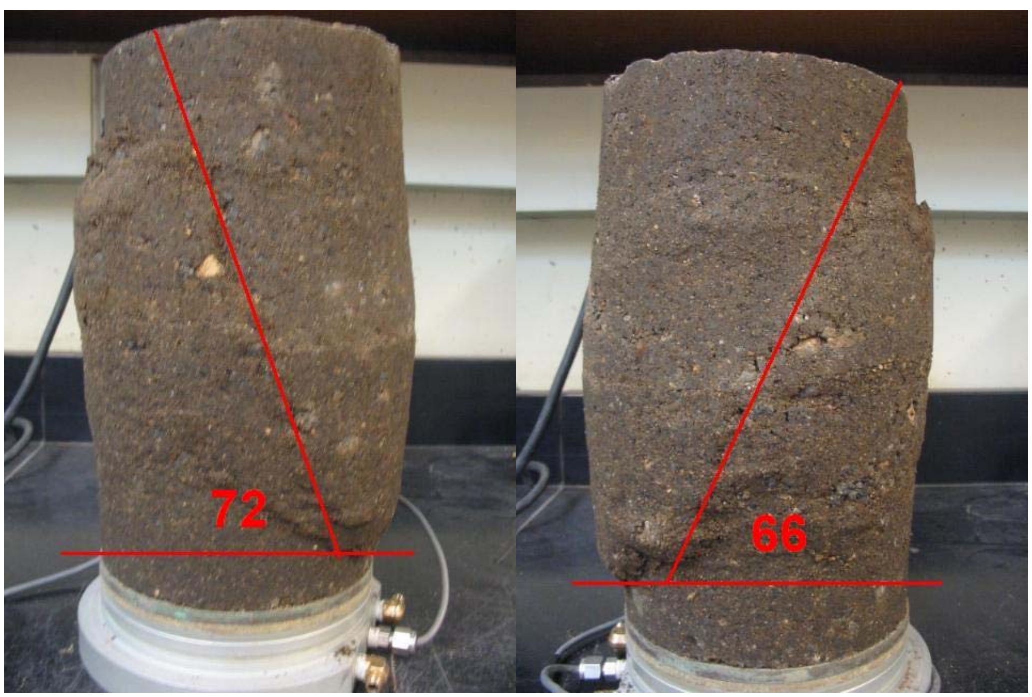

Figure D.86: V_5.2_2.

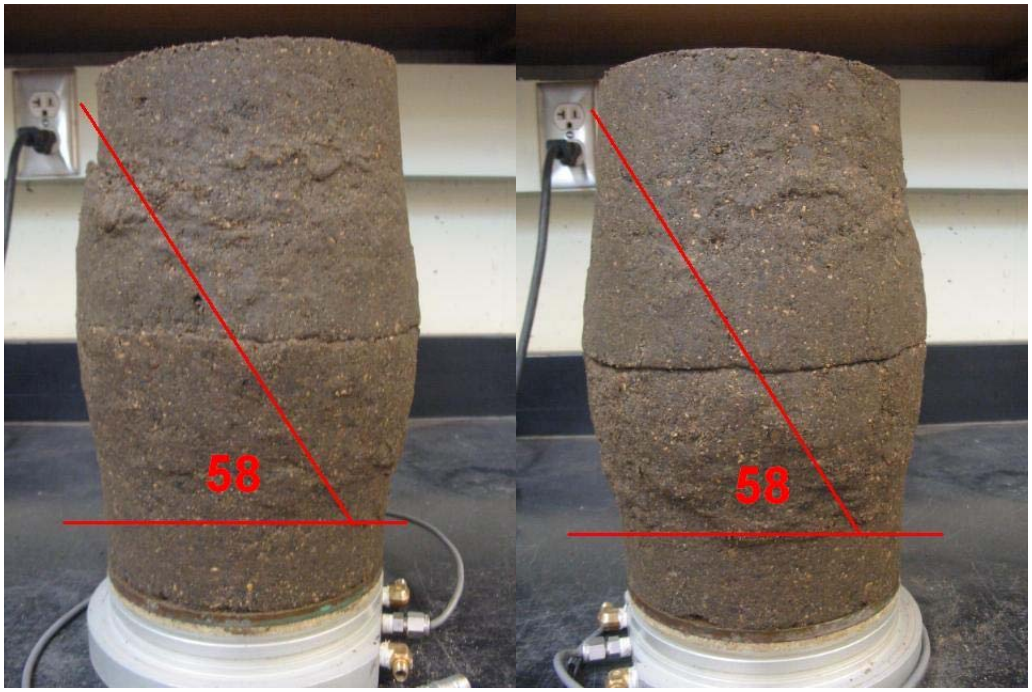

Figure D.87: V_8_1.

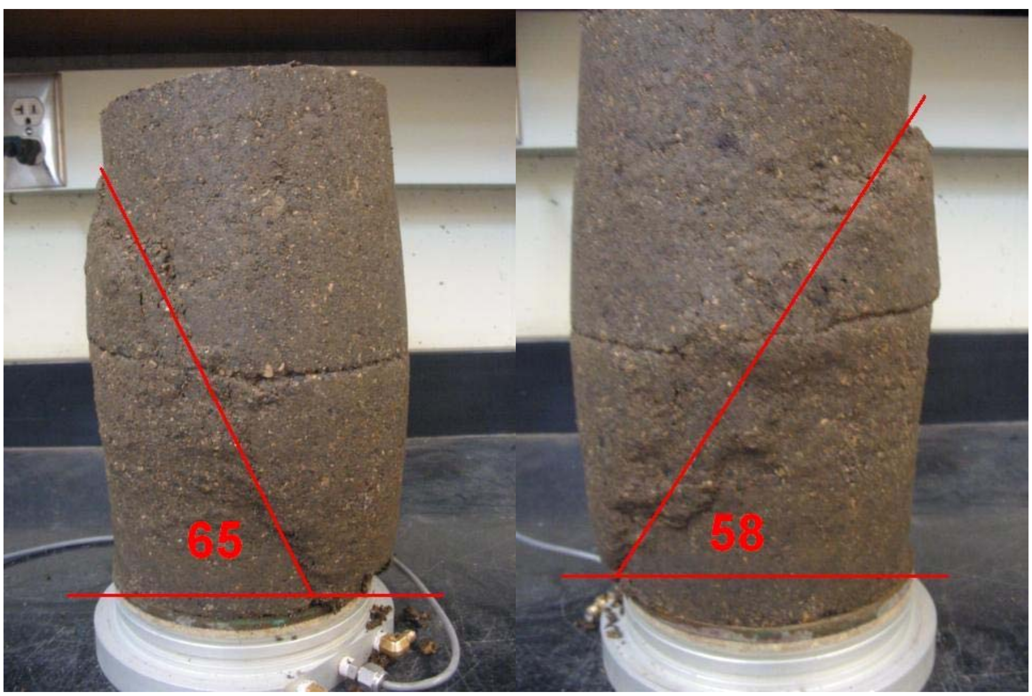

Figure D.88: V_8_2.

Figure D.89: W_4.7_1.

Figure D.90: W_4.7_2.

Figure D.91: W_7.2_1.

Figure D.92: W_7.2_2.

Figure D.93: X_3.5_1.

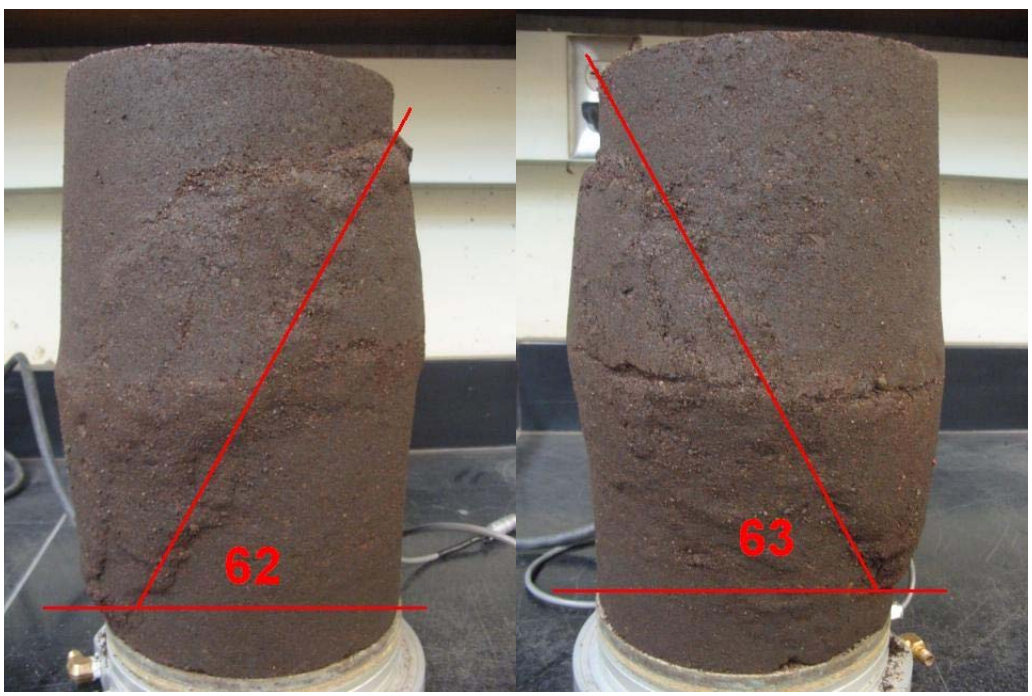

Figure D.94: X_3.5_2.

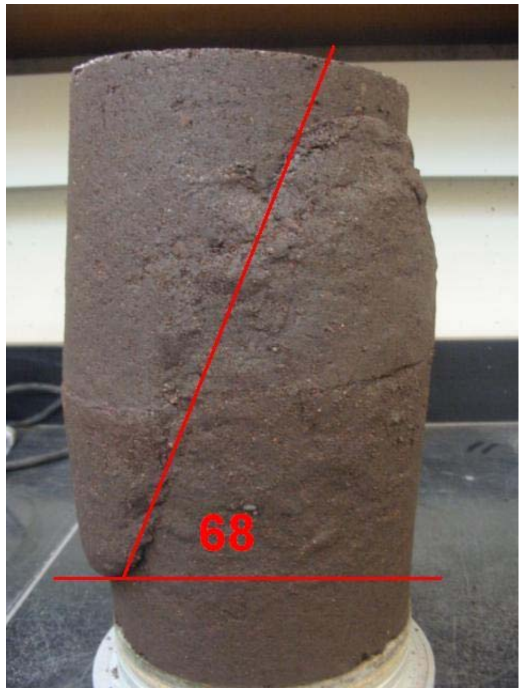

Figure .D.95: X_5.4_1.

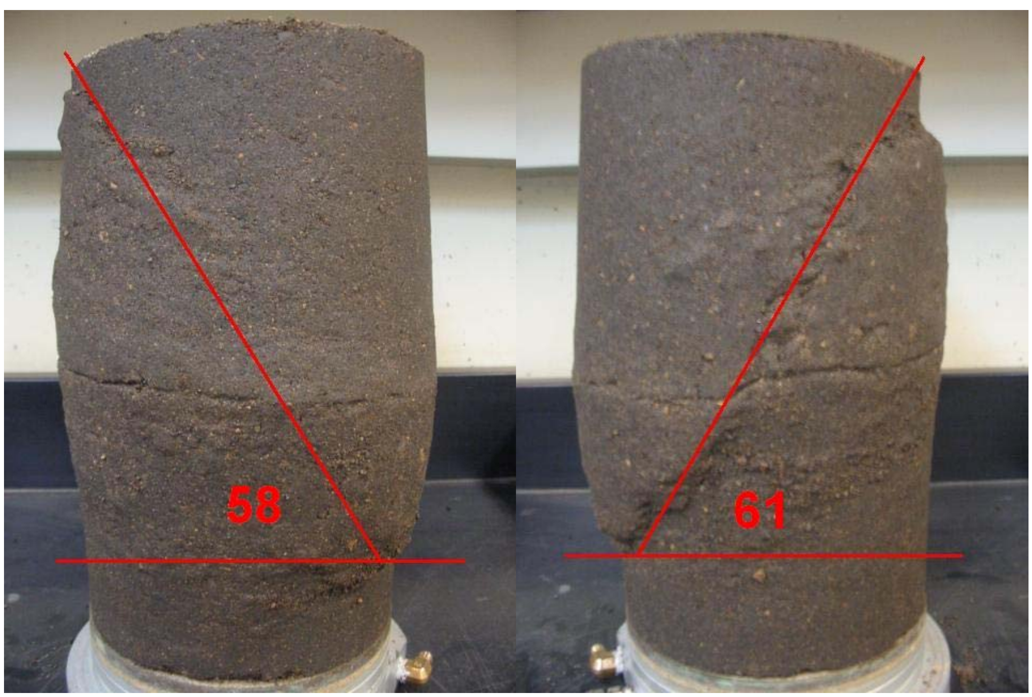

Figure D.96: Y_3.7_1.

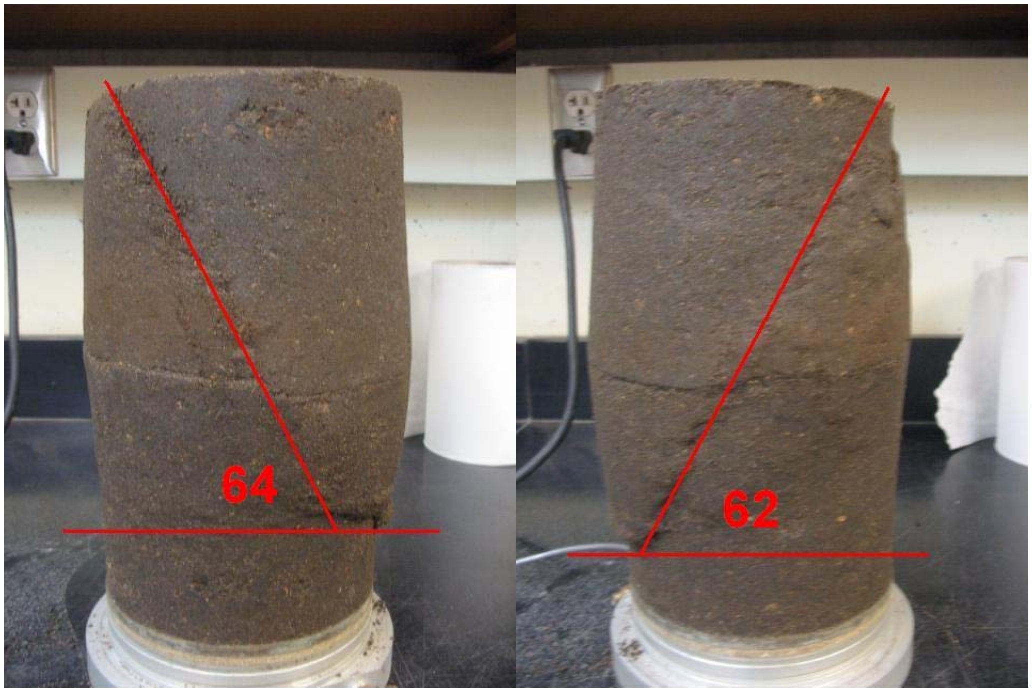

Figure D.97: Y_3.7_2.

Figure D.98: Y_5.7_2.

D.6 Cumulative Permanent Strain (ε_a^p)

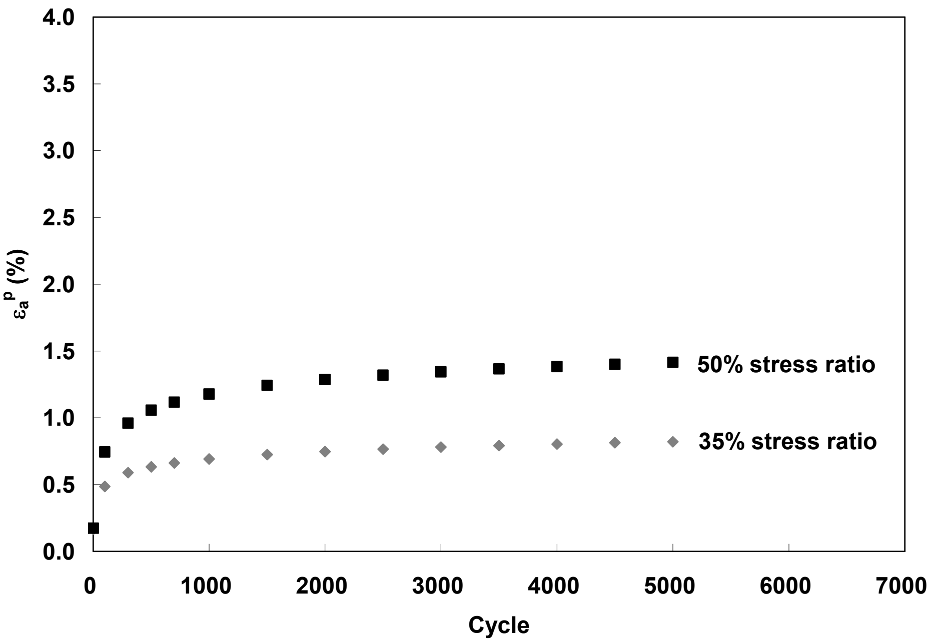

Figure D.99: Cumulative Permanent Strain (ε_a^p) of CR 3 In-situ Blend.

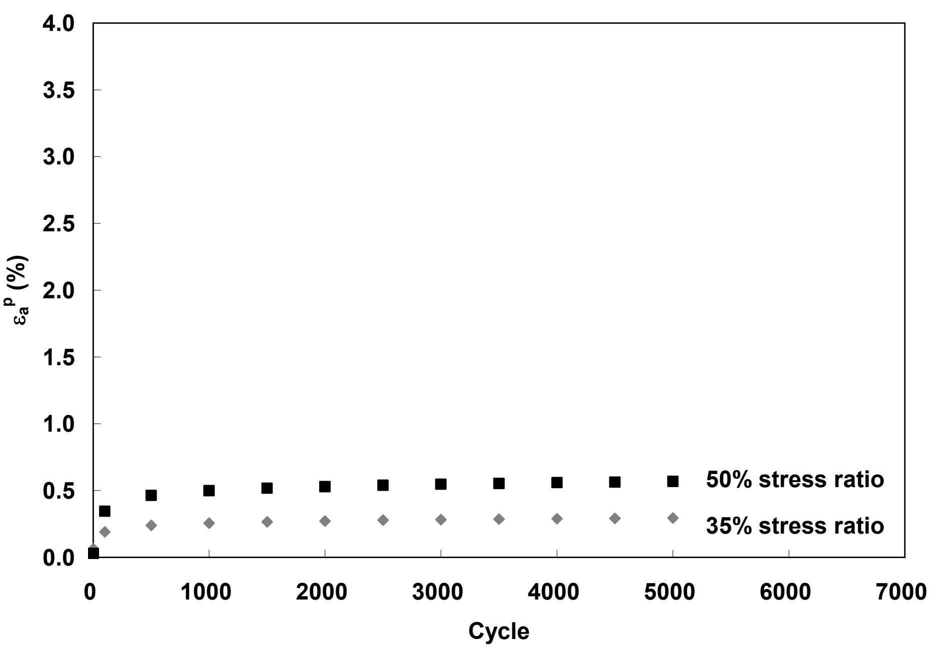

Figure D.100: Cumulative Permanent Strain (ε_a^p) of CR 3 100% Aggregate.

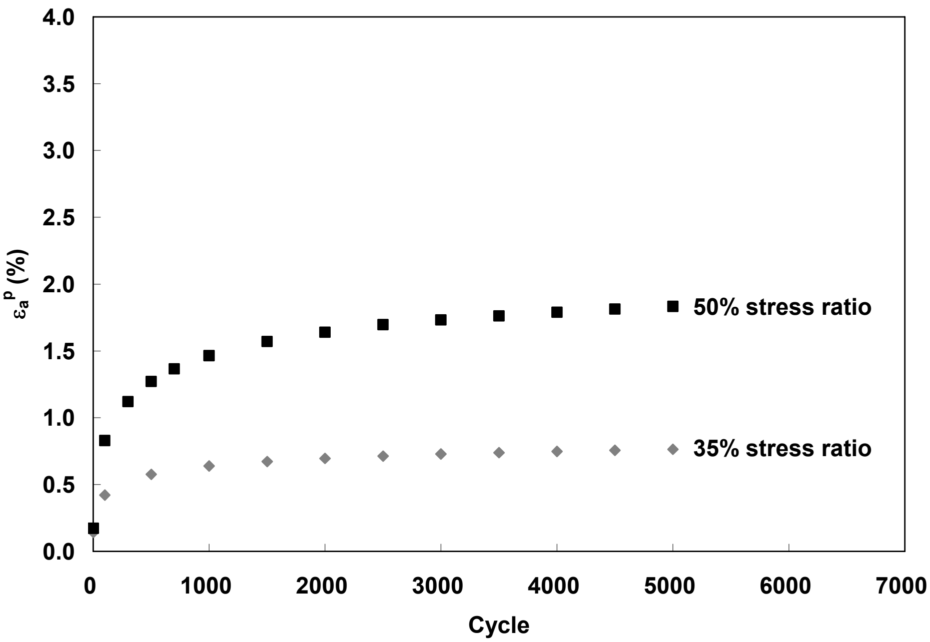

Figure D.101: Cumulative Permanent Strain (ε_a^p) of CR 3 75% Aggregate – 25% RAP.

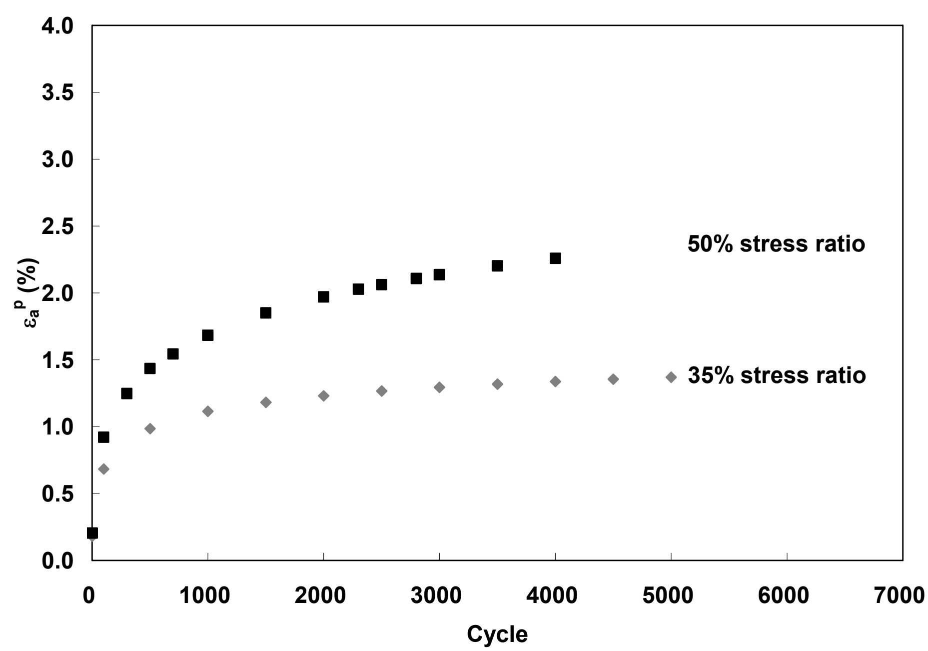

Figure D.102: Cumulative Permanent Strain (ε_a^p) of CR 3 50% Aggregate – 50% RAP.

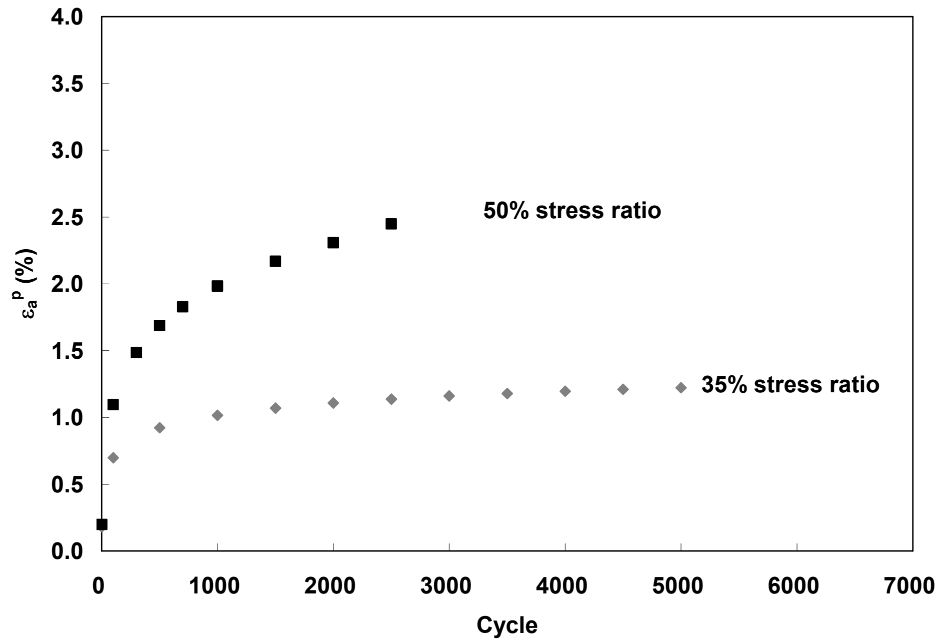

Figure D.103: Cumulative Permanent Strain (ε_a^p) of CR 3 25% Aggregate – 75% RAP.

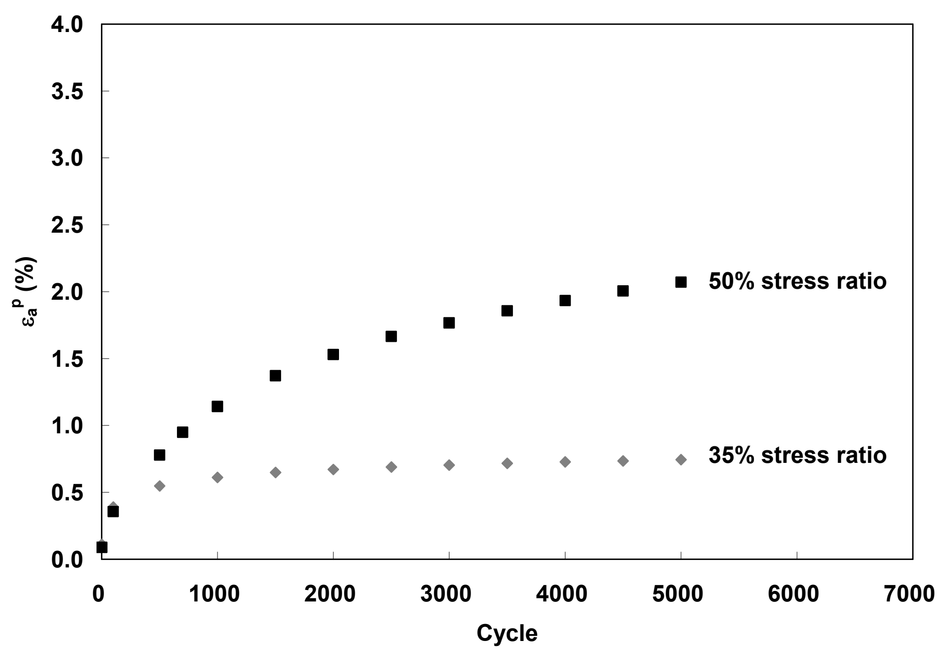

Figure D.104: Cumulative Permanent Strain (ε_a^p) of TH 23 In-situ Blend.

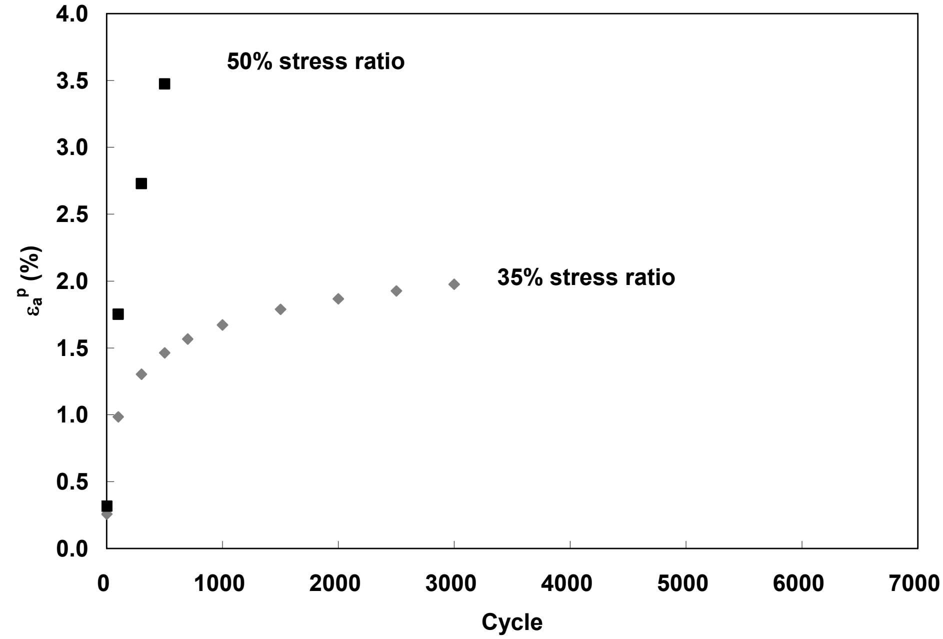

Figure D.105: Cumulative Permanent Strain (ε_a^p) of TH 200 In-situ Blend.

D.7 Young's Modulus (E_{secant})

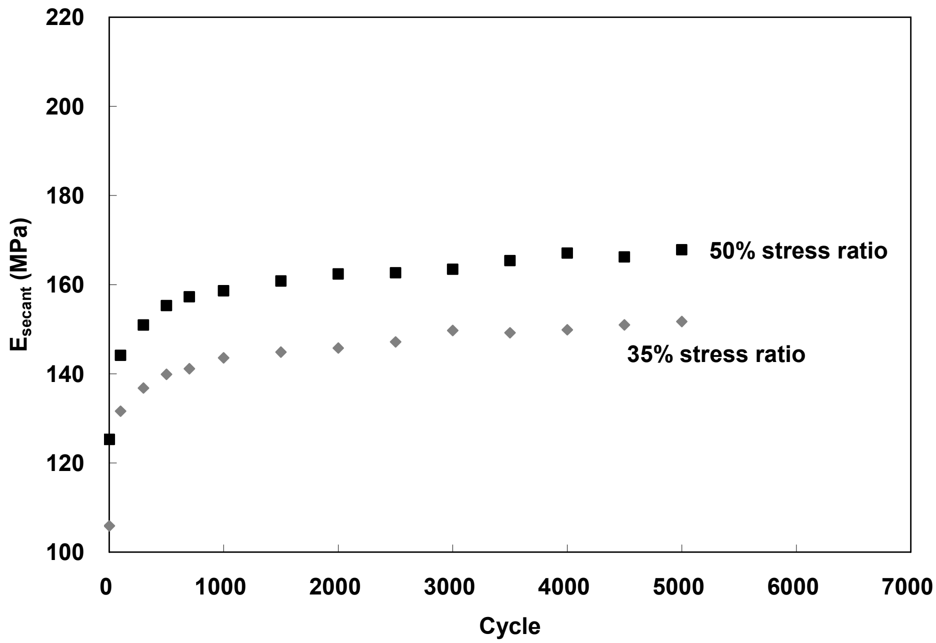

Figure D.106: Young's modulus (E_{secant}) of CR 3 In-situ Blend.

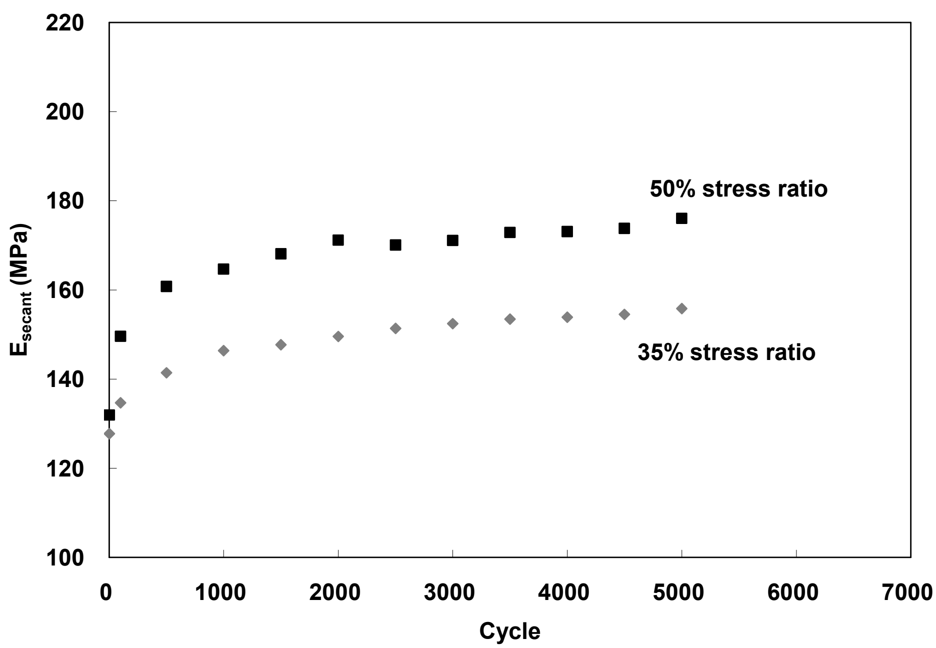

Figure D.107: Young's modulus (E_{secant}) of CR 3 100% Aggregate.

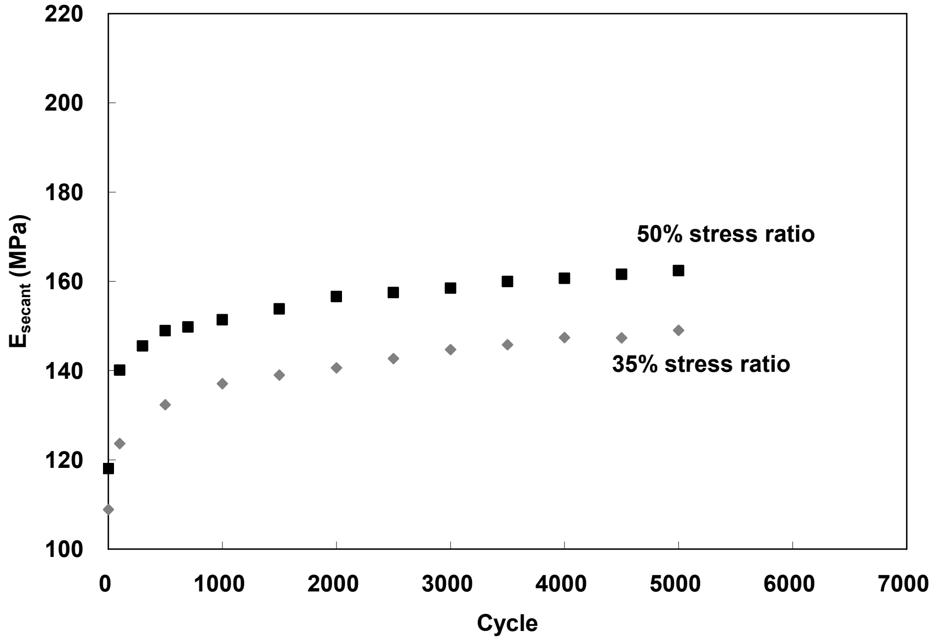

Figure D.108: Young's modulus (E_{secant}) of CR 3 75% Aggregate – 25% RAP.

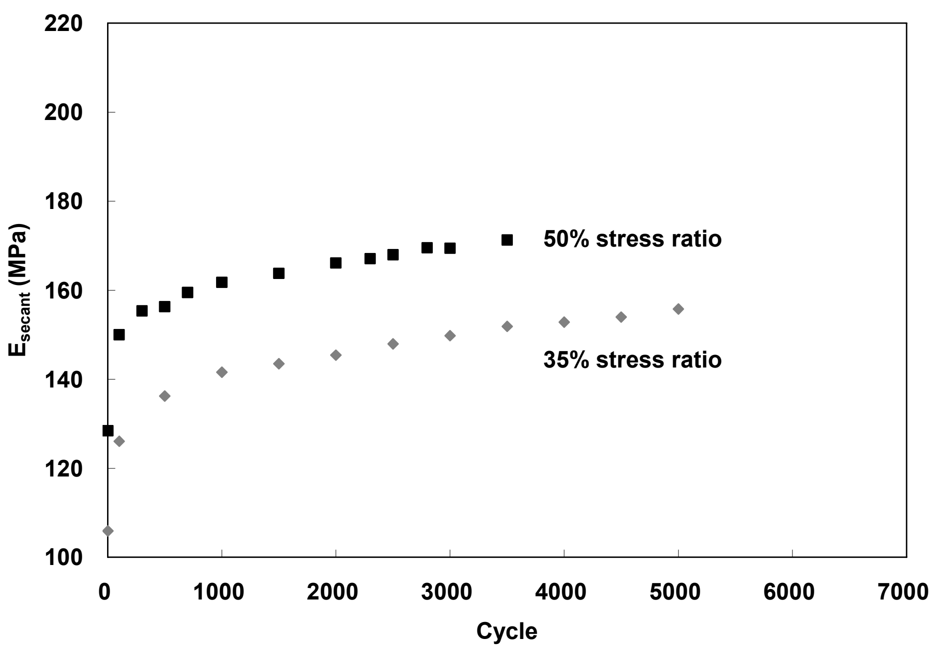

Figure D.109: Young's modulus (E_{secant}) of CR 3 50% Aggregate – 50% RAP.

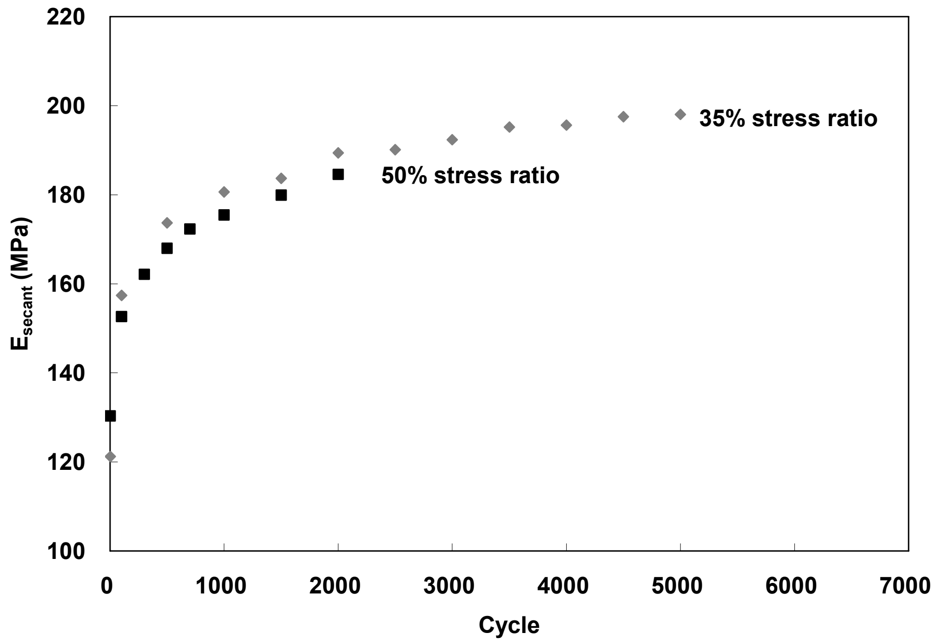

Figure D.110: Young's modulus (E_{secant}) of CR 3 25% Aggregate – 75% RAP.

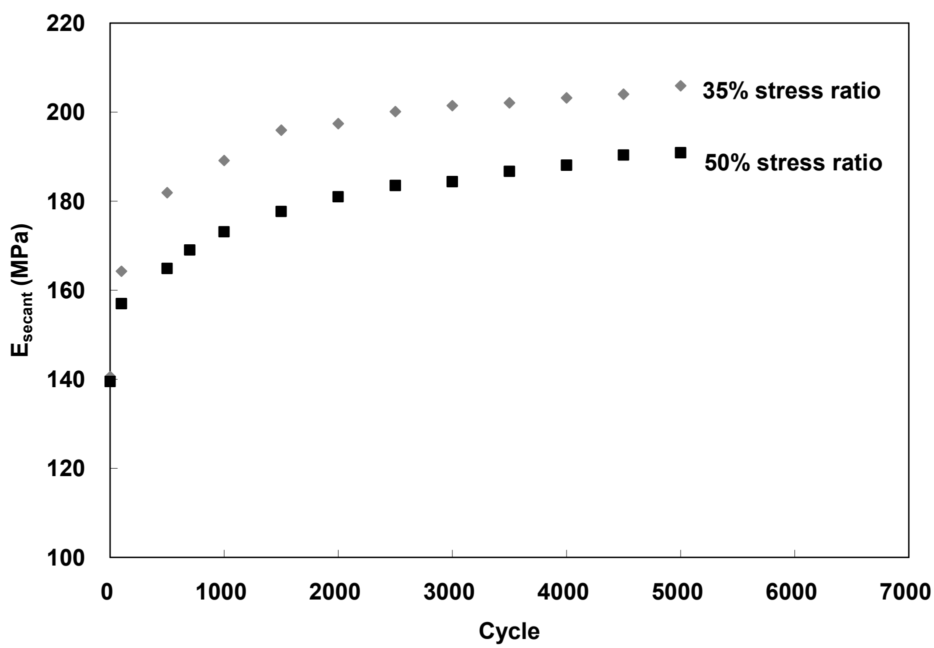

Figure D.111: Young's modulus (E_{secant}) of TH 23 In-situ Blend.

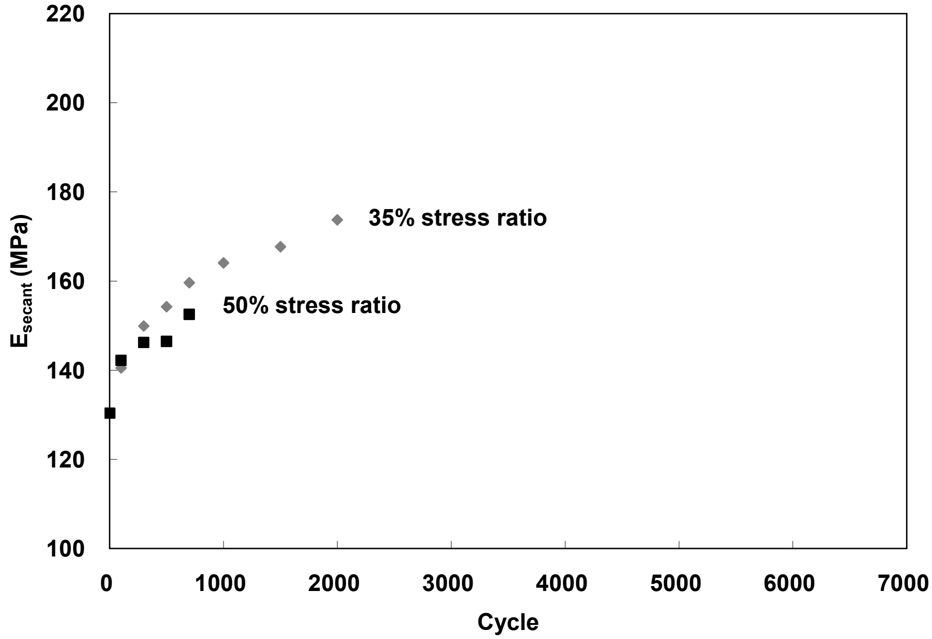

Figure D.112: Young's modulus (E_{secant}) of TH 200 In-situ Blend.

D.8 Energy Loss

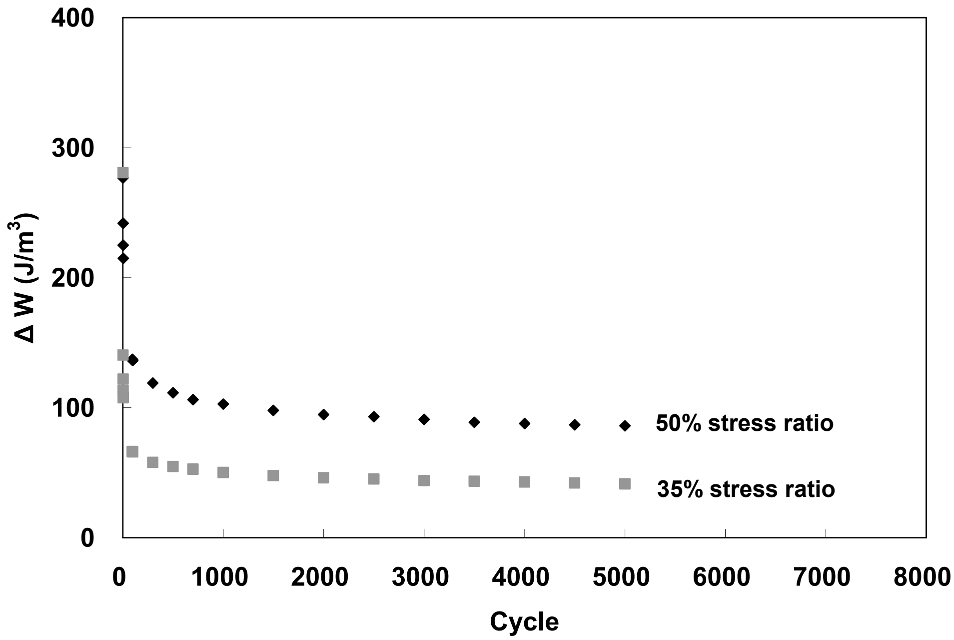

Figure D.113: Energy Loss of CR 3 In-situ Blend.

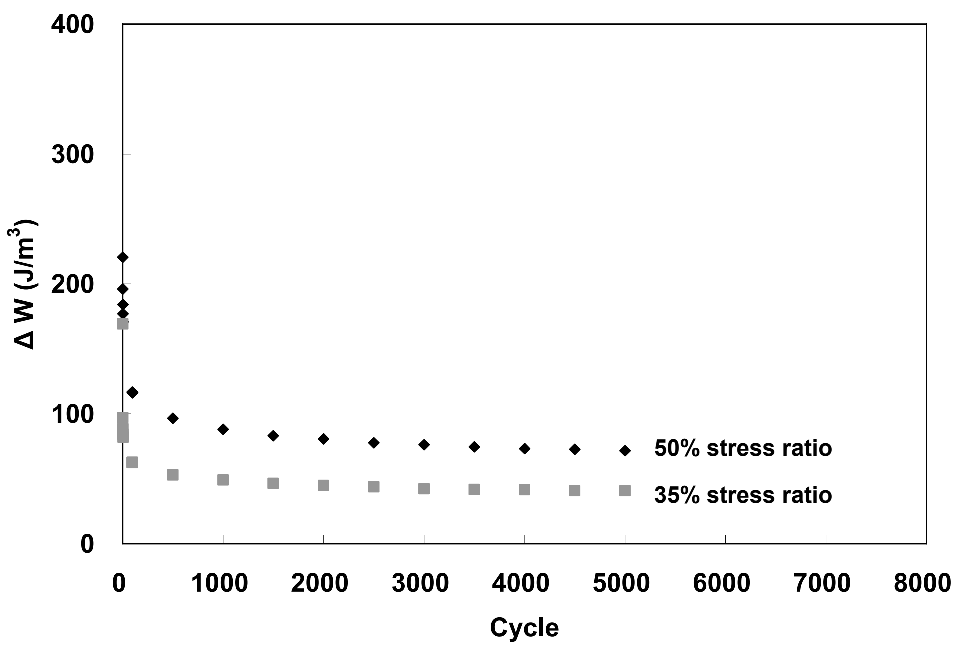

Figure D.114: Energy Loss of CR 3 100% Aggregate.

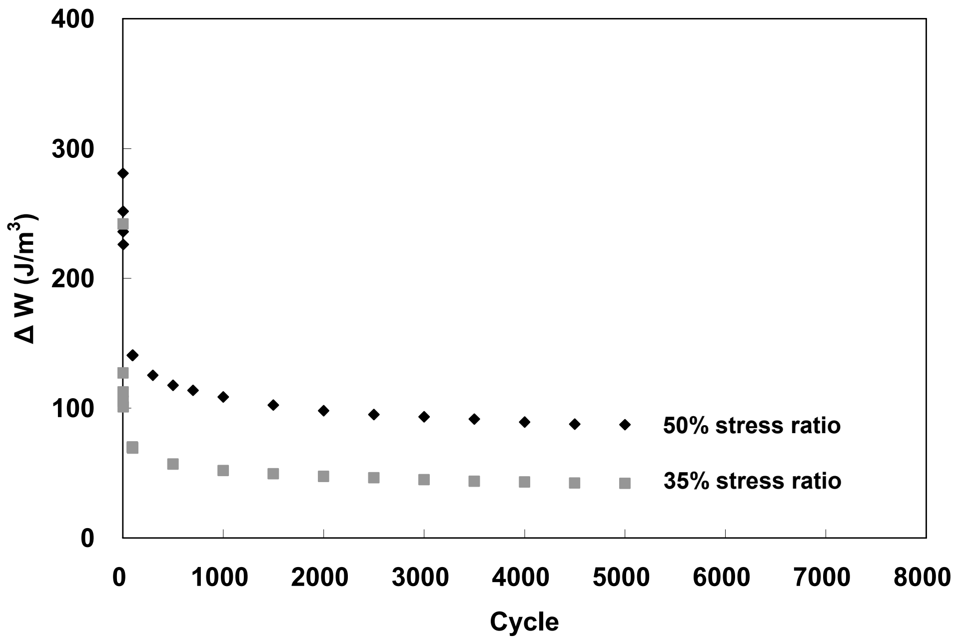

Figure D.115: Energy Loss of CR 3 75% Aggregate – 25% RAP.

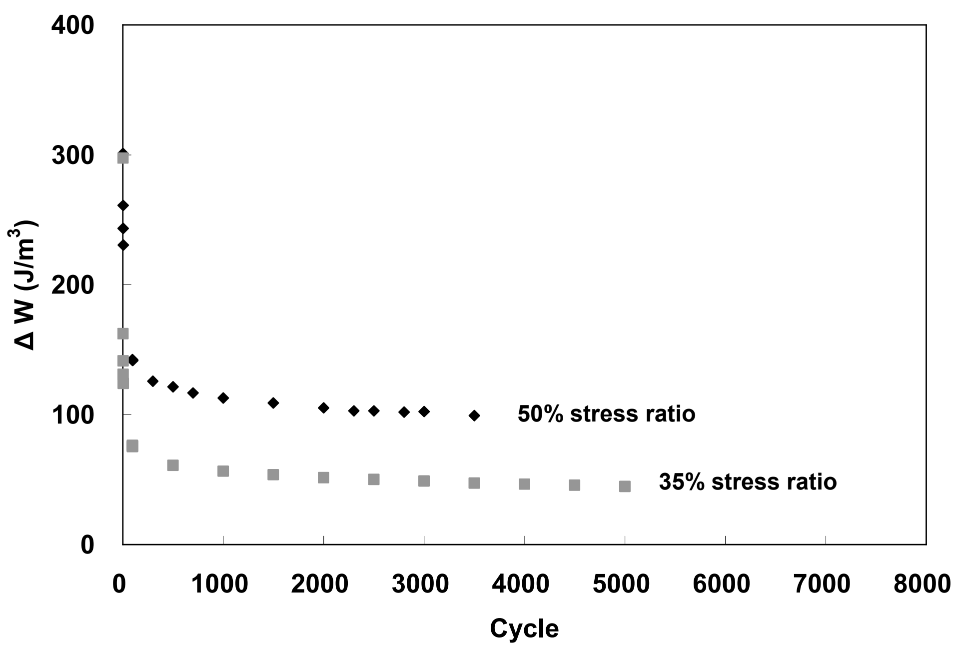

Figure D.116: Energy Loss of CR 3 50% Aggregate – 50% RAP.

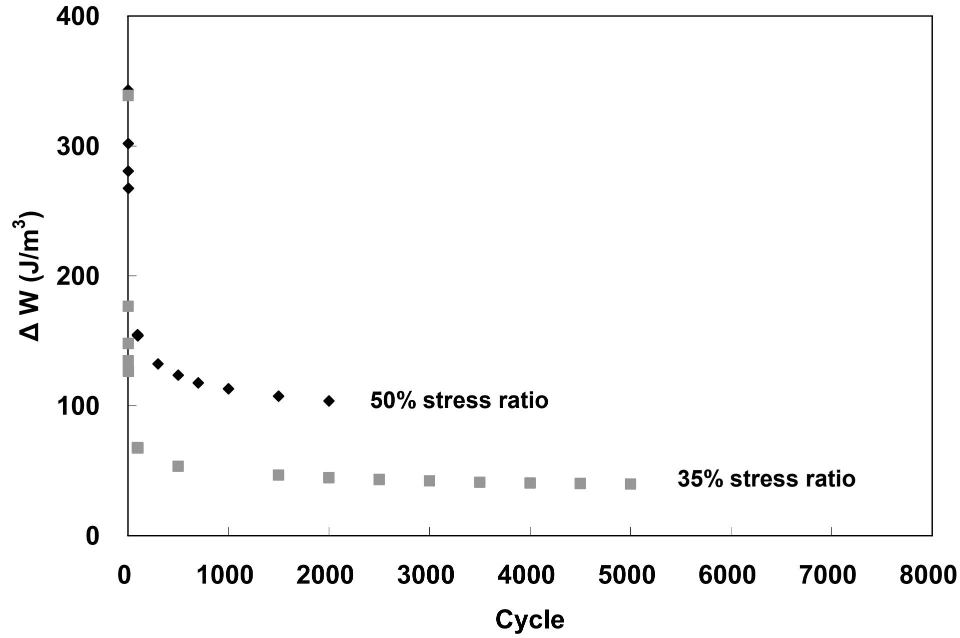

Figure D.117: Energy Loss of CR 3 25% Aggregate – 75% RAP.

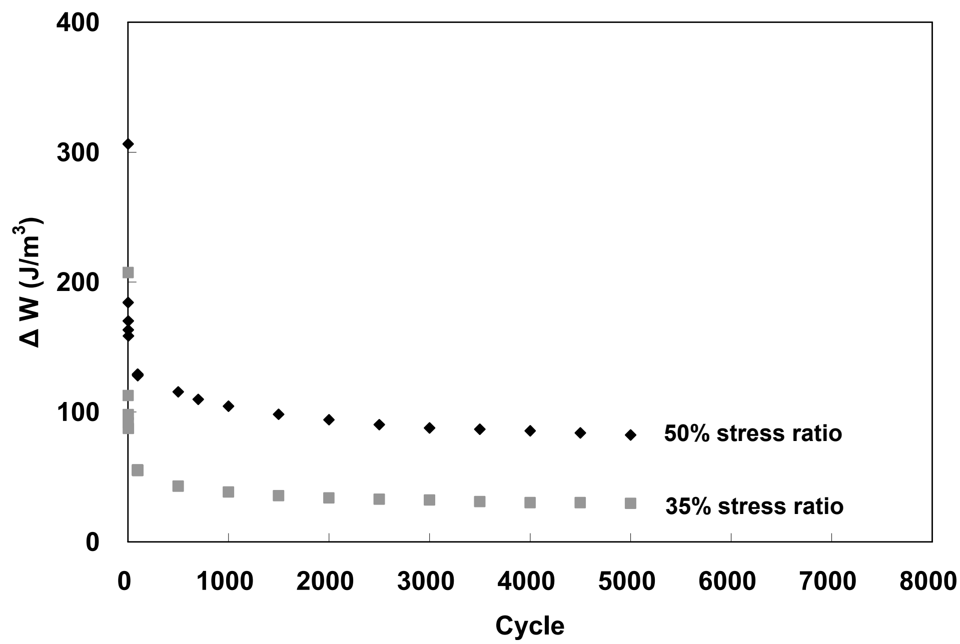

Figure D.118: Energy Loss of TH 23 % In-situ Blend.

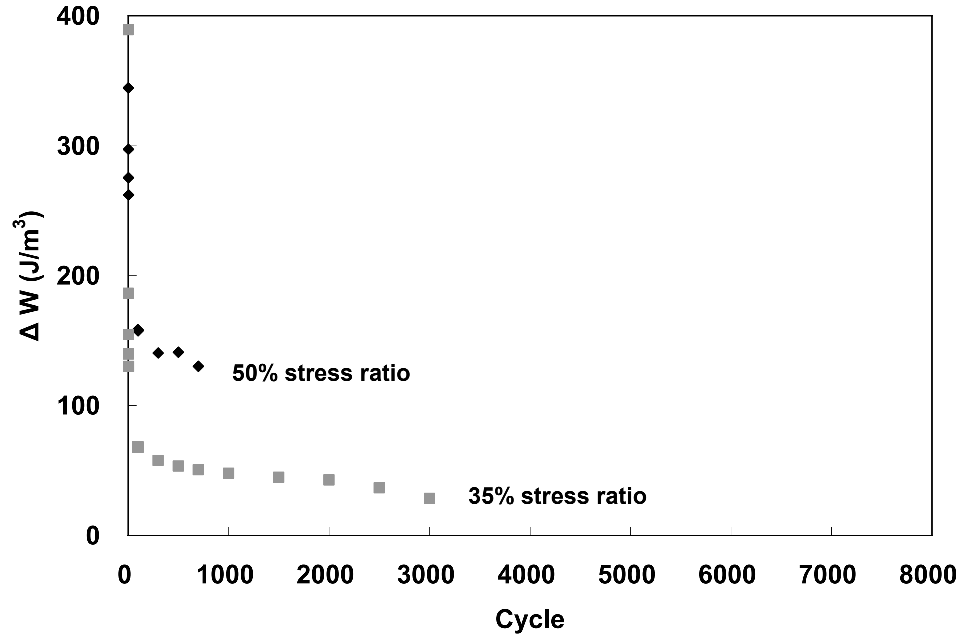

Figure D.119: Energy Loss of TH 200 % In-situ Blend.

D.9 QC / QA Criteria for M_R Testing

Table D32: QC / QA for S_5.1_1, CR 3_Blend_65%OMC_1

Sq	Cycle	Conf psi	Dev Stress Psi	SNR LVDT1	SNR LVDT2	SNR LVDT3	Rotation θ(°)	COV %	Pass Criteria	Mr psi
1	1	3	1.509	3.09	3.07	16.63	0.0009	4.14	Yes	41415.78
	2	3	1.511	2.71	3.04	23.83	0.0005		No	NA
	3	3	1.506	2.78	2.97	10.58	0.0004		No	NA
	4	3	1.504	3.10	2.97	8.00	0.0008		No	NA
	5	3	1.423	2.65	3.01	7.00	0.0004		No	NA
29	1	15	103.469	58.66	61.72	68.21	0.0337	0.10	Yes	65330.65
	2	15	103.555	56.70	58.97	66.00	0.0341		Yes	65386.27
	3	15	103.453	56.42	59.11	63.10	0.0336		Yes	65443.33
	4	15	103.532	52.21	55.26	60.34	0.0340		Yes	65499.92
	5	15	103.449	49.09	54.22	61.88	0.0334		Yes	65461.26
30	1	20	137.059	61.38	63.62	62.38	0.0424	0.19	No	NA
	2	20	137.251	63.69	59.84	59.17	0.0424		No	NA
	3	20	137.233	55.39	58.17	59.59	0.0421		No	NA
	4	20	137.148	55.32	56.97	56.22	0.0424		No	NA
	5	20	136.969	56.44	54.76	56.41	0.0419		No	NA

Table D33: QC / QA for S_5.1_2, CR 3_Blend_65%OMC_2

Sq	Cycle	Conf psi	Dev Stress psi	SNR LVDT1	SNR LVDT2	SNR LVDT3	Rotation θ(°)	COV %	Pass Criteria	Mr psi
1	1	3	1.478	2.65	1.66	infinite	0.0016	2.49	No	NA
	2	3	1.565	2.73	1.68	6.75	0.0016		No	NA
	3	3	1.479	2.34	1.79	infinite	0.0012		No	NA
	4	3	1.478	2.25	1.83	infinite	0.0012		No	NA
	5	3	1.474	2.28	1.91	9.37	0.0012		No	NA
2	1	6	2.844	3.04	2.42	3.38	0.0013	2.09	No	NA
	2	6	2.834	3.78	2.73	3.20	0.0013		No	NA
	3	6	2.834	3.68	2.69	2.96	0.0013		No	NA
	4	6	2.921	3.75	2.92	3.33	0.0012		No	NA
	5	6	2.922	3.72	2.63	3.62	0.0014		No	NA
3	1	10	4.923	4.96	3.65	5.89	0.0013	2.38	Yes	90378.73
	2	10	4.838	4.74	3.76	5.63	0.0014		Yes	92755.62
	3	10	4.924	5.23	3.69	6.35	0.0017		Yes	86937.91
	4	10	4.921	4.89	3.78	5.82	0.0013		Yes	90967.64
	5	10	4.922	4.97	3.65	5.42	0.0013		Yes	91188.02

Table D34: QC / QA for S_7.8_1, CR 3_Blend_100%OMC_1

Sq	Cycle	Conf psi	Dev Stress psi	SNR LVDT1	SNR LVDT2	SNR LVDT3	Rotation θ(°)	COV %	Pass Criteria	Mr psi
1	1	3	1.437	10.87		4.11				
	2	3	1.532	12.80		3.70				
	3	3	1.440	8.60		3.14				
	4	3	1.438	16.46		2.97				
	5	3	1.453	9.04		3.02				
2	1	6	2.851	10.00	5.62	32.77	0.0033	2.63	Yes	36265.14
	2	6	2.851	10.31	5.40	23.37	0.0033		Yes	36263.85
	3	6	2.765	9.69	5.61	infinite	0.0034		Yes	35034.57
	4	6	2.851	10.26	5.05	33.51	0.0031		Yes	37418.13
	5	6	2.854	10.62	5.79	infinite	0.0036		Yes	35279.40
6	1	3	2.878	15.41		62.20				
	2	3	2.882	17.93		43.12				
	3	3	2.883	17.47		27.40				
	4	3	2.877	17.49		25.19				
	5	3	2.871	17.99		35.31				
7	1	6	5.890	22.46	11.93	35.04	0.0050	1.15	Yes	33524.22
	2	6	5.799	21.12	12.16	37.74	0.0054		Yes	32564.84
	3	6	5.902	22.09	11.84	41.23	0.0051		Yes	33183.85
	4	6	5.898	22.78	10.99	31.08	0.0051		Yes	33164.54
	5	6	5.893	22.20	11.68	91.16	0.0054		Yes	32751.61
11	1	3	5.885	28.17		32.08				
	2	3	5.883	27.62		35.24				
	3	3	5.887	27.65		27.58				
	4	3	5.880	28.70		32.77				
	5	3	5.897	26.49		23.82				
12	1	6	11.752	43.87	23.71	32.26	0.0102	0.25	Yes	32192.96
	2	6	11.756	42.30	22.87	33.86	0.0107		Yes	31990.21
	3	6	11.748	40.28	24.17	28.27	0.0107		Yes	32038.57
	4	6	11.749	39.43	23.91	30.74	0.0104		Yes	32009.02
	5	6	11.752	43.52	25.04	28.88	0.0104		Yes	32047.47

Table D35: QC / QA for S_7.8_2, CR 3_Blend_100%OMC_2

Sq	Cycle	Conf psi	Dev Stress psi	SNR LVDT1	SNR LVDT2	SNR LVDT3	Rotation θ(°)	COV %	Pass Criteria	Mr psi
1	1	3	1.456	4.80	3.11	6.28	0.0019	4.31	Yes	26110.93
	2	3	1.457	4.25	3.11	6.27	0.0018		Yes	27021.31
	3	3	1.544	5.32	2.97	6.27	0.0019		No	NA
	4	3	1.463	4.06	2.41	6.53	0.0024		No	NA
	5	3	1.460	4.51	2.33	6.05	0.0020		No	NA
2	1	6	2.847	7.07	5.32	7.40	0.0016	2.72	Yes	38701.14
	2	6	2.848	7.13	5.31	7.80	0.0021		Yes	37491.00
	3	6	2.849	7.25	5.17	7.80	0.0021		Yes	37470.68
	4	6	2.847	7.16	5.12	7.88	0.0022		Yes	37376.61
	5	6	2.847	7.28	5.28	6.46	0.0020		Yes	39739.36
29	1	15	103.032	62.75	68.48	62.10	0.0385	0.16	Yes	56069.72
	2	15	103.028	63.91	66.66	58.62	0.0388		Yes	56195.41
	3	15	103.026	62.68	60.93	59.13	0.0388		Yes	56245.95
	4	15	103.024	54.50	60.91	57.04	0.0389		Yes	56294.26
	5	15	102.942	55.01	61.00	55.56	0.0390		Yes	56284.77
30	1	20	137.101	60.94	61.77	59.01	0.0508	0.12	No	NA
	2	20	137.105	57.65	59.98	56.14	0.0514		No	NA
	3	20	137.103	54.86	58.77	52.73	0.0512		No	NA
	4	20	137.101	50.99	55.47	52.69	0.0512		No	NA
	5	20	137.101	54.86	52.98	54.70	0.0509		No	NA

Table D36: QC / QA for T_5.7_1, CR 3_100%A_65%OMC_1

Sq	Cycle	Conf psi	Dev Stress psi	SNR LVDT1	SNR LVDT2	SNR LVDT3	Rotation θ(°)	COV %	Pass Criteria	Mr psi
1	1	3	1.464	2.88	3.07	infinite	0.0011	4.71	No	NA
	2	3	1.463	2.98	3.03	37.39	0.0015		No	NA
	3	3	1.464	3.76	2.94	infinite	0.0007		No	NA
	4	3	1.462	3.94	2.84	infinite	0.0012		No	NA
	5	3	1.549	3.13	3.03	26.52	0.0015		Yes	35166.62
2	1	6	2.858	5.13	4.14	8.01	0.0015	2.71	Yes	40745.57
	2	6	2.850	4.79	3.86	7.95	0.0020		Yes	43445.65
	3	6	2.850	4.89	3.71	7.84	0.0020		Yes	43494.21
	4	6	2.854	5.57	3.84	8.07	0.0018		Yes	42006.53
	5	6	2.853	5.58	3.79	7.86	0.0018		Yes	42094.91

Table D37: QC / QA for T_5.7_2, CR 3_100%A_65%OMC_2

Sq	Cycle	Conf psi	Dev Stress psi	SNR LVDT1	SNR LVDT2	SNR LVDT3	Rotation θ(°)	COV %	Pass Criteria	Mr psi
1	1	3	1.532	3.47	4.34	4.41	0.0010	4.00	Yes	34776.13
	2	3	1.433	3.77	4.49	4.10	0.0011		Yes	32030.70
	3	3	1.444	3.60	4.40	2.94	0.0015		No	NA
	4	3	1.444	2.98	4.09	3.04	0.0015		No	NA
	5	3	1.519	2.99	4.09	3.31	0.0016		No	NA
2	1	6	2.844	5.30	7.53	10.28	0.0022	1.98	Yes	41149.69
	2	6	2.849	4.94	7.04	10.49	0.0017		Yes	42345.62
	3	6	2.845	4.71	7.04	8.24	0.0017		Yes	42206.87
	4	6	2.848	5.01	6.37	8.03	0.0019		Yes	43251.11
	5	6	2.849	4.87	6.30	7.79	0.0019		Yes	43102.05

Table D38: QC / QA for T_8.8_1, CR 3_100%A_100%OMC_1

Sq	Cycle	Conf psi	Dev Stress psi	SNR LVDT1	SNR LVDT2	SNR LVDT3	Rotation θ(°)	COV %	Pass Criteria	Mr psi
1	1	3	1.461	7.55	9.69	9.88	0.0009	1.45	Yes	15434.48
	2	3	1.461	7.74	8.90	8.66	0.0009		Yes	15319.77
	3	3	1.462	7.70	8.99	7.87	0.0012		Yes	15886.29
	4	3	1.463	7.17	9.05	8.31	0.0013		Yes	15724.14
	5	3	1.463	7.45	8.85	9.26	0.0013		Yes	15632.13
29	1	15	103.008	86.77	78.54	67.40	0.0120	0.13	Yes	43168.84
	2	15	103.085	80.87	80.28	68.88	0.0121		Yes	43213.59
	3	15	103.173	82.53	75.62	64.37	0.0116		Yes	43239.41
	4	15	103.175	73.04	75.75	58.96	0.0122		Yes	43290.33
	5	15	102.829	78.01	73.36	57.88	0.0117		Yes	43143.94
30	1	20	136.598							
	2	20	136.598							
	3	20	136.596							
	4	20	136.763							
	5	20	136.596							

Table D39: QC / QA for T_8.8_2, CR 3_100%A_100%OMC_2

Sq	Cycle	Conf psi	Dev Stress psi	SNR LVDT1	SNR LVDT2	SNR LVDT3	Rotation θ(°)	COV %	Pass Criteria	Mr psi
1	1	3	1.433	7.41	1.11	7.23	0.0056	4.49	No	NA
	2	3	1.343	7.63	1.04	8.69	0.0056		No	NA
	3	3	1.435	7.23	0.97	8.33	0.0057		No	NA
	4	3	1.433	7.42	1.05	11.03	0.0055		No	NA
	5	3	1.432	7.72	1.05	12.93	0.0060		No	NA
2	1	6	2.848	12.14	1.17	20.17	0.0089	1.76	No	NA
	2	6	2.846	11.94	0.59	17.14	0.0097		No	NA
	3	6	2.761	11.05	0.59	17.40	0.0094		No	NA
	4	6	2.758	11.05	1.27	17.14	0.0088		No	NA
	5	6	2.753	11.04	1.24	15.04	0.0088		No	NA
3	1	10	4.927	11.02	6.87	71.42	0.0053	0.98	Yes	40389.55
	2	10	4.838	11.06	6.56	71.42	0.0053		Yes	39665.31
	3	10	4.924	11.12	6.52	infinite	0.0053		Yes	40402.98
	4	10	4.927	10.78	6.75	100.73	0.0053		Yes	40428.93
	5	10	4.924	11.11	7.63	infinite	0.0048		Yes	39709.65
4	1	15	7.387	10.32	12.87	infinite	0.0015	0.74	Yes	50942.24
	2	15	7.383	9.95	13.34	102.96	0.0019		Yes	51685.46
	3	15	7.377	10.43	13.38	102.96	0.0015		Yes	50906.56
	4	15	7.465	10.24	13.03	72.97	0.0015		Yes	51479.93
	5	15	7.361	10.83	13.56	33.25	0.0015		Yes	50875.03
8	1	10	9.868	22.30	20.75	infinite	0.0030	0.74	Yes	37042.49
	2	10	9.871	22.55	23.22	135.95	0.0024		Yes	37045.55
	3	10	9.863	19.23	22.67	191.98	0.0029		Yes	36728.65
	4	10	9.862	18.45	23.52	infinite	0.0029		Yes	36712.71
	5	10	9.855	17.81	22.50	132.72	0.0025		Yes	37379.30
24	1	15	73.845	82.38	132.90	88.45	0.0486	0.18	No	NA
	2	15	73.843	76.56	123.59	80.88	0.0476		No	NA
	3	15	73.931	69.87	118.97	81.61	0.0487		No	NA
	4	15	73.847	75.69	108.96	76.47	0.0486		No	NA
	5	15	73.845	66.21	111.54	74.00	0.0487		No	NA
25	1	20	98.532	84.58	110.43	92.83	0.0508	0.07	No	NA
	2	20	98.527	86.85	113.48	89.75	0.0504		No	NA
	3	20	98.525	89.80	105.35	79.83	0.0504		No	NA
	4	20	98.440	84.06	97.82	81.58	0.0500		No	NA
	5	20	98.528	83.10	103.94	77.63	0.0504		No	NA

Table D40: QC / QA for U_5.7_1, CR 3_75%A-25%R_65%OMC_1

Sq	Cycle	Conf psi	Dev Stress psi	SNR LVDT1	SNR LVDT2	SNR LVDT3	Rotation θ(°)	COV %	Pass Criteria	Mr psi
1	1	3	1.550	3.09	4.25	4.13	0.0007	2.60	Yes	39424.50
	2	3	1.551	2.81	4.27	3.66	0.0010		No	NA
	3	3	1.526	2.45	4.23	3.94	0.0010		No	NA
	4	3	1.521	3.47	4.56	3.69	0.0006		Yes	38315.17
	5	3	1.527	2.59	4.15	3.66	0.0010		No	NA

Table D41: QC / QA for U_5.7_2, CR 3_75%A-25%R_65%OMC_2

Sq	Cycle	Conf psi	Dev Stress psi	SNR LVDT1	SNR LVDT2	SNR LVDT3	Rotation θ(°)	COV %	Pass Criteria	Mr psi
1	1	3	1.394	0.62	2.93	0.91	0.0025	6.11	No	NA
	2	3	1.315	0.60	2.95	1.01	0.0026		No	NA
	3	3	1.394	0.78	2.39	0.96	0.0020		No	NA
	4	3	1.397	0.83	2.99	1.03	0.0025		No	NA
	5	3	1.393	0.83	2.57	1.05	0.0019		No	NA
2	1	6	2.844	2.36	4.89	3.40	0.0032	4.85	No	NA
	2	6	2.848	2.36	4.53	2.95	0.0028		No	NA
	3	6	2.845	2.36	4.55	3.01	0.0028		No	NA
	4	6	2.844	2.36	4.54	3.57	0.0027		No	NA
	5	6	2.930	2.31	4.56	3.75	0.0027		No	NA
3	1	10	4.925	2.34	9.87	5.07	0.0059	0.81	No	NA
	2	10	5.010	2.36	9.50	5.27	0.0059		No	NA
	3	10	4.924	2.32	9.19	5.30	0.0059		No	NA
	4	10	4.923	2.31	9.04	5.33	0.0059		No	NA
	5	10	4.925	2.40	9.34	5.35	0.0059		No	NA
6	1	3	2.941	2.51	5.89	4.92	0.0039	2.81	No	NA
	2	3	2.941	2.88	5.98	5.01	0.0037		No	NA
	3	3	2.939	2.36	6.12	4.68	0.0042		No	NA
	4	3	2.939	2.36	5.60	4.83	0.0037		No	NA
	5	3	2.936	2.56	5.60	4.89	0.0036		No	NA
29	1	15	103.022	72.82	74.84	56.38	0.0476	0.08	No	NA
	2	15	103.027	74.05	77.70	53.54	0.0471		No	NA
	3	15	103.022	76.30	78.27	57.42	0.0474		No	NA
	4	15	103.024	81.85	77.92	56.97	0.0472		No	NA
	5	15	103.023	76.26	78.00	55.62	0.0471		No	NA
30	1	20	137.019	67.78	72.79	49.66	0.0569	0.12	No	NA
	2	20	137.019	65.96	71.37	50.40	0.0569		No	NA
	3	20	137.019	65.53	68.41	50.17	0.0572		No	NA
	4	20	137.008	61.47	64.87	49.23	0.0574		No	NA
	5	20	136.932	61.24	63.24	45.85	0.0568		No	NA

Table D42: QC / QA for U_8.7_1, CR 3_75%A-25%R_100%OMC_1

Sq	Cycle	Conf psi	Dev Stress psi	SNR LVDT1	SNR LVDT2	SNR LVDT3	Rotation θ(°)	COV %	Pass Criteria	Mr psi
1	1	3	1.471	9.57	4.41	12.34	0.0023	2.55	Yes	21313.56
	2	3	1.472	8.72	4.35	8.53	0.0018		Yes	22106.19
	3	3	1.469	8.99	5.42	6.15	0.0022		Yes	20887.27
	4	3	1.472	9.18	5.26	5.97	0.0022		Yes	20915.51
	5	3	1.469	8.96	4.99	5.22	0.0023		Yes	21834.43
30	1	20	136.296							
	2	20	136.225							
	3	20	136.303							
	4	20	136.044							
	5	20	136.037							

Table D43: QC / QA for U_8.7_2, CR 3_75%A-25%R_100%OMC_2

Sq	Cycle	Conf psi	Dev Stress psi	SNR LVDT1	SNR LVDT2	SNR LVDT3	Rotation θ(°)	COV %	Pass Criteria	Mr psi
1	1	3	1.444	15.23	10.52	14.17	0.0006	2.31	Yes	11109.41
	2	3	1.449	13.77	10.63	17.54	0.0007		Yes	11044.04
	3	3	1.440	14.10	11.54	23.37	0.0011		Yes	11095.03
	4	3	1.361	13.52	11.03	13.74	0.0008		Yes	10537.40
	5	3	1.448	14.67	10.80	12.58	0.0008		Yes	11147.52
30	1	20	135.208							
	2	20	135.206							
	3	20	135.120							
	4	20	135.201							
	5	20	135.201							

Table D44: QC / QA for V_8_1, CR 3_50%A-50%R_100%OMC_1

Sq	Cycle	Conf psi	Dev Stress psi	SNR LVDT1	SNR LVDT2	SNR LVDT3	Rotation θ(°)	COV %	Pass Criteria	Mr psi
1	1	3	1.456	14.16	10.47	9.19	0.0035	0.43	Yes	12787.86
	2	3	1.455	14.08	9.60	9.95	0.0030		Yes	12903.46
	3	3	1.461	14.20	9.65	11.79	0.0030		Yes	12823.49
	4	3	1.453	14.46	9.53	12.78	0.0030		Yes	12773.45
	5	3	1.459	15.25	9.76	11.92	0.0030		Yes	12771.33
30	1	20	137.220							
	2	20	137.218							
	3	20	137.132							
	4	20	137.130							
	5	20	137.214							

Table D45: QC / QA for V_8_2, CR 3_50%A-50%R_100%OMC_2

Sq	Cycle	Conf psi	Dev Stress psi	SNR LVDT1	SNR LVDT2	SNR LVDT3	Rotation θ(°)	COV %	Pass Criteria	Mr psi
1	1	3	1.431	14.08	14.70	11.90	0.0028	2.31	Yes	10031.99
	2	3	1.429	14.13	13.50	12.08	0.0028		Yes	10004.68
	3	3	1.436	18.61	14.79	12.85	0.0028		Yes	9977.20
	4	3	1.444	18.81	14.57	14.69	0.0026		Yes	10120.01
	5	3	1.536	15.76	14.81	13.16	0.0028		Yes	10543.80
29	1	15	102.467	44.59	48.12	46.48	0.0412	0.19	No	NA
	2	15	102.391	42.06	45.10	45.18	0.0412		No	NA
	3	15	102.386	41.32	44.69	42.03	0.0413		No	NA
	4	15	102.381	40.72	43.69	40.81	0.0412		No	NA
	5	15	102.469	38.37	42.44	38.21	0.0412		No	NA
30	1	20	135.913							
	2	20	135.909							
	3	20	135.992							
	4	20	135.991							
	5	20	135.900							

Table D46: QC / QA for W_4.7_1, CR 3_25%A-75%R_65%OMC_1

Sq	Cycle	Conf psi	Dev Stress psi	SNR LVDT1	SNR LVDT2	SNR LVDT3	Rotation θ(°)	COV %	Pass Criteria	Mr psi
1	1	3	1.538	5.37	2.81	3.62	0.0017	5.54	No	NA
	2	3	1.544	5.09	2.54	3.62	0.0017		No	NA
	3	3	1.548	4.26	2.65	3.71	0.0014		No	NA
	4	3	1.544	4.07	2.58	3.14	0.0013		No	NA
	5	3	1.551	4.56	2.67	4.13	0.0018		No	NA
2	1	6	2.861	5.21	4.30	4.97	0.0012	2.11	Yes	58564.25
	2	6	2.859	6.63	4.66	5.00	0.0012		Yes	58225.78
	3	6	2.867	8.15	4.36	4.89	0.0012		Yes	58658.15
	4	6	2.860	12.28	4.51	5.23	0.0012		Yes	58313.08
	5	6	2.864	8.42	4.32	4.84	0.0008		Yes	61190.57

Table D47: QC / QA for W_7.2_2, CR 3_25%A-75%R_100%OMC_2

Sq	Cycle	Conf psi	Dev Stress psi	SNR LVDT1	SNR LVDT2	SNR LVDT3	Rotation θ(°)	COV %	Pass Criteria	Mr psi
1	1	3	1.458	6.49	7.09	1.32	0.0041	2.49	No	NA
	2	3	1.445	6.33	7.94	1.23	0.0040		No	NA
	3	3	1.524	6.18	7.08	1.23	0.0041		No	NA
	4	3	1.534	6.87	7.12	1.30	0.0041		No	NA
	5	3	1.529	9.25	7.97	1.42	0.0040		No	NA
2	1	6	2.838	11.29	8.88	2.53	0.0047	1.74	No	NA
	2	6	2.847	10.02	8.57	2.44	0.0047		No	NA
	3	6	2.843	10.62	8.90	2.57	0.0048		No	NA
	4	6	2.849	10.90	8.91	2.56	0.0048		No	NA
	5	6	2.845	10.93	8.92	2.44	0.0046		No	NA
3	1	10	4.849	11.86	13.59	4.43	0.0045	1.57	Yes	57518.87
	2	10	4.854	10.87	12.75	4.19	0.0045		Yes	57573.97
	3	10	4.939	12.16	14.02	4.39	0.0049		Yes	57067.07
	4	10	4.919	13.58	13.89	4.42	0.0044		Yes	58772.10
	5	10	4.923	13.05	12.35	4.31	0.0045		Yes	59195.80

Table D48: QC / QA for X_3.5_1, TH 23_Blend_65%OMC_1

Sq	Cycle	Conf psi	Dev Stress psi	SNR LVDT1	SNR LVDT2	SNR LVDT3	Rotation θ(°)	COV %	Pass Criteria	Mr psi
1	1	3	1.521	6.60	5.61	2.25	0.0027	3.19	No	NA
	2	3	1.434	6.69	5.80	2.30	0.0028		No	NA
	3	3	1.440	7.84	5.90	2.24	0.0028		No	NA
	4	3	1.448	8.49	5.97	2.20	0.0028		No	NA
	5	3	1.532	9.44	6.13	2.29	0.0028		No	NA
2	1	6	2.842	11.94	7.67	3.94	0.0029	1.72	Yes	42521.91
	2	6	2.843	10.41	7.61	3.75	0.0029		Yes	42637.55
	3	6	2.839	11.03	8.22	3.98	0.0033		Yes	41231.08
	4	6	2.843	9.91	7.57	3.64	0.0029		Yes	42737.76
	5	6	2.839	9.54	8.22	3.82	0.0033		Yes	41414.44
29	1	15	102.842							
	2	15	102.669							
	3	15	102.839							
	4	15	102.659							
	5	15	102.665							
30	1	20								
	2	20								
	3	20								
	4	20								
	5	20								

Table D49: QC / QA for X_3.5_2, TH 23_Blend_65%OMC_2

Sq	Cycle	Conf psi	Dev Stress psi	SNR LVDT1	SNR LVDT2	SNR LVDT3	Rotation θ(°)	COV %	Pass Criteria	Mr psi
1	1	3	1.533	5.77	6.07	4.11	0.0036	4.83	Yes	27729.72
	2	3	1.520	4.87	6.45	4.33	0.0037		Yes	28754.52
	3	3	1.526	5.17	6.57	3.70	0.0036		Yes	27424.49
	4	3	1.443	5.63	6.41	3.43	0.0036		Yes	25983.90
	5	3	1.448	5.06	6.01	3.06	0.0036		Yes	25565.27
29	1	15	102.576	52.84	60.56	53.95	0.0123	0.11	Yes	65055.82
	2	15	102.477	57.02	59.19	48.81	0.0127		Yes	65014.12
	3	15	102.647	49.37	57.80	49.03	0.0123		Yes	65036.82
	4	15	102.571	46.76	55.55	45.68	0.0117		Yes	65061.98
	5	15	102.649	51.32	54.07	47.37	0.0122		Yes	65196.23
30	1	20	136.183							
	2	20	136.094							
	3	20	136.091							
	4	20	136.086							
	5	20	136.001							

Table D50: QC / QA for X_5.4_2, TH 23_Blend_100%OMC_2

Sq	Cycle	Conf psi	Dev Stress psi	SNR LVDT1	SNR LVDT2	SNR LVDT3	Rotation θ(°)	COV %	Pass Criteria	Mr psi
1	1	3	1.428	5.79	7.86	4.35	0.0022	2.30	Yes	24628.72
	2	3	1.528	5.87	9.46	4.33	0.0026		Yes	24349.72
	3	3	1.446	6.50	10.33	4.28	0.0028		Yes	23607.97
	4	3	1.535	5.86	9.06	4.30	0.0028		Yes	25030.20
	5	3	1.534	7.76	8.26	4.49	0.0021		Yes	24889.60
7	1	6	5.903	17.65	26.60	13.89	0.0069	1.58	Yes	32689.09
	2	6	5.811	1.72	25.33	3.39	0.0070		No	NA
	3	6	5.814	17.48	24.56	14.02	0.0064		Yes	32678.32
	4	6	5.799	16.85	25.29	15.10	0.0069		Yes	32275.20
	5	6	5.897	16.44	23.86	14.65	0.0066		Yes	33598.73
29	1	15	102.662	68.25	66.28	60.05	0.0447	0.16	No	NA
	2	15	102.586	67.77	62.98	61.35	0.0446		No	NA
	3	15	102.749	62.17	60.66	57.22	0.0447		No	NA
	4	15	102.665	56.83	56.36	54.66	0.0445		No	NA
	5	15	102.493	55.38	57.51	52.28	0.0447		No	NA
30	1	20	136.525	61.08	60.17	55.09	0.0555	0.17	No	NA
	2	20	136.437	58.67	58.08	53.40	0.0554		No	NA
	3	20	136.438	55.91	55.14	51.66	0.0548		No	NA
	4	20	136.432	56.35	54.56	49.73	0.0552		No	NA
	5	20	136.438	54.28	52.83	49.14	0.0550		No	NA

Table D51: QC / QA for Y_3.7_1, TH 200_Blend_65%OMC_1

Sq	Cycle	Conf psi	Dev Stress psi	SNR LVDT1	SNR LVDT2	SNR LVDT3	Rotation θ(°)	COV %	Pass Criteria	Mr psi
1	1	3	1.476	6.20	5.37	6.37	0.0020	3.64	Yes	24055.18
	2	3	1.470	5.97	5.31	6.02	0.0017		Yes	24448.32
	3	3	1.556	5.66	5.69	5.55	0.0022		Yes	24750.01
	4	3	1.475	5.67	4.83	4.61	0.0030		Yes	24741.04
	5	3	1.466	6.22	5.11	4.68	0.0020		Yes	26422.56
30	1	20	137.072							
	2	20	137.158							
	3	20	137.171							
	4	20	137.075							
	5	20	137.483							

Table D52: QC / QA for Y_3.7_2, TH 200_Blend_65%OMC_2

Sq	Cycle	Conf psi	Dev Stress psi	SNR LVDT1	SNR LVDT2	SNR LVDT3	Rotation θ(°)	COV %	Pass Criteria	Mr psi
1	1	3	1.544	5.29	3.23	4.29	0.0028	4.85	Yes	30595.59
	2	3	1.369	5.51	3.23	3.89	0.0027		Yes	27002.68
	3	3	1.467	6.70	3.58	3.82	0.0034		Yes	27504.53
	4	3	1.459	4.84	3.01	3.71	0.0027		Yes	28615.60
	5	3	1.459	4.84	3.07	3.69	0.0026		Yes	28431.05
26	1	3	20.452	49.86	63.16	62.50	0.0402	0.21	No	NA
	2	3	20.456	42.36	62.94	60.59	0.0407		No	NA
	3	3	20.378	37.14	58.56	58.83	0.0402		No	NA
	4	3	20.455	32.48	59.48	59.46	0.0406		No	NA
	5	3	20.452	43.46	59.90	54.16	0.0402		No	NA
27	1	6	40.778	43.09	71.01	66.45	0.0398	0.27	Yes	42978.42
	2	6	40.786	63.06	70.55	66.60	0.0402		No	NA
	3	6	41.042	51.88	63.77	63.77	0.0400		Yes	43217.48
	4	6	40.864	50.74	65.02	60.08	0.0404		No	NA
	5	6	41.042	39.15	61.66	56.55	0.0404		No	NA

Table D53: QC / QA for Y_5.7_1, TH 200_Blend_100%OMC_1

Sq	Cycle	Conf psi	Dev Stress psi	SNR LVDT1	SNR LVDT2	SNR LVDT3	Rotation θ(°)	COV %	Pass Criteria	Mr psi
1	1	3	1.435	11.97	11.67	19.40	0.0034	2.47	Yes	10813.21
	2	3	1.445	11.60	10.96	31.68	0.0036		Yes	11011.59
	3	3	1.447	17.94	12.15	22.96	0.0036		Yes	10876.65
	4	3	1.538	10.82	13.84	15.85	0.0036		Yes	11387.05
	5	3	1.458	11.92	14.73	21.44	0.0038		Yes	10676.50
30	1	20	135.944							
	2	20	135.793							
	3	20	135.951							
	4	20	135.861							
	5	20	135.921							

Table D54: QC / QA for Y_5.7_2, TH 200_Blend_100%OMC_2

Sq	Cycle	Conf psi	Dev Stress psi	SNR LVDT1	SNR LVDT2	SNR LVDT3	Rotation θ(°)	COV %	Pass Criteria	Mr psi
1	1	3	1.438	10.18	12.56	12.88	0.0010	0.59	Yes	10974.06
	2	3	1.440	13.43	17.44	15.89	0.0010		Yes	10814.96
	3	3	1.450	15.21	13.46	18.43	0.0010		Yes	10862.97
	4	3	1.453	13.23	12.20	14.02	0.0005		Yes	10947.45
	5	3	1.438	10.28	12.80	16.64	0.0005		Yes	10913.49
30	1	20	134.385							
	2	20	134.648							
	3	20	134.634							
	4	20	134.607							
	5	20	134.612							